Oceanologia

Official Journal of the Polish Academy of Sciences: Institute of Oceanology and Committee on Maritime Research

This journal is supported by the Ministry of Science and Higher Education, Warsaw, Poland

Indexed in: ISI Journal Master List, Science Citation Index Expanded, Scopus, Current Contents, Zoological Record, Thomson Scientific SSCI, Aquatic Sciences and Fisheries Abstracts, DOAJ

IMPACT FACTOR ANNOUNCED FOR 2017 IN THE 'JOURNAL CITATION REPORTS' IS 1.614; 5-year IF is 1.585

Publisher
Elsevier Sp. z o.o.
22, Jana Pawła II Avenue
00-133 Warsaw, Poland

Associate Publisher
Chen Lin
c.lin@elsevier.com
+86-10-8520 8768

ISSN 0078-3234

Oceanologia (2019) 61, 179—196

Available online at www.sciencedirect.com

ScienceDirect

journal homepage: www.journals.elsevier.com/oceanologia/

REVIEW ARTICLE

Amphipods in estuarine and marine quality assessment — a review

Weronika Podlesińska [a,*], **Henryka Dąbrowska** [b]

[a] *Gdynia Aquarium, National Marine Fisheries Research Institute (NMFRI), Gdynia, Poland*
[b] *Department of Food and Environmental Chemistry, National Marine Fisheries Research Institute (NMFRI), Gdynia, Poland*

Received 4 June 2018; accepted 27 September 2018
Available online 17 October 2018

KEYWORDS
Ecotoxicology;
Marine sediments;
Amphipods;
Corophium spp.;
Bioassays

Summary Amphipods are a diverse and important group of invertebrates contributing to the functioning of aquatic ecosystems. In spite of their variety, many species of amphipods share important biological and ecological characteristics that make them suitable test organisms for assessment of the ecological quality of estuarine and marine sediments. Their pertinence as test organism includes ecological relevance, close association with sediments, sensitivity to environmental contaminants, and amenability for culture and experimentation. Amphipod bioassays are used to examine the effect of exposure to contaminants, as well as to assess whole sediment quality, improve bioassay methods, develop more sensitive endpoints, and compare sensitivity and utility of species in environmental quality assessment. This work reviews the developments in this area of research over the last decades, focusing on European amphipods. The most often used species, the type of bioassays and endpoints investigated, confounding factors influencing the bioassays outcome, and the main applications of the bioassays have been presented. This review also addresses some aspects of amphipod biology that are relevant for bioassay methods and results analysis.

* Corresponding author at: Gdynia Aquarium, National Marine Fisheries Research Institute (NMFRI), Gdynia, Poland. Tel.: +48 58 732 66 08.
E-mail address: weronika.podlesinska@mir.gdynia.pl (W. Podlesińska).
Peer review under the responsibility of Institute of Oceanology of the Polish Academy of Sciences.

Production and hosting by Elsevier

https://doi.org/10.1016/j.oceano.2018.09.002

1. Introduction

Benthic habitats represent significant compartments of aquatic ecosystems, often negatively influenced by various anthropogenic activities including sediment contamination, especially in estuarine and marine areas (Chapman et al., 2013). These environments support diverse communities and ecological functions of ecosystems, but the presence of contaminants in sediments can negatively impact their ecological balance and, indirectly, human health (Burton, 1992). The significance of benthic habitats in determining ecosystem's health status has been stressed by the EU Marine Strategy Framework Directive (MSFD 2008/56/EC).

Amphipods, due to their habitat and lifestyle, are widely used test organisms for assessment of marine and estuarine sediment quality (Chapman et al., 1992, 2013; Postma et al., 2002). Attributes that make amphipods highly suitable for this purpose include their habitat at or below the sediment–water interface which ensures continuous exposure to sediment contaminants. Most species are characterized by sensitivity to contaminants, relatively broad tolerance for a wide range of salinity, sediment particle sizes and organic matter content, which facilitates tests with a variety of sediment types. Ecological significance (important links in coastal food chains) and wide geographic distribution of some species allows for comparisons throughout regions. They are relatively simple to collect from the field, handle and maintain in laboratory conditions. They can be cultured and show high survival rates under laboratory conditions (Chapman et al., 2013; Conlan, 1994; Lourens et al., 1995; Stronkhorst, 2003). Amphipods can be exposed to sediment contaminants through interstitial and/or bottom waters, as well as through ingestion of detritus/organic matter and a fine fraction of sediment. For sediment quality assessment, both infaunal and epibenthic amphipods e.g., *Corophium* spp. and *Gammarus* spp., have been recommended and used (Casado-Martinez et al., 2007; Chapman and Wang, 2001; Costa et al., 2005; Kunz et al., 2010; Macken et al., 2008; Van Den Brink and Kater, 2006). Burrowing species (such as *Corophium* spp.) are considered particularly good bioindicators as they are directly exposed to harmful substances through gills and body surface absorption and due to ingestion of fine sediment particles (Burton, 1992).

The use of amphipods for sediment toxicity testing was firstly developed in North America in the 1970s (Burton, 1992). In the 1990s amphipod bioassays became increasingly important in regulation and sediment assessment in North America, less so in Europe since only a few such bioassays had been then developed for European species (Chapman et al., 1992). Since that time the research advanced in this area, and a number of guidelines and numerous papers have been published worldwide (Table 1). Generally, the sediment toxicity testing can be performed with relatively simple bioassays, however, for in-depth assessment of sediment quality, it is recommended that the assessment includes also sediment chemistry and in situ benthic community structure which comprises the so-called sediment quality triad (Chapman, 1990; Chapman and Wang, 2001). The bioassays advantage is that they integrate the interactive effects of the complex contaminant mixtures present in sediments providing an integrative measure of contaminant-induced biological effects (ASTM, 1991).

Burrowing amphipods recommended and used in marine or estuarine sediment toxicity studies in North America include *Ampelisca abdita*, *Corophium volutator*, *Rhepoxynius abronius*, *Eohaustorius washingtonianus*, *Eohaustorius estuarius*, *Amphiporeia virginiana*, *Foxiphalus xiximeus*, *Leptocheirus pinguis* (Anderson et al., 2007; Chapman et al., 1992; Environment Canada, 1992; Fay et al., 2000; Meador et al., 1993; Nipper et al., 2002). In Europe, the Corophium genus has been recommended by ICES as a standard species for marine and estuarine sediment toxicity testing (Roddie and Thain, 2001). It has been also used for regulatory purposes for testing chemical products that are liable to accumulation in sediments (Cesnaitis et al., 2014). OSPAR (2006) indicated *C. volutator* for testing chemicals used in the offshore oil industry. Although recommended, *C. volutator* is not common in Southern Europe, and locally available *Corophiidae* species have been proposed as alternatives, such as *Corophium orientale*, *Corophium arenarium*, *Corophium multisetosum* or *Monocorophium insidiosum* (OSPAR, 2006, 2013; Prato et al., 2010; SETAC-Europe, 1993). Various species of the Corophium genus as well as representatives of other genera such as Gammarus and Ampelisca, depending on their natural occurrence, availability, and existing methodologies, have been used in studies of sediment quality (Table 1). Some amphipods, such as deposit-feeding benthic, keystone species in the Baltic Sea, *Monoporeia affinis* and *Pontoporeia femorata*, have been recommended by HELCOM and ICES as indicators of reproductive effects associated with hazardous substances in the marine environment (HELCOM, 2017; Sundelin et al., 2008a).

As bioassays with amphipods are being increasingly applied in the marine and estuarine environmental assessment, reviewing the issues related to their application can be of interest to scientists and consulting agencies involved in this type of activity. The objective of this review was to provide an update on developments in this area of research during the last decades. The review presents the most often used amphipod species with emphasis on European studies, the type of bioassays employed, endpoints investigated, confounding factors influencing the bioassays outcome and species sensitivity, and the main applications of the bioassays. Moreover, some aspects of amphipod biology and ecology have been addressed.

2. Some aspects of amphipod biology and ecology

Amphipoda (Crustacea, Malacostraca) constitute an important biological group of marine, estuarine, and freshwater aquatic ecosystems. They inhabit pelagic and benthic compartments exhibiting different life patterns, habitat preferences, and feeding ecology. Amphipods are herbivores, detritivores or scavengers (grazing on algae), omnivores or predators, and represent important links in aquatic food chains. A number of amphipod species, considered as herbivorous shredders, show a high diversity in food spectrum, consuming various types of plant materials as well as invertebrates. An example is *Echinogammarus marinus* which has been shown to consume algae as well as hard-bodied isopods

Table 1 Studies on estuarine and marine sediment quality using amphipod species.

Test species	Objectives	Test duration and investigated endpoints	Investigated matrix (area)	Applied guidelines	Reference
Leptocheirus plumulosus	Study of effects of sediment-associated weathered slick oil.	28-d survival, growth, reproduction	Whole sediment (Gulf of Mexico, USA)	ASTM, 2008; USEPA, 2001a	Lotufo et al., 2016
Echinogammarus marinus	Assessment of the short-term in situ assay.	48-h survival; 30-, 60-, 120-min post-exposure feeding rates	Whole sediment (the Minho and Lima River estuaries, Spain)	Short-term in situ procedure was developed	Martinez-Haro et al., 2016
Monocorophium insidiosum[b]	Development of an evaluation tool for sediment toxicity detection	10-d survival	Whole sediment (Taranto Gulf, Italy)	ASTM, 1993a; ISO, 2001	Prato et al., 2015
Grandidierella bonnieroides	Assessment of sediment quality	10-d survival	Whole sediment (Macaé River Estuary, Brazil)	ASTM, 2008	Molisani et al., 2013
Corophium volutator	Study on burrowing activity as endpoint.	10-d survival, burrowing	Whole sediment, laboratory culture (highly contaminated harbor, Germany)	DIN EN ISO 16712, 2007	Siebeneicher et al., 2013
Corophium orientale, *Monocorophium insidiosum*[b]	Comparison of the sensitivity of two amphipods.	10-d survival	Whole sediment, two species sensitivity comparison (Livorno harbor, Italy)	ASTM, 1993a; ISO, 2001; SETAC-Europe, 1993	Prato et al., 2010
Corophium multisetosum	Comparison of the sensitivity of laboratory-cultured and field-collected amphipod.	10-d survival	Whole sediment	Casado-Martinez et al., 2007	Menchaca et al., 2010
Melita plumulosa	Comparison of in situ and laboratory tests results.	gametogenesis, fertilization, and embryo development	Whole sediment	Mann et al., 2009	Mann et al., 2010
Ampelisca abidita, *Leptocheirus plumulosus*	Comparison of acute and chronic toxicity methods.	10-d survival; 28-d survival, growth, reproduction	Whole sediment (New York/New Jersey Harbor)	USEPA, 2001a	Kennedy et al., 2009
Monocorophium insidiosum[b], *Gammarus aequicauda*	Comparison of response of the species from different evolutionary levels and habitats.	10-d survival	Whole sediment, three species comparison (Ionian Sea, Taranto, Italy)	ASTM, 1993b; SETAC-Europe, 1993	Narracci et al., 2009
Monocorophium insidiosum[b]	Optimization of methodology for a bioassay.	10-d survival	Whole sediment	ASTM, 1990, 1993a, 1997	Prato et al., 2008
Corophium multisetosum	Assessment of performance of the amphipod in toxicity testing.	10-d survival	Temperature, salinity, cadmium, laboratory culture	ASTM, 1992, 2008	Ré et al., 2009
Corophium volutator	Assessment of sediment with use of a battery of multi-trophic species and multiple exposure phases.	10-d survival	Whole sediment (Irish estuaries)	ISO, 2004; RIKZ, 1999; Roddie and Thain, 2001	Macken et al., 2008
Corophium orientale	Assessment of sensitivity and applicability of an amphipod in the bioassays.	96-h survival; 10-d survival	Water-only and whole sediment (Venice Lagoon)	Procedure was developed	Picone et al., 2008

Table 1 (*Continued*)

Test species	Objectives	Test duration and investigated endpoints	Investigated matrix (area)	Applied guidelines	Reference
Corophium volutator, Ampelisca brevicornis	Comparison of the sensitivity of amphipods to dredged sediments.	10-d survival,	Whole sediment, two-species comparison (Spanish harbor)	ASTM, 1991; USEPA, 1994	Casado-Martinez et al., 2007
Corophium volutator	Description of methods and confounding factors in chronic bioassay.	49-d survival, growth, reproduction	Salinity, ammonium, nitrate, oxygen, laboratory culture	ASTM, 1999; ISO, 2005; Roddie and Thain, 2001; USEPA, 2001a	Van Den Heuvel-Greve et al., 2007
Corophium multisetosum	Comprehensive estuarine sediment toxicity survey with acute and chronic assessment.	10-d survival; 21-d survival, growth, fecundity	Whole sediment (Ria de Aveiro estuary), laboratory cultures	Procedure was described	Castro et al., 2006
Melita plumulosa	Description of the chronic sublethal sediment toxicity bioassay.	10-d survival; 42-d survival, reproduction, bioaccumulation	Metal-spiked sediment, whole sediments (Cockle Bay, Warners Bay, Nords Wharf, Australia)	Procedure for chronic bioassay was developed	Gale et al., 2006
Corophium volutator	Assessment of ammonium toxicity in bioassays at high pH.	10-d survival	Ammonium toxicity in bioassays	Procedure was described	Kater et al., 2006
Leptocheirus plumulosus	Effects of contaminated harbor sediment in chronic exposure.	42-d survival, growth, reproduction, dry weight	whole sediment, laboratory culture (Baltimore Harbor, USA)	USEPA, 2001a,b	Manyin and Rowe, 2006
Gammarus aequicauda, Monocorophium insidiosum[b]	Evaluation of toxicity of copper, cadmium and mercury in 5 species.	10-d survival; 28-d survival, growth	Whole sediment	SETAC-Europe, 1993	Prato et al., 2006
Melita plumulosa	Development of a culturing procedures.	28-d survival, growth, reproduction	Optimal conditions for laboratory cultures	ASTM, 2003a, 2003b; USEPA, 2001a	Hyne et al., 2005
Mandibulophoxus mai, Monocorophium acherusicum, Haustorioides indivisus, Haustorioides koreanus	Development bioassay protocols for species native to Korea.	10-d survival, behavior	Whole sediment (Sihwa and Onsan industrial complexes, Korea)	ASTM, 1991; USEPA, 1994	Lee et al., 2005
Corophium colo	Assessment and comparison of the species sensitivity to contaminated sediments.	10-d survival	Whole sediment (Sydney Harbour, Australia)	ASTM, 1998	McCready et al., 2005
Gammarus locusta	Assessment of moderately toxic sediments in chronic exposures with biochemical endpoints.	28-d survival, reproduction[a], biochemical markers	Whole sediment (Sado and Tagus estuaries, Portugal)	Procedure was described	Neuparth et al., 2005
Corophium volutator	Study on the laboratory cultures for sediment toxicity testing.	71-d growth, reproduction	Laboratory cultures, fecundity, fertility, temperature preference	USEPA, 2001a	Peters and Ahlf, 2005

Table 1 (*Continued*)

Test species	Objectives	Test duration and investigated endpoints	Investigated matrix (area)	Applied guidelines	Reference
Gammarus aequicauda, Microdeutopus gryllotalpa	Sensitivity of the marine organisms in assessment of sediments.	10-d survival	Whole sediment, two-species comparison (Portmán Bay, Spain)	ASTM, 1997; USEPA, 1994	Cesar et al., 2004
Leptocheirus plumulosus	Evaluation of the relationship between laboratory and field responses to contaminants.	10-d survival, 28-d survival, growth, reproduction	Whole sediment (Baltimore Harbour/Patapsco River System)	USEPA, 1998	McGee et al., 2004
Corophium volutator, Ampelisca brevicornis	Comparison of toxicity of sediment contaminated with mining spill to two species.	10-d survival	Whole sediment (Bay of Cádiz, Spain)	ASTM, 1993b	Riba et al., 2003
Paracorophium excavatum	Assessment of suitability of the amphipod in sediment toxicity assessment.	10-d survival, 28-d survival	Whole sediment (Avon-Heathcote Estuary)	Bat and Raffaelli, 1998	Marsden et al., 2000
Corophium orientale	Assessment of suitability of the amphipods in harbor toxicity assessment.	10-d survival	Whole sediment (northern Tyrrhenian Sea, Italy)	Ciarelli, 1994	Onorati et al., 1999
Spiked-sediment exposures					
Leptocheirus plumulosus	Study on effects of long-term exposure to copper on survival, growth and reproduction.	28-d survival, growth, reproduction	Cu-spiked sediment	USEPA, 2001a	Ward et al., 2015
Monocorophium insidiosum[b]	Assessment of toxicity of three antiparasitic pesticides.	10-d survival	Antiparasitic pesticides-spiked sediment	USEPA, 1994	Tucca et al., 2014
Eohaustorius estuarius	Comparison of the sensitivities of toxicity test protocols.	10-d survival	Chlorpyrifos, copper, fluoranthene, permethrin, bifenthrin, and cypermethrin-spiked sediment	USEPA, 1994	Anderson et al., 2008
Corophium volutator	Development of a long-term assay with polychaete and amphipod.	10-d survival; 28-d survival, growth,	Toxicity of Ivermectin; UK	Roddie and Thain, 2001	Allen et al., 2007
Corophium volutator	Development of chronic toxicity test method.	28-d survival, growth, reproduction	Crude oil-spiked sediment	ASTM, 2000; USEPA, 2001a, 1994	Scarlett et al., 2007
Corophium volutator	Assessment of suitability of the amphipod in sediment biomonitoring.	behavioral responses	Bioban pesticide-spiked sediment	Procedure was described	Kirkpatrick et al., 2006
Melita plumulosa	Evaluation of chronic toxicity test.	10-d survival; 42-d survival, reproduction, bioaccumulation	Metal-spiked sediment, whole sediment (Cockle Bay, Warners Bay, Nords Wharf, Australia)	Procedure for chronic bioassay was developed	Gale et al., 2006

Table 1 (*Continued*)

Test species	Objectives	Test duration and investigated endpoints	Investigated matrix (area)	Applied guidelines	Reference
Paracorophium excavatum	Study on influence of the sediment copper on the amphipod reproduction.	28-d survival, growth	Cu-spiked sediment	Environment Canada, 1992	Marsden, 2002
Ampelisca abdita	Evaluation of the ecological significance of the laboratory tests.	10-d survival, 70-d survival, growth	Cd-spiked sediment	ASTM, 1993c	Kuhn et al., 2002
Ampelisca abdita	Study on the feasibility of the amphipod for sediment toxicity tests.	10-d survival, avoidance	2,6-DNT-spiked sediment	Procedure was described	Nipper et al., 2002
Ampelisca abdita	Determination of body residues associated with acute toxicity.	10-d survival	Non-ionic organics-spiked sediment	USEPA, 1994	Fay et al., 2000
Interlaboratory comparative studies					
Corophium volutator, Ampelisca brevicornis	Comparison of the sensitivity of amphipods to dredged materials.	10-d survival	Whole sediment, inter-laboratory, multispecies, comparisons	ASTM, 1991; RIKZ, 1999; SETAC-Europe, 1993; USEPA, 1994	Casado-Martinez et al., 2007
Eohaustorius estuarius	Determination of interlaboratory variability in sediment toxicity tests.	10-d survival	Whole sediment, inter-laboratory comparisons	ASTM, 1992; USEPA, 1994	Bay et al., 2003
Corophium volutator, Rhepoxynius abronius, Bathyporeia sarsi	Identification of the most useful sediment toxicity tests for regulatory purposes and general assessment.	10-d survival, reburial	Whole sediment, inter-laboratory comparisons	Procedure was described	Chapman et al., 1992

[a] Additional chronic endpoints: whole-body metal bioaccumulation, metallothionein induction, DNA strand breakage, and lipid peroxidation.
[b] Basionym: *Corophium insidiosum*.

and soft-bodied oligochaetes (Dick et al., 2005; Navarro-Barranco et al., 2013). Swimming species (e.g., *Gammarus* spp.) and burrowing species (e.g., *Corophium* spp.) have bodies compressed laterally and dorso-ventrally respectively. Their sexual dimorphism and reproductive strategies differ among species (Hyne, 2011). Generally, mature females can be recognized by a brood pouch (marsupium) with setae on the brood plates (oostegites; Fig. 1b). Fertilization and development of eggs take place in marsupium. Eggs hatch directly into a juvenile form and remain in the brood pouch until the next female molt. The development of embryos occurs concurrently with the maturation of a new batch of oocytes in the ovaries in preparation for the next spawning. There is a close link between moulting and oogenic cycles i.e., the onset of molting is delayed until the hatching and release of juveniles. This seems to facilitate the transfer of newly ovulated oocytes through the oviducts into marsupium when the new exoskeleton is still flexible. Mature males can be recognized by the presence of genital papillae at the seventh thoracic segment at the ventral side of a body (Fig. 1c). They are available for mating during most of their molt cycle, while females are sexually receptive for a short period during their moult cycle (Sutcliffe, 1992).

2.1. Biology and ecology of some relevant amphipod species

Corophiidae family species (suborder Senticaudata), like *C. volutator, C. multisetosum, C. orientale*, and *M. insidiosum*, are well studied and commonly used in sediment quality studies in Europe (Table 1). They are endobenthic, tube-dwelling species, inhabiting littoral zones of brackish or saline environment where they often occur in extremely high densities (Beukema and Flach, 1995; Casado-Martinez et al., 2007; Cunha et al., 2000a; Jażdżewski et al., 2005; Meadows, 1964). The corophioid amphipods exhibit three feeding modes i.e., suspension feeding from a current generated by the pleopods, deposit feeding by leaving the burrow

Figure 1 (a) *Corophium volutator* female and male; (b) Adult female — marsupium, clearly visible oostegites with developed setae holding eggs; (c) Adult male, arrows point to genital papillae (photos made by W. Podlesińska during the study of *C. volutator* from the Puck Bay).

and scraping surface detritus and microorganisms into the burrow with the second antennae, and epipsammic browsing, where the microbial biofilm is scraped off individual sediment grains (Gerdol and Hughes, 1994; Lowry and Myers, 2003). Abiotic factors such as temperature, salinity, and sediment texture play an important role in the distribution of the species. *C. volutator* is a euryhaline species usually living in silty areas, while *C. multisetosum* prefers oligohaline and mesohaline waters and seems to prefer sediments with a smaller amount of fines and organic matter content (Beukema and Flach, 1995; Meadows, 1964; Ré et al., 2009). *C. volutator*, similarly to other Corophiidae species, is mostly deposit-feeder whose source of nutrition is particulate matter, organic detritus, bacteria and diatoms (Nielsen and Kofoed, 1982). It is an important prey for demersal fish and invertebrates and it is also predated by shorebirds (Wilson and Parker, 1996). It typically produces two generations per year, while European populations from colder, northern zones normally produce only one generation (Cunha et al., 2000a,b; Peters and Ahlf, 2005; Wilson and Parker, 1996). Adult individuals show distinct sexual dimorphism, males in comparison to females have a considerably larger second pair of antennae (Fig. 1a). Natural populations of *C. volutator* have been shown to be dominated by females throughout most of the year (Dobrzycka and Szaniawska, 1993; Drolet and Barbeau, 2012; Peters and Ahlf, 2005). Guidelines for sediment toxicity testing using these species have been developed, as well as procedures for organism cultivation in laboratory conditions (Costa et al., 2005; Peters and Ahlf, 2005; Ré et al., 2009; Siebeneicher et al., 2013). Presence of polychaetes, like *Nereis diversicolor* or *Arenicola marina*, was observed to be a limiting biotic factor for the *Corophium* spp. occurrence. The worms can influence amphipod density and zonation through predation, sediment disturbance, and tubes damage. Resulting swimming behavior increases the risk of predation (Beukema and Flach, 1995; Cunha et al., 2000a, Podlesińska, unpublished data).

Gammarus locusta (Linnaeus, 1758) belongs to the Gammaridae family (suborder Senticauda). In contrary to *Corophium* spp., it is an epibenthic species. It is an established test species for sediment toxicity assessment in the western Europe marine areas of high salinity (Costa et al., 2005; Neuparth et al., 2002). Similarly to *Corophium* spp., it shows high sensitivity to a variety of contaminants and is easily cultured and handled in laboratory conditions. *G. locusta* is widely distributed along the North-East Atlantic from Norway to the Mediterranean Sea. Its populations are more frequently found in fully marine conditions, but the species inhabits less saline estuarine waters as well (Costa and Costa, 2000). Living in coastal and estuarine areas, it inhabits rocky substrates with seaweeds and sandy or muddy bottoms covered by *Zostera* spp. beds. Despite high affinity to marine salinities, *G. locusta* has a great potential for physiological adaptation. The majority of its life-history traits determined at a salinity of 20 does not differ from those at 33 (Neuparth et al., 2002). It is one of the main prey items for fish, birds, and marine invertebrates, therefore it plays a significant role in the energy flow in the ecosystem. Its life cycle and reproductive activity in natural environments might differ among geographical areas. In the Saldo estuary, the reproduction was reported to be continuous throughout the year (Costa et al., 2005). *G. locusta* was found the least common and least abundant species in a survey of malacostracan crustacea of the Baltic Sea, characterized by a low salinity (Jażdżewski et al., 2005).

M. affinis (Lindström, 1855) of the Pontoporeiidae family (suborder Amphilochidea) is one of the Baltic Sea glacial relicts. It is a deposit-feeder living in sub-thermocline soft bottoms, sandy and muddy sediments, mostly within the upper 5 cm sediment layer. It usually occurs in large densities, thus it is a significant element of the marine trophic web. The species is mobile during the night and during the day remains burrowed in sediment. Adult specimens are tolerant of low oxygen concentration, in contrast to their eggs and embryos. Males reach sexual maturity at the length of 6 mm, females at 9 mm. After mating in the autumn and bearing over the winter, the female gives birth to 20–40 juveniles, which only happens once during their lifespan of 2–4 years. The fecundity and population abundance of *M. affinis* can be influenced by a number of environmental factors including food shortage and limitation of essential fatty acids and amino acids (Sundelin et al., 2008b). In the Swedish National Marine Program, it is used as a sentinel species to monitor fertility, impaired growth, survival of juveniles, and embryo malformations as the key endpoints (Löf et al., 2016).

3. Assessment of sediment quality using bioassays with amphipods as test organisms

3.1. Exposure matrices

Sediment toxicity bioassays can be conducted using various exposure matrix. Most often whole sediment exposures have been applied, although pore (interstitial) waters, elutriates, and extracts exposures have been used as well. In the whole sediment exposures, the test organisms are subjected to all exposure routes without major changes in the physicochemical properties of sediments (Chapman and Wang, 2001). Burton and Johnston indicated that laboratory sediment exposures can produce artifacts leading to some differences in exposures compared to in situ conditions (Burton and Johnston, 2010). These artifacts can include changes in redox, pH, sorption and complexation, microbial activity, and food availability among others. Thus, bioassay guidelines recommend that basic parameters such as water temperature, dissolved oxygen concentration, pH, ammonia, salinity/conductivity, and nitrate levels are to be monitored during the bioassays.

3.2. Acute versus chronic bioassays

There are two types of bioassays: acute, with exposure time less than a full life cycle of the test organism, and chronic, covering at least one full life cycle of the test organism (Chapman, 1989). Acute bioassay usually does not differentiate low or moderately contaminated sediments which in natural environments occur more commonly than highly contaminated (Picone et al., 2016; Van Den Heuvel-Greve et al., 2007). In the chronic bioassays, in addition to survival, measurements of more sensitive sublethal endpoints are carried out. That allows extrapolating toxicological effects

at a population level. A number of studies compared acute and chronic exposures to evaluate their effectiveness in sediment toxicity assessment. For example, Castro et al. in the Ria de Aveiro estuary (Portugal) conducted 10-d and full life-cycle (21-d) exposures of *C. multisetosum* to sediment samples from 144 and 56 sites, respectively (Castro et al., 2006). The authors reported that the 10-d exposures yielded high survival and showed almost no toxic areas. While the chronic exposures also showed relatively good survival for most of the sites, the endpoints related to organismal growth and fecundity clearly depicted the more contaminated estuary areas. McGee et al. presented a study of the Baltimore Harbor/Patapsco River System (MD, USA) which involved 10-d and 28-d exposures of the indigenous amphipod *L. plumulosus* to sediment samples from 11 stations (McGee et al., 2004). The study showed an overall good agreement in the biological responses between the two types of exposures in depicting spatial differences in sediment contamination. Gale et al. (2006) performed a study of an estuarine amphipod, *Melita plumulosa*, exposed to heavy metals spiked sediments for 10 and 42 days. It was reported that survival, gravidity, fertility, and length did not differ between the short and long-term Cd-exposures. In the Cu-exposures, there was a significant growth reduction after 42-d compared to the 10-d exposure. Fertility was the most sensitive endpoint that distinguished the 10-d and 42-d exposures to Cu- and Zn-spiked sediments. Kennedy et al. (2009) examined the acute and chronic toxicity of the New York/New Jersey harbor sediments collected from nine sites of varying contamination levels to four invertebrate species with an overall objective to compare the performance of the two tests. The endpoint responses varied among the tests, from low to moderate and high. The 25-d exposure of *L. plumulosus* was the only chronic exposure that differentiated the sediments, and its endpoint magnitudes seemed to be related to sediment chemistry. A study by Allen et al. (2007), designed to develop a long-term sublethal sediment bioassay with *C. volutator*, tested 10-d and 28-d exposures to Ivermectin-spiked sediments. The study showed no significant difference in the LC_{50} values between the exposure periods, indicating that longer exposure period did not increase the amphipod sensitivity.

Generally, chronic bioassays require greater effort and time involvement than acute bioassays. Yet, they represent a useful tool for risk assessment in more environmentally realistic exposure scenarios, whereas acute bioassays are useful for identifying highly contaminated sediments, or assess an immediate effect of exposure to specific substances or conditions. It can be assumed that the sublethal endpoints, like growth and fertility, can illustrate sediment toxicity more plainly, however, the response can be contaminant and species-specific.

3.3. Toxicity endpoints

In the 10-d acute toxicity bioassays, survival is usually the sole endpoint measured. However a post-exposure burrowing ability in a uncontaminated sediment can be used as a more sensitive sublethal endpoint, as was shown in an extensive study of sediment toxicity from the Sydney Harbour and its vicinity (Australia) with an indigenous amphipod, *Corophium colo* (McCready et al., 2005). Similar findings were obtained by Siebeneicher et al. (2013), who tested the burrowing of *C. volutator* and proved that the burrowing activity depends also, as one would expect, on size and gender. Bat et al. (1998) investigating the accumulation of heavy metals, mortality, and burrowing behavior of *C. volutator*, reported that the metals affected the burrowing behavior in a dose-dependent manner. Hellou et al. (2008) in a study of Halifax harbor sediments (Canada) was able to relate the *C. volutator* sediment avoidance response to PAH bioaccumulation level. Behavioral responses most often pertain to avoidance and/or reburial ability, yet, behavioural endpoints can include a variety of activities (Hellou, 2011). De Backer et al. (2010) reported nine different behavioral activities of the *C. volutator* which can be applied to other tube-building amphipod species. These were: surface inactivity, surface crawling, swimming, scraping, flushing (removing the excess of grain and feces with the pleopods movement that create the water current in the tube), subsurface inactivity, ventilating and filter feeding, subsurface walking, and bulldozing (pushing the sediment grains out of the burrow with pleon). A short-term, novel sediment toxicity endpoint, has been recently proposed by Martinez-Haro et al. (2016) where post-exposure feeding inhibition was used as an endpoint in a study with amphipod *E. marinus*. In 30-min bioassay that measured *E. marinus* post-exposure feeding rates, clean and contaminated sites of the Minho and Lima River estuaries (Portuguese coast) could be discriminated. In general, behavioral bioassays represent a whole organism response and are valued for simplicity, as well as also their time- and cost-efficiency.

Sublethal endpoints bear importance for prediction of long-term effects and are ecologically more relevant (Costa et al., 2005). These endpoints most often include growth measurement (mg/individual/d; or length and dry weight) and fecundity (number of neonates per female), sometimes gravidity (presence of eggs in brood pouch) and other reproductive traits (Allen et al., 2007; Gale et al., 2006; Kennedy et al., 2009; McGee et al., 2004; Van Den Heuvel-Greve et al., 2007; Ward et al., 2015). In a study of a chronic toxicity of the Saldo and Tagus estuary sediments (Portuguese coast) to the amphipod *G. locusta*, Costa et al. (2005) examined the reproductive outcome in more details. The authors considered not only fecundity as an endpoint, but also sex ratio (the exposure began with 2—4 mm juveniles), the size (diameter and volume) and developmental stages of embryos. Furthermore, the same study included a number of biochemical endpoints, i.e. metal bioaccumulation, metallothionein induction, DNA strand breakage and lipid peroxidation (Neuparth et al., 2005).

Amphipod embryo malformation rate has been shown to be a sensitive endpoint in the field studies (Löf et al., 2016; Sundelin and Eriksson, 1998). In a study of *M. affinis* females in the Bothnian Bay and the Bothnian Sea with known pollution levels, apart from fecundity, Löf et al. (2016) investigated developmental stage of embryos and their aberrations which included malformed, membrane-damaged, and undifferentiated embryos with development arrested before gastrulation, as well as dead and partially dead broods. Based on the percentage of females with each type of embryo aberration, the authors found out that different types of aberrations were related to elevated

concentrations of specific contaminants in sediments. There was a strong correlation between the embryo malformation rate and distance from the source of pollution. The frequency of amphipod embryo malformations has been used in field studies which dealt with sediment quality assessment in the Baltic Sea. Berezina et al. (2017) investigated this endpoint in the amphipod *Gmelinoides fasciatus* in the Neva River estuary (the eastern Gulf of Finland, the Baltic Sea), whereas Strode et al. (2017) used *M. affinis* in the Gulf of Riga (the Baltic Sea). As all amphipod species show similar embryo development (despite differences in sexual behavior and embryogenesis), the method for embryo staging and malformations can be extended to other species (Sundelin et al., 2008a). Further studies regarding associations between groups of contaminants and specific malformations are encouraged (HELCOM, 2017).

3.4. Confounding factors

In sediment toxicity bioassays there are several confounding factors which can influence the measured endpoints. These factors are related to the water physicochemical characteristics, sediment geochemistry, and to the biology of test organisms. Temperature, salinity, and oxygen saturation are the basic factors modulating organismal responses. Some studies point out also to toxicants which can be present in sediments, but not always considered in the bioassays, i.e., ammonia (originating from anthropogenic discharges and natural decomposition process) and sulfides, which are common in estuarine sediments (as reviewed by Chapman and Wang, 2001; Neuparth et al., 2002; Postma et al., 2002; Van Den Heuvel-Greve et al., 2007).

Temperature is one of the key factors influencing metabolic and physiological processes including growth, reproduction, duration of the amphipod life cycle, and sensitivity to contaminants (Cunha et al., 2000b; Prato et al., 2008; Ré et al., 2009). An experimental study by Kater et al. (2008) with *Corophium* spp. showed negligible growth rate at a low temperature of 5°C, noticeable at 10°C, and an optimum at 15°C which did not differ from that at 25°C. A study involving *G. locusta* reported that at 20°C compared to 15°C (reference condition) there was an acceleration and condensation of the species life cycle i.e., faster individual and population growth, reduction in the lifespan, and shorter generation time (Neuparth et al., 2002). Peters and Ahlf (2005) who studied reproduction of *C. volutator* in laboratory conditions at 15, 19 and 23°C pointed out that the reproductive outcome (number of offspring per female) was significantly better at 15°C than 23°C. Prato et al. (2008) reported reduced mortality and sensitivity of *Corophium insidiosum* to contaminants at 10°C and 15°C compared to 20°C and 25°C, possibly due to decreased oxygen consumption and energy expenditure at lower temperatures. They suggested 15–20°C as the optimal temperature for bioassays with *M. insidiosum*.

Sediment grain size and organic matter content are two variables that, depending on their nature, can not only modify the availability of sediment-bound contaminants but have an influence on the test organism as well. For example, Costa et al. (2005) reported that *G. lacusta* had better growth rates and reproductive traits when chronically exposed to muddy sediments (9–11% of total volatile solids, TVS) than to sandy ones (0.4% TVS). This positive effect was attributed to a richer and more efficient diet provided by the muddy sediments (Costa et al., 2005). Picone et al. (2008), in an extensive evaluation of *C. orientale* as a bioindicator for the Venice Lagoon, reported that sediment grain size and organic carbon content (0.4–15%) were not influential factors for the 10-d mortality endpoint. As indicated by Burton, (1992), the responses of organisms to test sediments (bioassay endpoints) can be affected by their life stage and health condition, the acclimation to test conditions and exposure duration, the route of contaminant uptake, and the mode of toxicant action. Organisms that burrow freely in sediment compared to tube-building and epibenthic species are more directly exposed to contaminants present in interstitial water and have greater direct contact with contaminated particles, which results in their greater sensitivity. This has been shown in a laboratory study with two amphipods, *E. estuaries* (free-burrowing detritivore) and *A. abdita* (tube-dwelling feeder) exposed to contaminant-spiked sediments (Anderson et al., 2008) as well as in a field studies of sediment toxicity in the San Francisco Estuary (Anderson et al., 2007).

Biological factors that can influence bioassay endpoints were the subjects of several studies, which involved an exposure of amphipods to cadmium, zinc, and ammonia. McGee et al. (1998) in a study of the acute toxicity of aqueous cadmium to the estuarine amphipod *Leptocheirus plumulosus* reported that size, reproductive status, and molting cycle were significant factors influencing the sensitivity of individuals, which lead them to conclude that field-collected animals might exhibit seasonal variation in sensitivity. This aspect was further examined by Kater et al. (2000) in a study of *C. volutator* exposed to cadmium in the context of their origin (newly field-collected versus long-term laboratory-held organisms), exposure media (natural versus artificial seawater), body length, and percentage of gravid females. Their study showed significant seasonal variation in sensitivity (lower in the winter than the summer period; expressed as an LC_{50} value) irrespective of changes in the tested variables. Although the reproductive cycle did not seem to be important, it had been indicated that the sensitivity can be influenced by the molting cycle. In a study which examined the influence of life stage, gender, and a priori nutritional state on the uptake of zinc and cadmium in *E. marinus*, it has been shown that life stage and nutritional state were significant factors for bioaccumulation of both metals, whereas only cadmium bioaccumulation was gender-specific (Pastorinho et al., 2009). Another study regarding the effect of seasonality and body size on the sensitivity of *Corophium urdaibaiense* and *C. multisetosum* found that the sensitivity (greater during summer than winter) could be related to reproduction as the percentage of gravid females was significantly inversely related to the LC_{50} values (Pérez-Landa et al., 2008).

3.5. The sensitivity of amphipods to reference toxicants

Sediment toxicity bioassays are often accompanied by short-term reference toxicity tests for quality assurance purposes.

These are water-phase tests performed with a reference toxicant in order to obtain an information on the health condition of the test organisms and detect changes in species sensitivity that can influence the bioassay results (Kater et al., 2000). The outcome measured in these tests is mortality upon which an LC_{50} value (a concentration that causes 50% mortality of the test organisms) is being calculated. Commonly used and recommended reference toxicant for this purpose is cadmium (Kater et al., 2000; Picone et al., 2008; USEPA, 2001a,b).

The sensitivity of amphipods to cadmium and ammonia (which can be toxic if present during bioassays), expressed as LC_{50} values, is shown in Table 2. Some aspects of the sensitivity were also raised in the 3.4 section in the context of biological factors influencing bioassay results. As indicated by the LC_{50} values, cadmium is generally more toxic than ammonia (Kater et al., 2000, 2006; Pérez-Landa et al., 2008). In a given species the sensitivity has been shown to depend on its biological characteristics, among which the organism size seems to be most important. Smaller specimens are more sensitive than larger, as reported by McGee et al. (1998) for *L. plumulosus* exposed to cadmium and by Pérez-Landa et al. (2008) for *C. urdaibaiense* exposed to ammonia (data not presented). The season is another factor that influences the species sensitivity. Lower LC_{50} values for cadmium and ammonia obtained in warmer months indicate greater sensitivity in the summer period (Kater et al., 2000; Pérez-Landa et al., 2008). Furthermore, some variation in sensitivity can occur between laboratory-maintained and freshly field-collected specimens (Kater et al., 2000; Menchaca et al., 2010; Ré et al., 2009), and between different field populations (Onorati et al., 1999). Inter-species differences in sensitivity to cadmium were examined by Prato et al. (2010) in a study evaluating the suitability and applicability of *C. insidiosum* and *C. orientale* for sediment toxicity testing in southern Italy. This study showed that *C. insidiosum* was significantly more sensitive to cadmium than *C. orientale*.

3.6. Guidelines and standard methods

Guidelines and standard methods are based on best practices and support a unified approach to the sediment quality assessment (Table 1). Commonly used guidelines and recommendations are published by the International Organization for Standardization (ISO), the American Society for Testing and Materials (ASTM), the United States Environmental

Table 2 Sensitivity of amphipods to reference toxicants in water-only exposures.

Species	Toxicant	Organisms description, time	LC_{50} range or value (mg L^{-1})	Test duration, temperature (°C)	References
Corophium volutator	Cadmium	f.c., l.c	1.3–10[a]		Kater et al., 2000
Corophium volutator	Ammonia	f.c.	12–86[b]		Kater et al., 2006
Corophium insidiosum	Cadmium	f.c., 2–4 mm	1.30 ± 0.11	96-h, 16	Prato et al., 2010
Corophium orientale	Cadmium	f.c., 2–4 mm	3.03 ± 0.7	96-h, 16	
Corophium multisetosum	Cadmium	f.c., Aug	2.40	72-h, 15	Menchaca et al., 2010
	Cadmium	l.c., Aug	5.82	72-h, 15	
Corophium multisetosum	Cadmium	l.c.	0.71	96-h, 15	Ré et al., 2009
	Cadmium	l.c.	0.47, 0.58	96-h, 15	
	Cadmium	l.c.	0.23, 0.25	96-h, 18	
	Cadmium	l.c.	0.27, 0.33	96-h, 22	
	Cadmium	l.c	0.34	96-h, 22	
	Cadmium	f.c.	0.31	96-h, 22	
Corophium multisetosum	Ammonia	f.c., 4–7 mm, Sep	26	72-h, 15	Pérez-Landa et al., 2008
	Ammonia	f.c., 4–7 mm, Jan	115	72-h, 15	
	Cadmium	f.c., 4–7 mm, Sep	0.63	72-h, 15	
	Cadmium	f.c., 4–7 mm, Jan	31	72-h, 15	
Corophium urdaibaiense	Ammonia	f.c., 4–7 mm, May	27	72-h, 15	Pérez-Landa et al., 2008
	Ammonia	f.c., 4–7 mm, Aug	61	72-h, 15	
	Ammonia	f.c., 4–7 mm, Dec	110	72-h, 15	
	Cadmium	f.c., 4–7 mm, Feb	2.28	72-h, 15	
	Cadmium	f.c., 4–7 mm, Sep	0.88	72-h, 15	
Corophium orientale	Cadmium	f.c. A[c], 2–5 mm,	4.28 ± 1.35	96-h, 15	Onorati et al., 1999
	Cadmium	f.c. B[c], 2–5 mm,	2.91 ± 0.82	96-h, 15	
Leptocheirus plumulosus	Cadmium	l.c., 500 μm[d]	0.35	96-h, 25	McGee et al., 1998
	Cadmium	l.c., 710 μm[d]	0.65	96-h, 25	
	Cadmium	l.c., 1000 μm[d]	0.88	96-h, 25	

Ammonia refers to total ammonia; f.c. – field collected; l.c. – laboratory cultured.
[a] LC_{50} varied depending on month.
[b] LC_{50} varied depending on pH.
[c] Two field populations.
[d] Size sorted on nested 500-, 710-, and 1000 μm mesh sieves.

Table 3 Multi-species set of bioassays (including Amphipods) used with other lines of evidence for assessment of estuarine and marine sediments (selected studies).

Investigated lines of evidence	Matrix
The Gulf of Riga, eastern Baltic Sea (Strode et al., 2017):	
Amphipod response: 10-d survival bioassay with *Corophium volutator*, *Monoporeia affinis*, *Pontogammarus robustoides*, *Bathyporeia sarsi*[a] and *Hyalella azteca*	Whole sediment
Metal contaminants	Whole sediment
Benthic macroinvertebrate community	Whole sediment
Southern Baltic Sea (Dabrowska et al., 2017):	
Amphipod response: 10-d survival bioassay with *Monoporeia affinis*, *Bathyporeia sarsi*[a] and *Pontogammarus robustoides*	Whole sediment
Organic and metal contaminants	Whole sediment
Biomarkers and contaminants	Mussels
Biomarkers and contaminants	Fish
The Venice Lagoon (Picone et al., 2016):	
Amphipod response: 10-d survival bioassay with *Corophium volutator*	Whole sediment
Sea urchin response: sperm cell and embryo toxicity in *Paracentrotus lividus*	Elutriates
Bivalve response: embryo toxicity in *Crassostrea gigas*	Elutriates
Organic and metal contaminants	Whole sediment
Spanish sea ports (Khosrovyan et al., 2015):	
Amphipod response: 10-d survival bioassay with *Corophium volutator* and *Ampelisca brevicornis*	Whole sediment
Polychaete response: 10-d survival bioassay with *Arenicola marina*	Whole sediment
Bacteria response: contaminant accumulation and inhibition of luminescence in *Vibrio fisheri*	Elutriates
Sea urchin response: egg fertilization and embryogenesis in *Paracentrotus lividus*	Elutriates
Organic and metal contaminants	Whole sediment
Grand Harbour, the Sicily Channel (Romeo et al., 2015):	
Amphipod response: 10-d survival bioassay with *Corophium orientale*	Whole sediment
Sea urchin response: embryo toxicity in *Paracentrotus lividus*	Elutriates
Bacteria response: inhibition of luminescence in *Vibrio fisheri*	Elutriates
Organic and metal contaminants	Whole sediment
Benthic macroinvertebrate community	Whole sediment
Santos-São Vicente Estuarine System, Brazil (Buruaem et al., 2013):	
Amphipod response: 10-d survival bioassay with *Tiburonella viscana*	Whole sediment
Sea urchin response: embryo malformations in *Lytechinus variegatus*	Pore-water
Sea urchin response: embryo-larval development in *Lytechinus variegatus*	Elutriates
Organic and metal contaminants	Whole sediment
Benthic macroinvertebrate community	Whole sediment
North eastern Baltic Sea (Berezina et al., 2013):	
Amphipod response: 10-d survival bioassay with *Monoporeia affinis*, *Gmelinoides fasciatus*, *Hyalella azteca*	Whole sediment
Benthic macroinvertebrate community	Whole sediment
The Wadden Sea, The Netherlands (Van Den Brink and Kater, 2006):	
Amphipod response: 10-d survival bioassay with *Corophium volutator*	Whole sediment
Bivalve response: larval survival and deformations in *Crassostrea gigas*	Elutriates
Sea urchin response: survival, and re-burrowing in *Echinocardium cordatum*	Whole sediment
Bacteria response: inhibition of luminescence in *Vibrio fisheri*	Sediment suspensions
Organic and metal contaminants	Whole sediment
Dutch harbors (Stronkhorst, 2003):	
Amphipod response: 10-d survival bioassay with *Corophium volutator*	Whole sediment
Sea urchin response: 14-d survival and re-burrowing in *Echinocardium cordatum*	Whole sediment
Bacteria response: inhibition of luminescence in *Vibrio fisheri*	Sediment suspensions

[a] Originally described as *Bathyporeia pilosa* – now synonym of *Bathyporeia sarsi*.

Protection Agency (USEPA), the Environment Canada, the Convention for the Protection of the Marine Environment of the North-East Atlantic (OSPAR Convention), the International Council for the Exploration of the Sea (ICES), the National Oceanic and Atmospheric Administration (NOAA), the Society of Environmental Toxicology and Chemistry (SETAC) and the Helsinki Commission (HELCOM). The guidelines describe the optimal conditions to perform the bioassays for particular taxonomic groups or species. Amphipods to be used in bioassays can be either field-collected from uncontaminated sites or lab-cultured. Their availability from the field varies depending on the geographical region, ecosystem dynamics, and seasonal variability in population density and distribution (Hyne et al., 2005). Field-collected organisms, upon transferring to a laboratory, require an acclimation period to allow them to adapt to experimental conditions (temperature, food, salinity, light regime). A possibility to culture amphipods for use in bioassays is an advantage as the culture can provide organisms of similar age that came from similar conditions all year long (Peters and Ahlf, 2005). Yet, it requires a considerable knowledge of their ecology, biology, feeding, and reproduction. Laboratory cultures have been described and successfully performed with *C. volutator* (Kater et al., 2008; Peters and Ahlf, 2005; Siebeneicher et al., 2013; Van Den Heuvel-Greve et al., 2007), *C. multisetosum* (Castro et al., 2006; Menchaca et al., 2010; Ré et al., 2009), *M. insidiosum* (Nair and Anger, 1979), *L. plumulosus* (Manyin and Rowe, 2006) and *M. plumulosa* (Hyne et al., 2005; Mann et al., 2010; Table 1).

3.7. Bioassays in an integrated sediment assessment

Bioassays with amphipods are currently one of many lines of evidence (LOE) in the assessment of marine and estuarine sediments quality. Multi-species test batteries that include organisms from different trophic levels in addition to resident benthic communities are recommended and used in a number of studies (Table 3). For example, Khosrovyan et al. (2015) assessed the quality of sediments in Spanish harbors based on several different LOEs. These included a battery of toxicity bioassays (10-d survival of *C. volutator* and *Ampelisca brevicornis;* 10-d survival and contaminant accumulation in *A. marina*; the *Vibrio fisheri* inhibition of luminescence bioassay; and the *Paracentrotus lividus* bioassay with reproductive effects as endpoints) which were integrated with sediment organic and metal contaminants in a weight of evidence approach. According to Chapman (2007, 1990), a comprehensive sediment quality studies should involve chemical, toxicological, and resident benthic community structure, where sediment toxicity and benthic community data represent key criteria for addressing an association between stressors (contaminants) and effects. Examples of comprehensive studies are those performed by Buruaem et al. (2013) in the Santos-São Vicente Estuarine System in Brazil, by Strode et al. (2017) regarding the Gulf of Riga in the eastern Baltic Sea, and by Romeo et al. (2015) in respect to the Malta's Grand Harbour in the Sicily Channel. It has to be noted, however, that analysis of resident benthic communities require a substantial load of work and budget and are rarely included in the sediment assessment studies.

4. Conclusions

Bioassays with amphipods represent useful tools for the assessment of marine and estuarine environments. This review shows that over several decades more than 20 amphipod species have been used as test organisms. The Corophiidae amphipods have been most extensively employed for sediment toxicity testing and other purposes in Europe, North America and elsewhere, although the species used differ among geographical regions due to their natural occurrence and distribution. In Europe, most often used are *C. volutator* and *C. multisetosum*, although *C. orientale, M. insidiousm*, and other amphipod species have been considered in some European areas where the former two species do not occur. Bioassays employed for other purposes than environmental quality studies include assessment of dredged material quality and bioavailability of contaminants accumulated in the sediments, evaluation of the response of benthic organisms to specific contaminants, comparison of the sensitivity of different species to contaminants, and application for regulatory purposes.

Taking into consideration the exposure period, there are two types of bioassays, short-term (acute) and chronic (covering at least one full lifecycle), which are put into practice depending on the bioassay objectives. In the chronic bioassays, in addition to survival, more sensitive sublethal endpoints are examined like organismal growth, biochemical responses (e.g., bioaccumulation, physiological changes), and reproductive traits (e.g., fertility or fecundity). These measurements can reveal subtle biological responses allowing for more in-depth assessment of contaminant-elicited effects. Thus, although chronic bioassays require greater effort than acute bioassays, the exposure duration and biological responses reflect more realistically the environmental scenario. Worthy of note are behavioral endpoints such as post-exposure burial ability or feeding rate of sediment-dwelling amphipods, which can enhance the sensitivity of bioassays to discern negative effects.

Both abiotic and biological factors play an important role in the bioassays as they can influence the organisms' sensitivity (thus, the bioassay outcome) and hamper the interpretation of the results. These factors include the age/size of the species, molting stage, collection season, origin of the organisms, water temperature, salinity, pH, and photoperiod. They have to be taken into consideration when designing a bioassay.

Acknowledgments

The manuscript was prepared within the frames of two projects “Characteristics of the southern Baltic Sea sediments in respect to anthropogenic contaminants and their influence on benthic invertebrates” and “Application of *Corophium* spp. (Amphipoda) for sediment evaluation in the Gulf of Gdańsk and the Martwa nad Śmiała Rivers” financed by the Polish Ministry of Science and Higher Education.

References

Allen, Y.T., Thain, J.E., Haworth, S., Barry, J., 2007. Development and application of long-term sublethal whole sediment tests with *Arenicola marina* and *Corophium volutator* using Ivermectin as the test compound. Environ. Pollut. 146, 92—99, http://dx.doi.org/10.1016/j.envpol.2006.06.007.

Anderson, B., Hunt, J., Phillips, B., Thompson, B., Lowe, S., Taberski, K., Scott Carr, R., 2007. Patterns and trends in sediment toxicity in the San Francisco Estuary. Environ. Res. 105, 145—155, http://dx.doi.org/10.1016/j.envres.2006.07.005.

Anderson, B.S., Lowe, S., Phillips, B.M., Hunt, J.W., Vorhees, J., Clark, S., Tjeerdema, R.S., 2008. Relative sensitivities of toxicity test protocols with the amphipods *Eohaustorius estuarius* and *Ampelisca abdita*. Ecotoxicol. Environ. Saf. 69, 24—31, http://dx.doi.org/10.1016/j.ecoenv.2007.05.005.

ASTM, 1990. Standard guide for conducting 10-day static sediment toxicity test with marine and estuarine amphipods. E 1367-90. In: Annual Book of ASTM Standards, Water and Environmental Technology. Philadelphia, PA, 1—24.

ASTM, 1991. Standard guide for conducting 10-day static sediment toxicity tests with marine and estuarine amphipods. In: Annual Book of ASTM Standards. Philadelphia, PA, 4584—4610.

ASTM, 1992. Standard guide for conducting 10-days static sediment toxicity tests with marine and estuarine amphipods. E1367-92. In: Annual Book of ASTM Standards, vol. 11.04. Philadelphia, PA.

ASTM, 1993a. Standard guide for conducting sediment toxicity tests with freshwater invertebrates. E1383-93. In: Annual Book of ASTM Standards, Water and Environmental Technology, vol. 11.04. Philadelphia, PA.

ASTM, 1993b. Standard guide for conducting 10-d static sediment toxicity tests with marine and estuarine amphipods. E1367-92. In: Annual Book of ASTM Standards, Water and Environmental Technology, vol. 11.04. Philadelphia, PA.

ASTM, 1993c. Proposed new standard guide for conducting solid phase 10-day static sediment test with marine and estuarine amphipods. E 1367-92. Philadelphia, PA.

ASTM, 1997. Standard guide for conducting 10-day static sediment toxicity tests with marine and estuarine amphipods. E1367-92. In: Annual Book of ASTM Standards, Water and Environmental Technology. Philadelphia, PA, 731—756.

ASTM, 1998. Standard guide for conducting 10-day static sediment toxicity tests with marine and estuarine amphipods. E1367-92. In: Annual Book of ASTM Standards, Water and Environmental Technology, vol. 11.05. Philadelphia, PA, 732—757.

ASTM, 1999. Standard guide for conducting 10-day static sediment toxicity tests with marine and estuarine amphipods. In: Annual Book of ASTM Standards, Water and Environmental Technology, vol. 11.05. Philadelphia, PA, 733—758.

ASTM, 2000. Standard guide for conducting 10-day static sediment toxicity tests with marine and estuarine amphipods. E1367-99. In: Annual Book of ASTM Standards, Water and Environmental Technology. Philadelphia, PA.

ASTM, 2003a. Standard guide for conducting 10-day static sediment toxicity tests with marine and estuarine amphipods. E1367-99. In: Annual Book of ASTM Standards, Water and Environmental Technology, vol. 11.05, Philadelphia, PA, 674—700.

ASTM, 2003b. Standard guide for designing biological tests with sediments. E1525-02. In: Annual Book of ASTM Standards, Water and Environmental Technology, Vol. 11.05. Philadelphia, PA, 844—868.

ASTM, 2008. Standard test method for measuring the toxicity of sediment-associated contaminants with estuarine and marine invertebrates. E 1367-03. ASTM International, West Conshohocken, PA.

Bat, L., Raffaelli, D., 1998. Sediment toxicity testing: a bioassay approach using the amphipod *Corophium volutator* and the polychaete *Arenicola marina*. J. Exp. Mar. Bio. Ecol. 226, 217—239, http://dx.doi.org/10.1016/S0022-0981(97)00249-9.

Bat, L., Raffaelli, D., Marr, I.L., 1998. The accumulation of copper, zinc and cadmium by the amphipod *Corophium volutator* (Pallas). J. Exp. Mar. Bio. Ecol. 223, 167—184, http://dx.doi.org/10.1016/S0022-0981(97)00162-7.

Bay, S.M., Jirik, A., Stanford, A., 2003. Interlaboratory variability of amphipod sediment toxicity tests in a cooperative regional monitoring program. Environ. Monit. Assess. 81, 257—268.

Berezina, N.A., Strode, E., Lehtonen, K.K., Balode, M., Golubkov, S. M., 2013. Sediment quality assessment using *Gmelinoides fasciatus* and *Monoporeia affinis* (Amphipoda, Gammaridea) in the northeastern Baltic sea. Crustaceana 86, 780—801, http://dx.doi.org/10.1163/15685403-00003215.

Berezina, N.A., Gubelit, Y.I., Polyak, Y.M., Sharov, A.N., Kudryavtseva, V.A., Lubimtsev, V.A., Petukhov, V.A., Shigaeva, T.D., 2017. An integrated approach to the assessment of the eastern Gulf of Finland health: A case study of coastal habitats. J. Mar. Syst. 171, 159—171, http://dx.doi.org/10.1016/j.jmarsys.2016.08.013.

Beukema, J.J., Flach, E.C., 1995. Factors controlling the upper and lower limits of the intertidal distribution of two Corophium species in the Wadden Sea. Mar. Ecol. Prog. Ser. 125, 117—126, http://dx.doi.org/10.3354/meps125117.

Burton, G.A., 1992. Sediment Toxicity Assessment. Lewis Publishers, Chelsea, MI, 479 pp.

Burton, G.A., Johnston, E.L., 2010. Assessing contaminated sediments in the context of multiple stressors. Environ. Toxicol. Chem. 29, 2625—2643, http://dx.doi.org/10.1002/etc.332.

Buruaem, L.M., de Castro, Í.B., Hortellani, M.A., Taniguchi, S., Fillmann, G., Sasaki, S.T., Varella Petti, Mô. A., Sarkis, J.E.d.S., Bícego, M.C., Maranho, L.A., Davanso, M.B., Nonato, E.F., Cesar, A., Costa-Lotufo, L.V., Abessa, D.M.D.S., 2013. Integrated quality assessment of sediments from harbour areas in Santos-São Vicente Estuarine System, Southern Brazil. Estuar. Coast. Shelf Sci. 130, 179—189, http://dx.doi.org/10.1016/j.ecss.2013.06.006.

Casado-Martinez, M.C., Forja, J.M., DelValls, T.A., 2007. Direct comparison of amphipod sensitivities to dredged sediments from Spanish ports. Chemosphere 68, 677—685, http://dx.doi.org/10.1016/j.chemosphere.2007.01.077.

Castro, H., Ramalheira, F., Quintino, V., Rodrigues, A.M., 2006. Amphipod acute and chronic sediment toxicity assessment in estuarine environmental monitoring: an example from Ria de Aveiro, NW Portugal. Mar. Pollut. Bull. 53, 91—99, http://dx.doi.org/10.1016/j.marpolbul.2005.09.029.

Cesar, A., Marin, A., Marin-Guirao, L., Vita, R., 2004. Amphipod and sea urchin tests to assess the toxicity of Mediterranean sediments: the case of Portman Bay. Sci. Mar. 68, 205—213, http://dx.doi.org/10.3989/scimar.2004.68s1205.

Cesnaitis, R., Sobanska, M.A., Versonnen, B., Sobanski, T., Bonnomet, V., Tarazona, J.V., De Coen, W., 2014. Analysis of the ecotoxicity data submitted within the framework of the REACH Regulation. Part 3. Experimental sediment toxicity assays. Sci. Total Environ. 475, 116—122, http://dx.doi.org/10.1016/j.scitotenv.2013.10.059.

Chapman, P.M., 1989. Current approaches to developing sediment quality criteria. Environ. Toxicol. Chem. 8, 589—599, http://dx.doi.org/10.1002/etc.5620080706.

Chapman, P.M., 1990. The sediment quality triad approach to determining pollution-induced degradation. Sci. Total Environ. 97—98, 815—825, http://dx.doi.org/10.1016/0048-9697(90)90277-2.

Chapman, P.M., 2007. Do not disregard the benthos in sediment quality assessments! Mar. Pollut. Bull. 54, 633—635, http://dx.doi.org/10.1016/j.marpolbul.2007.03.006.

Chapman, P.M., Wang, F., 2001. Assessing sediment contamination in estuaries. Environ. Toxicol. Chem. 20, 3—22, http://dx.doi.org/10.1002/etc.5620200102.

Chapman, P., Swartz, R., Roddie, B., Phelps, H., van den Hurk, P., Butler, R., 1992. An international comparison of sediment toxicity tests in the North Sea. Mar. Ecol. Prog. Ser. 91, 253—264, http://dx.doi.org/10.3354/meps091253.

Chapman, P.M., Wang, F., Caeiro, S.S., 2013. Assessing and managing sediment contamination in transitional waters. Environ. Int. 55, 71—91, http://dx.doi.org/10.1016/j.envint.2013.02.009.

Ciarelli, S., 1994. Guideline for conducting 10-day static sediment toxicity tests using marine or estuarine amphipods. Report from the Tidal Water Division, Middelburg, The Netherlands. Report RIKZ-94.031.

Conlan, K.E., 1994. Amphipod crustaceans and environmental disturbance: a review. J. Nat. Hist. 28, 519—554, http://dx.doi.org/10.1080/00222939400770241.

Costa, F.O., Costa, M.H., 2000. Review of the ecology of *Gammarus locusta* (L.). Polish Arch. Hydrobiol. 47, 541—559.

Costa, F.O., Neuparth, T., Correia, A.D., Helena Costa, M., 2005. Multi-level assessment of chronic toxicity of estuarine sediments with the amphipod *Gammarus locusta*: II. Organism and population-level endpoints. Mar. Environ. Res. 60, 93—110, http://dx.doi.org/10.1016/j.marenvres.2004.08.005.

Cunha, M.R., Moreira, M.H., Sorbe, J.C., 2000a. The amphipod *Corophium multisetosum* (Corophiidae) in Ria de Aveiro (NW Portugal). II. Abundance, biomass and production. Mar. Biol. 137, 651—660, http://dx.doi.org/10.1007/s002270000385.

Cunha, M.R., Sorbe, J.C., Moreira, M.H., 2000b. The amphipod *Corophium multisetosum* (Corophiidae) in Ria de Aveiro (NW Portugal). I. Life history and aspects of reproductive biology. Mar. Biol. 137, 637—650, http://dx.doi.org/10.1007/s002270000384.

Dabrowska, H., Kopko, O., Lehtonen, K.K., Lang, T., Waszak, I., Balode, M., Strode, E., 2017. An integrated assessment of pollution and biological effects in flounder, mussels and sediment in the southern Baltic Sea coastal area. Environ. Sci. Pollut. Res. 24, 3626—3639, http://dx.doi.org/10.1007/s11356-016-8117-8.

De Backer, A., van Ael, E., Vincx, M., Degraer, S., 2010. Behaviour and time allocation of the mud shrimp, *Corophium volutator*, during the tidal cycle: A laboratory study. Helgol. Mar. Res. 64, 63—67, http://dx.doi.org/10.1007/s10152-009-0167-6.

Dick, J.T.A., Johnson, M.P., McCambridge, S., Johnson, J., Carson, V. E.E., Kelly, D.W., MacNeil, C., 2005. Predatory nature of the littoral amphipod *Echinogammarus marinus:* Gut content analysis and effects of alternative food and substrate heterogeneity. Mar. Ecol. Prog. Ser. 291, 151—158, http://dx.doi.org/10.3354/meps291151.

DIN EN ISO 16712, 2007. Wasserbeschaffenheit—Bestimmung der akuten Toxizität mariner Sedimente oder von Sedimenten aus Flussmündungen gegenüber Amphipoden. In: Deutsche Einheitsverfahren zur Wasser-, Abwasser- uns Schlamm-Untersuchung. Wiley, Berlin, DIN EN ISO 16712:2007(L50).

Dobrzycka, A., Szaniawska, A., 1993. Seasonal changes in energy value and lipid content in a population of *Corophium volutator* (Pallas, 1766) from the Gulf of Gdańsk. Oceanologia 35, 61—71.

Drolet, D., Barbeau, M.A., 2012. Population structure of resident, immigrant, and swimming *Corophium volutator* (Amphipoda) on an intertidal mudflat in the Bay of Fundy, Canada. J. Sea Res. 70, 1—13, http://dx.doi.org/10.1016/j.seares.2012.02.001.

Environment Canada, 1992. Biological test method: acute test for sediment toxicity using marine or estuarine amphipods. Report EPS 1/RM/26, Environmental Prot. Ser.

Fay, A.A., Brownawell, B.J., Elskus, A.A., McElroy, A.E., 2000. Critical body residues in the marine Amphipod *Ampelisca abdita*: sediment exposures with nonionic organic contaminants. Environ. Toxicol. Chem. 19, 1028, http://dx.doi.org/10.1002/etc.5620190432.

Gale, S.A., King, C.K., Hyne, R.V., 2006. Chronic sublethal sediment toxicity testing using the estuarine amphipod, *Melita plumulosa* (Zeidler): evaluation using metal-spiked and field-contaminated sediments. Environ. Toxicol. Chem. 25, 1887—1898, http://dx.doi.org/10.1897/05-468R.1.

Gerdol, V., Hughes, R.G., 1994. Feeding behaviour and diet of *Corophium volutator* in an estuary in southeastern England. Mar. Ecol. Prog. Ser. 114, 103—108, http://dx.doi.org/10.3354/meps114103.

HELCOM, 2017. Reproductive disorders: malformed embryos of amphipods. HELCOM supplementary indicator report. Online, HELCOM indicators.

Hellou, J., 2011. Behavioural ecotoxicology, an "early warning" signal to assess environmental quality. Environ. Sci. Pollut. Res. 18, 1—11, http://dx.doi.org/10.1007/s11356-010-0367-2.

Hellou, J., Cheeseman, K., Desnoyers, E., Johnston, D., Jouvenelle, M.L., Leonard, J., Robertson, S., Walker, P., 2008. A non-lethal chemically based approach to investigate the quality of harbour sediments. Sci. Total Environ. 389, 178—187, http://dx.doi.org/10.1016/j.scitotenv.2007.08.010.

Hyne, R.V., 2011. Review of the reproductive biology of amphipods and their endocrine regulation: Identification of mechanistic pathways for reproductive toxicants. Environ. Toxicol. Chem. 30, 2647—2657, http://dx.doi.org/10.1002/etc.673.

Hyne, R.V., Gale, S.A., King, C.K., 2005. Laboratory culture and life-cycle experiments with the benthic amphipod *Melita plumulosa* (Zeidler). Environ. Toxicol. Chem. 24, 2065—2073, http://dx.doi.org/10.1897/04-409R1.1.

ISO, 2001. Water quality determination of acute toxicity of marine or estuarine sediments to Amphipods. In: ISO/CD 16712. Committee Draft No. 98. TC 147/SC5/Wg2. 16 pp.

ISO, 2004. Water quality — determination of acute toxicity of marine or estuarine sediment to amphipods. International Standard, Geneva, Switzerland, FDIS 16712.

ISO, 2005. Water quality—determination of acute toxicity of marine or estuarine sediment to amphipods. Int. Organ. Stand. ISO 16712.

Jażdżewski, K., Konopacka, A., Grabowski, M., 2005. Native and alien malacostracan crustacea along the Polish Baltic Sea coast in the twentieth century. Oceanol. Hydrobiol. Stud. XXXIV 175—193, http://dx.doi.org/10.2478/s13545-011-0041-4.

Kater, B.J., Hannewijk, A., Postma, J.F., Dubbeldam, M., 2000. Seasonal changes in acute toxicity of cadmium To amphipod *Corophium volutator*. Environ. Toxicol. Chem. 19, 3032—3035.

Kater, B.J., Dubbeldam, M., Postma, J.F., 2006. Ammonium toxicity at high pH in a marine bioassay using *Corophium volutator*. Arch. Environ. Contam. Toxicol. 51, 347—351, http://dx.doi.org/10.1007/s00244-005-0163-z.

Kater, B.J., Jol, J.G., Smit, Mathijs, G.D., 2008. Growth of *Corophium volutator* under laboratory conditions. Arch. Environ. Contam. Toxicol. 54, 440—446, http://dx.doi.org/10.1007/s00244-007-9057-6.

Kennedy, A.J., Steevens, J.A., Lotufo, G.R., Farrar, J.D., Reiss, M.R., Kropp, R.K., Doi, J., Bridges, T.S., 2009. A comparison of acute and chronic toxicity methods for marine sediments. Mar. Environ. Res. 68, 118—127, http://dx.doi.org/10.1016/j.marenvres.2009.04.010.

Khosrovyan, A., Rodríguez-Romero, A., Antequera Ramos, M., Del-Valls, T.A., Riba, I., 2015. Comparative analysis of two weight-of-evidence methodologies for integrated sediment quality assessment. Chemosphere 120, 138—144, http://dx.doi.org/10.1016/j.chemosphere.2014.06.043.

Kirkpatrick, A.J., Gerhardt, A., Dick, J.T.A., McKenna, M., Berges, J.A., 2006. Use of the multispecies freshwater biomonitor to assess behavioral changes of *Corophium volutator* (Pallas, 1766) (Crustacea, Amphipoda) in response to toxicant exposure in sediment. Ecotoxicol. Environ. Saf. 64, 298—303, http://dx.doi.org/10.1016/j.ecoenv.2005.07.003.

Kuhn, A., Munns, W.R., Serbst, J., Edwards, P., Cantwell, M.G., Gleason, T., Pelletier, M.C., Berry, W., 2002. Evaluating the ecological significance of laboratory response data to predict population-level effects for the estruarine amphipod *Ampelisca abdita*. Environ. Toxicol. Chem. 21, 865—874, http://dx.doi.org/10.1002/etc.5620210425.

Kunz, P.Y., Kienle, C., Gerhardt, A., 2010. *Gammarus* spp. in aquatic ecotoxicology and water quality assessment: toward integrated multilevel tests. In: Whitacre, D. (Ed.), Reviews of Environmental Contamination and Toxicology. Springer, New York, 1—76, http://dx.doi.org/10.1007/978-1-4419-5623-1.

Lee, J.S., Lee, K.T., Kim, D.H., Kim, C.K., Lee, J.H., Park, K.H., Park, G.S., 2005. Application of indigenous benthic amphipods as sediment toxicity testing organisms. Ocean Sci. J. 40, 17—24, http://dx.doi.org/10.1007/BF03023462.

Löf, M., Sundelin, B., Bandh, C., Gorokhova, E., 2016. Embryo aberrations in the amphipod *Monoporeia affinis* as indicators of toxic pollutants in sediments: A field evaluation. Ecol. Indic. 60, 18—30, http://dx.doi.org/10.1016/j.ecolind.2015.05.058.

Lotufo, G.R., Farrar, J.D., Biedenbach, J.M., Laird, J.G., Krasnec, M. O., Lay, C., Morris, J.M., Gielazyn, M.L., 2016. Effects of sediment amended with Deepwater Horizon incident slick oil on the infaunal amphipod *Leptocheirus plumulosus*. Mar. Pollut. Bull. 109, 253—258, http://dx.doi.org/10.1016/j.marpolbul.2016.05.073.

Lourens, J.M., Vonck, A.P.M.A., vd Guchte, C., Hartnack, J., Stronkhorst, J., 1995. Sediment toxicity testing of lightly contaminated dredged material in The Netherlands. J. Aquat. Ecosyst. Heal. 4, 271—275, http://dx.doi.org/10.1007/BF00118007.

Lowry, J.K., Myers, A.A., 2003. A phylogeny and a new classification of the corophiidea leach, 1814 (Amphipoda). J. Crustac. Biol. 23, 443—485, http://dx.doi.org/10.1163/20021975-99990353.

Macken, A., Giltrap, M., Foley, B., McGovern, E., McHugh, B., Davoren, M., 2008. An integrated approach to the toxicity assessment of Irish marine sediments: validation of established marine bioassays for the monitoring of Irish marine sediments. Environ. Int. 34, 1023—1032, http://dx.doi.org/10.1016/j.envint.2008.03.005.

Mann, R.M., Hyne, R.V., Spadaro, D.A., Simpson, S.L., 2009. Development and application of a rapid amphipod reproduction test for sediment-quality assessment. Environ. Toxicol. Chem. 28, 1244—1254, http://dx.doi.org/10.1897/08-346.1.

Mann, R.M., Hyne, R.V., Simandjuntak, D.L., Simpson, S.L., 2010. A rapid amphipod reproduction test for sediment quality assessment: In situ bioassays do not replicate laboratory bioassays. Environ. Toxicol. Chem. 29, 2566—2574, http://dx.doi.org/10.1002/etc.306.

Manyin, T., Rowe, C.L., 2006. Chronic exposure of *Leptocheirus plumulosus* to Baltimore Harbor sediment: Bioenergetic and population-level effects. Mar. Environ. Res. 62, 116—130, http://dx.doi.org/10.1016/j.marenvres.2006.03.006.

Marsden, I.D., 2002. Life-history traits of a tube-dwelling corophioid amphipod, *Paracorophium excavatum*, exposed to sediment copper. J. Exp. Mar. Bio. Ecol. 270, 57—72, http://dx.doi.org/10.1016/S0022-0981(02)00010-2.

Marsden, I.D., Wong, C.H.T., Al-Mudaffar, N., 2000. Assessment of an estuarine amphipod (*Paracorophium excavatum*) as a bioindicator of contaminated sediment. Aust. J. Ecotoxicol. 6, 21—30.

Martinez-Haro, M., Acevedo, P., Pais-Costa, A.J., Taggart, M.A., Martins, I., Ribeiro, R., Marques, J.C., 2016. Assessing estuarine quality: a cost-effective in situ assay with amphipods. Environ. Pollut. 212, 382—391, http://dx.doi.org/10.1016/j.envpol.2016.01.071.

McCready, S., Greely, C.R., Hyne, R.V., Birch, G.F., Long, E.R., 2005. Sensitivity of an indigenous amphipod (*Corophium colo*) to chemical contaminants in laboratory toxicity tests conducted with sediments from Sydney Harbor, Australia, and vicinity. Environ. Toxicol. Chem. 24, 2545—2552, http://dx.doi.org/10.1897/04-457.1.

McGee, B.L., Wright, D.A., Fisher, D.J., 1998. Biotic factors modifying acute toxicity of aqueous cadmium to estuarine amphipod *Leptocheirus plumulosus*. Arch. Environ. Contam. Toxicol. 34, 34—40, http://dx.doi.org/10.1007/s002449900283.

McGee, B.L., Fisher, D.J., Wright, D.A., Yonkos, L.T., Ziegler, G.P., Turley, S.D., Farrar, J.D., Moore, D.W., Bridges, T.S., 2004. A field test and comparison of acute and chronic sediment toxicity tests with the estuarine amphipod *Leptocheirus plumulosus* in Chesapeake Bay, USA. Environ. Toxicol. Chem. 23, 1751—1761, http://dx.doi.org/10.1897/03-326.

Meadows, P.S., 1964. Experiments on substrate selection by Corophium species: films and bacteria on sand particles. J. Exp. Biol. 41, 499—511.

Meador, J.P., Varanasi, U., Krone, C.A., 1993. Differential sensitivity of marine infaunal amphipods to tributyltin. Mar. Biol. 116, 231—239, http://dx.doi.org/10.1007/BF00350012.

Menchaca, I., Belzunce, M.J., Franco, J., Garmendia, J.M., Montero, N., Revilla, M., 2010. Sensitivity comparison of laboratory-cultured and field-collected amphipod *Corophium multisetosum* in toxicity tests. Bull. Environ. Contam. Toxicol. 84, 390—394, http://dx.doi.org/10.1007/s00128-010-9960-9.

Molisani, M.M., Costa, R.N., Cunha, P., De Rezende, C.E., Ferreira, M. I.P., De Assis Esteves, F., 2013. Acute toxicity bioassay with the amphipod, *Grandidierella bonnieroides* S. after exposure to sediments from an urban estuary (Macaé River Estuary, RJ, Brazil). Bull. Environ. Contam. Toxicol. 90, 79—84, http://dx.doi.org/10.1007/s00128-012-0871-9.

Nair, K.K.C., Anger, K., 1979. Life cycle of *Corophium insidiosum* (Crustacea, Amphipoda) in laboratory culture. Helgoländer Wissenschaftliche Meeresuntersuchungen 32, 279—294, http://dx.doi.org/10.1007/BF02189586.

Narracci, M., Cavallo, R.A., Acquaviva, M.I., Prato, E., Biandolino, F., 2009. A test battery approach for ecotoxicological characterization of Mar Piccolo sediments in Taranto (Ionian Sea, Southern Italy). Environ. Monit. Assess. 148, 307—314, http://dx.doi.org/10.1007/s10661-008-0161-5.

Navarro-Barranco, C., Tierno-de-Figueroa, J.M., Guerra-García, J. M., Sánchez-Tocino, L., García-Gómez, J.C., 2013. Feeding habits of amphipods (Crustacea: Malacostraca) from shallow soft bottom communities: comparison between marine caves and open habitats. J. Sea Res. 78, 1—7, http://dx.doi.org/10.1016/j.seares.2012.12.011.

Neuparth, T., Costa, F.O., Costa, M.H., 2002. Effects of temperature and salinity on life history of the marine amphipod *Gammarus locusta*. Implications for ecotoxicological testing. Ecotoxicology 11, 61—73, http://dx.doi.org/10.1023/A:1013797130740.

Neuparth, T., Correia, A.D., Costa, F.O., Lima, G., Costa, M.H., 2005. Multi-level assessment of chronic toxicity of estuarine sediments with the amphipod *Gammarus locusta*: I. Biochemical endpoints. Mar. Environ. Res. 60, 69—91, http://dx.doi.org/10.1016/j.marenvres.2004.08.006.

Nielsen, M., Kofoed, L., 1982. Selective feeding and epipsammic browsing by the deposit-feeding amphipod *Corophium volutator*. Mar. Ecol. Prog. Ser. 10, 81—88, http://dx.doi.org/10.3354/meps010081.

Nipper, M., Carr, R.S., Biedenbach, J.M., Hooten, R.L., Miller, K., 2002. Toxicological and chemical assessment of ordinance compounds in marine sediments and porewaters. Mar. Pollut. Bull. 44, 789—806.

Onorati, F., Bigongiari, N., Pellegrini, D., Giuliani, S., 1999. The suitability of *Corophium orientale* (Crustacea, Amphipoda) in

harbour sediment toxicity bioassessment. Aquat. Ecosyst. Heal. Manag. 2, 465—473, http://dx.doi.org/10.1080/14634989908656984.

OSPAR, 2006. OSPAR Protocols on Methods for the Testing of Chemicals Used in the Offshore Oil Industry, Offshore Industry Series.

OSPAR, 2013. Background document and technical annexes for biological effects monitoring, Update 2013, Monitoring and Assessment Series.

Pastorinho, M.R., Telfer, T.C., Soares, A.M.V.M., 2009. Amphipod susceptibility to metals: cautionary tales. Chemosphere 75, 1423—1428, http://dx.doi.org/10.1016/j.chemosphere.2009.03.003.

Pérez-Landa, V., Belzunce, M.J., Franco, J., 2008. The effect of seasonality and body size on the sensitivity of marine amphipods to toxicants. Bull. Environ. Contam. Toxicol. 81, 548—552, http://dx.doi.org/10.1007/s00128-008-9550-2.

Peters, C., Ahlf, W., 2005. Reproduction of the estuarine and marine amphipod *Corophium volutator* (Pallas) in laboratory for toxicity testing. Chemosphere 59, 525—536, http://dx.doi.org/10.1016/j.chemosphere.2005.01.053.

Picone, M., Bergamin, M., Novelli Alessandra, A., Noventa, S., Delaney, E., Barbanti, A., Ghirardini, A.V., 2008. Evaluation of *Corophium orientale* as bioindicator for Venice Lagoon: Sensitivity assessment and toxicity-score proposal. Ecotoxicol. Environ. Saf. 70, 174—184, http://dx.doi.org/10.1016/j.ecoenv.2006.06.005.

Picone, M., Bergamin, M., Losso, C., Delaney, E., Arizzi Novelli, A., Ghirardini, A.V., 2016. Assessment of sediment toxicity in the Lagoon of Venice (Italy) using a multi-species set of bioassays. Ecotoxicol. Environ. Saf. 123, 32—44, http://dx.doi.org/10.1016/j.ecoenv.2015.09.002.

Postma, J.F., De Valk, S., Dubbeldam, M., Maas, J.L., Tonkes, M., Schipper, C.A., Kater, B.J., 2002. Confounding factors in bioassays with freshwater and marine organisms. Ecotoxicol. Environ. Saf. 53, 226—237, http://dx.doi.org/10.1006/eesa.2002.2195.

Prato, E., Biandolino, F., Scardicchio, C., 2006. Test for acute toxicity of copper, cadmium, and mercury in five marine species. Turkish J. Zool. 30, 285—290.

Prato, E., Scardicchio, C., Biandolino, F., 2008. Effects of temperature on the acute toxicity of cadmium to *Corophium insidiosum*. Environ. Monit. Assess. 136, 161—166, http://dx.doi.org/10.1007/s10661-007-9672-8.

Prato, E., Bigongiari, N., Barghigiani, C., Biandolino, F., 2010. Comparison of amphipods *Corophium insidiosum* and *C. orientale* (Crustacea: Amphipoda) in sediment toxicity testing. J. Environ. Sci. Heal.-Part A Toxic/Hazardous Subst. Environ. Eng. 45, 1461—1467, http://dx.doi.org/10.1080/10934529.2010.500941.

Prato, E., Biandolino, F., Libralato, G., 2015. A toxicity scoring system for the 10-day whole sediment test with *Corophium insidiosum* (Crawford). Environ. Monit. Assess. 187, 1—11, http://dx.doi.org/10.1007/s10661-015-4405-x.

Ré, A., Freitas, R., Sampaio, L., Rodrigues, A.M., Quintino, V., 2009. Estuarine sediment acute toxicity testing with the European amphipod Corophium multisetosum Stock, 1952. Chemosphere 76, 1323—1333, http://dx.doi.org/10.1016/j.chemosphere.2009.06.041.

Riba, I., DelValls, T.A., Forja, J.M., Gómez-Parra, A., 2003. Comparative toxicity of contaminated sediment from a mining spill using two amphipods species: *Corophium volutator* (Pallas, 1776) and Ampelisca brevicornis (A. Costa, 1853). Bull. Environ. Contam. Toxicol. 71, 1061—1068, http://dx.doi.org/10.1007/s00128-003-8878-x.

RIKZ, 1999. Standard operating procedure species-01 marine amphipod *Corophium volutator* mortality sediment toxicity test. Riijksinstituut voor Kust en Zee. RIKZ/AB-99.114x, the Netherlands.

Roddie, B.D., Thain, J.E., 2001. Biological effects of contaminants: *Corophium* sp. sediment bioassay and toxicity test. ICES Tech. Mar. Environ. Sci. 22.

Romeo, T., D'Alessandro, M., Esposito, V., Scotti, G., Berto, D., Formalewicz, M., Noventa, S., Giuliani, S., Macchia, S., Sartori, D., Mazzola, A., Andaloro, F., Giacobbe, S., Deidun, A., Renzi, M., 2015. Environmental quality assessment of Grand Harbour (Valletta, Maltese Islands): a case study of a busy harbour in the Central Mediterranean Sea. Environ. Monit. Assess. 187, 747, http://dx.doi.org/10.1007/s10661-015-4950-3.

Scarlett, A., Rowland, S.J., Canty, M., Smith, E.L., Galloway, T.S., 2007. Method for assessing the chronic toxicity of marine and estuarine sediment-associated contaminants using the amphipod *Corophium volutator*. Mar. Environ. Res. 63, 457—470, http://dx.doi.org/10.1016/j.marenvres.2006.12.006.

SETAC-Europe, 1993. Guidance document on sediment toxicity assessment for freshwater and marine environments. In: Hill, I.R., Matthiessen, P., Rigler, F.H. (Eds.), Workshop on Sediment Toxicity Assessment, Renesse, Netherlands. SETAC-Europe.

Siebeneicher, S., Wahrendorf, D.S., Wetzel, M.A., Jungmann, D., 2013. Analysis of burrowing ability as a sublethal endpoint in a marine sediment bioassay with Corophium volutator (Pallas). J. Soils Sediments 13, 197—206, http://dx.doi.org/10.1007/s11368-012-0619-5.

Strode, E., Jansons, M., Purina, I., Balode, M., Berezina, N.A., 2017. Sediment quality assessment using survival and embryo malformation tests in amphipod crustaceans: The Gulf of Riga, Baltic Sea AS case study. J. Mar. Syst. 172, 93—103, http://dx.doi.org/10.1016/j.jmarsys.2017.03.010.

Stronkhorst, J., 2003. Using marine bioassays to classify the toxicity of dutch harbor sediments. Environ. Toxicol. Chem. 22, 1525—1547, http://dx.doi.org/10.1002/etc.5620220716.

Sundelin, B., Eriksson, A.K., 1998. Malformations in embryos of the deposit-feeding amphipod Monoporeia affinis in the Baltic Sea. Mar. Ecol. Prog. Ser. 171, 165—180, http://dx.doi.org/10.3354/meps171165.

Sundelin, B., Eriksson Wiklund, A.-K., Ford, A.T., 2008a. Biological Effects of Contaminants: the use of embryo aberrations in amphipod crustaceans for measuring effects of environmental stressors. ICES Tech. Marine Environ. Sci. International Council for the Exploration of the Sea.

Sundelin, B., Rosa, R., Wiklund, A.K.E., 2008b. Reproduction disorders in the benthic amphipod Monoporeia affinis: An effect of low food resources. Aquat. Biol. 2, 179—190, http://dx.doi.org/10.3354/ab00048.

Sutcliffe, D.W., 1992. Reproduction in Gammarus (Crustacea, Amphipoda): basic processes. Freshw. Forum 2, 102—128.

Tucca, F., Díaz-Jaramillo, M., Cruz, G., Silva, J., Bay-Schmith, E., Chiang, G., Barra, R., 2014. Toxic effects of antiparasitic pesticides used by the salmon industry in the marine amphipod Monocorophium insidiosum. Arch. Environ. Contam. Toxicol. 67, 139—148, http://dx.doi.org/10.1007/s00244-014-0008-8.

USEPA, 1994. Methods for Assessing the Toxicity of Sediment-associated Contaminants with Estuarine and Marine Amphipods. EPA/600/R-94/025. US Environmental Protection Agency, Washington, DC.

USEPA, 1998. Method of assessing the chronic toxicity of sediment-associated contaminants with Leptocheirus plumululosus. 1st ed. August 1998 draft. Office of Research and Development, Duluth, MN.

USEPA, 2001a. Methods for assessing the chronic toxicity of marine and estuarine sediment-associated contaminants with the amphipod Leptocheirus plumulosus. EPA/600/R-01/020. US Environmental Protection Agency, Washington, DC.

USEPA, 2001b. Application of the 10-d acute and 28-d chronic *Leptocheirus plumulosus* sediment toxicity tests to the ambient toxicity assessment program. EPA/903/R-01/001. Chesapeake Bay Program, Annapolis, MD.

Van Den Brink, P.J., Kater, B.J., 2006. Chemical and biological evaluation of sediments from the Wadden Sea, The Netherlands. Ecotoxicology 15, 451—460, http://dx.doi.org/10.1007/s10646-006-0080-6.

Van Den Heuvel-Greve, M., Postma, J., Jol, J., Kooman, H., Dubbeldam, M., Schipper, C., Kater, B., 2007. A chronic bioassay with the

estuarine amphipod Corophium volutator: Test method description and confounding factors. Chemosphere 66, 1301—1309, http://dx.doi.org/10.1016/j.chemosphere.2006.07.022.

Ward, T.J., Gaertner, K.E., Gorsuch, J.W., Call, D.J., 2015. Survival, reproduction and growth of the marine amphipod, *Leptocheirus plumulosus*, following laboratory exposure to copper-spiked sediment. Bull. Environ. Contam. Toxicol. 95, 434—440, http://dx.doi.org/10.1007/s00128-015-1638-x.

Wilson, W.H., Parker, K., 1996. The life history of the amphipod Corophium volutator: the effect of temperature and shorebird predation. J. Exp. Mar. Bio. Ecol. 196, 239—250, http://dx.doi.org/10.1016/0022-0981(95)00133-6.

Oceanologia (2019) 61, 197—207

Available online at www.sciencedirect.com

ScienceDirect

journal homepage: www.journals.elsevier.com/oceanologia/

ORIGINAL RESEARCH ARTICLE

Effects of environmental variables on midsummer dinoflagellate community in the Neva Estuary (Baltic Sea)

Mikhail Golubkov *, **Vera Nikulina**, **Sergey Golubkov**

Zoological Institute of Russian Academy of Sciences, St. Petersburg, Russia

Received 13 June 2018; accepted 19 September 2018
Available online 4 October 2018

KEYWORDS
Gulf of Finland;
Phytoplankton;
Mixotrophy;
Eutrophication;
Climate change

Summary Dinoflagellates account for most of the harmful phytoplankton species but relatively little is known about the specific responses of different species to environmental variables. 21 dinoflagellate species were recorded in the plankton of the Neva Estuary since the mid-19th century. 14-year long data of midsummer dinoflagellate biomass was statistically analyzed in the Neva Estuary to show the changes in dinoflagellate species in relation to environmental factors. Biomasses of *Dinophysis norvegica* (Clapared & Lachmann 1859), *Prorocentrum lima* ((Ehrenberg) F.Stein 1878) and *Peridinium aciculiferum* (Lemmermann 1900) had very similar positive relationships with salinity, temperature, phosphorus and suspended particulate organic matter concentrations while the biomass of the other common species *Peridinium cinctum* ((Müller) Ehrenberg 1832) and *Peridinium* sp. mostly showed quite opposite trends. Climate fluctuations leading to changes in the environmental variables could significantly affect the composition and productivity of the dinoflagellate community. Biomass of *Glenodinium* sp. and *Peridinium* sp. positively correlated with primary production and biomass and chlorophyll *a* concentration, but did not show a positive relationship with phosphorus. This may be due to the fact that these species in the conditions of the Neva Estuary, apparently, are more consumers than producers of organic matter, feeding on algae and cyanobacteria of phytoplankton. Therefore, to interpret the relationships between the dinoflagellate biomass and environmental variables one should take into account that the species of this group is characterized by mixotrophy and, consequently, their biomass may depend not only on the conditions of autotrophic, but also heterotrophic nutrition.

* Corresponding author at: Zoological Institute of Russian Academy of Sciences, 199034, Universitetskaya emb. 1, St. Petersburg, Russia. Tel.: +7 8123280311; fax: +7 8123282941.
E-mail address: golubkov_ms@mail.ru (M. Golubkov).
Peer review under the responsibility of Institute of Oceanology of the Polish Academy of Sciences.

ELSEVIER Production and hosting by Elsevier

https://doi.org/10.1016/j.oceano.2018.09.001

1. Introduction

It is generally recognized that there have been more algal blooms, often of greater geographic extent and/or longer duration, with more toxic species observed, in the past decade than in previous decades (Heisler et al., 2008). In fact, dinoflagellates account for about 75% of all harmful phytoplankton species (Smayda and Reynolds, 2003). They have often formed huge red tides, which have sometimes caused large-scale mortalities of fin-fish and shellfish and thus great losses to the aquaculture and tourist industries of many countries (Anderson et al., 2002; Heisler et al., 2008; Zhou et al., 2017). This includes the proliferation of both spring and summer species (Jaanus et al., 2006; Klais et al., 2011; Smayda, 2002; Smayda and Reynolds, 2003; Smayda and Trainer, 2010). In the Baltic Sea the role of dinoflagellates in phytoplankton has increased everywhere from the northern to the southern regions (Golubkov et al., 2017; Jaanus et al., 2006; Klais et al., 2011; Kremp et al., 2008; Olli and Trunov, 2010; Wasmund and Uhlig, 2003).

Several reasons have been proposed to explain the observed prosperity of dinoflagellates. Eutrophication of coastal waters is the one of main reasons by which harmful algae appear to be increasing in extent and duration in many locations (Anderson et al., 2002; Heisler et al., 2008; Price et al., 2017; Xiao et al., 2018). For instance, there is a definite dinoflagellate cyst which is considered as eutrophication signal along the estuaries of the NW Atlantic, thus confirming their value as indicators of water quality change and anthropogenic impact (Price et al., 2017).

The abundance of some species in the NW Atlantic region positively correlated to summer water temperatures (Price et al., 2017). Therefore, climate change may also contribute to their success. However, these changes are not so unambiguous. In the Gulf of Bothnia, the role of dinoflagellate in the phytoplankton community was higher in the colder period (Kuosa et al., 2017).

One of the most important features of dinoflagellates is their ability to become mixotrophic (uses both autotrophy and heterotrophy for growth). Many species are able to consume low molecular weight organic compounds, such as urea and amino acids, suspended organic matter, bacteria and other phytoplankton species (Hansen, 2011). Therefore, the proliferation of dinoflagellate can be associated with the increase in runoff of organic substances especially in coastal areas and with global warming. All climate projections predict an increase in average global humidity and so an increase in total rainfall. More locally, the mid-latitudes are predicted to become drier, while the wet regions, that is the tropics and polar and sub-polar regions, get wetter (Eggleton, 2018). Thus, the change in phytoplankton communities may be a result of proliferation of allochthonous organic matter-based food web (Kuosa et al., 2017), which is known to be important in northern parts of Europe (the Gulf of Bothnia) (Sandberg et al., 2004) and America (Gagnon, 2005). In some cases, the occurrence of red tides was associated with the introduction of alien species of dinoflagellates. For example, the invasion of *Prorocentrum minimum* ((Pavillard) Schiller 1933) into the southern part of the Baltic Sea led to blooms in the area (Telesh et al., 2016). The prosperity of this species was facilitated by their resistance to changes in the salinity of coastal waters, which can also be caused by climate-induced changes in surface runoff (Skarlato et al., 2018).

In the Russian part of the eastern Gulf of Finland (Neva Estuary), studies of dinoflagellate began in the mid-19th century (Brandt, 1845) and continue to the present time. However, these data are poorly represented in international databases (e.g., HELCOM, 1996, 2004). Recent studies have shown that biomass of dinoflagellates has increased significantly over the past two decades. Before the late 1990s the dominant group of phytoplankton was diatoms (Bacillariophyta). In summer, the share of Dinophyta in total biomass did not exceed 3% (Nikulina, 2003). In 2000s their biomass considerably increased and in 2013–2014 this group of phytoplankton together with Cryptophyta became dominant and subdominant in midsummer phytoplankton in the upper and middle parts of the estuary respectively (Golubkov et al., 2017).

The mechanisms of bloom-species selection, and the causes of the shifts in phytoplankton community structure favoring flagellate taxa and their blooms, are major unresolved issues. Dinoflagellates have multiple life-form strategies consistent with their diverse habitat specializations. Indigenous phytoplankton communities are assembled from an extensive array of species of diverse size, shape and overlapping autecology, from which bloom species are selected (Smayda and Reynolds, 2003). However, the conditions, factors and mechanisms selecting for the genus, and species for bloom time windows remain poorly understood especially in variable coastal environments, and the outcome is thus highly unpredictable. Life-forms are selected primarily on specific habitat conditions like eutrophication and physical–chemical habitat templates. Identifying quantitative relationships between environmental variables and proliferation of certain algal species is very challenging and complex. Models of harmful algal blooms (HABs) need to include autecological characteristics of the HAB species (Glibert et al., 2010; Hense, 2010). Therefore, to predict future trends in assembly of dinoflagellate communities more information about specific habitat conditions for different species are needed.

The purpose of this study was to analyze, based on 14-year data, the effects of the environmental variables on biomass of different dinoflagellate species in the Neva Estuary. We analyzed environmental conditions such as water temperature, salinity, concentration of total phosphorus, primary production and mineralization of organic matter in order to relate them with dinoflagellate species composition and biomass in the upper, middle and lower parts of the Neva Estuary in midsummer. We tested a hypothesis that biomass of different species may be significantly correlated with these environmental variables. End of July–early August period was chosen for long-term observations because of maximum development of summer phytoplankton at this period in the Neva Estuary (Golubkov, 2009; Nikulina, 2003). The second task was to summarize the results of previous studies on the composition of the dinoflagellate community in the eastern Gulf of Finland.

2. Material and methods

2.1. Study site and sampling

The Neva Estuary receives water from the Neva River, a relatively short canal (74 km) between Lake Ladoga and

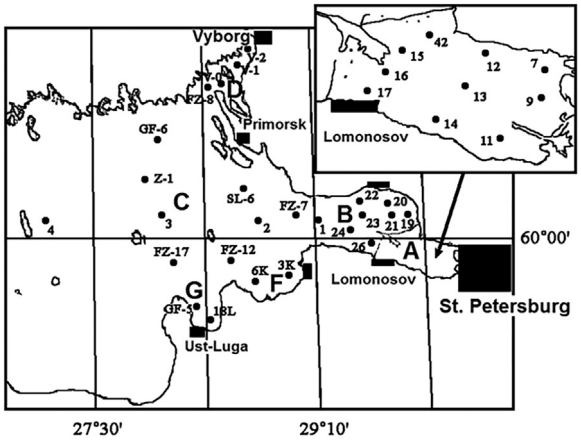

Figure 1 The Neva Estuary with indication of the sample stations (A — Neva Bay; B — Inner Estuary; C — Outer Estuary, D — Gulf of Vyborg; F — Koporskaya Bay; G — Luga Bay).

the Gulf of Finland. The catchment area of the Neva River exceeds 280,000 km^2, and its water discharge averages 2490 m s^{-1} (78.6 km^3 yr^{-1}). The Neva Estuary consists of three parts: the upper freshwater — Upper Estuary (Neva Bay), the brackish Middle (Inner) Estuary, and the Lower (Outer) Estuary. The surface area of the Neva Bay (Fig. 1) is about 400 km^2, the salinity — 0.07—0.2 PSU, with the exception of short-term surge events when brackish waters from the Middle estuary come to the Neva Bay and mix there with fresh waters. The depth of the bay is 3.5—5 m. At the end of 1980s, the Neva Bay was separated from the lower part of the estuary by the flood protection barrier (Dam). It has several sluices in its northern part and a broad ship lock in the southern part. There is no temperature stratification in this part of the estuary. Low water transparency, which does not exceed 1.8 m of Secchi depth in summer time, constrains the distribution of bottom vegetation in the bay. Dense reeds of 300—600 m width belt encircle its shallow coastal zone.

The Inner Estuary is a slightly brackish-water basin in the eastern Gulf of Finland and is located between the Dam and the longitude ca. 29°E. The salinity of surface waters in this part of the Neva Estuary ranges from 1 to 3 PSU and depth from 12 to 14 m in the eastern part and up to 30 m in its western part. There is temperature stratification in this part of the estuary: the warm water upper layer (epilimnion) and cold water deep layer (hypolimnion). The Outer Estuary is located to the west of the ca. 29°E and has a depth up to 50 m and salinity 3—7 PSU.

Ten stations in the Neva Bay and eight stations in the Inner Estuary, thirteen stations in the Outer Estuary and four stations in the Gulf of Vyborg (Fig. 1) were sampled from 20th of July to 5th of August 2003—2016. The number of stations varied in different years. Secchi depth (Sec), salinity and temperature were measured at each station. Temperature and salinity was measured by the CTD90 m probe (Sea&-Sun Tech., Germany) every 20 cm from the surface to the bottom in the whole water column. Taking into account that according to these measurements the whole water column in the shallow Neva Bay was mixed, we collected five water samples (2 l each): from the surface, half a meter from the bottom and from three equal depths between them. Samples from different depths were taken in order to avoid errors associated with the vertical distribution of different dinoflagellate species in the water column. These samples were mixed to make up an integrated sample (10 l). Samples of total phosphorus, chlorophyll *a*, suspended particulate matter and suspended particulate organic matter (three replicates) were taken from the integrated samples.

In the Inner and Outer Estuaries and in the Gulf of Vyborg, integrated water samples were taken from the two water layers: above (epilimnion) and below (hypolimnion) of the thermocline (the steepest slope of the temperature gradient from the surface to the bottom). Five water samples (2 l each) were taken from the epilimnion: from the surface, thermocline and from three equal depths between them. These samples were mixed to make up an integrated sample (10 l). Integrated water samples from hypolimnion were collected in the same way from thermocline to the bottom. Samples of chlorophyll *a* and total phosphorus (three replicates) were taken from the epilimnion integrated samples.

2.2. Sample analysis

Three hundred milliliters of water was filtered through 0.85 μm membrane filters (Millipore AAWP) for the determinations of chlorophyll *a* (C) concentration, followed by a 90% acetone extraction and spectrophotometric determination (Grasshoff et al., 1999). Total phosphorus (TP) was determined after acid hydrolysis with the molybdate blue method (Grasshoff et al., 1999). Suspended particulate matter (SPM) concentration was determined after filtration through Whatman GF/F filters with a gravimetric technique. Suspended particulate organic matter (SOM) was determined after filtration with Whatman GF/F filters (with the dichromate acid oxidation) (Grasshoff et al., 1999).

The primary production of plankton (PP) and the mineralization of organic matter (D) in water column were measured by means of the oxygen method of light and dark bottles (Hall et al., 2007; Vernet and Smith, 2007). Ratio (R) between PP and D under 1 m^2 was calculated as R = PP/D. The method of determination and design of experiments were described in details in the Golubkov et al. (2017).

2.3. Autotrophic dinoflagellate assemblages

Phytoplankton (volume 0.3 l) was taken in one replicate from epilimnion integrated samples and fixed with acid Lugol's solution. Since in shallow Neva Bay the whole water column was mixed, we collected only one integrated water sample from the whole column in the same way as in the Inner Estuary. The phytoplankton taxa were identified and counted in sedimentation chambers (10—25 ml) with an inverted Hydro-Bios microscope. Phytoplankton biomass was calculated in total volume of algal cells according to Olenina et al. (2006) and expressed in WW mg l^{-1}. Identification of dinoflagellate taxa was conducted according to Kiselev (1954), Pankov (1976) and Tikkanen (1986). Phytoplankton species have been listed in the modern nomenclature according to Guiry and Guiry (2018).

2.4. Statistical analysis

Statistical analyses were performed using the R software (version 3.4.0; R Development Core Team, 2017; www.

r-project.org/). Non-metric Multidimensional Scaling (NMDS) was used to analyse changes within the dinoflagellate communities by ordinating samples based on the dissimilarities of environmental conditions (function "metaMDS", R package 'vegan', Oksanen et al., 2017). NMDS is an ordination technique that uses rank orders to collapse information from multiple dimensions, so they can be visualised and interpreted. The range of data values was so large that the data were square root transformed, and then submitted to Wisconsin double standardization, or species divided by their maxima, and stands standardized to equal totals. We used the Bray-Curtis dissimilarity as the distance metric in the NMDS. In the NMDS ordination space, the samples position themselves based on their taxon specific biomass. To overlaying environmental information onto ordination diagrams we use function "envfit" (R package "vegan", Oksanen et al., 2017). The arrow points to the direction of most rapid change in the environmental variable. This is called the direction of the gradient. The length of the arrow is proportional to the correlation between ordination and environmental variable. This is called the strength of the gradient. We add the fitted vectors to an ordination using "plot" command and limit plotting to most significant variables with argument "p. max = 0.05".

3. Results and discussion

3.1. Species composition and abundance of autotrophic dinoflagellates

A total of 134 phytoplankton midsummer samples were processed, and 9 dinoflagellates species were identified across the samples. Four dinoflagellates groups were identified only to genus (Table 1). Since the number of stations where phytoplankton samples were collected varied over the years, we did not analyze the interannual variability of the composition and biomass of the dinoflagellate community.

The most common species for the Neva Estuary were *Ceratium hirundinella* ((Müller) Dujardin 1841), *Peridinium aciculiferum* and *Glenodinium* sp. These species were found in the samples 34–42 times; had high biomass and were distributed in all parts of the estuary, almost every year (Table 1). *C. hirundinella* was also common in plankton during the summers 1911–1912, 1914, 1920–1921 and 1923 (Kiselev, 1924; Vislouh, 1913, 1921) (Table 2), giving a maximum biomass in late July–early August. In summer 1930 it was found in the Outer Estuary in Koporskaya Bay (Kiselev, 1948). In addition, it was a subdominant species in the summer phytoplankton of the Neva Bay in 1982–1984, 2000 and 2002 (Lange, 2006; Nikulina, 1987). This dinoflagellate species was found throughout the Baltic Sea in areas with low salinity (HELCOM, 2004). *P. aciculiferum* was common in the Neva Estuary in 1982–1984 (Nikulina, 1987). But this species was not in the list of dinoflagellates found in the Baltic Sea published by HELCOM (2004). This may be due to the fact that it is mainly a freshwater species, which does not withstand a significant increase in water salinity (Craveiro et al., 2016). However, the water salinity in the Neva Estuary is rather low, and it was found in all its parts.

Peridinium cinctum, another freshwater species, which was found in the Neva Bay and the Inner estuary mainly in 2014–2016, had the highest biomass (Table 1). This species was also previously recorded in the Neva Estuary (Nikulina, 1987), Arkona Basin, Gulf of Riga and the western Gulf of Finland (HELCOM, 2004). *Gymnodinium* sp. reached to similar biomasses. *Gymnodinium simplex* ((Lohmann) Kofoid & Swezy 1921) was the rarest species of dinoflagellates in the Neva Estuary. We found this marine species, which occurred throughout the Baltic Sea (HELCOM, 2004), only once in the Outer Estuary station in 2014. *Amphydinium* spp., and *Dinophysis rotundata* (Clapared & Lachmann 1859) were also rare (Table 1).

21 taxa of dinoflagellate were noted in the Russian part of the Gulf of Finland since the mid-19th century (Table 2). The first data on phytoplankton of the Neva Estuary belong to Brandt, 1845 (Table 2). Working in the summer 1843 near the southern coast of the Neva Estuary, 40 km to the west of Lomonosov town, he found one species of dinoflagellates: *Prorocentrum micans* (Ehrenberg 1834). This marine species

Table 1 Species composition and biomass of dinoflagellates in midsummer 2003–2016 in the Neva Estuary.

Species	The number of occurrence	The year of occurence	The station where species were found	Biomass [mg m^{-3}]
Amphidinium spp.	2	2003	6k, FZ-17	43.4–180.1
Ceratium hirundinella	42	2003, 2004, 2006, 2007, 2009, 2010, 2013–2016	Everywhere	17.6–1760.0
Dinophysis norvegica	9	2006–2008, 2014	16, 1, 2, 3, 4, 6k	5.0–124.3
D. rotundata	4	2003	18L, GF-5, z-1, FZ-17	12.3–49.3
Glenodinium sp.	34	2003–2006, 2008, 2010–2014, 2016	Every where	0.5–275.5
Gymnodinium sp.	13	2011, 2014, 2015	Neva Bay, Inner Estuary	5.2–2304
Gymnodinium simplex	1	2004	1	10.9
Peridinium sp.	9	2003, 2012, 2013,	Everywhere	13.4–544.5
Peridinium aciculiferum	36	2003–2006, 2008–2009, 2014–2016	Everywhere	1.6–977.3
P. cinctum	18	2004, 2014–2016	Neva Bay, Inner Estuary	18.7–2664
Peridiniella catenata	3	2005, 2010	Inner Estuary	49.5–85.5
Protoperidinium bipes	9	2004–2007, 2009, 2014	Inner Estuary, Outer Estuary	8.3–832
Prorocentrum lima	7	2005–2006	1, 2, 4, GF-5, 3k, FZ-17,	1.0–411.5

Table 2 Species composition of dinoflagellates in the Neva Estuary in different years (according to Brandt, 1845; Kiselev, 1924, 1948; Lange, 2006; Nikulina, 1987; Shishkin et al., 1989; Tereshenkova, 2006; Vislouh, 1913, 1921 and own data).

Species	1843	1911–1912, 1914	1920–1921	1930–1937	1982–1984	1988	1997	1999–2002	2003–2016
	July–August			All seasons	August	All seasons	All seasons	August	July–August
Amphidinium sp.									+
Ceratium hirundinella		+	+	+	+			+	+
C. longipes				+					
Dinophysis norvegica									+
D. ovum var. *baltica*				+					
D. rotundata									+
Diplopsalis lenticular				+					
Glenodinium sp.					+			+	+
Glenodinium paululum								+	
Gymnodinium sp.					+			+	+
Gymnodinium simplex									+
Peridinium sp.								+	+
Peridinium aciculiferum					+				+
P. cinctum			+	+	+			+	+
P. divergens var. *oblongum*				+					
P. inconspicuum			+		+				
Peridiniella catenata				+		+	+		+
Protoperidinium bipes				+	+				+
P. granii				+					
Prorocentrum micans	+								
P. lima									+

is capable of forming blooms but is usually considered as harmless. Recent incidents with *P. micans* involving shellfish mortality was attributed to oxygen depletion (Faust and Gulledge, 2002). In our study we did not found this species.

Further studies of dinoflagellates were continued at the beginning of the 20th century (Kiselev, 1924; Vislouh, 1913, 1921). Ten species of photosynthetic dinoflagellate were found in phytoplankton in the outer part of the Neva Estuary in Koporskaya Bay and near Seskar Island in 1930: *Dinophysis ovum* var. *baltica* (Paulsen 1908), *P. cinctum*, *Diplopsalis lenticula* (Bergh 1881), *C. hirundinella*, *Ceratium longipes* ((Bailey) Gran 1902), *Peridinium divergens* var. *oblongum* (Aurivillius 1898), *Protoperidinium granii* ((Ostenfeld) Balech 1974), *Protoperidinium bipes* ((Paulsen) Balech 1974), *Protoperidinium pyriforme* subsp. *breve* ((Paulsen) E.Balech 1988), *Peridiniella catenata* ((Levander) Balech 1977) (Kiselev, 1948). Although the author did not provide numerical values of biomass, he noted that *P. catenata* was on the fourth place in the biomass of phytoplankton in Koporskaya Bay. This cold-loving species, found throughout the Baltic Sea (HELCOM, 2004), was found in 2003–2016 only three times in the samples from the Inner Estuary (Table 1). However, in 1935–1937, 1988 and 1997 this species was a sub-dominant species in phytoplankton of brackish water part of the Neva Estuary (Kiselev, 1948; Shishkin et al., 1989; Tereshenkova, 2006) (Table 2). Moreover, the dinoflagellate spring blooms of the mid 1990s in the Baltic Sea were dominated by *P. catenata* (Wasmund et al., 2011). This contrasted with the previous decade, when HELCOM (1996) did not report *P. catenata* in the list of the five most important spring species in 1979–1983.

Among other species found in the estuary in 2003–2016, *D. norvegica* is a typical species for the Baltic Sea (HELCOM, 2004). *P. lima* is a marine species found in the Kattegat and the Belt Sea, Arkona Basin, preferring coastal waters in these areas (HELCOM, 2004). In the Neva Estuary *P. lima* had the lowest abundance, although in some years their biomass was significant (Table 1). Its presence in the Neva Estuary was somewhat unexpected, as it has not been previously found in this part of the Baltic Sea. In the Neva Estuary, it occurred in the most marine part in 2005–2006, and its biomass was higher at the stations with higher salinity. After 2006, this species was not found. Perhaps his appearance was associated with an inoculation with ballast water by sea vessels. The fact is, that the sea traffic in this area is quite active; several cargo ports are located along the coast of the estuary. However, the conditions for this species in the estuary are not particularly suitable and after 2006 it disappeared. This dinoflagellate is also interesting because it releases toxins, which are dangerous for humans (Lassus et al., 2016).

Amphydinium spp., *Dinophysis rotundata* (Clapared & Lachmann 1859) and *P. bipes* that rarely occurred in brackish water part of the Neva Estuary in 2003–2016 (Table 1) are marine species found throughout the Baltic Sea (HELCOM, 2004).

3.2. Relationships between environmental factors and dinoflagellate community structure

The NMDS method used in this study provides insights about the abundance and distribution of dinoflagellate taxa,

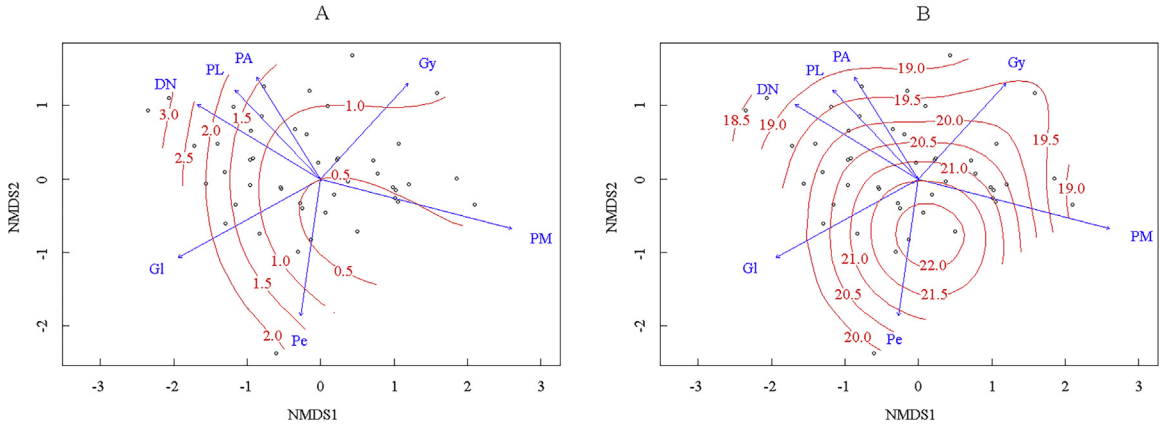

Figure 2 Dinoflagellates biomass vectors based on NMDS result and environmental variables in the Neva Estuary 2003–2016. Plot A: dinoflagellate biomass vectors and salinity (PSU), plot B: dinoflagellate biomass vectors and temperature (°C). DN — *Dinophysis norvegica*, PL — *Prorocentrum lima*, PA — *Peridinium aciculiferum*, PM — *Peridinium cinctum*, Pe — *Peridinium* sp., Gy — *Gymnodinium* sp., Gl — *Glenodinium* sp.

including some potentially toxic and bloom-forming species, along physiochemical gradients in an estuary under chronic anthropogenic nutrient enrichment. It enabled insight what environmental factors best explain dominant species composition and overall dinoflagellate assemblage structure and how they may be related to climate changes. We analyzed the factors influencing the composition of dinoflagellate community in the estuary and revealed species whose biomass significantly ($p < 0.05$) correlates with the studied environmental factors. These were 7 of 13 species that have been repeatedly encountered in the phytoplankton of the estuary and can be regarded as the most significant in the dinoflagellate community (Table 1). Biomasses of the other six species that were found in the estuary in different years did not show significant correlations with the studied factors. In most cases, this was explained by the fact that these were single findings (Table 1) and their number was insufficient for reliable correlations. Among these species, only *C. hirundinella* was found in all parts of the estuary at any studied environmental parameters.

Unidirectional vectors in a multidimensional space, for example, corresponding to the *D. norvegica*, *P. lima* and *P. aciculiferum* in Figs. 2–6, mean that changes in the biomass of these species, as a rule, are related similarly to the changes in some environmental factors. It is known that salinity and temperature are significant parameters influencing dinoflagellate assemblages in many regions (Price et al., 2017; Zonneveld et al., 2013).

In the Neva Estuary, the biomasses of *D. norvegica*, *P. aciculiferum* and *P. lima* were positively related to water salinity. These species showed higher biomasses with increasing water salinity (Fig. 2A). The marine species *D. norvegica* and *P. lima* were mainly found in the lower most marine part of the estuary. In contrast, *P. aciculiferum* was widely distributed throughout the estuary (Table 1), but higher biomass was in more saline waters. The oppositely directed *P. cinctum* vector means that this species reacted in the opposite way to the changes in the same environmental factors. The biomass of freshwater *P. cinctum* was higher in less saline waters (Fig. 2A). The transverse vectors of the *Peridinium* sp.,

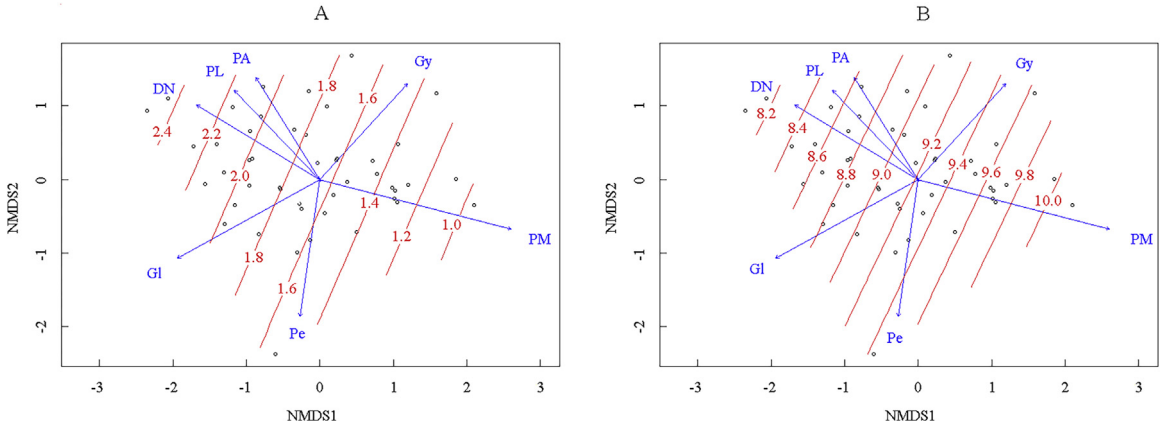

Figure 3 Dinoflagellates biomass vectors based on NMDS result and environmental variables in the Neva Estuary 2003–2016. Plot A: dinoflagellate biomass vectors and water transparency [m], plot B: dinoflagellate biomass vectors and concentrations of SPM [g m^{-3}]. DN — *Dinophysis norvegica*, PL — *Prorocentrum lima*, PA — *Peridinium aciculiferum*, PM — *Peridinium cinctum*, Pe — *Peridinium* sp., Gy — *Gymnodinium* sp., Gl — *Glenodinium* sp.

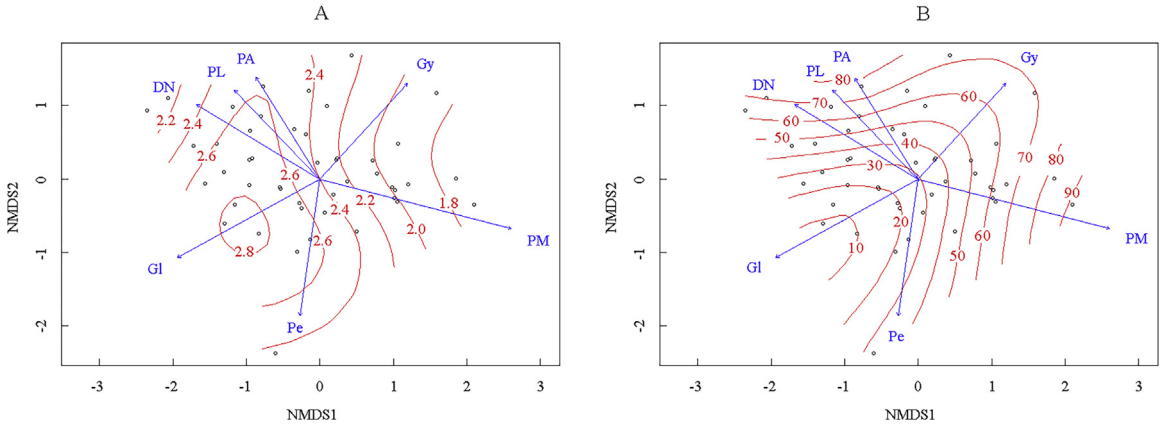

Figure 4 Dinoflagellates biomass vectors based on NMDS result and environmental variables in the Neva Estuary in 2003–2016. Plot A: dinoflagellate biomass vectors and the concentration of particulate organic matte [g m^{-3}], plot B: dinoflagellate biomass vectors and the concentration of total phosphorus [mg m^{-3}]. DN – *Dinophysis norvegica*, PL – *Prorocentrum lima*, PA – *Peridinium aciculiferum*, PM – *Peridinium cinctum*, Pe – *Peridinium* sp., Gy – *Gymnodinium* sp., Gl – *Glenodinium* sp.

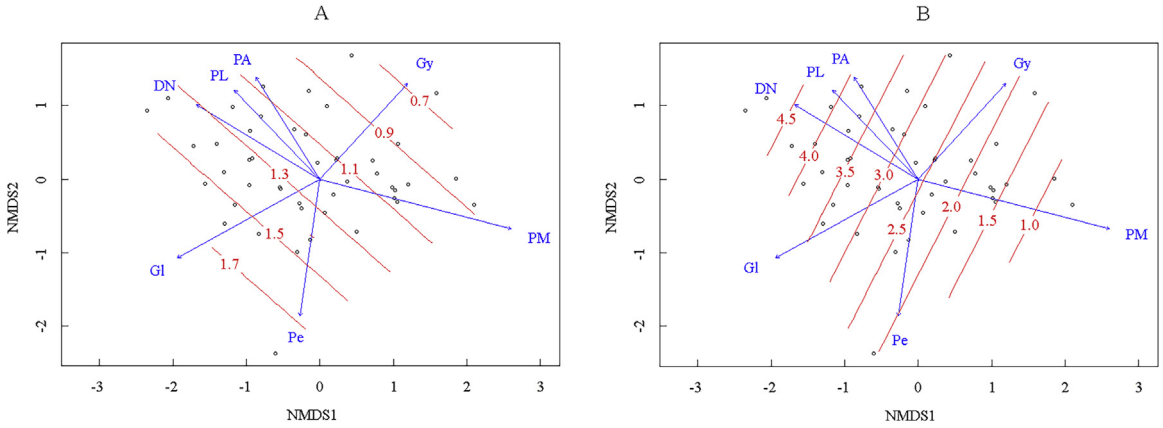

Figure 5 Dinoflagellates biomass vectors based on NMDS result and environmental variables in the Neva Estuary 2003–2016. Plot A: dinoflagellate biomass vectors and the rates of plankton primary production [gC m^{-2} day^{-1}], plot B: dinoflagellate biomass vectors and the rates of mineralization of organic matter [gC m^{-2} day^{-1}]. DN – *Dinophysis norvegica*, PL – *Prorocentrum lima*, PA – *Peridinium aciculiferum*, PM – *Peridinium cinctum*, Pe – *Peridinium* sp., Gy – *Gymnodinium* sp., Gl – *Glenodinium* sp.

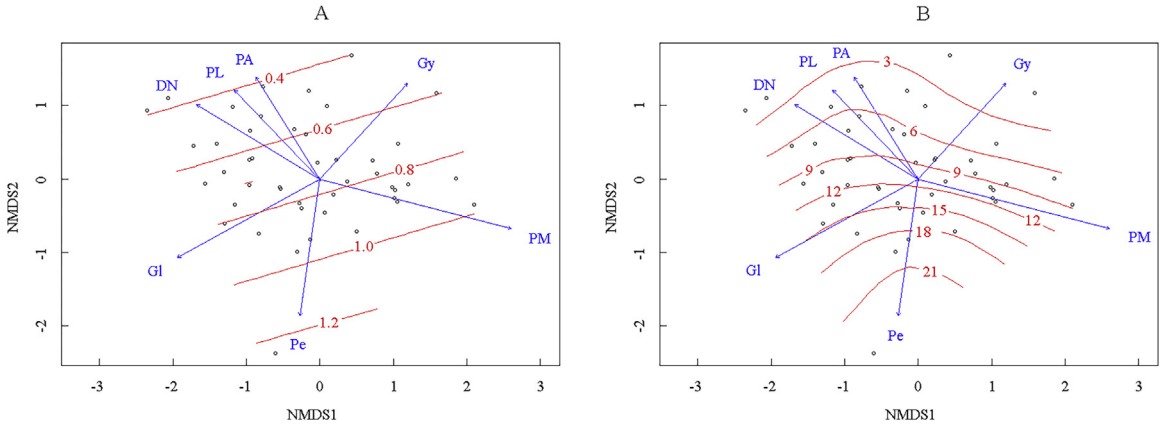

Figure 6 Dinoflagellates biomass vectors based on NMDS result and environmental variables in the Neva Estuary in 2003–2016. Plot A: dinoflagellate biomass vectors and PP/D ratio, plot B: dinoflagellate biomass vectors and chlorophyll *a* concentration [mg m^{-3}]. DN – *Dinophysis norvegica*, PL – *Prorocentrum lima*, PA – *Peridinium aciculiferum*, PM – *Peridinium cinctum*, Pe – *Peridinium* sp., Gy – *Gymnodinium* sp., Gl – *Glenodinium* sp.

Gymnodinium sp. and *Glenodinium* sp. mean that other, different from the first group, environmental factors significantly influenced their biomass, although these species preferred relatively salt waters. The biomass of these species did not show a significant correlation with water salinity, i.e., salinity was not a significant factor for them.

The temperature also had an effect on dinoflagellates in the Neva Estuary. Most species preferred relatively low temperatures. Only *Peridinium* sp. showed high biomass at the temperatures above 20°C. Biomasses of the other species were higher at lower temperatures (Fig. 2B). Similar result was obtained in the East China Sea, where two obvious picks of dinoflagellate pigments were recorded at temperatures ~18°C and ~25°C (Xiao et al., 2018). Well-known late spring dinoflagellate blooms (*Gymnodinium* and *Prorocentrum* species) in the East China Sea occured at the temperatures of ~18°C (Guo et al., 2014). In the Baltic Sea many dinoflagellates prefer low temperatures in summer perhaps due to nutrients coming up to surface by vertical mixing in cold weather and during cold water period. For example, the largest biomass of *D. norvegica* in the Baltic Sea was recorded at the thermocline boundary at about 12°C, as higher temperatures did not contribute to the growth of this species (Carpenter et al., 1995). Another closely related species, *D. rotundata*, also widespread in the Baltic Sea (HELCOM, 2004), was registered in 2003 at four stations in the south-western part of the estuary (Table 1) in the period of intensive upwelling of bottom cold waters in that area.

The negative reaction of most species of dinoflagellate in the Neva Estuary to the increase in summer water temperature may be partly explained by sharp domination in phytoplankton of toxin producing cyanobacteria in the years with high temperature (Nikulina and Gubelit, 2011). This should adversely affect other species of phytoplankton, including dinoflagellates (Carpenter et al., 1995; Codd and Poon, 1988; Sivonen et al., 1989). In recent years, a trend to lower water temperatures in summer was observed in St. Petersburg region caused by the predominance of cloudy and rainy weather (Golubkov and Golubkov, 2018) that might contribute to the development of dinoflagellate species.

Transparency of the water was important for photosynthetic dinoflagellates. The biomass of *P. cinctum* was higher in the waters with low transparency and high concentration of SPM (Fig. 3). The biomasses of *D. norvegica*, *P. aciculiferum* and *P. lima* were significantly higher in relatively transparent waters with low concentration of SPM. Water transparency and SPM concentrations did not have a significant effect on the biomasses of *Gymnodinium* sp., *Glenodinium* sp. and *Peridinium* sp. (Fig. 3).

The biomass of most species was lower at relatively high concentrations of SOM (Fig. 4A). High concentration of SOM especially negatively affected the biomass of *P. cinctum*. Only biomass of *Glenodinium* sp. was higher in the waters with high SOM concentration. The biomass of *Gymnodinium* sp. has not shown relationships with this environmental parameter (Fig. 4A). The reaction of various dinoflagellates to water transparence and the amounts of SPM and SOM was completely different. This is possibly explained by the ability of dinoflagellates to mixotrophic feeding. Practically all phototrophic dinoflagellates are suggested to be mixotrophic (Jeong et al., 2008). The mixotrophic and heterotrophic dinoflagellates are able to feed on diverse prey items including bacteria, picoeukaryotes, nanoflagellates, diatoms, other dinoflagellates, heterotrophic protists, metazoans and probably organic particles due to their diverse feeding mechanisms (Burkholder et al., 2008; Hansen, 2011; Jeong et al., 2010). For instance, mixotrophy appears to be quite common among species of *Dinophysis*, *Prorocentrum* (Hansen, 2011; Jeong et al., 2010). Food uptake of some *Dinophysis* species may provide them with ~80% of their carbon needs at high prey concentrations (Riisgaard and Hansen, 2009).

The total phosphorus concentration positively influenced most dinoflagellate species in the Neva Estuary. The biomass of *D. norvegica, P. lima, P. aciculiferum, P. cinctum* and *Gymnodinium* sp. was higher in the waters with higher concentration of total phosphorus (Fig. 4B). This suggests that autotrophy was also important trophic mode for these species. For instance, there was a definite *Prorocentrum* cyst eutrophication signal in some estuaries of the North-Western Atlantic, thus confirming their value as indicators of water quality change and anthropogenic impact (Price et al., 2017). A negative relationship was observed only for *Glenodinium* sp. *Peridinium* sp. did not show any correlation with total phosphorus concentration (Fig. 4B).

The biomass of dinoflagellates was also related to the rate of plankton primary production. The biomass of *Glenodinium* sp. and *Peridinium* sp. were higher in the waters with high primary production, whereas *Gymnodinium* sp. was more abundant in the waters with lower primary production (Fig. 5A). Biomass of *D. norvegica, P. lima* and *P. aciculiferum* did not show relationships with primary production. At the same time, these species had a larger biomass in the waters with high rate of organic matter mineralization (Fig. 5B). This probably indicated that bacteria played an important role in the feeding of these species. Although the dinoflagellates may have difficulty in detecting and capturing tiny bacterium cells, some species fed on a single bacterium cell like filter/interception feeders; they generate feeding currents using the flagella (Jeong et al., 2008).

The ratio of primary production and mineralization of organic matter shows which processes prevail. The PP/D ratio above one indicates eutrophication of water area. The biomass of *Peridinium* sp. was significantly higher in the waters with high PP/D (Fig. 6A). On the contrary, the biomasses of *D. norvegica*, *P. aciculiferum* and *P. lima* were higher with the predominance of mineralization processes over primary production. Biomass of *Gymnodinium* sp., *Glenodinium* sp. showed no relation with this parameter.

A similar pattern was demonstrated by the relationship between the biomass of dinoflagellates and the concentration of chlorophyll *a*. The biomass of *Peridinium* sp. was higher in the waters with high chlorophyll *a* concentration, whereas the biomasses of *D. norvegica*, *P. aciculiferum* and *P. lima* were higher at the stations with lower concentrations of the pigment (Fig. 6B). Unlike SOM concentration (Fig. 4B), this parameter did not affect the biomasses of *P. cinctum* and *Glenodinium* sp. Consequently, their biomasses were influenced by the concentration of SOM, which was not related to algae.

Biomass of *Glenodinium* sp. and *Peridinium* sp. positively correlated with primary production, and biomass of *Peridinium* sp. also positively reacted to an increase in the concentration of chlorophyll *a* and the PP/D ratio

(Figs. 5A and 6). However, these species did not show a positive relationship with phosphorus (Fig. 4B). This may be due to the fact that *Glenodinium* sp. and *Peridinium* sp. in the conditions of the Neva Estuary, apparently, are more consumers than producers of organic matter, feeding on algae and cyanobacteria of phytoplankton. Therefore, they responded positively to the increase in biomass and productivity of other phytoplankton species.

The proliferation of dinoflagellate could be due to an increase in runoff of organic substances from the catchment area induced by climate change. Model simulations predict that the climate change in the Baltic Sea region will result in a strong increase in precipitation and river discharge which, in turn, will lead to an increase in nutrient load and runoff of particulate and dissolved organic matter from the catchment area (Friedland et al., 2012; Meier et al., 2012). In this case, the changing conditions will contribute to the development of species that react positively to the increase in suspended and dissolved organic matter and associated bacteria, as well as an increase in nutrient load.

4. Conclusions

Twenty one dinoflagellate species were noted in the plankton of the Russian part of the Gulf of Finland at different times since the mid-19th century. Thirteen distinct species were observed in the present investigation and nine of them could be identified to species level. The statistical analysis showed that different species of dinoflagellates differ in relation to changes in environmental factors. Biomasses of *D. norvegica*, *P. lima* and *P. aciculiferum* had very similar relationships with investigated environmental variables that included salinity, temperature, phosphorus and suspended particulate organic matter concentrations. The biomasses of the other common species, *P. cinctum* and *Peridinium* sp., showed quite opposite trends. Current climate fluctuations leading to changes in temperature, salinity, nutrient and organic matter runoff from the catchment area could significantly affect the composition and productivity of the dinoflagellate community. At the same time, when interpreting the results of the analysis, it should be taken into account that the species of this group is characterized by mixotrophy and, consequently, their biomass may depend not only on the conditions of autotrophic, but also heterotrophic nutrition.

Acknowledgements

This work was supported by the Presidium of the Russian Academy of Sciences, program no. 41 “Biodiversity of natural systems and biological resources of Russia” and by the Russian Ministry of Science and Higher Education, project no. AAAA-A17-117021310121-0. We thank two anonymous reviewers for valuable comments that substantially improved the manuscript.

References

Anderson, D.M., Glibert, P.M., Burkholder, J.M., 2002. Harmful algal blooms and eutrophication: nutrient sources, composition and consequences. Estuaries 25 (4), 704—726, http://dx.doi.org/10.1007/BF02804901.

Brandt, J.F., 1845. Über mehrere der Nähe von St. Petersburg im Sommer des Jahres 1843 beobachtete Infusorienarten. Bull. de la classe phys.-math. de l'Ac. Imp. des Science de St. Petersburg 3 (2), 26—28.

Burkholder, J.M., Glibert, P.M., Skelton, H.M., 2008. Mixotrophy, a major mode of nutrition for harmful algal species in eutrophic waters. Harmful Algae 8 (1), 77—93, http://dx.doi.org/10.1016/j.hal.2008.08.010.

Carpenter, E.J., Janson, S., Boje, R., Pollehne, F., Chang, J., 1995. The dinoflagellate *Dinophysis norvegica*: biological and ecological observations in the Baltic Sea. Eur. J. Phycol. 30 (1), 1—9, http://dx.doi.org/10.1080/09670269500650751.

Codd, G.A., Poon, G.K., 1988. Cyanobacterial toxins. In: Rogers, L.J., Gallon, J.G. (Eds.), Biochemistry of the Algae and Cyanobacteria. Clarendon Press, Oxford, 283—296.

Craveiro, S.C., Daugbjerg, N., Moestrup, Ø., Calado, A.J., 2016. Studies on *Peridinium aciculiferum* and *Peridinium malmogiense* (=*Scrippsiella hangoei*): comparison with *Chimonodinium lomnickii* and description of *Apocalathium* gen. nov. (Dinophyceae). Phycologia 56 (1), 21—35, http://dx.doi.org/10.2216/16-20.1.

Eggleton, T., 2018. Future physical changes. In: Phillips, B.F., Pérez-Ramírez, M. (Eds.), Climate Change Impacts on Fisheries and Aquaculture. A Global Analysis. Volume I. Wiley Blackwell, Chichester, New York, 23—44.

Faust, M.A., Gulledge, R.A., 2002. Identifying harmful marine dinoflagellates. Contributions from the United States National Herbarium, vol. 42, 1—144.

Friedland, R., Neumann, T., Schernewski, G., 2012. Climate change and the Baltic Sea action plan: model simulations on the future of the western Baltic Sea. J. Marine Syst. 105-108, 175—186, http://dx.doi.org/10.1016/j.jmarsys.2012.08.002.

Gagnon, R., 2005. Growth stimulation of *Alexandrium tamarense* (Dinophyceae) by humic substances from the Manicouagan river (Eastern Canada). J. Phycol. 41 (3), 489—497, http://dx.doi.org/10.1111/j.1529-8817.2005.00077.x.

Glibert, P.M., Allen, J.I., Bouwman, A.F., Brown, C.W., Flynn, K.J., Lewitus, A.J., Madden, C.J., 2010. Modeling of HABs and eutrophication: Status, advances, challenges. J. Marine Syst. 83 (3—4), 262—275, http://dx.doi.org/10.1016/j.jmarsys.2010.05.004.

Golubkov, M.S., 2009. Phytoplankton primary production in the Neva Estuary at the turn of the 21st Centaury. Inland Water Biol. 2 (4), 312—318, http://dx.doi.org/10.1134/S199508290904004X.

Golubkov, M.S., Golubkov, S.M., 2018. The effect of weather conditions on eutrophication in the Neva Estuary. Dokl. Biol. Sci. 480 (1), 110—113, http://dx.doi.org/10.1134/S0012496618030122.

Golubkov, S., Golubkov, M., Tiunov, A., Nikulina, L., 2017. Long-term changes in primary production and mineralization of organic matter in the Neva Estuary (Baltic Sea). J. Marine Syst. 171, 73—80, http://dx.doi.org/10.1016/j.jmarsys.2016.12.009.

Grasshoff, K., Ehrhardt, M., Kremling, K., 1999. Methods of Seawater Analysis, 3rd ed. Wiley-VCH, Weinheim, New York, Chichester, Brisbane, Singapore, Toronto, 600 pp.

Guiry, M.D., Guiry, G.M., 2018. AlgaeBase. World-wide Electronic Publication. Natnl. Univ. Ireland, Galway, http://www.algaebase.org.

Guo, S., Feng, Y., Wang, L., Dai, M., Liu, Z., Bai, Y., Sun, J., 2014. Seasonal variation in the phytoplankton community of a continental-shelf sea: the East China Sea. Mar. Ecol. Prog. Ser. 516, 103—126, http://dx.doi.org/10.3354/meps10952.

Hall Jr., R.O., Thomas, S., Gaiser, E.E., 2007. Measuring freshwater primary production and respiration. In: Fahey, T.J., Knapp, A.K. (Eds.), Principles and Standards for Measuring Primary Production. Oxford University Press, Oxford, New York, 175—203.

Hansen, P.J., 2011. The role of photosynthesis and food uptake for the growth of marine mixotrophic Dinoflagellates. J. Eukaryot. Microbiol. 58 (3), 203—214, http://dx.doi.org/10.1111/j.1550-7408.2011.00537.x.

Heisler, J., Glibert, P.M., Burkholder, J.M., Anderson, D.M., Cochlan, W., Dennison, W.C., Dortch, Q., Gobler, C.J., Heil, C.A., Humphries, E., Lewitus, A., Magnien, R., Marshall, H.G., Sellner, K., Stockwell, D.A., Stoecker, D.K., Suddleson, M., 2008. Eutrophication and harmful algal blooms: a scientific consensus. Harmful Algae 8, 3—13, http://dx.doi.org/10.1016/j.hal.2008.08.006.

HELCOM, 1996. Third periodic assessment of the state of the marine environment of the Baltic Sea, 1989—1993. BSEP 64 (B), 1—252.

HELCOM, 2004. Checklist of Baltic Sea phytoplankton species. BSEP 95, 1—210.

Hense, I., 2010. Approaches to model the life cycle of harmful algae. J. Marine Syst. 83 (3—4), 108—114, http://dx.doi.org/10.1016/j.jmarsys.2010.02.014.

Jaanus, A., Hajdu, S., Kaitala, S., Andersson, A., Kaljurand, K., Ledaine, I., Lips, I., Olenina, I., 2006. Distribution patterns of isomorphic cold-water dinoflagellates (Scrippsiella/Woloszynskia complex) causing 'red tides' in the Baltic Sea. Hydrobiologia 554 (1), 137—146, http://dx.doi.org/10.1007/s10750-005-1014-7.

Jeong, H.J., Seong, K.A., Yoo, Y.D., Kim, T.H., Kang, N.S., Kim, S., Park, J.Y., Kim, J.S., Kim, G.H., Song, J.Y., 2008. Feeding and grazing impact by small marine heterotrophic dinoflagellates on hetertrophic bacteria. J. Eukaryot. Microbiol. 55 (4), 271—288, http://dx.doi.org/10.1111/j.1550-7408.2008.00336.x.

Jeong, H.J., Yoo, Y.D., Kim, J.S., Seong, K.A., Kang, N.S., Kim, T.H., 2010. Growth, feeding and ecological roles of the mixotrophic and heterotrophic dinoflagellates in marine planktonic food webs. Ocean Sci. J. 45 (2), 65—91, http://dx.doi.org/10.1007/s12601-010-0007-2.

Kiselev, I.A., 1924. Phytoplankton of the Neva Bay and the eastern part of the Gulf of Finland. Hydrological and hydrobiological studies of the Neva Bay. Studies of the Neva River and its basin. Russian Hydrol. Inst., Leningrad, 55 pp. (in Russian).

Kiselev, I.A., 1948. About the phytoplankton of the brackish-water part of the Gulf of Finland. In: Zhadin, V.I. (Ed.), In Memory of Academician S.A. Zernov. Academy of Sciences of the USSR, Leningrad, 192—205, (in Russian).

Kiselev, I.A., 1954. The Determinant of Freshwater Algae of the USSR. Soviet Science, Moscow, 212 pp. (in Russian).

Klais, R., Tamminen, T., Kremp, A., Spilling, K., Olli, K., 2011. Decadal-scale changes of dinoflagellates and diatoms in the anomalous Baltic Sea spring bloom. PLoS ONE 6 (6), e21567, http://dx.doi.org/10.1371/journal.pone.0021567.

Kremp, A., Tamminen, T., Spilling, K., 2008. Dinoflagellate bloom formation in natural assemblages with diatoms: nutrient competition and growth strategies in Baltic spring phytoplankton. Aquat. Microb. Ecol. 50 (2), 181—196, http://dx.doi.org/10.3354/ame01163.

Kuosa, H., Fleming-Lehtinen, V., Lehtinen, S., Lehtiniemi, M., Nygård, H., Raateoja, M., Raitaniemi, J., Tuimala, J., Uusitalo, L., Suikkanen, S., 2017. A retrospective view of the development of the Gulf of Bothnia ecosystem. J. Marine Syst. 167, 78—92, http://dx.doi.org/10.1016/j.jmarsys.2016.11.020.

Lange, E.K., 2006. Analysis of structural indicators of the midsummer phytoplankton of the Neva Bay for a 90-year period. In: Lavrent'eva, G.M., Susloparova, O.N. (Eds.), Ecological Aspects of the Impact of Hydro Construction on the Biota of the Eastern Part of the Gulf of Finland, FGNU GosNIORH, St. Petersburg, 122—146, (in Russian).

Lassus, P., Chomérat, N., Hess, P., Nézan, E., 2016. Toxic and harmful microalgae of the World Ocean. Micro-algues toxiques et nuisibles de l'Océan Mondial. In: International Society for the Study of Harmful Algae/Intergovernmental Oceanographic Commission of UNESCO. Copenhagen, 523 pp.

Meier, H.E.M., Hordoir, R., Andersson, H.C., Dieterich, C., Eilola, K., Gustafsson, B.G., Höglund, A., Schimanke, S., 2012. Modeling the combined impact of changing climate and changing nutrient loads on the Baltic Sea environment in an ensemble of transient simulations for 1961—2099. Clim. Dynam. 39 (9—10), 2421—2441, http://dx.doi.org/10.1007/s00382-012-1339-7.

Nikulina, V.N., 1987. Dynamics of numbers and biomass of phytoplankton. In: Vinberg, G.G., Gutelmakher, B.L. (Eds.), Neva Bay: Hydrobiological Investigations. Nauka, Leningrad. 20—29, (in Russian).

Nikulina, V.N., 2003. Seasonal dynamics of phytoplankton in the shallow zone of the eastern part of the Gulf of Finland in the 1980s and 1990s. Oceanologia 45 (1), 25—39.

Nikulina, V.N., Gubelit, Y.I., 2011. Cyanobacteria and macroalgae in ecosystem of the Neva estuary. Knowl. Manag. Aquat. Ecosyst. 402 (06), 12 pp., http://dx.doi.org/10.1051/kmae/2011049.

Oksanen, J., Blanchet, F.G., Friendly, M., Kindt, R., Legendre, P., McGlinn, D., Minchin, P.R., O'Hara, R.B., Simpson, G.L., Solymos, P., Stevens, M.H.H., Szoecs, E., Wagner, H., 2017. Vegan: Community Ecology Package (Version 2.4-5) [Software], Retrieved from: https://CRAN.R-project.org/package=vegan.

Olenina, I., Hajdu, S., Edler, L., Andersson, A., Wasmund, N., Busch, S., Göbel, J., Gromisz, S., Huseby, S., Huttunen, M., Jaanus, A., Kokkonen, P., Ledaine, I., Niemkiewicz, E., 2006. Biovolumes and size-classes of phytoplankton in the Baltic Sea. BSEP 106, 1—144.

Olli, K., Trunov, K., 2010. Abundance and distribution of vernal bloom dinoflagellate cysts in the Gulf of Finland and Gulf of Riga (the Baltic Sea). Deep-Sea Res. Pt. II 57 (3—4), 235—242, http://dx.doi.org/10.1016/j.dsr2.2009.09.009.

Pankov, H., 1976. Algenflora der Ostsee 1. Plankton, Fischer-Verlag, Stuttgart, 493 pp.

Price, A.M., Coffin, M.R.S., Pospelova, V., Latimer, J.S., Chmura, G. L., 2017. Effect of nutrient pollution on dinoflagellate cyst assemblages across estuaries of the NW Atlantic. Mar. Pollut. Bull. 121 (1—2), 339—351, http://dx.doi.org/10.1016/j.marpolbul.2017.06.024.

R Development Core Team, 2017. The R Project for Statistical Computing (Version 3.4.0) [Software], Retrieved from: http://www.r-project.org.

Riisgaard, K., Hansen, P.J., 2009. Role of food uptake for photosynthesis, growth and survival of mixotrophic dinoflagellate *Dinophysis acuminata*. Mar. Ecol. Prog. Ser. 381, 51—62.

Sandberg, J., Andersson, A., Johansson, S., Wikner, J., 2004. Pelagic food web structure and carbon budget in the northern Baltic Sea: potential importance of terrigenous carbon. Mar. Ecol. Prog. Ser. 268, 13—29.

Shishkin, B.A., Nikulina, V.N., Maksimov, A.A., Silina, N.I., 1989. The main characteristics of the biota of the upper part of the Gulf of Finland and its role in the formation of water quality. Investigations of the Neva River, the Neva Bay and the eastern part of the Gulf of Finland. Gidrometeoizdat, Leningrad, 96 pp. (in Russian).

Sivonen, K., Kononen, K., Esaca, A.L., Niiemela, S.I., 1989. Toxicity and isolation of the cyanobacterium *Nodularia spumigena* from the southern Baltic Sea in 1986. Hydrobiologia 185, 3—8.

Skarlato, S., Filatova, N., Knyazev, N., Berdieva, M., Telesh, I., 2018. Salinity stress response of the invasive dinoflagellate *Prorocentrum minimum*. Estuar. Coast. Shelf Sci. 211, 199—207, http://dx.doi.org/10.1016/j.ecss.2017.07.007.

Smayda, T.T., 2002. Adaptive ecology, growth strategies and the global bloom expansion of dinoflagellates. J. Oceanogr. 58 (2), 281—294.

Smayda, T.T., Reynolds, C.S., 2003. Strategies of marine dinoflagellate survival and some rules of assembly. J. Sea Res. 49, 95—106, http://dx.doi.org/10.1016/S1385-1101(02)00219-8.

Smayda, T.J., Trainer, V.L., 2010. Dinoflagellate blooms in upwelling systems: Seeding, variability, and contrasts with diatom bloom behaviour. Prog. Oceanogr. 85 (1—2), 92—107, http://dx.doi.org/10.1016/j.pocean.2010.02.006.

Telesh, I.V., Schubert, H., Skarlato, S.O., 2016. Ecological niche partitioning of the invasive dinoflagellate *Prorocentrum minimum* and its native congeners in the Baltic Sea. Harmful Algae 59, 100—111, http://dx.doi.org/10.1016/j.hal.2016.09.006.

Tereshenkova, T.V., 2006. Comparative characteristics of the mid-summer phytoplankton of the Gulf of Vyborg, the Luga and Koporsk Bay, the Bierkesund Strait and the eastern part of the Gulf of Finland. In: Lavrent'eva, G.M., Susloparova, O.N. (Eds.), Ecological Aspects of the Impact of Hydro Construction on the Biota of the Eastern Part of the Gulf of Finland, FGNU GosNIORH, St. Petersburg, 37—86, (in Russian).

Tikkanen, T., 1986. Kasviplannktonpas. Suomen Luonnosujelun Tuki Oy, Helsinki. 278 pp.

Vernet, M., Smith, R.C., 2007. Measuring and modeling primary production in marine pelagic ecosystems. In: Fahey, T.J., Knapp, A.K. (Eds.), Principles and Standards for Measuring Primary Production. Oxford University Press, Oxford, New York, 142—174.

Vislouh, S.M., 1913. A Brief Report on Biological Investigations of the Neva Bay in 1911—1913, St. Petersburg, 98 pp. (in Russian).

Vislouh, S.M., 1921. To the knowledge of the microorganisms of the Neva Bay. Proc. Russian Hydrol. Inst. 1—3, 83—96, (in Russian).

Wasmund, N., Uhlig, S., 2003. Phytoplankton trends in the Baltic Sea. ICES J. Mar. Sci. 60 (2), 177—186, http://dx.doi.org/10.1016/S1054-3139(02)00280-1.

Wasmund, N., Tuimala, J., Suikkanen, S., Vandepitte, L., Kraberg, A., 2011. Long-term trends in phytoplankton composition in the western and central Baltic Sea. J. Marine Syst. 87 (2), 145—159, http://dx.doi.org/10.1016/j.jmarsys.2011.03.010.

Xiao, W., Liu, X., Irwin, A.J., Laws, E.A., Wang, L., Chen, B., Zeng, Y., Huang, B., 2018. Warming and eutrophication combine to restructure diatoms and dinoflagellates. Water Res. 128, 206—218, http://dx.doi.org/10.1016/j.watres.2017.10.051.

Zhou, Z.X., Yu, R.C., Zhou, M.J., 2017. Seasonal succession of microalgal blooms from diatoms to dinoflagellates in the East China Sea: A numerical simulation study. Ecol. Model. 360, 150—162, http://dx.doi.org/10.1016/j.ecolmodel.2017.06.027.

Zonneveld, K.A.F., Marret, F., Versteegh, G.J.M., Bogus, K., Bonnet, S., Bouimetarhan, I., Crouch, E., de Vernal, A., Elshanawany, R., Edwards, L., Esper, O., Forke, S., Grøsfjeld, K., Henry, M., Holzwarth, U., Kielt, J.-F., Kim, S.-Y., Ladouceur, S., Ledu, D., Chen, L., Limoges, A., Londeix, L., Lu, S.-H., Mahmoud, M.S., Marino, G., Matsouka, K., Matthiessen, J., Mildenhal, D.C., Mudie, P., Neil, H.L., Pospelova, V., Qi, Y., Radi, T., Richerol, T., Rochon, A., Sangiorgi, F., Solignac, S., Turon, J.-L., Verleye, T., Wang, Y., Wang, Z., Young, M., 2013. Atlas of modern dinoflagellate cyst distribution based on 2405 data points. Rev. Palaeobotany Palyno 191, 1—197, http://dx.doi.org/10.1016/j.revpalbo.2012.08.003.

Oceanologia (2019) 61, 208–217

Available online at www.sciencedirect.com

ScienceDirect

journal homepage: www.journals.elsevier.com/oceanologia/

ORIGINAL RESEARCH ARTICLE

Trophic connectivity between intertidal and offshore food webs in Mirs Bay, China

Jiajia Ning [a,b,c], **Feiyan Du** [a,b,c,*], **Xuehui Wang** [a,b,c], **Lianggen Wang** [a,b,c], **Yafang Li** [a,b,c]

[a] *South China Sea Fisheries Research Institute, Chinese Academy of Fishery Sciences, Guangzhou, China*
[b] *Guangdong Provincial Key Laboratory of Fishery Ecology and Environment, Guangzhou, China*
[c] *Key Laboratory of South China Sea Fishery Resources Exploitation & Utilization, Ministry of Agriculture and Rural Affairs, Guangzhou, China*

Received 2 August 2018; accepted 11 October 2018
Available online 22 October 2018

KEYWORDS
Food webs;
Trophic connectivity;
Carbon pathways;
Stable isotopes;
Mirs Bay

Summary Trophic interactions are common worldwide, both within and between ecosystems. This study elucidated the trophic connectivity between intertidal and offshore zone, in Mirs Bay, China. The contributions of offshore suspended particulate organic matter (SPOM), intertidal macroalgae and epiphytes to consumer biomass were assessed, and the trophic pathways were identified through the use of stable isotope ratios of carbon ($\delta^{13}C$) and nitrogen ($\delta^{15}N$) of basal sources and consumers. Mean $\delta^{13}C$ values of basal sources had a wide range (−19.6‰ to −11.8‰) and were generally well separated in Mirs Bay. The average $\delta^{13}C$ of consumers in Mirs Bay ranged from −19.2‰ to −11.8‰, reflecting a carbon source integrated from different primary producer signals. IsoSource model solutions indicated consumers assimilated organic carbon from a mixture of basal sources. Offshore SPOM carbon was the primary carbon source supporting most consumers in both intertidal and offshore zones. Intertidal macroalgae and epiphytes also accounted for a large fraction for some consumers. $\delta^{15}N$ data indicated 5 trophic levels in Mirs Bay. Intertidal consumers, except for *Capitulum mitella*, had a TP (trophic position) between 2 and 3, and mainly included filter-feeders and grazers. In contrast, almost all offshore consumers had a TP of between 3 and 4 except for filter-feeders (zooplankton), planktivores (*Clupanodon punctatus* and *Sardinella aurita*) and piscivores (*Gymnura japonica*). The basal sources fueled consumers

* Corresponding author at: 231 Xingangxi Road, Guangzhou 510300, China. Tel.: +86 20 34063761. Fax: +86 20 84451442.
E-mail address: feiyanegg@163.com (F. Du).

Peer review under the responsibility of Institute of Oceanology of the Polish Academy of Sciences.

ELSEVIER Production and hosting by Elsevier

https://doi.org/10.1016/j.oceano.2018.10.001

through two trophic pathways, each of which involved organisms of both intertidal and offshore zones, implying trophic connectivity between them in the Mirs Bay ecosystem.

1. Introduction

Food webs among different habitats vary greatly in the abundances of their basal sources, community composition and productivity, leading to food webs being spatially heterogeneous. Trophic interactions are common among habitats because the nutrients, detritus, prey and consumers that comprise food webs often cross-habitat boundaries (Polis and Strong, 1996). Cross-habitat exchanges of materials can be of great importance to effective natural source dynamics both within and between ecosystems (Polis et al., 1997; Savage et al., 2012). For instance, in a deciduous forest and stream ecotone the populations of birds and fish, subsidized by aquatic insect and terrestrial invertebrate input, respectively, accounted for 25.6% and 44.0% of the annual total energy budget of the bird and fish assemblages (Nakano and Murakami, 2001). Abundant mangrove leaf litter from the intertidal zone promoted populations of the commercially important fisheries in adjacent coastal waters (Day et al., 2012).

Bays are complex ecosystems consisting of different habitats such as intertidal and offshore zones, which can be considered as interacting habitats (Jansson, 1988). The rhythmic movement of the tide is responsible for the materials exchange between intertidal and offshore zones and carries a diverse and abundant potential food source for consumers (Polis et al., 1997). In addition, consumers can move to forage across habitats according to prey availability (Mittelbach and Osenberg, 1993; Randall, 1965). Elucidating the trophic connectivity between intertidal and offshore zones is urgent because bay ecosystems are impacted by human activities in many regions of the world. For example, a large amount of intertidal areas has been destroyed by reclamation, which often changes the living environment and community structure of intertidal organisms (Lu et al., 2002). The result may be damage to the trophic interactions between intertidal and offshore zones. Thus, a current goal in ecological research is to quantitatively assess trophic relationships among spatially heterogeneous and contiguous, connected habitats (Claudino et al., 2015; Conway-Cranos et al., 2015). Knowledge of trophic relationships is crucial for researchers' understanding of bio-population ecology and natural resource management.

It is, however, difficult to elucidate trophic relationships using traditional methods. Stable isotopes have recently been used successfully to study trophic connectivity (Claudino et al., 2015; Selleslagh et al., 2015). Carbon stable isotope ratios ($\delta^{13}C$) change predictably between diet and consumer, and have been used in ecological studies to trace the flow of sources of organic matter in marine and freshwater ecosystems (Fry and Sherr, 1984; Peterson and Fry, 1987). In ecosystems, $\delta^{13}C$ values differ among phytoplankton (offshore zone) and macroalgae and epiphytes (intertidal zone) (Kang et al., 2008; Ouisse et al., 2012). Thus, $\delta^{13}C$ values can distinguish the basal sources of consumers, and researches can estimate the relative contribution of these primary producers to consumer biomass through IsoSource model of Phillips and Gregg (2003). In contrast, consumers are typically enriched in ^{15}N by 3–4‰ relative to their diet (Deniro and Epstein, 1981; Minagawa and Wada, 1984; Peterson and Fry, 1987). Therefore, stable nitrogen isotope ratios ($\delta^{15}N$) can be used to define their trophic position (TP), based on the pathways of energy flow (Post, 2002; Vander Zanden and Rasmussen, 1999).

In this context, the aims of this study were to (1) quantitatively assess the basal sources that support consumer biomass of intertidal and offshore zones to determine whether there is trophic interaction between these two zones in Mirs Bay; and (2) identify the main trophic pathways between the intertidal and offshore zones to highlight the importance of trophic connectivity.

2. Material and methods

2.1. Site description

Mirs Bay is northeast of Hong Kong and south of Shenzhen, south China. It is close to the Pearl River Estuary to the west and Daya Bay to the east. The Bay, part of the South China Sea, is semi-enclosed and has an area of 320 km^2 and a mean depth of 18 m. The coastline extends about 100 km, and is mostly rocky (Zhang et al., 2013). The sediment is sandy (Xia et al., 2005). The water movement in Mirs Bay is influenced primarily by the tide because no large river flows into it.

2.2. Sample collection and preparation

This research was undertaken at three intertidal zones and four offshore stations of Mirs Bay (Fig. 1). Samples were collected from intertidal zones and offshore stations representing different bio-community. The basal sources and consumers sampled at intertidal zones mainly included macroalgae, epiphyte and bivalves, barnacles, chitons, limpets, crabs as well as whelks. In contrast, the samples collected at offshore stations consisted of phytoplankton, zooplankton, fishes, shrimps, mantis shrimps, squids and crabs. Because the intertidal zones can submerge for several hours during high tides, so basal sources can exchange and consumers can forage between intertidal zones and offshore stations. Sampling was conducted in September 2013.

The most abundant basal sources (macroalgae and epiphytes) and the most common consumers (macroinvertebrates) were sampled during low tide at intertidal zones. All macroalgae and macroinvertebrates samples were collected by hand. Epiphyte samples were gently scraped from

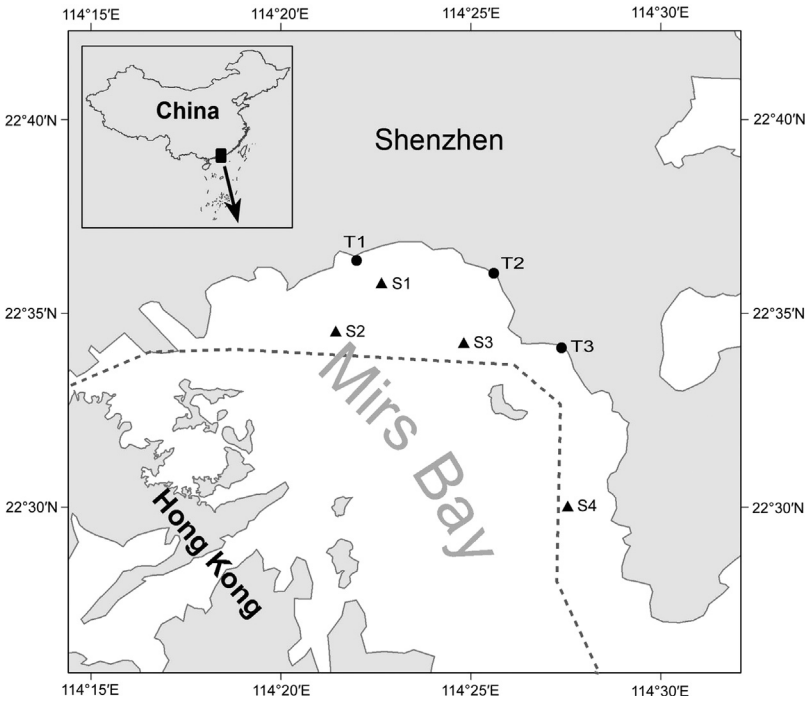

Figure 1 Map of Mirs Bay, China, showing the location of sampling stations and zones. Black triangles indicate location of offshore sampling stations; black circles indicate intertidal sampling zones.

rocks using a wire or nylon brush and carefully re-suspended in filtered seawater. They were then filtered onto precombusted (500°C, 4 h) Whatman GF/F filters. Experimental trawling was undertaken in four off-shore stations (ranging in depth from 12 to 19 m) from a commercial trawler. The catches (fish and macroinvertebrates) from each haul were stored in the field. Suspended particulate organic matter (SPOM) samples were obtained by filtering 5–7 L water at two depths (0.5 m and 10 m) using 4 L Niskin bottles from off-shore stations through pre-combusted (500°C, 4 h) Whatman GF/F filters, followed by manual removal of all visible zooplankton and other contaminants under a dissecting microscope (40× magnification). The SPOM samples were used to represent phytoplankton (Hill et al., 2006; Kaehler et al., 2000; Markel and Shurin, 2015). Mesozooplankton and macrozooplankton were sampled from vertical tows at off-shore stations using a zooplankton net with 505 μm mesh size. Zooplankton samples were maintained alive in filtered seawater for 2 h to allow gut evacuation. All samples were stored on ice and transported to the laboratory and frozen at −20°C.

In the laboratory, as copepods accounted for the majority of zooplankton abundance in Mirs Bay (unpublished data), they were handpicked under a dissecting microscope and transferred to pre-combusted tin cups immediately. Fish and macroinvertebrate samples were defrosted and then sorted, with specimens being identified to the lowest possible taxonomic level. A small piece of white muscle tissue was dissected from the dorsum of large fish. For small fish, the head and viscera were removed, and the remainder of the body (consisting primarily of white muscle) was retained for isotope analysis. Only muscle tissue was processed for macroinvertebrate samples. Because of low individual weight, a composite tissue sample from more than one individual of the same taxon was used for some macroinvertebrates, including small mollusks and crabs. All samples except zooplankton were washed with distilled water, dried (60°C, 48 h), ground to a fine powder and stored in glass vials for later isotope analysis.

2.3. Stable isotope analysis

Stable isotope analysis was conducted at the Chinese Academy of Agricultural Sciences Environmental Stable Isotope Laboratory, Beijing, China. To determine the $\delta^{13}C$ and $\delta^{15}N$ values for each sample, approximately 1–2 mg ground tissue was combusted using an NCE elemental analyzer (Vario PYRO Cube, Elementar) interfaced via continuous flow to an Isoprime 100 isotope-ratio mass spectrometer. Stable isotope ratios were expressed in the delta (δ) notation, defined as parts per thousand (per mil, ‰) deviation from a certified standard:

$$\delta^{13}C \text{ or } \delta^{15}N = \left[\left(\frac{R_{sample}}{R_{standard}}\right) - 1\right] \times 1000,$$

where $R = {}^{13}C/{}^{12}C$ or ${}^{15}N/{}^{14}N$. For carbon isotopes, the standard was Vienna Pee Dee Belemnite limestone, and atmospheric nitrogen was the nitrogen standard. Analytical errors were 0.08‰ for both $\delta^{13}C$ and $\delta^{15}N$.

2.4. Data analysis

Many species were collected from only one or two intertidal zones and offshore stations, preventing analysis of spatial variability within them. Therefore, data from different intertidal zones or offshore stations were pooled.

IsoSource model of Phillips and Gregg (2003) was used to estimate the percent contribution of basal sources to con-

sumer biomass. It allows multiple sources to be evaluated for each consumer using $\delta^{13}C$ measurements, and to apply this approach the $\delta^{13}C$ measurements of consumers were corrected for trophic fractionation (Post, 2002) using the TP assignments discussed below. Trophic fractionation of $\delta^{13}C$ for consumers was set at 0.4‰, representing the average value from reported fractionations (Post, 2002). Source increment was set at 1% and tolerance at 0.1%. In Mirs Bay the macroalgae *Amphiroa zonata* and *Enteromorpha* spp. had similar $\delta^{13}C$ values and were combined into the variable macroalgae.

The TP of each consumer was calculated as:

$$TP = 2 + (\delta^{15}N_{consumer} - \delta^{15}N_{baseline})/3.4,$$

where $\delta^{15}N_{consumer}$ was the $\delta^{15}N$ value of the consumer being evaluated, $\delta^{15}N_{baseline}$ was the average $\delta^{15}N$ value of the consumers used to estimate the base of the food web (*i.e.* mollusk species in this study) and 3.4‰ was the per trophic level fractionation of $\delta^{15}N$ according to Post (2002).

3. Results

3.1. Isotope signatures of basal sources

Three major potential basal sources for consumers were identified in Mirs Bay: the most abundant macroalgae species (*Enteromorpha* spp. and *Amphiroa zonata*) and epiphytes (consisting mainly of epilithic diatoms) collected from intertidal zones, and SPOM collected from offshore zones. The mean $\delta^{13}C$ values of basal sources had a wide range (−19.6‰ to −11.8‰): SPOM had the most depleted $\delta^{13}C$ value, and epiphytes had the most enriched values (Fig. 2). Macroalgae values were intermediate and had similar mean values between species (*Enteromorpha* spp. = −16.1‰ and *A. zonata* = −14.9‰).

SPOM samples had similar $\delta^{15}N$ values to epiphyte samples, and both of them were lower than those of the two macroalgae species (*Enteromorpha* spp. = 9.6‰ and *A. zonata* = 9.1‰).

3.2. Isotope signatures of consumers

A total of 32 species of consumers was collected and subjected to stable isotope analysis, comprising 9 intertidal macroinvertebrate taxa and 23 offshore species of animals.

The $\delta^{13}C$ signatures of consumers sampled at intertidal zones were relatively more variable than those collected from adjacent offshore zones (Fig. 2). The intertidal consumers had a range of $\delta^{13}C$ signatures from −17.9 (*Perna viridis*) to −11.8‰ (*Liolophura japonica*), whereas the offshore consumers varied between −19.2 (zooplankton) and −14.4‰ (*Gymnura japonica*). In intertidal zones, the bivalves (*P. viridis*, *Crassostrea rivularis* and *Arcopsis sculp-*

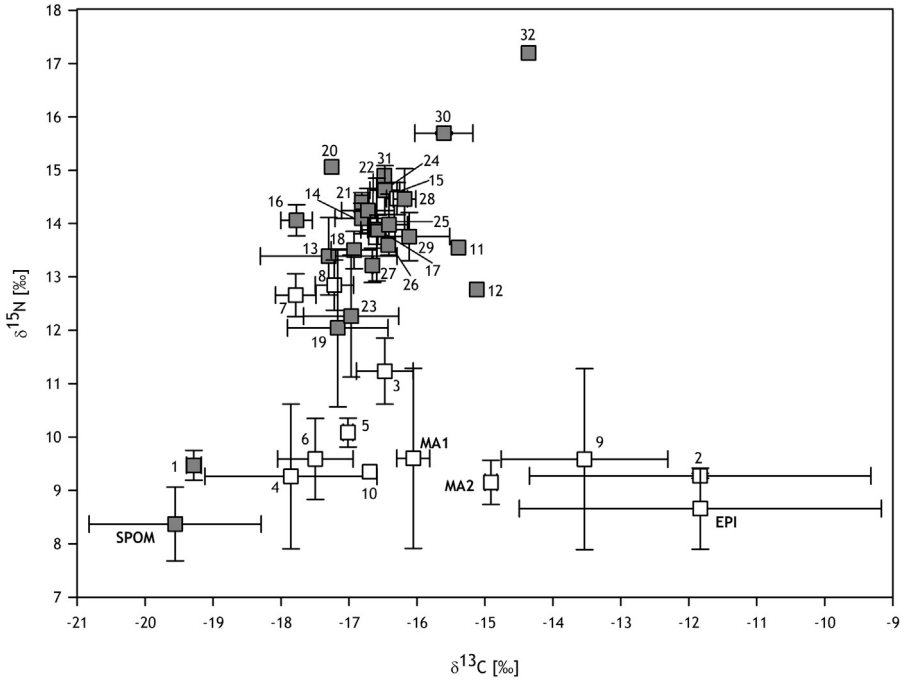

Figure 2 Mean $\delta^{13}C$ and $\delta^{15}N$ values (±SD) in basal sources and consumers from Mirs Bay, China. White squares and gray squares represent samples from intertidal zones and offshore stations, respectively. Abbreviations are as follows, SPOM = suspended particulate organic matter; MA1 = macroalgae *Enteromorpha* spp.; MA2 = macroalgae *Amphiroa zonata*; EPI = epiphytes. Numbers correspond to consumers discussed within the text. 1 = Zooplankton; 2 = *Liolophura japonica*; 3 = *Thais clavigera*; 4 = *Perna viridis*; 5 = *Crassostrea rivularis*; 6 = *Arcopsis sculptilis*; 7 = *Balanus* sp.; 8 = *Capitulum mitella*; 9 = *Cellana grata*; 10 = *Gaetice depressus*; 11 = *Charybdis feriatus*; 12 = *Portunus trituberculatus*; 13 = *Metapenaeus affinis*; 14 = *Oratosquilla oratoria*; 15 = *Loligo duvaucelii*; 16 = *Collichthys lucidus*; 17 = *Decapterus maruadsi*; 18 = *Caranx kalla*; 19 = *Clupanodon punctatus*; 20 = *Thrissa dussumieri*; 21 = *Nemipterus japonicus*; 22 = *Leiognathus brevirostris*; 23 = *Sardinella aurita*; 24 = *Polynemus sextarius*; 25 = *Trichiurus haumela*; 26 = *Gastrophysus spadiceus*; 27 = *Apogon striatus*; 28 = *Pagrosomus major*; 29 = *Rhabdosargus sarba*; 30 = *Gerres japonicus*; 31 = *Muraenesox cinereus*; 32 = *Gymnura japonica*.

Table 1 Means and ranges of basal source contributions (%) to consumer biomass in Mirs Bay, China, from IsoSource models. Bold values indicate high contributions from a single source.

Location	Species	SPOM		Macroalgae		Epiphytes	
		Mean	Range	Mean	Range	Mean	Range
Intertidal zone	*Liolophura japonica*	2.5	0–6	5.8	0–13	**91.8**	87–96
	Thais clavigera	**53.3**	37–69	30.7	0–63	15.9	0–33
	Perna viridis	**73.8**	64–83	17.3	0–36	8.9	0–19
	Crassostrea rivularis	**60.8**	47–74	25.7	0–53	13.4	0–28
	Arcopsis sculptilis	**68.3**	54–79	20.9	0–43	10.8	0–23
	Balanus sp.	**81.3**	74–88	12.3	0–26	6.4	0–14
	Capitulum mitella	**70.1**	59–80	19.8	0–41	10.1	0–21
	Cellana grata	14.0	0–29	29.9	0–62	**56.0**	38–73
	Gaetice depressus	**53.3**	37–69	30.7	0–63	15.9	0–33
Offshore zone	Zooplankton	**99.0**	98–100	1.0	0–2	0.0	0–1
	Charybdis feriatus	38.5	18–58	**40.4**	0–82	21.1	0–43
	Portunus trituberculatus	31.0	8–53	**45.4**	0–92	23.6	0–48
	Metapenaeus affinis	**73.8**	64–83	17.3	0–36	8.9	0–19
	Oratosquilla oratoria	**66.3**	54–78	22.2	0–46	11.4	0–24
	Loligo duvaucelii	**57.1**	42–71	28.2	0–58	14.7	0–30
	Collichthys lucidus	**83.1**	76–89	11.3	0–24	5.6	0–12
	Decapterus maruadsi	**60.8**	47–74	25.7	0–53	13.4	0–28
	Caranx kalla	**66.3**	54–78	22.2	0–46	11.4	0–22
	Clupanodon punctatus	**68.3**	57–79	20.9	0–43	10.8	0–23
	Thrissa dussumieri	**75.6**	66–84	16.3	0–34	8.1	0–17
	Nemipterus japonicus	**66.3**	54–78	22.2	0–46	11.4	0–22
	Leiognathus brevirostris	**64.5**	52–76	23.5	0–48	12.0	0–25
	Sardinella aurita	**64.5**	52–76	23.5	0–48	12.0	0–25
	Polynemus sextarius	**60.8**	47–74	25.7	0–53	13.4	0–28
	Trichiurus haumela	**60.8**	47–74	25.7	0–53	13.4	0–28
	Gastrophysus spadiceus	**57.1**	42–71	28.2	0–58	14.7	0–30
	Apogon striatus	**57.1**	42–71	28.2	0–58	14.7	0–30
	Pagrosomus major	**55.2**	39–70	29.4	0–61	15.3	0–32
	Rhabdosargus sarba	**51.6**	35–67	31.7	0–65	16.7	0–34
	Gerres japonicus	**47.9**	30–65	34.2	0–70	17.9	0–37
	Muraenesox cinereus	**60.8**	47–74	25.7	0–53	13.4	0–28
	Gymnura japonica	27.4	3–51	**47.7**	0–97	25.0	0–51

tilis) and barnacles (*Balanus* sp. and *Capitulum mitella*) had lower $\delta^{13}C$ signatures while the chiton *L. japonica* and limpet *Cellana grata* had higher values. The $\delta^{13}C$ values of whelk *Thais clavigera* and crab *Gaetice depressus* were intermediate. By contrast, offshore consumer $\delta^{13}C$ values were mainly distributed between −18.0 and −15.0‰ except for zooplankton (−19.2‰) and *G. japonica* (−14.4‰).

The $\delta^{15}N$ ranges of intertidal consumers were more depleted and less variable than those of offshore consumers, with values ranging from 9.3 (*P. viridis*) to 12.8‰ (*C. mitella*) and 9.6 (zooplankton) to 17.2‰ (*G. japonica*).

3.3. Contributions of basal sources supporting consumers

IsoSource solutions showed that consumers assimilated organic carbon from a mixture of basal sources. In offshore zones, SPOM was the most important production source supporting the biomass of most consumers (Table 1). Macroalgae also accounted for a large fraction, especially for the crabs *Portunus trituberculatus* and *Charybdis feriatus* and the fish *G. japonica*. In contrast, model results suggested that epiphytes likely made minor contributions.

In intertidal habitats, epiphytes accounted for significant fractions of the *L. japonica* and *C. grata* biomass and contributed smaller fractions to other consumers. SPOM was the main basal source of organic carbon for most consumers except *L. japonica* and *C. grata* similar to patterns in offshore zones. Consumers also appeared to rely on macroalgae as part of their carbon source.

3.4. TP of consumers

$\delta^{15}N$ data indicated ~5 trophic levels in Mirs Bay (Fig. 3). Apart from *C. mitella*, intertidal consumers had a TP of between 2 and 3. The consumers with the lowest trophic levels were mainly bivalves (*P. viridis*, *A. sculptilis* and *C. rivularis*), chiton (*L. japonica*) and limpet (*C. grata*) as well as crab (*G. depressus*). In contrast, almost all offshore consumers had a TP of between 3 and 4 except for the zooplankton and fish *Clupanodon punctatus*, *Sardinella aurita* and *G. japonica*. Trophic-level 2 included the zooplankton, fish *C.*

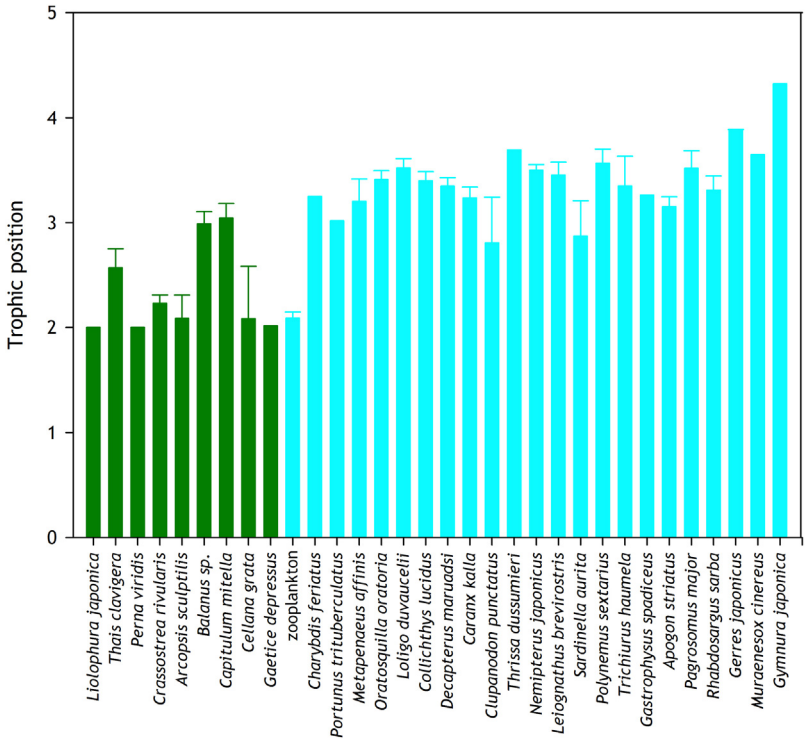

Figure 3 Mean trophic positions (± SD) of consumers in Mirs Bay, China, based on $\delta^{15}N$ values. Green bars and blue bars represent samples from intertidal zones and offshore stations, respectively.

punctatus and *S. aurita*, and the highest TP was occupied by *G. japonica* (TP = 4.32).

4. Discussion

4.1. Carbon isotopic composition of basal sources

Along the rocky shores of Mirs Bay, the most abundant macroalgae in the low- and mid-intertidal zones were *Enteromorpha* spp. and *Amphiroa zonata*. Their $\delta^{13}C$ signatures were in the range of values documented in intertidal beds in a mega-tidal system near Roscoff, France (Ouisse et al., 2012) and coastal areas on the Mexican Eastern Pacific coast (Nava et al., 2014). SPOM displayed similar $\delta^{13}C$ signatures to those demonstrated by Deegan and Garritt (1997), Douglass et al. (2011) and Kang et al. (2008). Epiphytes of the intertidal zones also had $\delta^{13}C$ values close to those reported in Uchiumi and Fukuura Bays, Japan (Doi et al., 2008) and Shark Bay, Australia (Belicka et al., 2012). These $\delta^{13}C$ values of basal sources had a wide range (−19.6‰ to −11.8‰) and were generally well separated, which created favorable conditions for assessing the relative contributions of carbon sources to consumer biomass in Mirs Bay.

4.2. Potential use of basal sources by consumers

In intertidal zones, the filter-feeders were mostly represented by the bivalves *Perna viridis*, *Arcopsis sculptilis* and *Crassostrea rivularis*, and by the barnacles *Balanus* sp. and *Capitulum mitella*, and showed high dependence on offshore SPOM, while intertidal macroalgae and epiphytes also contributed to them. Such species live on rocks, Kang et al. (2008) and Little and Kitching (1996) reported that, on rocky shores, suspension-feeding invertebrates depended on composite sources of macroalgae and phytoplankton. Filter-feeders may feed on macroalgal detritus or exudates in the interface of the water-rock boundary (Kang et al., 2008; Schaal et al., 2010). In addition, epiphytes (as detritus in SPOM) might be part of the diet of filter-feeders (Doi et al., 2008). These findings also indicated the presence of suspended macroalgal and epiphyte detritus in the water column in intertidal zones. For the grazer chiton *Liolophura japonica*, the similarity in $\delta^{13}C$ signatures and trophic enrichment of $\delta^{15}N$ with respect to epiphytes clearly revealed that it depended on materials from epiphytes as its food source. The IsoSource solutions confirmed that epiphytes showed the highest contribution to *L. japonica* nutrition. The chiton scraped off epiphytic organic matter from hard surfaces with radulae (Takai et al., 2004). Another grazer in the current study was the limpet *Cellana grata*, which did not only rely on epiphytes (like *L. japonica*) but also on some macroalgae, according to the IsoSource solutions. This species is generally referred to as a generalist grazer on many rocky shores, grazing on epilithic biofilm and macroalgae (Burnett et al., 2014). The intertidal varunid crab *Gaetice depressus* is considered to be an omnivore, relying on mixed SPOM, macroalgae and epiphytes as well as on heterotrophic detritus as its food source, as already observed in a boulder shore ecosystem (Wahyudi et al., 2013). However, Wahyudi et al. (2013) found that *G. depressus* used macroalgae as its main diet, which differed from the finding in the present study. This disagreement may be explained by local availability of food sources. Wahyudi et al. (2013) stated that

G. depressus preferred to feed upon SPOM and epiphytes when macroalgae were insufficiently abundant. Carbon in the whelk *Thais clavigera* also originated from a mixture of sources, as it did in the crab *G. depressus*; however, *T. clavigera* did not use these sources directly. Although the TP of *T. clavigera* was 2.57 in this study, it is generally referred to as a carnivore, preying primarily on bivalves, limpets and barnacles (Blackmore, 2000; Wada et al., 2013; Wai et al., 2008). Its prey fed on SPOM, macroalgae and epiphytes, as discussed above, and in turn contributed to the diet of *T. clavigera*. A similar result for this species was also found in another ecosystem (Wai et al., 2008). This result also suggested that a lower $\delta^{15}N$ trophic fractionation of 3.4‰ might be present for *T. clavigera*. McCutchan et al. (2003), compiling published studies, concluded that consumers feeding on invertebrate diets had the $\delta^{15}N$ trophic fractionation of 1.4 $\pm$ 0.20‰, which was significantly lower than that for those consumers feeding on other high-protein diets (vertebrates; microbes; and animal-based prepared diets). If we had used the $\delta^{15}N$ trophic fractionation of 1.4‰ to calculate the TP of *T. clavigera* in the present study, its mean TP would have been 3.36, which conformed to its feeding habit.

In offshore zones, the $\delta^{13}C$ signatures of zooplankton closely matched that of SPOM, with TP (2.09) clearly suggesting that they filtered SPOM. IsoSource solutions showed that SPOM accounted for almost all zooplankton biomass, implying that zooplankton depended on organic matter from SPOM almost entirely as its sole food source. The dominant zooplankton species during the investigation were *Subeucalanus subcrassus* and *Temora turbinata* (unpublished data), both known to be small-particle filter-feeders (Li et al., 2012). SPOM mainly comprised of phytoplankton in the offshore zone (Ouisse et al., 2012; Schaal et al., 2010) compared with the SPOM of intertidal zone, which was composed of a greater amount of macroalgal debris (Duggins and Eckman, 1997; Golléty et al., 2010) and epiphytic algae detritus (Doi et al., 2008), as well as phytoplankton. According to Bouillon et al. (2000), quantities of debris and detritus in the intertidal water column were generally greater than those of locally produced phytoplankton. This may explain why filter-feeders in offshore zones relied less on macroalgae and epiphytes than those in intertidal zones. The planktivorous fishes *Clupanodon punctatus* and *Sardinella aurita* displayed lower $\delta^{15}N$ values than other consumers, except for zooplankton in offshore zones. Their TP (2.81 and 2.87, respectively) indicated that these organisms mostly fed on primary consumers and basal sources, and confirmed that they mainly ate diatoms, copepods, Macrura larvae and fish larvae (Huang et al., 2008; Wang and Qiu, 1986). IsoSource solutions showed that SPOM-derived carbon was the major contributor for these two planktivorous fishes. Macroalgae made an important contribution to the carbon source of the crabs *Portunus trituberculatus* (TP = 3.02) and *Charybdis feriatus* (TP = 3.25) and of butterfly ray *Gymnura japonica* (TP = 4.32), followed by SPOM and epiphytes. The $\delta^{13}C$ values of these two crabs were similar to those of the macroalgae, suggesting that they mainly relied on energy derived from macroalgae. However, their TP indicated an indirect use of macroalgae. Their $\delta^{13}C$ values were similar to those of the grazer (*C. grata*), omnivore (*G. depressus*) and carnivore (*T. clavigera*) as well as to piscivore fishes (*Gerres japonicus* and *G. japonica*), which also consumed macroalgae as their important carbon source. This suggests that there is probably a trophic relationship between these two crabs and those organisms. The remaining consumers (17 of 23 species including shrimps, mantis shrimps, squids and fishes) sampled in offshore zones depended more heavily on SPOM, and to a lesser extent on intertidal macroalgae and epiphytes. Such species were mainly carnivorous and had a TP above 3, indicating that they can incorporate integrated basal sources indirectly through trophic interaction.

4.3. Major trophic pathways in Mirs Bay

Trophic connectivity between intertidal and offshore zones mainly followed either of two carbon pathways in Mirs Bay (Fig. 4).

The first and most enriched carbon pathway involved a combination of intertidal macroalgae and epiphytes, grazers, omnivores and their predators, and this provided the first clue about the degree of trophic linkage. Grazers included the intertidal limpet *C. grata* and chiton *L. japonica*, which mainly relied on epiphytes and macroalgae (see above 4.2). The intertidal varunid crab *G. depressus* and whelk *T. clavigera* were classified as an omnivore and a carnivore, respectively, and *G. depressus* fed on macroalgae and epiphytes while *T. clavigera* ate limpets as part of their diet. The offshore crabs *P. trituberculatus* (TP = 3.02) and *C. feriatus* (TP = 3.25) were predators in the present study and their major prey items included mollusks, crustaceans and fishes (Huang, 2004; Jiang et al., 1998). According to the $\delta^{13}C$ values and TP, the intertidal limpet *C. grata*, varunid crab *G. depressus* and whelk *T. clavigera* were assumed to provide the diet for these two crabs, and they might be further preyed on by silver biddy (*G. japonicus*) and butterfly ray (*G. japonica*). The silver biddy was already observed to feed on benthic invertebrates almost exclusively (Cyrus and Blaber, 1982), and the butterfly ray mainly ate teleosts, crustaceans and cephalopods (Capapé, 1986; Jacobsen et al., 2009; Raje, 2003).

Another carbon pathway mainly comprising offshore SPOM, which was incorporated by filter-feeders, omnivores and their predators. The filter-feeders consisted of planktonic zooplankton and intertidal bivalves, both of them consuming SPOM as their main biomass. These filter-feeders acted as trophic intermediates between primary producers and consumers. Zooplankton were preyed on not only by planktivorous fishes such as *C. punctatus* (Huang et al., 2008) and *S. aurita* (Wang and Qiu, 1986) which also fed on SPOM, but also by intertidal barnacles (Lu et al., 1996). The intertidal omnivore *G. depressus* and carnivore *T. clavigera* were also involved in the second carbon pathway besides the first, since *G. depressus* mainly fed on SPOM while *T. clavigera* preyed on bivalves and barnacles. The predators (including shrimps, mantis shrimps, crabs, squids and some fishes at trophic-level 3) conformed well to their known feeding habits. For example, shrimp *Metapenaeus affinis* mainly preys on polychaetes, crustaceans, fish larvae and bivalves (Yu et al., 2016); and mantis shrimp *Oratosquilla oratoria* mainly consumes bivalves, crabs, shrimps and fishes (Ning et al., 2016). Squid are considered to be carnivores as they not only eat fishes, crustaceans and Mollusca, but also show cannibalistic behavior each other (Castro and Huber, 2007). For the fishes, most teleosts are carnivores (Castro and

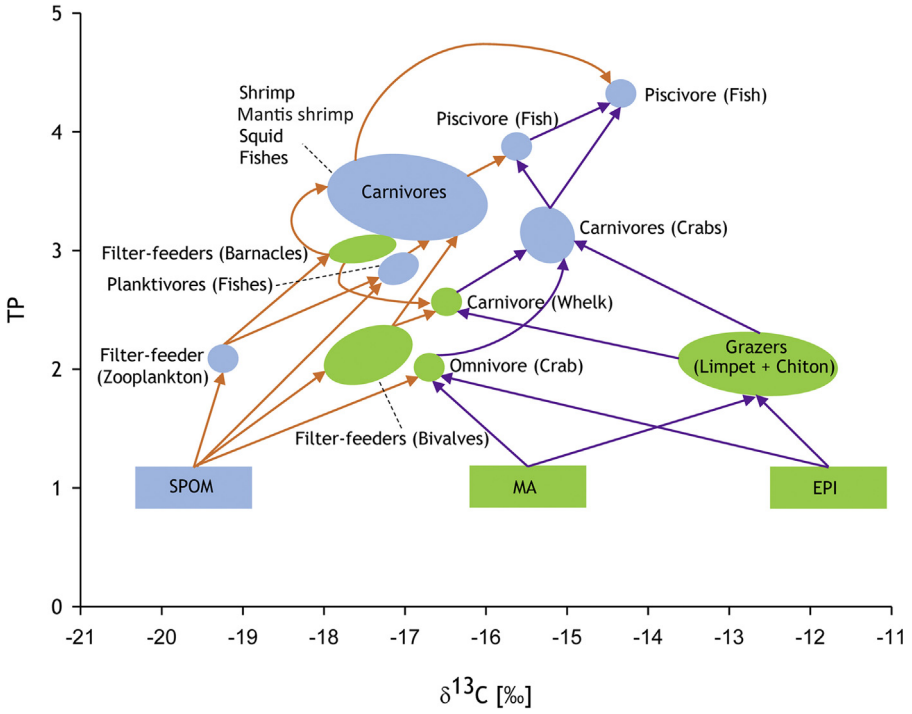

Figure 4 Trophic model of the food web in Mirs Bay, China, delineating the two major carbon pathways. SPOM = suspended particulate organic matter epiphytes; MA = macroalgae; EPI = epiphytes. Green and blue areas represent samples from intertidal zones and offshore stations, respectively. Purple arrows represent the first carbon pathway; orange arrows represent the second carbon pathway.

Huber, 2007), including all the teleosts here except for the planktivorous fishes *C. punctatus* and *S. aurita*. These upper trophic level predators were fueled by mixed basal sources through integrated multiple trophic pathways thought to be common in food webs (Belicka et al., 2012; Rooney et al., 2006). They were further eaten by the piscivore fishes *G. japonicus* and the top predator *G. japonica*.

5. Conclusions

Offshore SPOM carbon was the primary carbon source supporting most consumers not only in the offshore zone, but also in intertidal zones, emphasizing the importance of offshore primary production to intertidal consumers. Intertidal filter-feeders play an important role in retaining offshore primary production. Similarly, intertidal macroalgae and epiphytes also make some contributions to offshore consumers through transfer from prey. The basal sources fueled consumers through two trophic pathways, each of which involved organisms of both intertidal and offshore zones. The coupling of basal sources from different habitats to consumers suggested trophic interaction between intertidal and offshore zones in Mirs Bay. Future protection and preservation of bay ecosystems should consider the whole food web, not just offshore or intertidal food webs, to maintain ecological structure and function.

Further studies should carry out fatty acid biomarkers analysis because this will provide detailed tracking of carbon substrates in food webs not available to stable isotopes. Seasonal analysis should also be included, to enhance understanding of the temporal interactions of trophic dynamics.

Acknowledgments

This work was supported by the following funding projects: Guangdong Natural Science Foundation, China [grant number 2018A030313037]; Chinese Ministry of Science and Technology [grant number 2013BAD13B06]. We thank Dr. Yangguang Gu for sample collection and figures drawing. We also thank Dr. Linbao Zhang for the help during laboratory work. We also would like to thank the two anonymous referees, whose comments greatly contributed to the improvement of the manuscript.

Appendix A. Supplementary data

Supplementary data associated with this article can be found, in the online version, at https://doi.org/10.1016/j.oceano.2018.10.001.

References

Belicka, L.L., Burkholder, D., Fourqurean, J.W., Heithaus, M.R., Macko, S.A., Jaffe, R., 2012. Stable isotope and fatty acid biomarkers of seagrass, epiphytic, and algal organic matter to consumers in a pristine seagrass ecosystem. Mar. Freshwater Res. 63 (11), 1085–1097, http://dx.doi.org/10.1071/MF12027.

Blackmore, G., 2000. Field evidence of metal transfer from invertebrate prey to an intertidal predator, *Thais clavigera* (Gastropoda: Muricidae). Estuar. Coast. Shelf. Sci. 51 (2), 127–139, http://dx.doi.org/10.1006/ecss.2000.0643.

Bouillon, S., Mohan, P.C., Sreenivas, N., Dehairs, F., 2000. Sources of suspended organic matter and selective feeding by zooplankton in an estuarine mangrove ecosystem as traced by stable isotopes.

Mar. Ecol.-Prog. Ser. 208 (1), 79–92, http://dx.doi.org/10.3354/meps208079.

Burnett, N.P., Villarta, K.A., Williams, G.A., 2014. Rasping patterns of the high-shore limpet *Cellana grata*. J. Mollus. Stud. 80 (4), 456–459, http://dx.doi.org/10.1093/mollus/eyu022.

Capapé, C., 1986. General data on the diet of Gymnuridae and Mobulidae (Pisces, Selachii). Arch. Inst. Pasteur Tunis 63 (2–3), 241–246.

Castro, P., Huber, M.E. (Eds.), 2007. Marine Biology. McGraw-Hill Higher Education, New York, 480 pp.

Claudino, M.C., Pessanha, A.L.M., Araújo, F.G., Garcia, A.M., 2015. Trophic connectivity and basal food sources sustaining tropical aquatic consumers along a mangrove to ocean gradient. Estuar. Coast. Shelf. Sci. 167 (16), 45–55, http://dx.doi.org/10.1016/j.ecss.2015.07.005.

Conway-Cranos, L., Kiffney, P., Banas, N., Plummer, M., Naman, S., MacCready, P., Bucci, J., Ruckelshaus, M., 2015. Stable isotopes and oceanographic modeling reveal spatial and trophic connectivity among terrestrial, estuarine, and marine environments. Mar. Ecol.-Prog. Ser. 533, 15–28, http://dx.doi.org/10.3354/meps11318.

Cyrus, D.P., Blaber, S.J.M., 1982. Mouthpart structure and function and the feeding mechanisms of *Gerres* (Teleostei). Zool. Afr. 17 (3), 117–121, http://dx.doi.org/10.1080/02541858.1982.11447790.

Day, J.W., Crump, B.C., Kemp, W.M., Yáñez-Arancibia, A. (Eds.), 2012. Estuarine Ecology. Wiley-Blackwell, New Jersey, 550 pp.

Deegan, L.A., Garritt, R.H., 1997. Evidence for spatial variability in estuarine food webs. Mar. Ecol.-Prog. Ser. 147 (1–3), 31–47, http://dx.doi.org/10.3354/meps147031.

Deniro, M.J., Epstein, S., 1981. Influence of diet on the distribution of nitrogen isotopes in animals. Geochim. Cosmochim. Acta 45 (3), 341–351, http://dx.doi.org/10.1016/0016-7037(81)90244-1.

Doi, H., Chang, K.H., Obayashi, Y., Yoshihara, M., Shime, M., Yamamoto, T., Nishibe, Y., Nakano, S., 2008. Attached microalgae contribute to planktonic food webs in bays with fish and pearl oyster farms. Mar. Ecol.-Prog. Ser. 353 (01), 107–113, http://dx.doi.org/10.3354/meps07202.

Douglass, J.G., Emmett Duffy, J., Canuel, E.A., 2011. Food web structure in a Chesapeake Bay eelgrass bed as determined through gut contents and ^{13}C and ^{15}N isotope analysis. Estuar. Coast. 34 (4), 701–711, http://dx.doi.org/10.1007/s12237-010-9356-4.

Duggins, D.O., Eckman, J.E., 1997. Is kelp detritus a good food for suspension feeders? Effects of kelp species, age and secondary metabolites. Mar. Biol. 128 (3), 489–495, http://dx.doi.org/10.1007/s002270050115.

Fry, B., Sherr, E.B., 1984. $\delta^{13}C$ measurements as indicators of carbon flow in marine and freshwater ecosystems. Contr. Mar. Sci. 27, 13–47.

Golléty, C., Riera, P., Davoult, D., 2010. Complexity of the food web structure of the Ascophyllum nodosum zone evidenced by a $\delta^{13}C$ and $\delta^{15}N$ study. J. Sea Res. 64 (3), 304–312, http://dx.doi.org/10.1016/j.seares.2010.04.003.

Hill, J.M., McQuaid, C.D., Kaehler, S., 2006. Biogeographic and nearshore-offshore trends in isotope ratios of intertidal mussels and their food sources around the coast of southern Africa. Mar. Ecol.-Prog. Ser. 318, 63–73, http://dx.doi.org/10.3354/meps318063.

Huang, M., 2004. Study on feeding habit and nutrient level of *Portunus argentatus*, *P. sanguinolentus* and *Charybdis feriatu* in Fujian sea area. J. Oceanogr. Taiwan Strait 23 (2), 159–166, (in Chinese).

Huang, L., Zhang, Y., Pan, J., Wu, Y., Cui, Y., 2008. Food web of fish in Xiamen eastern waters. J. Oceanogr. Taiwan Strait 27 (1), 64–73, (in Chinese).

Jacobsen, I.P., Johnson, J.W., Bennett, M.B., 2009. Diet and reproduction in the Australian butterfly ray *Gymnura australis* from northern and north-eastern Australia. J. Fish Biol. 75 (10), 2475–2489, http://dx.doi.org/10.1111/j.1095-8649.2009.02432.x.

Jansson, B.O., 1988. Coastal-Offshore Ecosystem Interactions. Springer-Verlag, Berlin, 367 pp.

Jiang, W., Meng, T., Chen, R., Sheng, W., 1998. Diet of *Charybdis japonica* (A. Miline-Edwards) and *Portunus trituberculatus* (Miers) in the Bohai Sea. Mar. Fish. Res. 19 (1), 53–59, (in Chinese).

Kaehler, S., Pakhomov, E.A., McQuaid, C.D., 2000. Trophic structure of the marine food web at the Prince Edward Islands (Southern Ocean) determined by $\delta^{13}C$ and $\delta^{15}N$ analysis. Mar. Ecol.-Prog. Ser. 208, 13–20, http://dx.doi.org/10.3354/meps208013.

Kang, C.K., Choy, E.J., Son, Y., Lee, J.Y., Kim, J.K., Kim, Y., Lee, K.S., 2008. Food web structure of a restored macroalgal bed in the eastern Korean peninsula determined by C and N stable isotope analyses. Mar. Biol. 153 (6), 1181–1198, http://dx.doi.org/10.1007/s00227-007-0890-y.

Li, K., Tan, Y., Huang, L., Yin, J., Song, X., 2012. Feeding of planktonic copepods in the Pearl River Estuary. J. Trop. Oceanogr. 31 (6), 90–96, (in Chinese), https://doi.org/10.3969/j.issn.1009-5470.2012.06.014.

Little, C., Kitching, J.A. (Eds.), 1996. The Biology of Rocky Shores. Oxford University Press, New York, 235 pp.

Lu, J., Cai, R., Qian, Z., Wei, S., Qian, J., 1996. Stomach contents of the several barnacles in Zhoushan waters. Dongahi Mar. Sci. 14 (1), 28–35, (in Chinese).

Lu, L., Goh, B.P.L., Chou, L.M., 2002. Effects of coastal reclamation on riverine macrobenthic infauna (*Sungei Punggol*) in Singapore. J. Aquat. Ecosyst. Stress Recov. 9 (2), 127–135, http://dx.doi.org/10.1023/A:1014483804331.

Markel, R.W., Shurin, J.B., 2015. Indirect effects of sea otters on rockfish (*Sebastes* spp.) in giant kelp forests. Ecology 96 (11), 2877–2890, http://dx.doi.org/10.1890/14-0492.1.

McCutchan, J.H., Lewis, W.M., Kendall, C., McGrath, C.C., 2003. Variation in trophic shift for stable isotope ratios of carbon, nitrogen, and sulfur. Oikos 102 (2), 378–390, http://dx.doi.org/10.1034/j.1600-0706.2003.12098.x.

Minagawa, M., Wada, E., 1984. Stepwise enrichment of ^{15}N along food chains: Further evidence and the relation between $\delta^{15}N$ and animal age. Geochim. Cosmochim. Acta 48 (5), 1135–1140, http://dx.doi.org/10.1016/0016-7037(84)90204-7.

Mittelbach, G.G., Osenberg, C.W., 1993. Stage-structured interactions in bluegill: consequences of abult resource variation. Ecology 74 (8), 2381–2394, http://dx.doi.org/10.2307/1939589.

Nakano, S., Murakami, M., 2001. Reciprocal subsidies: dynamic interdependence between terrestrial and aquatic food webs. Proc. Natl. Acad. Sci. U.S.A. 98 (1), 166–170, http://dx.doi.org/10.1073/pnas.98.1.166.

Nava, H., Ramirez-Herrera, M.T., Figueroa-Camacho, A.G., Villegas-Sanchez, B.M., 2014. Habitat characteristics and environmental factors related to boring sponge assemblages on coral reefs near populated coastal areas on the Mexican Eastern Pacific coast. Mar. Biodivers. 44 (1), 45–54, http://dx.doi.org/10.1007/s12526-013-0182-3.

Ning, J., Du, F., Wang, X., Gu, Y., Wang, L., Li, Y., 2016. Feeding habits of mantis shrimp based on stable isotope analysis. J. Fish. China 40 (6), 903–910, (in Chinese), https://doi.org/10.11964/jfc.20151110177.

Ouisse, V., Riera, P., Migne, A., Leroux, C., Davoult, D., 2012. Food web analysis in intertidal *Zostera marina* and *Zostera noltii* communities in winter and summer. Mar. Biol. 159 (1), 165–175, http://dx.doi.org/10.1007/s00227-011-1796-2.

Peterson, B.J., Fry, B., 1987. Stable isotopes in ecosystem studies. Annu. Rev. Ecol. Syst. 18 (1), 293–320, http://dx.doi.org/10.1146/annurev.es.18.110187.001453.

Phillips, D.L., Gregg, J.W., 2003. Source partitioning using stable isotopes: coping with too many sources. Oecologia 136 (2), 261—269, http://dx.doi.org/10.1007/s00442-003-1218-3.

Polis, G.A., Strong, D.R., 1996. Food web complexity and community dynamics. Am. Nat. 147 (5), 813—846, http://dx.doi.org/10.1086/285880.

Polis, G.A., Anderson, W.B., Holt, R.D., 1997. Toward an integration of landscape and food web ecology: the dynamics of spatially subsidized food webs. Annu. Rev. Ecol. Syst. 28 (1), 289—316, http://dx.doi.org/10.1146/annurev.ecolsys.28.1.289.

Post, D.M., 2002. Using stable isotopes to estimate trophic position: models, methods, and assumptions. Ecology 83 (3), 703—718, http://dx.doi.org/10.2307/3071875.

Raje, S.G., 2003. Some aspects of biology of four species of rays off Mumbai water. Indian J. Fish. 50 (1), 89—96.

Randall, J.E., 1965. Grazing effect on sea grasses by herbivorous reef fishes in the West Indies. Ecology 46 (3), 255—260.

Rooney, N., McCann, K., Gellner, G., Moore, J.C., 2006. Structural asymmetry and the stability of diverse food webs. Nature 442 (7100), 265—269, http://dx.doi.org/10.1038/nature04887.

Savage, C., Thrush, S.F., Lohrer, A.M., Hewitt, J.E., 2012. Ecosystem services transcend boundaries: Estuaries provide resource subsidies and influence functional diversity in coastal benthic communities. PLoS ONE 7 (8), e42708, http://dx.doi.org/10.1371/journal.pone.0042708.

Schaal, G., Riera, P., Leroux, C., 2010. Trophic ecology in a Northern Brittany (Batz Island, France) kelp (*Laminaria digitata*) forest, as investigated through stable isotopes and chemical assays. J. Sea Res. 63 (1), 24—35, http://dx.doi.org/10.1016/j.seares.2009.09.002.

Selleslagh, J., Blanchet, H., Bachelet, G., Lobry, J., 2015. Feeding habitats, connectivity and origin of organic matter supporting fish populations in an estuary with a reduced intertidal area assessed by stable isotope analysis. Estuar. Coast. 38 (5), 1431—1447, http://dx.doi.org/10.1007/s12237-014-9911-5.

Takai, N., Yorozu, A., Tanimoto, T., Hoshika, A., Yoshihara, K., 2004. Transport pathways of microphytobenthos-originating organic carbon in the food web of an exposed hard bottom shore in the Seto Inland Sea, Japan. Mar. Ecol.-Prog. Ser. 284 (1), 97—108, http://dx.doi.org/10.3354/meps284097.

Vander Zanden, M.J., Rasmussen, J.B., 1999. Primary consumer $\delta^{13}C$ and $\delta^{15}N$ and the trophic position of aquatic consumers. Ecology 80 (4), 1395—1404, http://dx.doi.org/10.1890/0012-9658(1999)080[1395:pccana]2.0.co;2.

Wada, Y., Iwasaki, K., Yusa, Y., 2013. Changes in algal community structure via density- and trait-mediated indirect interactions in a marine ecosystem. Ecology 94 (11), 2567—2574, http://dx.doi.org/10.1890/12-0725.1.

Wahyudi, A.J., Wada, S., Aoki, M., Hama, T., 2013. Stable isotope signature and pigment biomarker evidence of the diet sources of *Gaetice depressus* (Crustacea: Eubrachyura: Varunidae) in a boulder shore ecosystem. Plankton Benthos Res. 8 (2), 55—67, http://dx.doi.org/10.3800/pbr.8.55.

Wai, T.C., Ng, J.S.S., Leung, K.M.Y., Dudgeon, D., Williams, G.A., 2008. The source and fate of organic matter and the significance of detrital pathways in a tropical coastal ecosystem. Limnol. Oceanogr. 53 (4), 1479—1492, http://dx.doi.org/10.4319/lo.2008.53.4.1479.

Wang, J., Qiu, S., 1986. On the feeding habit of *Sardinella Aurita* val. in South Fujian-East Guangdong coastal waters. J. Oceanogr. Taiwan Strait 5 (1), 86—93, (in Chinese).

Xia, Z., Zheng, Z., Lin, J., 2005. Integrated analysis of the marine geological environment and hazards in the Dapeng Bay. Geol. China 32 (1), 148—154, (in Chinese).

Yu, J., Chen, P., Feng, X., 2016. Food habits and trophic levels for 4 species of economical shrimps in the Pearl River estuary shallow waters. J. South. Agric. 47 (5), 736—741, (in Chinese), https://doi.org/10.3969/j.issn.2095-1191.2016.05.736.

Zhang, S., Sun, X., Wang, W., Huang, R., Lai, Y., Liu, Y., Zhu, L., Song, T., Jin, X., Zhang, H., 2013. Features of coastal landforms in Dapeng Peninsula of Shenzhen, China. Trop. Geogr. 33 (6), 647—658, (in Chinese), https://doi.org/10.13284/j.cnki.rddl.002475.

Oceanologia (2019) 61, 218—226

Available online at www.sciencedirect.com

ScienceDirect

journal homepage: www.journals.elsevier.com/oceanologia/

ORIGINAL RESEARCH ARTICLE

An eco-friendly strategy using flax/polylactide composite to tackle the marine invasive sponge *Celtodoryx ciocalyptoides* (Burton, 1935)

Charline Gentric, Pierre Sauleau *

University Bretagne-Sud, Lorient, France

Received 19 March 2018; accepted 14 October 2018
Available online 26 October 2018

KEYWORDS
Artificial substrate;
Biocomposite;
Celtodoryx ciocalyptoides;
Marine invaders;
Polylactide

Summary Discovered in the 1990s in the river of Etel (Morbihan, France), the marine invasive sponge *Celtodoryx ciocalyptoides* originating from the Chinese Yellow Sea is now well implanted on concrete pilings inside the Etel marina (Morbihan, France). Novel eco-friendly strategies are urgently needed in order to limit its adhesion on concrete and the risk of dispersal outside the marina. In this study, the anti-settlement and anti-attachment properties of flax/PLA, a biocomposite made of polylactide reinforced with flax fibres, were evaluated on sponge propagules' behaviour. First, flax/PLA panels were immersed into the Etel marina for six years. The coverage onto PLA panels of marine invertebrates was estimated twice a year. In a second step, PLA panels were used as artificial support for invasive sponge transplants. In comparison, specimens were transplanted in mesh bags. Sponge weight increase was measured twice a year. Results indicated that the occurrence of the invasive sponge was delayed for two years on biocomposite in comparison with concrete. At the end of the six-year study, macrofouling by marine invertebrates did not exceed 70% of the surface of the panels and no *C. ciocalyptoides* specimens were observed. Once transplanted on PLA panels, sponge specimens were able to survive the first year without growing. After two years, none of the transplants survived while specimens in mesh bags increased their weight by 100%. These findings highlight the potential interest of biocomposite in the development of coastal and marine infrastructures.

* Corresponding author at: University Bretagne-Sud, EA 3884, LBCM, IUEM, F-56100 Lorient, France. Tel.: +33 297 874 519; fax: +33 297 874 610.
E-mail address: pierre.sauleau@univ-ubs.fr (P. Sauleau).
Peer review under the responsibility of Institute of Oceanology of the Polish Academy of Sciences.

ELSEVIER Production and hosting by Elsevier

https://doi.org/10.1016/j.oceano.2018.10.002

1. Introduction

Discovered in 1996 in the Etel River (Brittany, France), the marine sponge *Celtodoryx ciocalyptoides* originating from the Chinese Yellow Sea is now well established and considered as an invasive species (Henkel and Janussen, 2011; Perez et al., 2006). In the Etel marina, this species was recently shown to cover on its own up to 17.4% of the surface of the concrete pilings (Gentric and Sauleau, 2016). The species is also present in the Gulf of Morbihan (Perez et al., 2006), in the river of Penerf (Sauleau, Personal communication), in the Oostershelde (Netherlands) (Van Soest et al., 2007) and has recently been observed in the harbour of Le Havre (Normandy, France) (Berno et al., 2016).

One possibility to limit invasive species adhesion on artificial hard substrate is the use of antifouling paints. Copper-based antifouling paints are applied on immersed structures to limit the growth of fouling organisms. However, by reducing biodiversity, competition with endemic species, and by inducing tolerance to copper pollution, antifouling paints are thought to enhance invasions (McKenzie et al., 2012; Piola et al., 2009). Thus novel antifouling strategies such as the use of self-polishing matrices for controlled release of natural antifouling substances were developed (Thouvenin et al., 2003).

Among self-polishing polymers, polylactide (PLA) is probably one of the most promising erodible polymers due to the fact that PLA is biodegradable, recyclable, compostable, biocompatible and eco-friendly produced. PLA is obtained using the ring-opening polymerization of lactide, a cyclic monomer derived from plant resources (corn starch, cane molasses, etc.). PLA showed relative biocompatibility as suture material, orthopaedic devices and drug release delivery systems for medical application (Farah et al., 2016; Hamad et al., 2015; Ulery et al., 2011; Walczak et al., 2015). In contrast to traditional highly durable plastics, PLA showed good biodegradability in soil and compost (Hakkarainen et al., 2000; Karjomaa et al., 1998; Pranamuda et al., 1997; Sukkhum et al., 2009). The mechanism of degradation includes both chemical hydrolysis and biodegradation. The polymer initially degraded through abiotic hydrolysis leading to the release of shorter oligomer chains and monomers of lactic acid (LA). This chemical hydrolysis is followed and accelerated by biodegradation (assimilation) by micro-organisms leading to carbon dioxide and water.

The direct contribution of the biodegradable polymer to the overall antifouling effect was recently investigated by Ishimaru et al. (2012) who prevented the attachment of barnacle cypris larvae using a polyethylene/PLA blend. Among hydrolysis products, LA was suggested to participate in the anti-barnacle attachment property of PLA. In addition, LA is known to have antibacterial effects by reducing the pH while low molecular weight PLA were suggested to have prolonged antimicrobial effects (Ariyapitipun et al., 1999). The use of bacteriostatic PLA against *Pseudomonas aeruginosa* and *Staphylococcus aureus* was also proposed in the conception of tympanostomy ear tube for children (Ludwick et al., 2006). Eventually, PLA microspheres were shown to be slightly bacteriostatic towards a *Pseudoalteromonas* sp. (Faÿ et al., 2008) while PLA film may have bacteriostatic activity against *Salmonella typhymurium* (Theinsathid et al., 2012).

It is well known that biofilms composed of bacteria, diatoms, protozoa or fungi are the prerequisite for the settlement of invertebrate larvae (Qian et al., 2007; Whalan and Webster, 2014). Thus, the hypothesis of our study was that the biodegradable and/or potential antimicrobial properties of PLA could be used as an eco-friendly biomaterial to limit propagules settlement. In order to assess the anti-settlement properties of PLA, biocomposite panels made of polylactide reinforced with flax fibres were immersed into the Etel marina for six years. The coverage onto those panels by the invasive sponge and other marine invertebrates was estimated twice a year. Since sponge overgrowth occurs also by lateral colonization, we evaluated the anti-attachment effects of flax/PLA on *C. ciocalyptoides* transplants bound to the biocomposite panels for the same period of time. As far as we know, this is the first time an eco-friendly strategy is developed to get rid of an invasive sponge on the North-East Atlantic coast.

2. Material and methods

2.1. Study site

Experiments were performed from April 2011 to March 2017 in the Etel marina (47.659°, −3.207°) located at the mouth of the river of Etel (Brittany, France). This river, 15 km long, is located between Lorient and Vannes (Morbihan, France) and belongs to the Natura 2000 network areas (FR5300028).

2.2. Sponge collection

Sponge samples were collected by SCUBA diving at a depth of 10—15 m during neap tides in April 2011 along the Magouër site situated 200 m west of the marina. *C. ciocalyptoides* specimens freshly collected were immediately transferred to the marina for transplantation. Samples were cut in approximately 125 cm^3 pieces, weighed, tagged, and let in a nylon mesh bag for control or separately bound onto a flax/PLA panel with an iron wire (Fig. 1).

2.3. Experimental set-up and design

Poly(L-lactic acid) (PLLA, Biomer® L9000) was purchased from Biomer (Germany). The polymer has a high molecular weight (220,000 g mol^{-1}) with a L- and D-isomer ratio of approximately 98:2. Flax fibres of the Marylin variety (1 mm length) were incorporated in PLA polymer (20% in weight) as previously described (Le Duigou et al., 2014).

The support structure (1 m^3) was made with PVC tubes (25 mm diameter). Each face was divided in five columns with a nylon rope, strengthened every 20 cm, each length containing 5 replicates i.e. 5 nylon mesh bags (36 × 29 cm, 3 mm mesh). Each mesh bag contained two sponge specimens, one let free into the net and another one bound with an iron wire to the panel (9.8 cm × 14.7 cm × 0.18 cm) made of flax/PLA. Both specimens were separated to avoid fusion. A total of 80 mesh bag were fixed to the 4 PVC quadrats linked each other. On the top of the structure, additional panels made of flax/PLA were attached all around the piling for settlement experiments. Panels were immersed at a depth of 9 m below sea level and fixed around the north-western piling of the

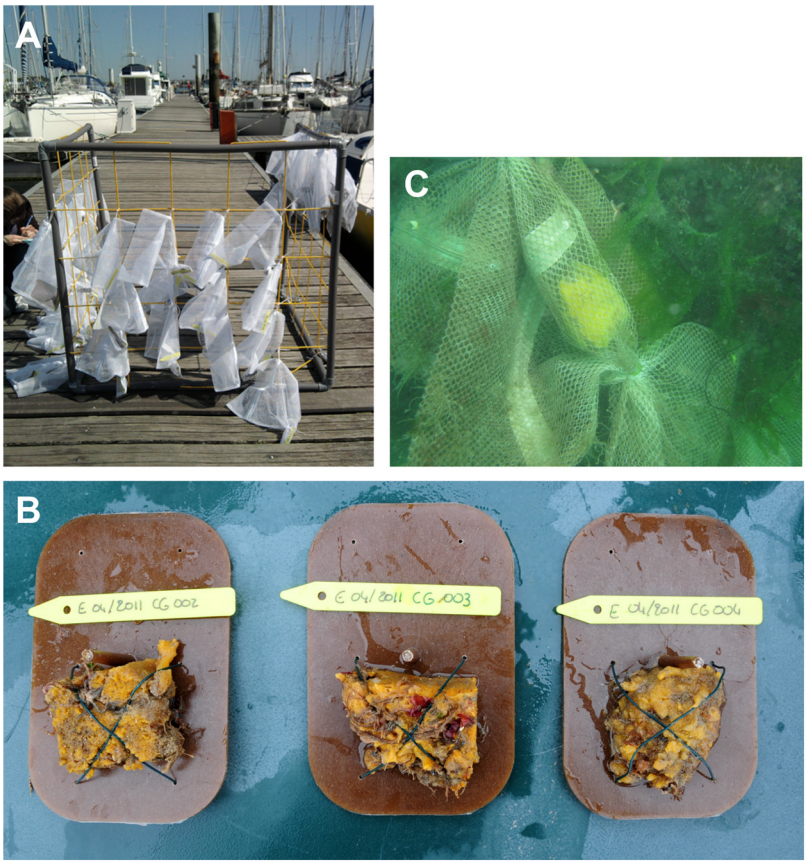

Figure 1 (A) The support structure. (B) *Celtodoryx ciocalyptoides* samples (125 cm^3) bound with an iron wire to tagged flax/PLA panels. (C) Mesh bags containing two sponge specimens: one let free inside the net and the other one bound separately onto the PLA panel.

marina. To respect hydrodynamic conditions, the distance between the piling and the support structure was 30 cm.

In order to assess sponge capacity to colonize any artificial substrate which may vary according to life cycle, the fauna covering a surface of 0.1 m^2 at 7 m deep was scraped off the concrete piling (Fig. 2a) at the beginning of the study. Sponge settlement on this area was observed in situ every 6 months by underwater pictures (Canon G10).

2.4. Sponge monitoring

In order to assess sponge survival and growth after transplantation in a new marine environment, percentage weight increase and elemental composition were measured. Five mesh bags were sampled by SCUBA every 6 months. Fresh sponge samples were gently removed from the net, directly weighed on the pontoons of the marina, bring back to the lab and kept at −80°C before lyophilization.

The percentage weight increase was calculated with the formula:

$$\%\,\text{Weight Increase} = \frac{(W_m - W_0)}{W_0} \times 100,$$

where W_m is the sponge weight after m months of growth and W_0 the sponge weight at the beginning of the experiment.

The following Metallic Trace Elements (MTEs) Ba, Cd, Co, Cr, Cu, Fe, Mg, Mn, Mo, Ni, Si, Sr and Zn which are vital for the growth and development of sponges were quantified in transplanted specimens and compared to wild specimens collected outside the marina from the natural site (Magouër). The elemental content was determined every year during a monitoring period of three years (2012, 2013 and 2014) by Inductively Coupled Plasma Atomic Emission Spectrometer (ICP-AES) by the University of Caen as previously described (Mahaut et al., 2013). Analyses were performed in triplicate on a mixture of 5 sponge specimens.

2.5. Covering and growth on PLA panels

The presence of micro- and macro-foulers on both faces of the flax/PLA settling panels ($n = 10$) was observed every 6 months by Scanning Electron Microscopy (SEM) (JSM-6460LV, Jeol) and underwater pictures, respectively. Spicules characteristic of the skeleton of *C. ciocalyptoides* were observed by SEM. Percentage cover of macrofoulers was calculated by using ImageJ software. Sponge growth was estimated by calculating the percentage weight increase as described in Section 2.4.

2.6. Statistical analyses

Transplants weight increase under the two conditions (on flax/PLA plates or on nylon mesh bags), MTEs composition between wild and transplanted specimens, and seasonal

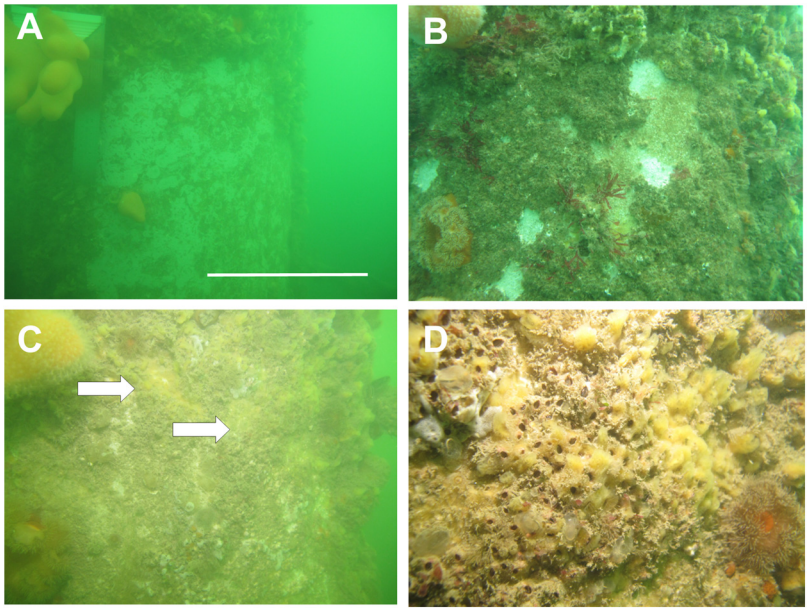

Figure 2 Fouling by the marine sponge *Celtodoryx ciocalyptoides* on concrete piling within the Etel marina. (A) A 0.1 m^2 area was scraped on the piling (scale bare = 25 cm). (B) The scraped area was rapidly covered by mainly barnacles after 6 months and (C) fouled by *C. ciocalyptoides* specimens (white arrows) after 1 year. (D) A zoom showed the sponge cover on the shells of barnacles competing with the hexacorallian *Metridum senile* and the tunicate *Diplosoma spongiforme*.

covering rate between spring and winter were compared using Wilcoxon-type test. All analyses were performed with Rstudio 1.0.143.

3. Results

3.1. Anti-settlement properties of the flax/PLA biocomposite

During the first 6 months of this study, the fouling at the surfaces of the panels was dominated by microfoulers such as diatoms, bacteria and hydrozoans (Fig. 3). In some cases, few macrofoulers such as tube worms *Pomatoceros* sp. and barnacles *Balanus* sp. were observed on both faces of the PLA panels (Fig. 4a and b) covering up to 4.6 ± 0.3% of the area (Fig. 5). In comparison, the PVC structure was covered of hydrozoans and tunicates such as *Ciona intestinalis* (Fig. 4a). During the next two years of immersion, both surfaces were partially (37.5 ± 8.7%) covered of mainly bivalves *Anomia* sp., mussels, tube worms *Pomatoceros* sp., few anemones *Metridium senile*, and tunicates but no *C. ciocalyptoides* specimens were observed (Figs. 4c and 5). After three years (Fig. 4d), half of the surface of PLA panels (48.7 ± 7.2%) were covered mainly of *Balanus* sp., *Anomia* sp. and *Mytilus* sp. In few cases, *Crassostrea gigas* and *Crepidula fornicata* were also observed. Sponge cells with spicules consisting part of the skeleton of *C. ciocalyptoides* (Fig. 6) were finally observed onto barnacle shells covering up to 25.5% of the panel. After 6 years of immersion, the fouling covered more than two thirds of the panel surface (70.6 ± 7.6%) but neither invasive sponge specimens nor barnacles were observed (Fig. 4e). During the six-year study, the percentage cover of macrofoulers did not decrease significantly each winter (p-value > 0.05) (Fig. 5).

3.2. Anti-attachment activity of the flax/PLA biocomposite

After one year, the weight of sponge transplants bound with an iron wire onto the flax/PLA panels severely dropped

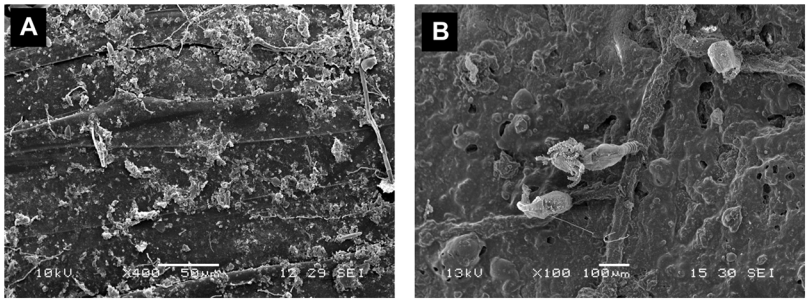

Figure 3 SEM micrographs of the flax/PLA panels after 3 months of immersion showing fouling by (A) micro-organisms and (B) hydrozoans.

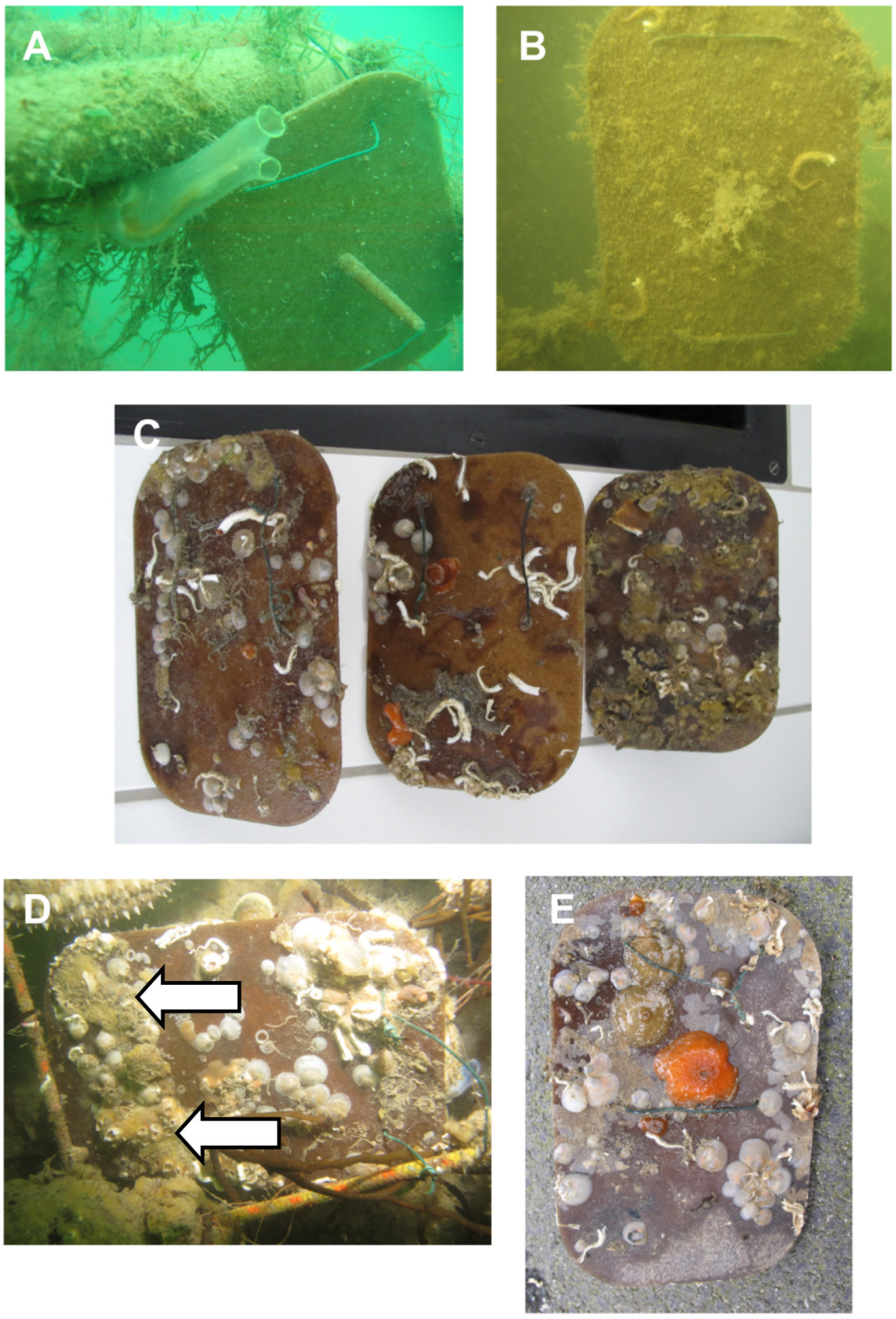

Figure 4 Fouling dominated by marine macro-organisms on PLA panels immersed into the Etel marina during (A) 90 days, (B) 6 months, (C) 2 years, (D) 3 years (showing barnacles with the marine sponge *Celtodoryx ciocalyptoides* (white arrows)), and (E) 6 years.

(Fig. 7). During 2012, the mean weight gain was significantly higher for specimens in nylon mesh bags than for those on PLA plates ($p < 0.05$). After two years (i.e. April 2013), *C. ciocalyptoides* specimens transplanted onto the PLA panels did not survive. Instead, both faces of the panels were covered of macrofoulers such as *Balanus* sp. and *Anomia* sp. This result suggests sponge cells did not find optimal conditions to adhere, survive and grow on flax/PLA biocomposite.

3.3. Transplantation efficiency of sponge

Measures of the weight of specimens let free in nylon mesh bags indicate no gain during the first year of transplantation while the increase in weight reached 100% the second year (Fig. 7). The composition in Metallic Trace Elements (MTEs) was quantified in transplanted specimens and compared with that from the natural site during the first three years (Fig. 8).

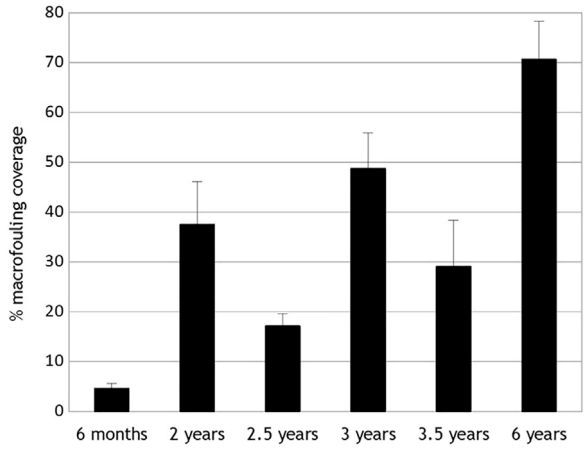

Figure 5 Percentage cover of marine organisms on PLA panels immersed into the Etel marina during the six-year study. Results are expressed as the mean ± SE of three replicates.

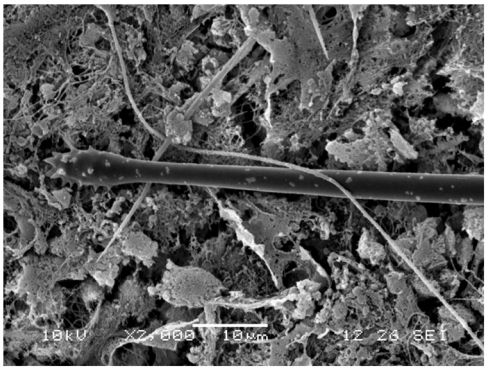

Figure 6 SEM micrograph of a flax/PLA panel showing a tylote constituting part of the skeleton of the species *Celtodoryx ciocalyptoides*.

Most of those MTEs, essential for sponge physiology, were at the same levels between transplanted and wild sponge specimens during the three first years of the study. Si levels remained particularly low in transplanted specimens but statistical analysis indicated no significant differences ($p > 0.05$) in comparison with wild ones. These results suggest transplantation in the Etel marina had no deleterious effects on the filtering activity of individuals which found favourable environmental conditions in the marina to survive and grow.

3.4. Sponge settlement on concrete substrate

After 5 months, fouling by barnacles *Balanus* sp., hydrozoans and rhodobionts covered approximately 75% of the surface of the scraped area on the concrete piling (Fig. 2b). In one year, the marine sponge *C. ciocalyptoides* was observed on the shells of barnacles, covering 13% of the initial area and competing with the hexacorallian *M. senile* and the tunicate *Diplosoma spongiforme* (Fig. 2c and d). At last, after two years, the scraped area got its original aspect with a density and thickness of *C. ciocalyptoides* similar to the other concrete pilings of the marina. This result confirms the sponge showed a rapid population growth during at least the first two years of our study.

4. Discussion

The colonization of artificial hard substrates by non-indigenous species is one of the major stumbling block in the development of coastal and marine infrastructure (Firth et al., 2016). In our study, we showed for the first time that a bio-based and biodegradable composite made of flax/PLA had promising anti-settlement and anti-attachment properties against the marine invasive sponge *C. ciocalyptoides*.

The recent observation of *C. ciocalyptoides* in the Etel marina close to shellfish farming activities suggests the possibility of its introduction through the Japanese Oyster *C. gigas* importation in Brittany during the 1970s. Once discharged in harbours, ports, and marinas sponge propagules found favourable conditions to establish on piers, pontoons, pilings, seawalls or buoys. Those artificial hard substrates are considered as providing new habitats facilitating the establishment, persistence and spread of non-indigenous and potentially invasive species (Glasby et al., 2007; Ruiz et al., 2009; Vaz-Pinto et al., 2014). We showed in this study that the colonization by *C. ciocalyptoides* on concrete pilings took place in a year by planktonic propagules (or competent sponge larvae) settlement and/or by spreading sponge colonies growing laterally. Finally, the marine invasive sponge *C. ciocalyptoides* was shown to cover up to 17.4% of the surface of concrete pilings of the Etel marina forming a mat of 5—

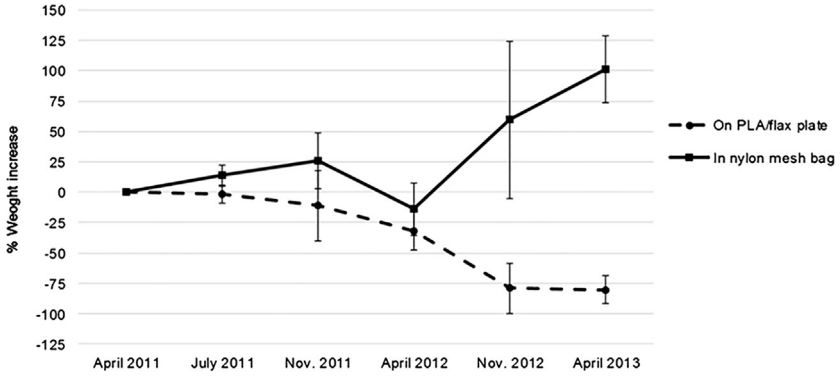

Figure 7 Weight variation of *Celtodoryx ciocalyptoides* transplants during the first two years. Results are expressed as the means ± SE of five replicates.

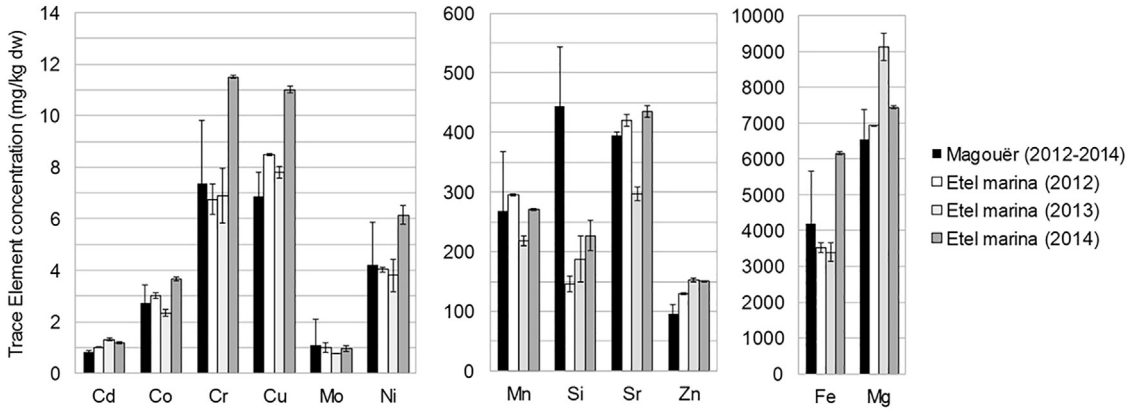

Figure 8 Elemental composition of the marine sponge *Celtodoryx ciocalyptoides*. Sponge specimens were transplanted into the Etel marina and their elemental composition was compared with that of wild specimens from the Magouër site during the first three years of the study (2012–2014). Results are expressed as the mean ± SE of three replicates.

6 cm of thickness from 5 to 9 m deep, between the mussel belt and the bottom of the marina (Gentric and Sauleau, 2016). Surprisingly, as shown in our study, fouling by marine organisms on flax/PLA biocomposite was delayed and reduced. After three years of immersion, fouling by successive macrofoulers such as barnacles, oysters and mussels covered half of the surface of the biocomposite. Specimens of *C. ciocalyptoides* were finally observed mainly on the shell of barnacles and in a lesser extent onto the flax/PLA panels. After six years of immersion, no invasive sponge cells were observed anymore. Further long-term studies are needed to assure sponge regression is due to PLA effect and not simply to a seasonal regression as already mentioned among non-indigenous species (Vaz-Pinto et al., 2014).

Concerning the anti-settlement and anti-attachment properties of the biocomposite, one can hypothesize that the bulk erosion of PLA and the release of lactic acid (LA) are incriminated in those phenomena. PLA degradation in compost and soil is already well documented (Jeon and Kim, 2013; Karjomaa et al., 1998; Nakamura et al., 2001; Sakai et al., 2001). Two steps are usually described in the degradation process of the polymer. Previous studies have shown that PLA degradation occurs mechanically and/or chemically depending on the water uptake, UV, pH, and temperature leading to the release of shorter oligomer chains and monomers of LA. In parallel, micro-organisms such as fungi and bacteria participate in the biofragmentation of the polymer by growing within the materials and provoking cracks. The second concomitant step is the enzymatic biodegradation by micro-organisms leading to carbon dioxide and/or methane and water. The biosynthesis of lipases, esterases, ureases and serine proteases (Lee et al., 2014; Matsuda et al., 2005; Sukkhum et al., 2009) cleaves the polymeric molecules into assimilable by-products. In contrast to terrestrial conditions, only few limited studies have been carried out on PLA biodegradation in the marine environment. PLA showed insignificant degradability in sea-water conditions at low temperature (18–21°C) even after immersion for 9 weeks (Zenkiewicz et al., 2012) or at 25°C for 10 weeks (Tsuji and Suzuyoshi, 2002). During tests conducted by the American Society of Testing and Materials (ASTM), the biodegradation of PLA was evaluated at 30°C. After 12 months of testing, results showed only 8% of the PLA sample biodegraded into carbon dioxide (CDRRR, 2012). In the Etel marina where our experiment was conducted, the seawater exceptionally reaches 20°C during summer in the first few metres. This low temperature may explain the relative slow degradation of PLA compared to soil or compost. Biopolymers reinforced with natural fibres provide biocomposites whose properties are comparable to those of traditional glass/polyester composites (Le Duigou et al., 2009). During a three-month immersion in seawater, the behaviour of PLA reinforced with 30% by weight of flax fibres showed a significant reduction in mechanical properties, in particular, a molecular weight decrease of almost 50% at 20°C. In comparison, the molecular weight of PLA decreased by 14% in the same conditions (Le Duigou et al., 2009). During ageing, water can diffuse by capillarity at the fibre/matrix interface and through the fibre itself (Le Duigou et al., 2009). This mechanism contributes to the hydrolysis of the matrix and may explain the long-term diffusion of small molecular weight PLA and LA from the core to the external layer of the PLA. As shown previously, a decrease in PLA molecular weight and increase in LA concentration directly depresses the attachment ratio of cypris larvae and inhibit the network formation of cement proteins involved in barnacle attachment (Ishimaru et al., 2012). Marine invertebrate larvae settlement is not completely understood but it seems that phototropism, biofilm formation and substrate topography play an important role in this process (Whalan and Webster, 2014; Whalan et al., 2015). In the perspective of a marine invasive species management, it will be of interest to understand the microbial biofilm formation at the interface between abiotic (i.e. flax/PLA biocomposite) and biotic (i.e. *C. ciocalyptoides* propagules) substrates.

To evaluate the anti-attachment properties of the biocomposite, sponge transplants were bound with an iron wire on PLA panels and their growth was compared with specimens let into nylon nets. To ascertain whether the transplantation itself had no direct effect on sponge growth and development, trace elements composition was measured as an indicator of the filter-feeding activity and compared with specimens living outside the marina. The roles of trace elements such as cadmium, copper, iron, silicon or zinc in sponge physiology seem to be essential (Mayzel et al., 2014). For example, silicon is required for the spiculogenesis in

Demospongiae. In our study, we showed transplants maintained a sufficient trace elements uptake during the first three years reflecting a normal pumping activity. The increasing levels of Ba, Cr, Cu and Ni measured in transplants are probably attributed to anthropogenic origins (urban runoff, antifouling biocides, etc.). For example, in marina, copper-based antifouling paints are largely applied onto ship hulls to limit the growth of fouling organisms. It's interesting to note that this sponge species accumulated Cu up to 11 mg kg^{-1} dry weight. In comparison, specimens living on the shore, outside the marina, accumulated in average 6.9 mg kg^{-1} dry weight. This copper tolerance confirms the inefficiency of copper-based antifouling paints to get rid of invasive species (McKenzie et al., 2012). In contrast, Si concentration was shown to be two times lower in transplanted samples. The Si uptake seemed, however, to increase by 15—20% each year suggesting sponge transplants adapted well to their new environment. Furthermore, weight gains indicated transplants let into mesh bags had a 100% increase in biomass after two years while transplants formerly bound on PLA panels did not survive. All these results indicated that the transplantation did not affect significantly sponge development and that the decline observed of our sponge transplants was due to the flax/PLA itself.

As harbours and marina are considered as the main entrance for invasive species, novel antifouling strategies are urgently needed. In this sense, an environmentally friendly approach using flax/PLA biocomposite was adopted to tackle the marine invasive sponge *C. ciocalyptoides*. In the present study, the occurrence of marine invasive sponge specimens was delayed for two years in comparison with concrete. In addition, fouling by marine invertebrates did not exceed 70% of the surface of flax/PLA panels even after 6 years of immersion. Artificial substrates such as pier pilings, boys, floats and pipes made of or coated with such biodegradable biopolymers may be useful in marina to slow or limit temporarily on their surfaces settlement by invasive species. Due to the increasing use of biopolymers for various application, many more studies on their biodegradation in marine environment are required.

Acknowledgments

We are grateful to the UBS for providing financial support to this “Epavart” project. We're also grateful to A. Magueresse for SEM micrographs, P. Jacquemin from the Lycée technique Marcelin Berthelot de Questembert (Brittany, France) for PLA panels extrusion, to Oxéa association, to B. Legrand and M. Le Corguillé, administrators of the marina of Etel for diving permission, and to A. Taranne for proofreading.

References

Ariyapitipun, T., Mustapha, A., Clarke, A.D., 1999. Microbial shelf life determination of vacuum-packaged fresh beef treated with polylactic acid, lactic acid, and nisin solutions. J. Food Protect. 62 (8), 913—920, http://dx.doi.org/10.4315/0362-028X-62.8.913.

Berno, A., Dancie, C., Pinsivy, L., Corthésy, D., Breton, G., 2016. First observation of the alien and invasive sponge *Celtodoryx ciocalyptoides* (Burton, 1935) (Porifera: Coelosphaeridae) in the port of Le Havre (English Channel). Hydroécol. Appl. 20, 131—144, (in French), https://doi.org/10.1051/hydro/2016002.

CDRR (California Department of Resources Recycling and Recovery), 2012. PLA and PHA Biodegradation in the Marine Environment, http://www.calrecycle.ca.gov/publications/Documents/1435%5C20121435.pdf, (accessed 12.12.17).

Farah, S., Anderson, D.G., Langer, R., 2016. Physical and mechanical properties of PLA, and their functions in widespread applications — a comprehensive review. Adv. Drug Deliv. Rev. 107, 367—392, http://dx.doi.org/10.1016/j.addr.2016.06.012.

Faÿ, F., Linossier, I., Legendre, G., Vallée-Réhel, K., 2008. Microencapsulation and antifouling coatings: development of poly(lactic acid) microspheres containing bioactive molecules. Macromol. Symp. 272, 4551, http://dx.doi.org/10.1002/masy.200851205.

Firth, L.B., Browne, K.A., Knights, A.M., Hawkins, S.J., Nash, R., 2016. Eco-engineered rock pools: a concrete solution to biodiversity loss and urban sprawl in the marine environment. Environ. Res. Lett. 11 (9), 094015, http://dx.doi.org/10.1088/1748-9326/11/9/094015.

Gentric, C., Sauleau, P., 2016. Distribution, abundance and pollution tolerance of the marine invasive sponge *Celtodoryx ciocalyptoides* (Burton, 1935) in the Etel river. Cah. Biol. Mar. 57, 57—64, http://dx.doi.org/10.21411/CBM.A.7079EADE.

Glasby, T.M., Connell, S.D., Holloway, M.G., Hewitt, C.L., 2007. Nonindigenous biota on artificial structures: could habitat creation facilitate biological invasions? Mar. Biol. 151 (3), 887—895, http://dx.doi.org/10.1007/s00227-006-0552-5.

Hakkarainen, M., Karlsson, S., Albertsson, A.C., 2000. Rapid (bio) degradation of polylactide by mixed culture of compost microorganisms — low molecular weight products and matrix changes. Polymer 41 (7), 2331—2338, http://dx.doi.org/10.1016/S0032-3861(99)00393-6.

Hamad, K., Kaseem, M., Yang, H.W., Deri, F., Ko, Y.G., 2015. Properties and medical applications of polylactic acid: a review. Express Polym. Lett. 9 (5), 435—455, http://dx.doi.org/10.3144/expresspolymlett.2015.42.

Henkel, D., Janussen, D., 2011. Redescription and new records of *Celtodoryx ciocalyptoides* (Demospongiae: Poecilosclerida) — a sponge invader in the north east Atlantic Ocean of Asian origin? J. Mar. Biol. Ass. U.K. 91 (2), 347—355, http://dx.doi.org/10.1017/S0025315410001487.

Ishimaru, N., Tsukegi, T., Wakisaka, M., Shirai, Y., Nishida, H., 2012. Effects of poly(L-lactic acid) hydrolysis on attachment of barnacle cypris larvae. Polym. Degrad. Stab. 97 (11), 2170—2176, http://dx.doi.org/10.1016/j.polymdegradstab.2012.08.012.

Jeon, H.J., Kim, M.N., 2013. Biodegradation of poly(L-lactide) (PLA) exposed to UV irradiation by a mesophilic bacterium. Int. Biodeterior. Biodegrad. 85, 289—293, http://dx.doi.org/10.1016/j.ibiod.2013.08.013.

Karjomaa, S., Suortti, T., Lempiäinen, R., Selin, J.F., Itävaara, M., 1998. Microbial degradation of poly-(L-lactic acid) oligomers. Polym. Degrad. Stab. 59 (1—3), 333—336, http://dx.doi.org/10.1016/S0141-3910(97)00204-8.

Le Duigou, A., Davies, P., Baley, C., 2009. Seawater ageing of flax/poly(lactic acid) biocomposites. Polym. Degrad. Stab. 94 (7), 1151—1162, http://dx.doi.org/10.1016/j.polymdegradstab.2009.03.025.

Le Duigou, A., Bourmaud, A., Davies, P., Baley, C., 2014. Long term immersion in natural seawater of Flax/PLA biocomposite. Ocean Eng. 90, 140—148, http://dx.doi.org/10.1016/j.oceaneng.2014.07.021.

Lee, S.H., Kim, I.Y., Song, W.S., 2014. Biodegradation of polylactic acid (PLA) fibers using different enzymes. Macromol. Res. 22 (6), 657—663, http://dx.doi.org/10.1007/s13233-014-2107-9.

Ludwick, J.J., Rossmann, S.N., Johnson, M.M., Edmonds, J.L., 2006. The bacteriostatic properties of ear tubes made of absorbable polylactic acid. Int. J. Pediatr. Otorhinolaryngol. 70 (3), 407—410, http://dx.doi.org/10.1016/j.ijporl.2005.05.025.

Mahaut, M.-L., Basuyaux, O., Baudinière, E., Chataignier, C., Pain, J., Caplat, C., 2013. The porifera *Hymeniacidon perlevis* (Mon-

tagu, 1818) as a bioindicator for water quality monitoring. Environ. Sci. Pollut. Res. 20 (5), 2984–2992, http://dx.doi.org/10.1007/s11356-012-1211-7.

Matsuda, E., Abe, N., Tamakawa, H., Kaneko, J., Kamio, Y., 2005. Gene cloning and molecular characterization of an extracellular poly(L-lactic acid) depolymerase from *Amycolatopsis* sp. strain K104-1. J. Bacteriol. 187 (21), 7333–7340, http://dx.doi.org/10.1128/JB.187.21.7333-7340.2005.

Mayzel, B., Aizenberg, J., Ilan, M., 2014. The elemental composition of demospongiae from the Red Sea, Gulf of Aqaba. PLOS ONE 9 (4), e95775, http://dx.doi.org/10.1371/journal.pone.0095775.

McKenzie, L.A., Johnston, E.L., Brooks, R., 2012. Using clones and copper to resolve the genetic architecture of metal tolerance in a marine invader. Ecol. Evol. 2 (6), 1319–1329, http://dx.doi.org/10.1002/ece3.241.

Nakamura, K., Tomita, T., Abe, N., Kamio, Y., 2001. Purification and characterization of an extracellular poly(L-lactic acid) depolymerase from a soil isolate, *Amycolatopsis* sp. strain K104-1. Appl. Environ. Microbiol. 67 (1), 345–353, http://dx.doi.org/10.1128/AEM.67.1.345-353.2001.

Perez, T., Perrin, B., Carteron, S., Vacelet, J., Boury-Esnault, N., 2006. *Celtodoryx girardae* gen. nov. sp. nov., a new sponge species (Poecilosclerida: Demospongiae) invading the Gulf of Morbihan (North East Atlantic, France). Cah. Biol. Mar. 47, 205–214, http://dx.doi.org/10.21411/CBM.A.1E48CEBD.

Piola, R.F., Dafforn, K.A., Johnston, E.L., 2009. The influence of antifouling practices on marine invasions. Biofouling 25 (7), 633–644, http://dx.doi.org/10.1080/08927010903063065.

Pranamuda, H., Tokiwa, Y., Tanaka, H., 1997. Polylactide degradation by an *Amycolatopsis* sp. Appl. Env. Microbiol. 63 (4), 1637–1640.

Qian, P.Y., Lau, S.C.K., Dahms, H.U., Dobretsov, S., Harder, T., 2007. Marine biofilms as mediators of colonization by marine macroorganisms: implications for antifouling and aquaculture. Mar. Biotechnol. 9 (4), 399–410, http://dx.doi.org/10.1007/s10126-007-9001-9.

Ruiz, G.M., Freestone, A.L., Fofonoff, P.W., Simkanin, C., 2009. Habitat distribution and heterogeneity in marine invasion dynamics: The importance of hard substrate and artificial structure. In: Wahl, M. (Ed.), Marine Hard Bottom Communities. Springer, Berlin-Heidelberg, 321–332, http://dx.doi.org/10.1007/b76710_23.

Sakai, K., Kawano, H., Iwami, A., Nakamura, M., Moriguchi, M., 2001. Isolation of a thermophilic poly-L-lactide degrading bacterium from compost and its enzymatic characterization. J. Biosci. Bioeng. 92 (3), 298–300, http://dx.doi.org/10.1016/S1389-1723(01)80266-8.

Sukkhum, S., Tokuyama, S., Tamura, T., Kitpreechavanich, V., 2009. A novel poly(L-lactide) degrading actinomycetes isolated from Thai forest soil, phylogenic relationship and the enzyme characterization. J. Gen. Appl. Microbiol. 55, 459–467, http://dx.doi.org/10.2323/jgam.55.459.

Theinsathid, P., Visessanguan, W., Kruenate, J., Kingcha, Y., Keeratipibul, S., 2012. Antimicrobial activity of lauric arginate-coated polylactic acid films against *Listeria monocytogenes* and *Salmonella typhimurium* on cooked sliced ham. J. Food Sci. 77 (2), M142–M149, http://dx.doi.org/10.1111/j.1750-3841.2011.02526.x.

Thouvenin, M., Langlois, V., Briandet, R., Langlois, J.Y., Guerin, P.H., Peron, J.J., Haras, D., Vallee-Rehel, K., 2003. Study of erodable paint properties involved in antifouling activity. Biofouling 19 (3), 177–186, http://dx.doi.org/10.1080/08927014.2003.10382980.

Tsuji, H., Suzuyoshi, K., 2002. Environmental degradation of biodegradable polyesters 2, poly(ε-caprolactone), poly[(R)-3-hydroxybutyrate], and poly(L-lactide) films in natural dynamic seawater. Polym. Degrad. Stab. 75 (2), 357–365, http://dx.doi.org/10.1016/S0141-3910(01)00239-7.

Ulery, B.D., Nair, L.S., Laurencin, C.T., 2011. Biomedical applications of biodegradable polymers. J. Polym. Sci. Pol. Phys. 49 (12), 832–864, http://dx.doi.org/10.1002/polb.22259.

Van Soest, R.W.M., de Kluijver, M.J., van Bragt, P.H., Faasse, M., Nijland, R., Beglinger, E.J., de Weerdt, W.H., de Voogd, N.J., 2007. Sponge invaders in Dutch coastal waters. J. Mar. Biol. Ass. U.K. 87 (6), 1733–1748, http://dx.doi.org/10.1017/S002531540705816X.

Vaz-Pinto, F., Torrontegi, O., Prestes, A.C.L., Alvaro, N.V., Neto, A.I., Martins, G.M., 2014. Invasion success and development of benthic assemblages: effect of timing, duration of submersion and substrate type. Mar. Environ. Res. 94, 72–79, http://dx.doi.org/10.1016/j.marenvres.2013.12.007.

Walczak, M., Brzezinska, M.S., Sionkowska, A., Michalska, M., Jankiewicz, U., Deja-Sikora, E., 2015. Biofilm formation on the surface of polylactide during its biodegradation in different environments. Colloids Surf. B Biointerfaces 136, 340–345, http://dx.doi.org/10.1016/j.colsurfb.2015.09.036.

Whalan, S., Webster, N.S., 2014. Sponge larval settlement cues: the role of microbial biofilm in a warming ocean. Sci. Rep. 4, 4072, http://dx.doi.org/10.1038/srep04072.

Whalan, S., Abdul Wahab, M.A., Sprungala, S., Poole, A.J., de Nys, R., 2015. Larval settlement: the role of surface topography for sessile coral reef invertebrates. PLoS ONE 10 (2), e0117675, http://dx.doi.org/10.1371/journal.pone.0117675.

Zenkiewicz, M., Malinowski, R., Rytlewski, P., Richert, A., Sikorska, W., Krasowska, K., 2012. Some composting and biodegradation effects of physically or chemically crosslinked poly(lactic acid). Polym. Test. 31 (1), 83–92, http://dx.doi.org/10.1016/j.polymertesting.2011.09.012.

Oceanologia (2019) 61, 227—238

Available online at www.sciencedirect.com

ScienceDirect

journal homepage: www.journals.elsevier.com/oceanologia/

ORIGINAL RESEARCH ARTICLE

Life in sympatry: coexistence of native *Eurytemora affinis* and invasive *Eurytemora carolleeae* in the Gulf of Finland (Baltic Sea)

Natalia Sukhikh [a,*], Anissa Souissi [b], Sami Souissi [b], Anne-Catherine Holl [c], Nikolaos V. Schizas [d], Victor Alekseev [a]

[a] *Zoological Institute, Russian Academy of Sciences, Saint Petersburg, Russia*
[b] *Lille University, CNRS, ULCO, LOG, Wimereux, France*
[c] *Lille University of Science and Technology, CNRS, Villeneuve d'Ascq Cedex, France*
[d] *Department of Marine Sciences, University of Puerto Rico, Mayagüez, Puerto Rico*

Received 18 June 2018; accepted 2 November 2018
Available online 22 November 2018

KEYWORDS
Eurytemora species;
Copepoda;
Zooplankton;
Invasive and native species;
Gulf of Finland

Summary The invasion of exotic species into native ecosystems is becoming a crucial issue in global biology. Over the last ten years, at least 45 invasions of aquatic species have been reported in the eastern part of the Gulf of Finland; the majority of them were introduced through ballast water. Recently, invasion of the estuarine calanoid copepod *Eurytemora carolleeae* (Temoridae), originating from North America, has been reported in several European estuaries and particularly in the Gulf of Finland. This species is morphologically very similar to the native *Eurytemora affinis*, but it is easily discriminated by molecular markers. In this study, we monitored the distribution area of the invasive copepod species in European waters, as well as the population structure of (native) *E. affinis* and (invasive) *E. carolleeae*, from 2006 to 2018 in the Gulf of Finland. The population density of *E. affinis* was significantly higher, compared to *E. carolleeae*, during most of the study period. The only exception was Neva Bay in 2010, wherein the invasive species dominated possibly due to high temperatures and differences in the levels of fish predation. The reproductive performance of *E. carolleeae* was also higher than that of *E. affinis*. These results show different population dynamics between the two species. It was revealed that invasive *E. carolleeae* develops in some of the very

* Corresponding author at: Zoological Institute, Russian Academy of Sciences, 1 Universitetskaya emb., St.-Petersburg, 199034, Russia. Tel.: +7 812 328 13 11; fax: +7 812 328 02 21.
E-mail addresses: Susikh1@mail.ru (N. Sukhikh), anissa.ben-radhia@univ-lille1.fr (A. Souissi), Sami.Souissi@univ-lille1.fr (S. Souissi), Anne-Catherine.Holl@univ-lille1.fr (A.-C. Holl), nschizas@gmail.com (N.V. Schizas), alekseev@zin.ru (V. Alekseev).
Peer review under the responsibility of Institute of Oceanology of the Polish Academy of Sciences.

ELSEVIER Production and hosting by Elsevier

https://doi.org/10.1016/j.oceano.2018.11.002

same habitats as native *E. affinis*, thereby potentially becoming a significant component of the zooplankton in the studied area. Moreover, invader has the potential to displace native *E. affinis*.

1. Introduction

An estimated 140—171 aquatic invasions have been reported in the Baltic Sea during the last two centuries (www.stateofthebalticsea.helcom.fi; www.corpi.ku.lt). The geologically young ecosystem of the Baltic Sea, in combination with salinity gradients, has resulted in many new ecological niches. These factors have been hypothesized to provide the key necessary conditions for the spread of new invasive species and their naturalization in the area (Leppäkoski et al., 2002a,b). Previous and ongoing intensive maritime traffic, however, results in the displacement of million of tons of ballast water from site to site (www.helcom.fi/Lists/Publications). These transfers are impacting the Baltic's flora and fauna, and they may be a major factor in the multiple invasions recorded in the region during the last century (Ojaveer and Kotta, 2015).

The Gulf of Finland is one of the most dense maritime traffic areas in the Baltic Sea; it includes several active international shipping routes and large ports (Pollumaea and Valjataga, 2004). Consequently, more than 40 alien species have been found during the last ten years in only the eastern part of the Gulf of Finland, most of which were invertebrates (Lehtiniemi et al., 2016). Most of these species were introduced through ballast water (Berezina et al., 2011; Katajisto et al., 2013; Lehtiniemi et al., 2016; Panov et al., 2003; www.helcom.fi/Lists/Publications; www.stateofthebalticsea.helcom.fi), including: *Cercopagis pengoi* (Ostroumov, 1891) (Crustacea: Cladocera), *Mytilopsis leucophaeata* (Conrad, 1831), (Mollusca: Bivalvia), *Palaemon serratus* (Pennant, 1777) (Crustacea: Decapoda), *Eriocheir sinensis* (Milne-Edwards, 1853) (Crustacea: Decapoda), *Palaemon elegans* (Martin Rathke, 1837) (Crustacea: Decapoda), *Neogobius melanostomus* (Pallas, 1814) (Fish).

The invasive species list includes several copepod species, among which there is a report of a subtle invasion in 2007 of the estuarine North American copepod *Eurytemora carolleeae* Alekseev and Souissi, 2011 in the eastern part of the Gulf of Finland (Alekseev et al., 2009; Sukhikh et al., 2013). Later, this species was also detected in the Gulf of Riga and in the Amsterdam channels (Sukhikh et al., 2013), as well as in additional locations (Wasmund et al., 2013), namely: Kiel Bight, Mecklenburg Bight, Arkona Sea, Bornholm Sea, and in Eastern Gotland Sea.

It is interesting that, according to pictures and descriptions of *Eurytemora* species in English waters (Gurney, 1931), *E. carolleeae* already inhabited this area of water at the beginning of 20th century. Possibly, it was an invasion through ship ballast water, similar to the case of *Eurytemora americana* Williams, 1906, which was originally discovered in 1933 in the same area (Sukhikh et al., 2016a). Recent genetic studies of *Eurytemora* populations have not revealed the presence of *E. carolleeae* in English waters (Lee, 2000; Sukhikh et al., 2016b; Winkler et al., 2011). However, genetic studies targeted few crustacean specimens, and it is likely that they missed *E. carolleeae*. In addition, early morphological studies may have misidentified this species as *Eurytemora affinis* (Poppe, 1880).

The *E. affinis* species complex is a group of species inhabiting the Holarctic (Sukhikh et al., 2013). The species complex is currently represented by three species: *E. affinis* with Palearctic distribution; North American *E. carolleeae*; and Asian *Eurytemora caspica* Sukhikh and Alekseev, 2013. All of these species inhabit estuaries and freshwater reservoirs where they are the dominant pelagic species and constitute the main food source for animals at higher trophic levels (e.g. Devreker et al., 2008, 2010; Dur et al., 2009; Lee, 2000).

The *E. affinis* species complex has been well studied (Devreker et al., 2008, 2010; Dur et al., 2009; Hirche, 1992; Knatz, 1978; Lajus et al., 2015; Lloyd et al., 2013). Experimental studies comparing the reproductive traits (development time, clutch size and longevity) of *E. affinis* (from the Seine estuary, France) and *E. carolleeae* (from St. Lawrence salt marshes, Canada; and Chesapeake Bay, USA) have confirmed the higher fitness of the North American population (Beyrend-Dur et al., 2009; Devreker et al., 2012) compared to the European one (Devreker et al., 2009, 2012). In addition, field measurements have suggested that, in both populations, egg production decreased when temperatures rose above 18°C (Lloyd et al., 2013; Pierson et al., 2016). This corroborates results from laboratory experiments (Devreker et al., 2012).

In this paper, we investigated the coexistence of these two *Eurytemora* species in the Gulf of Finland. The presence of both species in the Baltic Sea is the result of secondary contact. Historically, only *E. affinis* inhabited the studied region, whereas the native habitat of *E. carolleeae* was the North American Atlantic coast. *E. affinis* and *E. carolleeae* diverged approximately 5.1 million years ago, dating to the time of the Miocene/Pliocene boundary (Lee, 2000). They have a mean sequence divergence of 15% in part of the mitochondrial cytochrome c oxidase I (COI) gene.

The detection of these related species in Baltic waters is likely the result of recent invasion by *E. carolleeae* via the ballast water of ships (Alekseev et al., 2009; Sukhikh et al., 2013). The most likely source of this invasion is the Atlantic coast of the United States (Alekseev et al., 2009; Sukhikh et al., 2013).

E. carolleeae and *E. affinis* are very similar morphologically and it appears as though they occupy, more or less, the same ecological niches. Like other invasive species, however, displacements can be detrimental to ecosystem stability. At the beginning of the invasion, sibling species cause unidentifiable changes in biological diversity, followed by rearran-

gement of the aquatic communities (Gelembiuk et al., 2006). In fact, such species can exhibit distinct habitat preferences defined by depth, salinity, or exposure. Successional differences between sibling species, reflecting temporal partitioning of resources in response to seasonal change or disturbance, have also been documented (Knowlton, 1993). This may be the result of different physiologies. Moreover, hybridization experiments, between these North American and European species, have shown reproductive incompatibility among them (S. Souissi, unpublished). For example, six *Tubifex tubifex* (oligochaetes) lineages living sympatrically differed in their tolerance to cadmium (Sturmbauer et al., 1999) and in their resistance to infection by *Myxobolus cerebralis* (Beauchamp et al., 2001).

Previous data on the region's zooplankton community is rather limited and has been published mainly in Russian. The zooplankton community of the eastern part of the Gulf of Finland is represented mainly by freshwater species. The bulk of zooplankton, by mass, usually consists of Cladocera (Pollumae and Kotta, 2007; Uitto et al., 1999), while copepods dominate numerically (Ogorodnikova and Volkhonskaya, 2006; Ostov, 1971; Ryabova and Pogrebov, 1991). In general, zooplankton in the Russian Gulf of Finland are distributed irregularly, and the areas of highest zooplankton abundance are located in the southern and eastern regions (Ostov, 1971). Depending on the year of the study, zooplankton biomasses have varied from 140 to 1000 mg m^{-3} (Antsulevich et al., 1995; Basova, 1983; Lavrentieva and Finogenova, 1999). As a result, Luga Bay and Neva Bay (both situated in the southeastern Gulf of Finland) serve as the main areas for fish feeding and breeding (Golubkov, 2009). The main consumers of zooplankton in the Gulf of Finland are Baltic herring. Since the mid-1990s, however, Sprat (*Sprattus sprattus* (Linnaeus)), which is recovering from overfishing in the 1970s, has also begun to play a significant role as a zooplankton predator (Alimov et al., 2004).

Zooplankton aggregations are represented by both brackish and freshwater species in Luga Bay. Studies (Lavrentieva and Finogenova, 1999; Ogorodnikova and Volkhonskaya, 2006; Ryabova and Pogrebov, 1991; Sergeev et al., 1971) have shown that different species have dominated aggregations in different years: *Keratella quadrata* (Muller); *Keratella cochlearis* (Gosse); *Synchaeta baltica* Ehrenberg; *Synchaeta oblonga* Ehrenberg; *Bosmina obtusirostris* Sars; *Acartia clausi* Giesbrecht; *Daphnia cristata* Sars; *Daphnia cucullata* Sars; and *Eurytemora* spp. Generally speaking, these dominant species occur in others parts of the Gulf of Finland as well (Pollumae and Kotta, 2007; Uitto et al., 1999). *Eurytemora* spp. are invariably present in these species lists (Uitto et al., 1999). It is one of the dominant members in the Gulf of Finland (https://www.st.nmfs.noaa.gov/copepod/time-series/fi-30103/), and they reach up to 50% of all zooplankton biomass in the study area (Sukhikh, unpublished data). *Eurytemora* spp. consist up to 45% of all stomachs of cyprinid species and are abundantly found in the stomachs of sticklebacks (Demchuk et al., 2017).

Little is known about local *Eurytemora* spp. populations and even less is known about the new invasive species, *E. carolleeae*, in the Baltic Sea. This is the first study of the population structure and reproductive traits of two related species living together in the Baltic Sea: native *E. affinis* and invasive *E. carolleeae* (of western Atlantic origin). We have used genetic markers to examine the potential for hybridization between these two closely related species (*E. affinis* and *E. carolleeae*) which are living in sympatry.

As the invasion of *E. carolleeae* seems to be a recent and rapid process, we hypothesize here that it has the potential to displace native *E. affinis* in the Gulf of Finland ecosystem and possibly in the entire Baltic Sea. Such an outcome is especially possible under certain conditions, such as force majeure events that cause profound environmental changes. We seek to clarify spatial and temporal differences in their distributions that are related to, or dependent on, environmental parameters in order to gain a better understanding of the potential for native *E. affinis* to be displaced by invasive *E. carolleeae*.

2. Material and methods

2.1. Sampling

In order to reveal the distribution of invasive *E. carolleeae* in European waters, copepods were collected from 11 European sites between 2004 and 2017: channels in Amsterdam; the Elbe, Seine, Schelde, Loire, and Gironde estuaries; the Lake of the Bois de Boulogne (Paris); Umeå Seaport (Sweden); Vistula Lagoon; the Gulfs of Riga and Finland (the Baltic Sea); and the Northern Dvina River (Fig. 1, Table 1). Three sites were analyzed in the Gulf of Finland: the Gulf of Vyborg, Neva Bay and Luga Bay.

Monitoring of invasive species has been carried out periodically since 2004 in Neva Bay and since 2006 in Luga Bay. To estimate the relative percentage of the two *Eurytemora* species in Neva and Luga Bays, samplings were performed once per year, usually during August when high population densities are observed; Luga Bay sampling in 2010 was an exception and occurred in September. The total number of studied specimens ranged from 15 to 181 per site (the number of specimens obtained in three replicates, three nets in each).

Seasonal monitoring of adult population densities (*E. affinis* and *E. carolleeae*) in Luga Bay (Gulf of Finland) was carried out from 10.06 to 27.08 in 2006, from 19.04 to 17.09 in 2008 and from 16.06 to 27.09 in 2015. Sampling was performed at the mouth of Luga River, every ten days in 2006 and in 2008, and every twenty days in 2015. Water salinity and temperature at the mouth of the Luga River were measured using a COM-100 waterproof combination meter (HM Digital, USA).

Samples were collected with 100 μm or 230 μm mesh plankton nets by vertical tows from depth to surface in three replicates and preserved in 96% ethanol or in 4% formalin solution (sampling information is given in Table 1).

2.2. Species identification

Identification of adult *E. affinis* and *E. carolleeae* copepods was accomplished by following published taxonomical keys (Alekseev and Souissi, 2011; Sukhikh and Alekseev, 2013). Morphological analysis of adult copepods was performed under an SZX2 dissection microscope (Olympus) with a 5 μm resolution ocular micrometer. *E. carolleeae* type material from the Russian Academy of Sciences Zoological Insti-

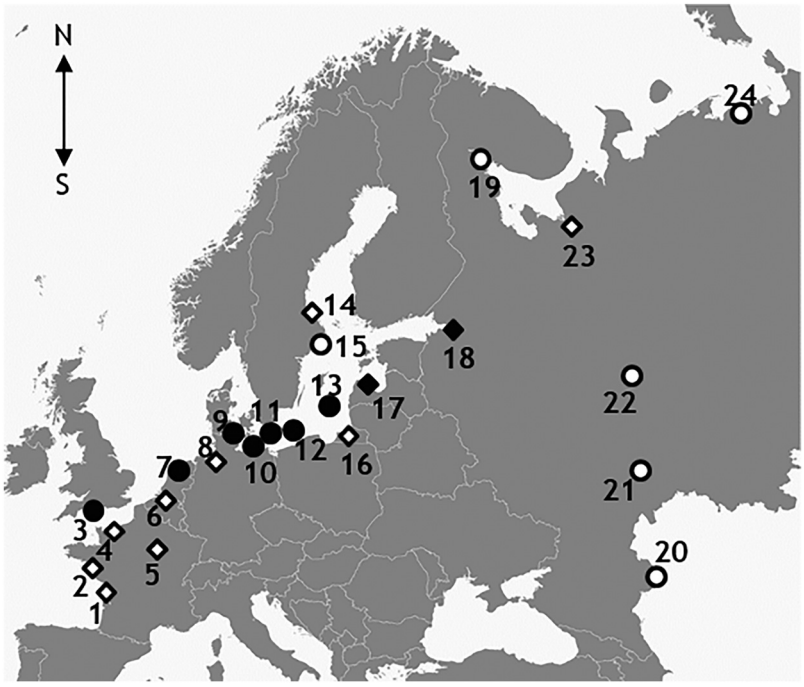

Figure 1 Sampling locations analyzed by the authors (rhombi) and literature data on the distribution of invasive *Eurytemora carolleeae* in Europe (circles). Black figures represent the presence of invasive *Eurytemora carolleeae* in studied area. 1 — Gironde Estuary; 2 — Loire Estuary; 3 — Chelson Meadow, Plymouth, British waters (Gurney, 1931); 4 — Seine Estuary; 5 — Lake in Bois de Boulogne (Paris); 6 — Scheldt Estuary; 7 — Amsterdam channels (Sukhikh et al., 2013); 8 — Elbe Estuary; 9—13: 9 — Kiel Bight, 10 — Mecklenburg Bight, 11 — Arkona Sea, 12 — Bornholm Sea and 13 — Eastern Gotland Sea (Wasmund et al., 2013); 14 — Gulf of Bothnia, Umeå; 15 — Stockholm (Gorokhova et al., 2013); 16 — Vistula lagoon; 17 — Gulf of Riga; 18 — Gulf of Finland; 19 — the White Sea (Sukhikh et al., 2016a,b and pers. comm. of Polyakova N.V.); 20—22 — the Caspian Sea and the drainage basin of Volga River (Lazareva et al., 2018; Sukhikh et al., 2018); 23 — Northern Dvina River; 24 — Pechora Estuary (Cherevichko, 2017; Fefilova, 2015).

tute collection was used for reference in this study (type collection #55052-55054). Identification of specimens from the Schelde River, Seine estuary, Gulf of Riga, Gulf of Finland, Vistula Lagoon, Loire estuary, Lake in the Bois de Boulogne, and Northern Dvina River was also supported by DNA sequencing of a portion of the mitochondrial cytochrome oxidase subunit 1 gene (COI, see below). In studying and estimating population densities in Luga Bay, only adult stages of *E. affinis* and *E. carolleeae* were analyzed as there are no clear morphological features distinguishing the juvenile stages (nauplii and copepodites) of these closely related species. Moreover, an additional *Eurytemora* species, *Eurytemora lacustris* (Poppe, 1887), was present in the zooplankton community of the sampled area. The juvenile stages of *E. lacustris* are also indistinguishable from those of *E. affinis* and *E. carolleeae*. As a result, it was impossible for us to separately distinguish or estimate nauplii and copepodites densities for these three *Eurytemora* species.

2.3. Morphological and reproductive traits measurements

For measurement of reproductive parameters, 20 *E. carolleeae* females and 23 *E. affinis* females were randomly selected from the same sample collected in July 2015 in Luga Bay (water temperature 17.3°C). The number of eggs per clutch and the egg diameters of 5—10 eggs from each clutch were calculated for each female of both species. In addition, the lengths and widths of the prosome and the egg sac were measured under a dissection microscope (as above).

2.4. Statistical analysis

Differences between the species, in terms of reproductive parameters as well as in the lengths and widths of prosomes and egg sacs, were quantified using the nonparametric Kruskal—Wallis test as implemented in the Statistica 7 software package. The relationships between female prosome length and clutch size, in both studied species, were shown by linear regression analysis (Statistica 7). The significance limit was set at $p < 0.05$.

2.5. Material used for genetic analysis

The nuclear ribosomal 18S gene, ITS regions (including 5.8S), and one mitochondrial (COI) gene were analyzed in the present study. Specimens used for genetic analysis were obtained from: Neva Bay (Russia), July 2014 (*E. affinis*, *E. carolleeae*); the Loire and Seine Rivers (France), April 2011 (*E. affinis*); the Saint-Lawrence estuary (France), September 2014 (*E. carolleeae*); and a laboratory collection (*E. carolleeae*), originally from Chesapeake Bay (U.S.A.). A total of 18 *E. affinis* individuals and 23 *E. carolleeae* individuals were analyzed with genetic tools.

Table 1 Sampling locations of populations of *Eurytemora affinis* and *Eurytemora carolleeae*.

Sampling locations	Sampling date	Sample size for genetic analysis[a]	Sample size for morphological analysis[b]	Latitude	Longitude
Elbe estuary	March 2006		50	53°53′24N	09°08′44E
Scheldt River	April 2011	7	15	51°13′42N	04°23′86E
Antwerp	April 2011	1	15	51°N	04°E
Duaene					
Seine estuary	April 2011	37	10	49°28′33N	00°27′54W
	May 2008		8	49°28′33N	00°27′54W
	July 2008		9	49° N	00°W
Gulf of Riga	Aug. 2008	14	29	57° 04′44N	23°04′44E
City Port					
Gulf of Finland:	Sep. 2007	35	10	60°23′39N	28°26′74E
Gulf of Vyborg	Aug. 2009	30	110	59°32′36N	29°28′17E
Neva R. estuary	Aug. 2010	30	227	59°24′13N	28°11′06E
Luga R. estuary	Aug. 2004, 2007, 2010–12, 2014–15				
	Aug. 2006–09, 2011, 2015				
	Sep. 2010				
Vistula Lagoon	Oct. 2007	5	30	54°65′02N	20°23′37E
	Jun. 2015		30		
Northern Dvina River	Aug. 2015	5	10	64°33′00N	40°32′00E
Gulf of Bothnia, Umeå	May 2010		10	63°49′30″N	20°15′50″E
Loire estuary	April 2011	52	10	47°17′23N	02°01′52W
St.1	July 2009		9		
St.2					
Gironde estuary	May 2005		10	45°04′10N	00°38′30W
St.1	July 2009		4		
St.3					
Lake in the Bois de Boulogne (Paris)	July 2010	3		48°51′48N	2°15′07E
Saint-Lawrence Estuary	Sep. 2014	4		48°1′1N	69°20′8W
Chesapeake Bay	Feb. 2013	3		38°36′15N	76°4′54W

[a] Number of individuals sequenced per location.
[b] Number of individuals analyzed with morphological method.

2.6. DNA extraction, amplification, and sequencing

Genomic DNA was extracted from single adult copepods preserved in 96% ethanol using a standard method described by Aljanabi and Martinez (1997) or using a cell lysis buffer with Proteinase-K protocol modified from Hoelzel and Green (1992) and Lee (2000). Polymerase chain reaction (PCR), in order to achieve cytochrome oxidase subunit 1 (COI) amplification, utilized both universal (COIH, COIL) and specific (EuF1, EuR2) primers. Their sequences are: COIH 2198 (5′-TAAACTTCAGGGTGACCAAAAAATCA-3′); COIL 1490 (5′-GGTCAACAAATCATAAAGATATTGG-3′; Folmer et al., 1994); EuF1 (5′-CGTATGGAGTTGGGACAAGC-3′); and EuR2 (5′-CAAAATAAGTGTTGGTATAAAATTGGA-3′; Winkler et al., 2011). Two thermocycling programs, modified from Lee (2000), were used for PCR amplification. The first was 5 cycles of 90°C (30 s), 45°C (60 s), 72°C (90 s); followed by 27 cycles of 90°C (30 s), 55°C (45 s), 72°C (60 s); and ending with 5 min at 72°C. The second program featured an initial denaturation at 95°C for 30 s; followed by 5 cycles of 90°C (30 s), 55°C (60 s), 72°C (90 s); followed by 27 cycles of 90°C (30 s), 55°C (45 s), 72°C (60 s); and ending with 5 min at 72°C. These conditions and methods were used in our previous work (Sukhikh et al., 2016a,b).

Complete 18S rDNAs were amplified using the primer pair 18A1 mod (5′-CTGGTTGATCCTGCCAGTCATATGC-3′) and 1800 mod (5′-GATCCTTCCGCAGGTTCACCTACG-3′) (Raupach et al., 2009). The ITS-4 and ITS-5 universal nITS (nuclear ribosomal DNA internal transcribed spacer) primers (White et al., 1990) were used for amplification of the ITS1-5.8SrRNA-ITS2 region. PCR conditions for both sets of primers (18SrRNA and nITS) were: initial denaturation at 95°C for 30 s; followed by 38 cycles of 95°C (30 s), annealing (50°C for nITS or 55°C for 18SrRNA) for 30 s, 72°C (70 s); and a final extension at 72°C for 7 min.

Amplified products were purified with a QIAquick PCR purification kit (Qiagen, Valencia, CA, USA) and sequenced using an ABI 3100 or 3130 automated sequencer (Applied Biosystems Inc., Foster City, CA, USA). Both DNA strands were sequenced to confirm the accuracy of each sample sequence.

Sequences were aligned using the CLUSTAL W algorithm (Thompson et al., 1994) implemented in BIOEDIT v.7.2 (Hall, 1999) with manual editing of ambiguous sites. The number of

polymorphic sites was estimated using DNASP v6 (Librado and Rozas, 2009). The level of nucleotide differences between the species was calculated using the Tamura-Nei 93 model with the MEGA 6.06 software package (Tamura et al., 2013).

3. Results

3.1. Distribution of invasive species in European waters

Apart from the Gulf of Finland, the presence of invasive American *Eurytemora* species was monitored at 11 sampling locations (Table 1) over the last 12 years. As a result, *E. carolleeae* was detected in Riga Bay and in Amsterdam channels. The density of American *Eurytemora* in Riga Bay did not exceed 2% of total density (both *Eurytemora* species). In contrast, *E. carolleeae* was more prevalent in Amsterdam channels with a total of about 30% of the combined *Eurytemora* density. *E. carolleeae* was absent from all samples from the Schelde, Seine, Loire, and Gironde estuaries, and also absent from the Bois de Boulogne (Paris), Vistula Lagoon, the Gulf of Bothnia (the Baltic Sea), and Northern Dvina River.

3.2. Coexistence of native and invasive *Eurytemora* species in the Gulf of Finland

During the entire study period, *E. affinis* numerically dominated the *Eurytemora* species assemblage in the Gulf of Finland (Fig. 3a, b). *Eurytemora carolleeae* accounted for 2–30% in Luga Bay and from 0% to 100% in Neva Bay. During the whole study period, *E. carolleeae* occurred in fewer numbers than *E. affinis* in Neva and Luga Bay regions in the Gulf of Finland. The maximum *E. carolleeae* density percentages were observed in 2010 and 2015 (Fig. 3a). At the same time, the densities of *E. carolleeae* adult females during the unusual temperature conditions in 2010 and 2015, were similar to those seen during the thermally normal year 2011, in which *E. affinis* was prevalent (631 $\pm$ 259 ind m^{-3}). Indeed, the density of *E. carolleeae* adult females in mid September 2010 in Neva Bay was 24 $\pm$ 11 ind m^{-3}. In July 2011, the density of *E. carolleeae* adult females was about 16 $\pm$ 10 ind m^{-3}. In mid August 2015, the density of *E. carolleeae* adult females was 24 $\pm$ 8 ind m^{-3}. *E. affinis* adult females densities in 2010 and 2015 were low: 108 $\pm$ 51 ind m^{-3} and 1 $\pm$ 1 ind m^{-3}, respectively.

3.3. Salinity and temperature conditions in Luga Bay, Gulf of Finland

Water salinity in the studied area at the mouth of the Luga River changed from 0.67 to 2.31 psu during the monitoring period. Temperatures during the summers of 2006, 2008, 2015, and 2017 ranged from a minimum of 12.8°C (in June 2015) to a maximum of 23.2°C (in July 2006) (Fig. 2). In this region of the Gulf of Finland, mean water temperature in July is usually between 18 and 20°C (http://weatherarchive.ru). During 2010, 2015, and 2017, however, water temperatures were unexpectedly different. In 2010, for example, 23.5°C was recorded. Yet, the summers of 2015 and 2017, by contrast, were rather cool and mean July temperatures were 17.1°C and 15.8°C, respectively (http://weatherarchive.ru).

3.4. Density changes in adult *E. affinis* and *E. carolleeae* populations

The average density of the zooplankton community (represented mainly by Rotifera, Cladocera, and Copepoda) was about 10^5 ind m^{-3} in all studied periods. The Order Copepoda dominated the summer zooplankton community (~50,000 ind m^{-3}). The predominant zooplankton species were the rotifer *Keratella quadrata*, the calanoid copepod *E. affinis*, and the cladoceran *Bosmina longispina*. *E. carolleeae* was present in all of the Gulf of Finland study locations. Seasonal monitoring of *E. carolleeae* and *E. affinis* in Luga Bay showed that both species exhibited two summer population density peaks (in years 2015 and in 2008) and one strong peak in 2006 (Fig. 4). In 2006, the major peak for both species was observed in the end-of-June to beginning-of-July time frame, yet with an almost five fold higher density for *E. affinis* than for *E. carolleeae*. A minor peak was noted for *E. affinis* at the beginning of August, as well as a slight increase at the end of the month (Fig. 4a).

In 2008, the highest density was observed between mid-June and the beginning of July for *E. affinis*, and a second peak was recorded at the end of August. At the same times, two peaks of density were also observed for *E. carolleeae* but of smaller magnitude (Fig. 4b).

In 2015, the first density peak, for both species, was recorded during mid-June and the beginning of July, and the second one was observed at the beginning of September (Fig. 4c). Neva Bay sampling in summer 2017 (24.07.17) did not detect any *Eurytemora* specimens.

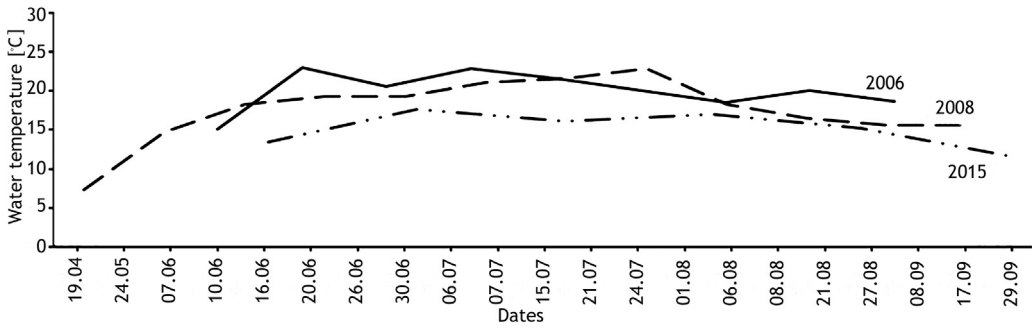

Figure 2 Mean changes in Luga Bay, Gulf of Finland, surface water temperature (°C) during spring, summer, and early autumn in the years: 2006 (full line); 2008 (dotted line); and 2015 (dashed line).

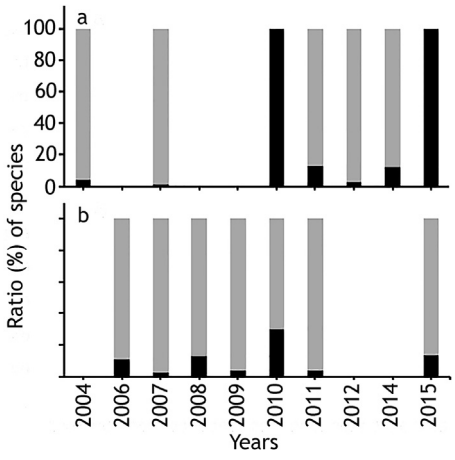

Figure 3 Percent ratio of invasive *Eurytemora carolleeae* (black sector) and native *Eurytemora affinis* (gray sector), during the last 10 years, in Neva (a) and Luga Bays (b), Gulf of Finland.

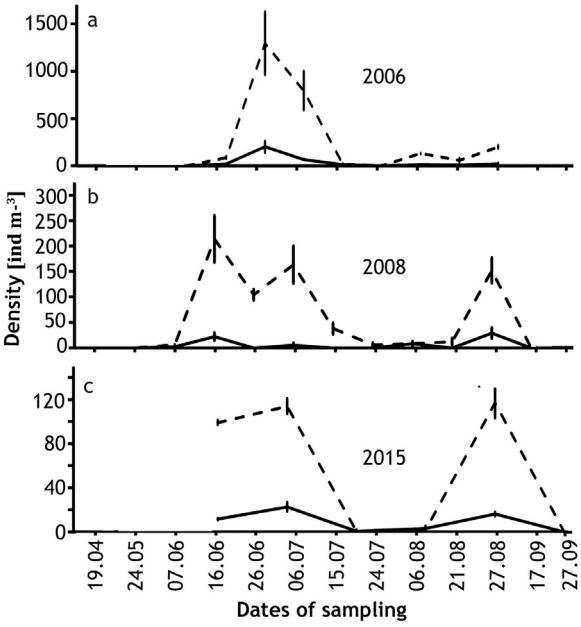

Figure 4 Population density changes in adult *Eurytemora affinis* (dotted line) and *Eurytemora carolleeae* (solid line) during the 2006 (a), 2008 (b), and 2015 (c) summer seasons.

Overall, *E. affinis* population densities were generally several times higher than those of *E. carolleeae*. The maximal densities were observed for both species in 2006, namely 1295 ind m^{-3} for *E. affinis*, and 201 ind m^{-3} for *E. carolleeae*. The minimal population densities were observed during the summer of 2015 in which no more than 117 ind m^{-3} were observed for *E. affinis* and 24 ind m^{-3} for *E. carolleeae*.

In Fig. 5, the detailed densities of males and females, of both species, are shown. During 2006 and 2008, there were more males than females in both *E. affinis* (Fig. 5a, b) and *E. carolleeae* populations (Fig. 5d, e). However, during 2015 (Fig. 5c, f), the opposite occurred, and the sex ratio was generally in favor of females except for one date (beginning of July, *E. affinis*) (Fig. 5c).

3.5. Reproductive parameters of *Eurytemora* females

The two *Eurytemora* species studied in the Gulf of Finland were significantly different ($p < 0.05$) in their morphological (prosome length and width, egg sac width) and reproductive (clutch size) characteristics (Table 2). The respective prosome lengths and widths were 830.2 ± 7.0 μm and 310.1 ± 6.4 μm in *E. carolleeae* and 744.0 ± 15.5 μm and 247.9 ± 5.3 μm in *E. affinis*.

Clutch size was almost two times larger in *E. carolleeae* than in *E. affinis*: 61.7 ± 2.4 and 34.0 ± 1.4, respectively Analysis of egg size and egg sac length did not reveal substantial differences between the two species. The difference in egg sac width between the two species (252.3 ± 11.5 μm in *E. carolleeae* versus 226.9 ± 5.1 μm in *E. affinis*) reflects differences in the shape of the sac, which is more rounded in *E. carolleeae* and more oval in *E. affinis*. At the same time, prosome lengths and clutch sizes in females of both species had a linear relationship (*E. affinis*, $r^2 = 0.59$, $p < 0.05$; *E. carolleeae*, $r^2 = 0.35$, $p < 0.05$).

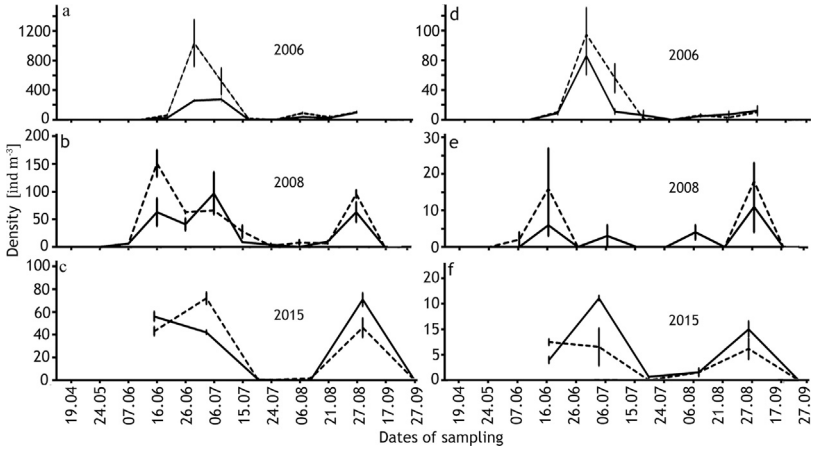

Figure 5 Population density changes in males (dotted lines) and females (solid lines) of *Eurytemora affinis* (a, b, c) and *Eurytemora carolleeae* (d, e, f) during the 2006 (a, d), 2008 (b, e), and 2015 (c, f) summer seasons.

Table 2 Mean values of reproductive parameters in females of *Eurytemora carolleeae* and *Eurytemora affinis* from the Gulf of Finland. Mean ± standard deviation.

Species/measuring	Egg number	Egg size	Prosome L (μm)	Prosome W (μm)	Clutch L (μm)	Clutch W (μm)	Number of studied individuals
E. carolleeae	61.7 ± 2.4	76.7 ± 0.8	830.2 ± 7.0	310.1 ± 6.4	476.6 ± 14.7	252.3 ± 11.5	20
E. affinis	34.0 ± 1.4	77.6 ± 0.57	744.0 ± 15.5	247.9 ± 5.3	466.8 ± 11.1	226.9 ± 5.1	23

3.6. DNA polymorphism data and hybridization between the species

Morphological observation revealed clear differences between the two species, and specimens exhibiting intermediate characters were not typically seen during the study period. Very rare specimens (about 1%) with intermediate features were observed and they were tentatively presumed to be hybrids.

These intermediate phenotypes usually featured intermediate numbers of eggs in the egg sac, intermediate egg sizes, body sizes, or caudal rami shapes. Some had segment-like divisions in setae and genital somite with outgrowth, as in *E. carolleeae*, yet they always differed from the morphology of *E. carolleeae* type specimens by a wing-like outgrowth in the distal part of body, a diagnostic character of *E. affinis*.

Genetic analyses were performed with a complete data set of 86 sequences (75 original and 11 previously published; Sukhikh et al., 2016b). The obtained sequences were compared with existing sequences of *Eurytemora* and deposited in GenBank (accession numbers 18SrRNA KX400968–KX400986; COI KX400987–KX401004, KX401042–KX401328; nITS KX401005–KX401041). The ITS and 18S nuclear genes were analyzed together with the COI gene in order to determine whether hybridization occurs and, if so, whether only F1 individuals are observed or are there subsequent generations of introgression.

Sixteen *E. carolleeae* COI sequences and thirteen *E. affinis* COI sequences were analyzed. Samples sources were: eight *E. carolleeae* and eight *E. affinis* sampled from Neva Bay, four *E. affinis* and four *E. carolleeae* sampled from Luga Bay and 3 *E. carolleeae* from Chesapeake Bay. In both species, a 544 b.p. COI product was amplified. Overall, *E. carolleeae* (COI) sequences contained 38 polymorphic sites and 13 haplotypes; *E. affinis* sequences contained 4 polymorphic sites and 4 haplotypes. The level of pairwise divergence in the COI gene between the two species was 15%, which is indicative of high divergence between these 2 species.

In terms of the 18SrRNA gene (length of 1690 bp), 15 sequences were successfully obtained for *E. carolleeae* and 9 for *E. affinis*. There were no observed nucleotide differences between the species and no polymorphic sites were observed. This suggests that the 18SrRNA gene is more useful in wide phylogenetic analysis of Copepoda, and less useful in work with closely related species.

ITS gene sequences were obtained and analyzed (*E. carolleeae* $n = 17$; *E. affinis* $n = 12$) from samples collected as follows: 14 *E. carolleeae* and 12 *E. affinis* sampled from Neva Bay; and three *E. carolleeae* from Chesapeake Bay. Due to polymorphism, ITS amplicons were 791 bp from *E. carolleeae* and 783 bp from *E. affinis*. Overall, *E. carolleeae* ITS sequences (794 bp in length, including sites with alignment gaps) contained one polymorphic site, whereas *E. affinis* ITS sequences (795 bp in length, including sites with alignment gaps) had no polymorphic sites. The level of pairwise divergence, in the ITS1-5.8SrRNA-ITS2 region between the two species, was 4.9%. *E. affinis* sequences from the Loire and Seine Rivers were not available.

4. Discussion

4.1. Distribution of invasive *E. carolleeae* in Europe

The presence of the invasive *E. carolleeae* species in European waters has only been reported in specific locations, namely: the Gulf of Finland, the Gulf of Riga, Amsterdam channels (Sukhikh et al., 2013), Kiel Bight; Mecklenburg Bight, the Arkona Sea, the Bornholm Sea, the Eastern Gotland Sea (Wasmund et al., 2013) and perhaps in British waters (Gurney, 1931) (Fig. 1). The presence of *E. carolleeae* in these areas is a noteworthy result since there are many previous reports, from a wide variety of European fresh and marine waters, showing no evidence of *E. carolleeae*.

Accurate identification of different species is necessary due to the fact that they feature evident differences in physiology, and those differences may cause harmful changes in ecosystem function or productivity. Population shifts may eventually have important consequences for biodiversity, biogeography, conservation, or fisheries management (Gelembiuk et al., 2006; Knowlton, 1993; Lee, 2000). Such invasions might have important implications for disease transmission as well. *Eurytemora* are major hosts of many pathogens, including *Vibrio cholerae*, *V. vulnificus*, and *V. parahaemolyticus* (Colwell, 2004; Lee et al., 2007; Piasecki et al., 2004). They are also probable hosts and vectors for plerocercoids that can infect some fish species (Arnold and Yue, 1997).

E. carolleeae was not found in the Elbe, Schelde, Seine, Loire or Gironde estuaries, nor was it detected in the lake near Paris, the Vistula Lagoon, or the Gulf of Bothnia (the Baltic Sea) in 2006–2011 (Table 1). In addition, we have previously shown that it is not present in samples from White Sea rock pools (Sukhikh et al., 2016a,b), in the White Sea itself (pers. comm. of Polyakova N.V.), or in the Northern Dvina River. In addition, species lists from the Pechora Estuary (Cherevichko, 2017; Fefilova, 2015), the Caspian Sea, and the Volga River drainage basin (Lazareva et al., 2018; Sukhikh et al., 2018) did not include *E. carolleeae*. Finally, previous genetic studies of the *E. affinis* species complex in a number of locations (the Swedish coast – Gorokhova et al., 2013;

Winkler et al., 2011; the Elbe, Schelde, Seine, Loire, and Gironde estuaries – Winkler et al., 2011) have not detected *E. affinis*.

4.2. Population dynamics of *E. carolleeae* and *E. affinis* in the Gulf of Finland

Seasonal study of *E. carolleeae* and *E. affinis* in Luga Bay revealed no substantial differences in their population dynamics. The highest densities were observed during early summer of 2006 for both species (Fig. 4a). These maximal densities may be the result of dredging activity in the Luga Bay study area that occurred during the summer of 2006 (Spiridonov et al., 2011). This event caused resuspension of nutrients in the water column which, in result, induced an increase of phytoplankton (the main food source for *Eurytemora*) density (Spiridonov et al., 2011).

The lowest population densities (both species) were observed during the summer of 2015 (Fig. 4c). The period was characterized by unusually low temperatures, including a minimum of 12.8°C in June. The conditions likely reduced phytoplankton densities, and the effect is a possible reason for the decreased population densities recorded for both *E. affinis* and *E. carolleeae*. Nevertheless, no overall correlation was found between population density and water temperature during the summer.

The absence of *Eurytemora* species in the 2017 samples was possibly due to a shift of the resident marine zooplankton community to a riverine one, since summer 2017 was rather rainy and river flow had increased. During the same sampling period, *Eurytemora* species were observed in more or less usual densities in the central part of Neva Bay of the Gulf of Finland (pers. comm. of Litvinchuk L.), an area unaffected by river outflow-associated salinity decreases. In the summer 2018, *E. carolleeae* in Luga Bay was also observed in usual density.

Throughout the study period, the population density of *E. affinis* was several times higher than that of *E. carolleeae* in Luga Bay (Fig. 4). However, in September 2010 and in August 2015, Neva Bay samples contained only *E. carolleeae*; this suggests a major shift in zooplankton populations, featuring a replacement of *E. affinis* by invasive *E. carolleeae* (Fig. 3). However, the shift in zooplankton was temporary since samples devoid of *E. affinis* were recorded only those two times. Interestingly, both summers 2010 and 2015 featured unusual temperatures: hot 2010 and cold 2015. Record heat levels were observed in summer 2010, resulting in the warmest summer of the last 100 years in the region (https://en.wikipedia.org; https://en.wikipedia.org/wiki/2010_Northern_Hemisphere_summer_heat_waves). Consequently, during that summer, the warmest water temperatures were also recorded. Water temperatures above 15–20°C are known to be unfavorable for *E. affinis* (Devreker et al., 2008, 2010; Dur et al., 2009; Hirche, 1992; Knatz, 1978).

These uncommon temperature conditions probably negatively affected native *E. affinis* populations, yet without reducing population densities of invasive *E. carolleeae*. The temperature tolerance of the invasive copepod species is possibly wider as water temperatures in its native Chesapeake Bay range between 5 and 25°C (Kimmel et al., 2006). *E. carolleeae* is also characterized by high egg productivity (Pierson et al., 2016), which could favor its rapid spread in the area. In the eastern part of the Gulf of Finland, yearly mean water temperature varied between 0 (winter) and 18–20°C (summer) (http://weatherarchive.ru/Sea/Ust-luga/July). In such an environment, invasive species may be more successful than native ones in fast changing environmental and temperature conditions. Furthermore, *E. carolleeae* densities were not observed to depend on summer temperatures in different years.

In 2010 and 2015, analysis of Luga Bay samples did not reveal replacement of *E. affinis* by *E. carolleeae*. This indicates that site-specific factors likely play a significant role in the population dynamics of the species. In fact, the population density trends are similar to the other years studied (Fig. 3) even though the proportions of *E. carolleeae* were slightly higher during these two years (30% in 2010 and 14% in 2015). The relatively lower 2010 densities of *E. carolleeae* in Luga Bay, in comparison to Neva Bay, could be due to the sample collection timing. Plankton samples were not collected during August, as in other years, but later, at the end of September, when water temperature was 18°C. However, during September of 2008 and 2015, water temperatures were not higher than 15°C, and neither *Eurytemora* species was found there. These observations reinforce the possibility that temperature fluctuations may affect the development of both species in the Gulf of Finland.

Luga Bay is known to be one of the most important regions in the Gulf of Finland for fish feeding, breeding, and spawning (Golubkov, 2009). Therefore, it is possible that fish predation on copepods was higher in Luga Bay. Prosome size (length and width) was larger in *E. carolleeae* than in *E. affinis* (Table 2); this makes them more susceptible to visual predators. It has been demonstrated that fish eat larger zooplankton first and small ones afterwards (Brooks and Dodson, 1965). In addition, this invasive species has a larger egg sac (Table 2), and it was shown by Mahjoub et al. that fish prefer to feed on ovigerous females. Therefore, with their bigger prosomes and egg sacs, *E. carolleeae* may be more visible to fish predators and more susceptible to subsequent predation. Therefore, in addition to temperature, fish predation pressure may be one of the limiting factors in population growth of *E. carolleeae* in Luga Bay. Ideally, laboratory experiments would test these hypotheses.

4.3. Reproductive characteristics of the studied species

Study of the reproductive parameters of the two *Eurytemora* species living in sympatry revealed a significant difference in clutch size, but not in egg size. *E. carolleeae*, from a summer 2015 sample, was characterized by higher reproductive potential. The invasive *E. carolleeae* produced almost double the clutch size (62 eggs female^{-1}) than that of the native *E. affinis* (34 eggs female^{-1}). In Chesapeake Bay (the native habitat of *E. carolleeae)*, the species is characterized by salinity tolerance, temperature tolerance, and high fecundity (Pierson et al., 2016). Beyrend-Dur et al. (2009) compared two formerly transatlantic *Eurytemora* populations collected from the Seine estuary (France) and from the Saint Lawrence salt marshes (Canada) and showed that American *Eurytemora* had higher fecundity, higher salinity tolerance, shorter

development time, and a longer life span (Beyrend-Dur et al., 2009). These reproductive and physiological differences may enhance the ability of *E. carolleeae* to invade and spread into new areas. This ability may further be enhanced in regions where conditions have become more favorable, over time, due to climate change. A general trend of decreasing salinity in the Baltic Sea is one such example (https://www.st.nmfs.noaa).

4.4. Comparison between invasive and native *E. carolleeae* populations

In comparisons between the invasive *E. carolleeae* found in the Gulf of Finland (this study) and the native *E. carolleeae* from Chesapeake Bay (Lloyd et al., 2013), native *E. carolleeae* had a lower clutch size (around 50 eggs female^{-1}) and a smaller prosome length (about 780 μm) at the same water temperatures. Chesapeake Bay is a possible source of invasive copepods (Sukhikh et al., 2013), and it is likely that invasive *E. carolleeae* encountered more favorable environmental conditions in the Gulf of Finland than in its native area. This interpretation is supported by Lajus et al. (2015), who compared levels of fluctuating asymmetry (FA) for populations of *E. carolleeae* from Chesapeake Bay and from the Gulf of Finland. Fluctuating asymmetry represents random deviations from perfect symmetry, and is a proxy for developmental instability (Zakharov, 1989). FA is often used to monitor stress of different origins (Beasley et al., 2013; Graham et al., 2010).

FA was larger for native *E. carolleeae* (Chesapeake Bay), compared to invasive *E. carolleeae* (Gulf of Finland). Interestingly, *E. affinis* from the Gulf of Finland has almost the same FA as the invasive *E. carolleeae* species. This may be the result of generally less stressful environmental conditions in the Gulf of Finland in comparison to Chesapeake Bay. The Gulf features different temperature conditions and fewer salinity changes due to the absence of tides. In fact, the *E. affinis* population from the Seine estuary, with its high tides, had the highest FA of all of the studied populations (Lajus et al., 2015). Those findings fits with our data showing higher FA for native *E. carolleeae* (from Chesapeake Bay) than for invasive *E. carolleeae* (from the Baltic).

4.5. Interaction between sympatric species

Long-term monitoring of the population densities of the two *Eurytemora* species living in sympatry, as well as analysis of their morphological and reproductive parameters, revealed that invasive *E. carolleeae* and native *E. affinis* have remained reproductively isolated from one another. However, rare individuals with intermediate morphological features were observed. Similar cases are known, and hybrids within zooplankton species/lineages are not unheard of in studies of planktonic dispersers, and in particular within Copepoda (Makino and Tanabe, 2009; Parent et al., 2012; Petrusek et al., 2008; Pritchard et al., 2012; Taylor and Hebert, 1993).

Analysis of nuclear ITS genes confirmed that the gene pools of the two studied species have remained largely genetically isolated. More variable (and thus more powerful) molecular markers should be developed to test for the presence of subtle introgression between these two closely related and sympatric species.

5. Conclusion

We have demonstrated that two *Eurytemora* species (native *E. affinis* and invasive *E. carolleeae*) co-exist in the same area in the Gulf of Finland. Although previously published work has established the presence of these species in the Gulf of Riga and in Amsterdam channels, Wasmund et al. (2013) have demonstrated their expanded co-distribution in Kiel Bight, Mecklenburg Bight, Arkona Sea, Bornholm Sea, and in Eastern Gotland Sea.

The population dynamics of both species are largely parallel. Invasive *E. carolleeae* is usually second to *E. affinis* in terms of density. In addition, the larger body size and different reproductive traits of *E. carolleeae* confer a potential for it to displace native *E. affinis* species. Future work which aims to assess the prospects for further geographic expansion of *E. carolleeae* should take into consideration not only interspecific competition between these two closely related *Eurytemora* species, but also species present at higher and lower trophic levels that interact with *Eurytemora* copepods.

Acknowledgments

We are very grateful to G. Winkler, J. Pierson, O. Glippa, M. Tackx, L. Samchishina, J. Polunina, E. Naumenko, S. Maljavin, and S. Korochin for their help in sampling. We thank the staff of the GEPV laboratory, Lille University, and especially Vincent Castric for providing the genetic work and valuable comments on this paper. We thank the staff of the Zoological Institute Laboratory of Molecular-Genetic Systematics, where the genetic analysis was performed. We are thankful to L.F. Litvinchuk, V.I. Lazoreva, and N.V. Polyakova for information on the distribution of *E. carolleeae* in European waters. We thank anonymous reviewers for valuable comments that substantially improved the manuscript. For this work, the Federal Collection N 96-03-16, Zoological Institute of the Russian Academy of Sciences (St. Petersburg, Russia) was used. This work was conducted in accordance with the national initiative АААА-А17-117041910019-2 and supported by: the BIODISEINE; ZOOGLOBAL Seine Aval project; and the Mechnikov postdoctoral program in France; the "Biodiversity" grant from the Presidium of the Russian Academy of Sciences; and Russian Foundation for Basic Research (РФФИ 17-04-00027 А). We are also grateful to Edward Ramsay for English editing.

References

Alekseev, V., Souissi, A., 2011. A new species within the *Eurytemora affinis* complex (Copepoda: Calanoida) from the Atlantic Coast of USA, with observations on eight morphologically different European populations. Zootaxa 2767, 41–56.

Alekseev, V.R., Abramson, N.I., Sukhikh, N.M., 2009. Introduction of sibling species to the ecosystem of the Baltic Sea. Dokl. Biol. Sci. 429 (5), 694–697.

Alimov, A.F., Bogutskaya, N.G., et al., 2004. Biological Invasions in Aquatic and Terrestrial Ecosystems. Fellowship of Scientific Publications KMC, Moscow, St. Petersburg, 424 pp., (in Russian).

Aljanabi, S.M., Martinez, I., 1997. Universal and rapid salt-extraction of high quality genomic DNA for PCR-based techniques. Nucleic Acids. Res. 25—22, 4692—4693.

Antsulevich, A.E., Ryabova, V.N., Stogov, I.A., 1995. The current state of zooplankton in the Luga Bay of the Gulf of Finland. Bull. St. Petersburg State Univ. 3 (3), 3—9, (in Russian).

Arnold, J.D., Yue, H.S., 1997. Prevalence, relative abundance, and mean intensity of plerocercoids of Proteocephalus sp. in young striped bass in the Sacramento-San Joaquin estuary. California Fish Game 83 (3), 105—117.

Basova, S.L., 1983. Survey of the pollution status of the eastern part of the Gulf of Finland by hydrobiological indicators in 1983, Leningrad, 86 pp., (in Russian).

Beasley, D.E., Bonisoli-Alquati, A., Mousseau, T.A., 2013. The use of fluctuating asymmetry as a measure of environmentally induced developmental instability: a meta-analysis. Ecol. Indic. 30, 218—226.

Beauchamp, K.A., Kathman, R.D., McDowell, Hedrick, R.P., 2001. Molecular phylogeny of tubificid oligochaetes with special emphasis on *Tubifex tubifex* (Tubificidae). Mol. Phylogenet. Evol. 19, 216—224.

Berezina, N.A., Petryashev, V.V., Razinkovas, A., Lesutiene, J., 2011. Alien malacostraca in the eastern Baltic Sea: pathways and consequences. In: Galil, B.S., Clark, P.F., Carlton, J.T. (Eds.), In the Wrong Place — Alien Marine Crustaceans: Distribution, Biology and Impacts Invading Nature, Springer Series, Invasion Ecol., 63, 301—322. .

Beyrend-Dur, D., Souissi, S., Devreker, D., Winkler, D., Hwang, J.S., 2009. Life cycle traits of two transatlantic populations of *Eurytemora affinis* (Copepoda: Calanoida): salinity effects. J. Plankt. Res. 31 (7), 713—728.

Brooks, J.L., Dodson, S.I., 1965. Predation, body size, and composition of plankton. The effect of a marine planktivore on lake plankton illustrates theory of size, competition, and predation. Sci. New Ser. 150 (3692), 28—35.

Cherevichko, A.V., 2017. Zooplankton of water bodies of seaside marches of Malozemelskaya Tundra. Biol. Inl. Waters 2, 88—93, (in Russian).

Colwell, R.R., 2004. Infectious disease and environement: cholera as a paradigm for waterborne disease. Int Microbiol 7, 285—289.

Demchuk, A., Uspenskiy, A., Golubkov, S., 2017. Feeding patterns of the abundant coastal fish species in the Eastern Gulf of Finland, Tallinn, Gulf of Finland Science Days, 16 October. , http://dx.doi.org/10.13140/RG.2.2.18238.38724.

Devreker, D., Souissi, S., Molinero, J.C., Nkubito, F., 2008. Trade-offs of the copepod *Eurytemora affinis* in mega-tidal estuaries. Insights of high frequency sampling in the Seine estuary. J. Plankton Res. 30, 1329—1342.

Devreker, D., Souissi, S., Molinero, J.C., Beyrend-Dur, D., Gomez, F., Forget-Leray, J., 2010. Tidal and annual variability of the population structure of *Eurytemora affinis* in the middle part of the Seine estuary during 2005. Estuar. Coast. Shelf. Sci. 89 (4), 245—255.

Devreker, D., Pierson, J., Souissi, S., Kimmel, D., Roman, M., 2012. An experimental approach to estimate egg production and development rate of the calanoid copepod *Eurytemora affinis* in Chesapeake Bay, USA. J. Exp. Mar. Bio. Ecol. 416—417, 72—83.

Dur, G., Souissi, S., Devreker, D., Ginot, V., Schmitt, F.G., Hwang, J. S., 2009. An individual based model to study the reproduction of egg bearing copepods: application to *Eurytemora affinis* (Copepoda; Calanoida) from the Seine estuary. Ecol. Model. 8, 1073—1089.

Fefilova, E.B., 2015. Fauna of the European North-East of Russia. Copepods (Copepoda), 12. 319 pp., (in Russian).

Folmer, O., Black, M., Hoeh, W., Lutz, R., Vriyenhoek, R., 1994. DNA primers for amplification of mitochondrial cytochrome c oxidase subunit I from diverse metazoan invertebrates. Mol. Mar. Biol. Biotechnol. 3, 294—299.

Gelembiuk, G.W., May, G.E., Lee, C.E., 2006. Phylogeography and systematics of zebra mussels and related species. Mol. Ecol. 15, 1033—1050.

Golubkov, S.M., 2009. Changes of biological communities in the eastern Gulf of Finland during the last century. Proc. Zooll. Instit. RAS 313 (4), 406—418.

Gorokhova, E., Lehtiniemi, M., Motwani, N.H., 2013. Trade-offs between predation risk and growth benefits in the copepod *Eurytemora affinis* with contrasting pigmentation. PLoS ONE 8 (8), e71385.

Graham, J.H., Raz, S., Hel-Or, H., Nevo, E., 2010. Fluctuating Asymmetry: Methods, Theory, and Applications, Symmetry, 2, 46—540.

Gurney, R., 1931. British Fresh-water Copepoda, vol. 1. Ray Society, London, 384 pp.

Hall, T.A., 1999. Bioedit: a user-friendly biological sequence alignment editor and analysis program for Windows 95/98/NT. Nucleic Acids Res. 41, 95—98.

Hirche, H.-J., 1992. Egg production of *Eurytemora affinis*-effect of k-strategy. Estuar. Coast. Shelf Sci. 35, 395—407.

Hoelzel, A.R., Green, A., 1992. Analysis of population-level variation by sequencing PCR-amplified DNA. In: Hoelzel, A.R. (Ed.), Molecular Genetic Analysis of Populations: A Practical Approach. Oxford Univ. Press, New York, 159—188.

Katajisto, T., Kotta, J., Lehtiniemi, M., Malavin, S.A., Panov, V.E., 2013. *Palaemon elegans Rathke*, 1837 (Caridea: Palaemonoidea: Palaemonidae) established in the Gulf of Finland. BioInvas. Rec. 2 (2), 125—132.

Kimmel, D.G., Miller, W.D., Roman, M.R., 2006. Regional scale climate forcing of mesozooplankton dynamics in Chesapeake Bay. Estuar. Coasts 29 (3), 375—387.

Knatz, G., 1978. Succession of copepod species in a middle Atlantic estuary. Estuaries 1, 68—71.

Knowlton, N., 1993. Sibling species in the sea. Annu. Rev. Ecol. Syst. 24, 189—216.

Lajus, D., Sukhikh, N., Alekseev, V., 2015. Cryptic or pseudocryptic: can morphological methods inform copepod taxonomy? An analysis of publications and a case study of the *Eurytemora affinis* species complex. Ecol. Evol. 5 (12), 2374—2385.

Lavrentieva, G.M., Finogenova, N.P., 1999. Hydrobiological characteristics of the Vyborg Gulf, the Bierkesund Strait, the Batareinoy Bay and the Luga Bay (Eastern part of the Gulf of Finland), The Gulf of Finland in the conditions of anthropogenic impact, St. Petersburg, 242 pp., (in Russian).

Lazareva, V.I., Sabitova, R.Z., Sokolova, E.A., 2018. Features of the structure and distribution of the late summer (august) zooplankton in the Volga reservoirs. Biol. Inl. Waters 82, 28—51, (in Russian).

Lee, C.E., 2000. Global phylogeography of a cryptic copepod species complex and reproductive isolation between genetically proximate populations. Evolution 54, 2014—2027.

Lee, C.E., Remfert, J.L., Chang, Y., 2007. Response to selection and evolvability of invasive species. Genetica 129 (2), 179—192.

Lehtiniemi, M., Antsulevich, A., Kotta, J., Maximov, A., Ojaveer, H., Orlova, M., 2016. Non-indigenous species. In: Raateoja, M., Setälä, O. (Eds.), Reports of the Finnish Environment Institute. The Gulf of Finland Assessment. Finnish Environ. Inst., Helsinki, 264—275.

Leppäkoski, E., Gollasch, S., Gruszka, P., Ojaveer, H., Olenin, S., Panov, V., 2002a. The Baltic — a sea of invaders. Can. J. Fish Aquat. Sci. 59, 1175—1188.

Leppäkoski, E., Olenin, S., Gollasch, S., 2002b. The Baltic Sea — a field laboratory for invasion biology. In: Leppäkoski, E., Gollasch, S., Olenin, S. (Eds.), Invasive Aquatic Species of Europe — Distribution, Impacts, Management. Dordrecht, The Netherlands, Kluwer Academic Publ., 253—259.

Librado, P., Rozas, J., 2009. DnaSP v5: A software for comprehensive analysis of DNA polymorphism data. Bioinformatics 25, 1451—1452.

Lloyd, S., Elliott, D., Roman, M., 2013. Egg production by the copepod, *Eurytemora affinis*, in Chesapeake Bay turbidity maximum regions. J. Plankton. Res. 35 (2), 299—308, http://dx.doi.org/10.1093/plankt/fbt003.

Makino, W., Tanabe, A.S., 2009. Extreme population genetic differentiation and secondary contact in the freshwater copepod *Acanthodiaptomus pacificus* in the Japanese Archipelago. Mol. Ecol. 18, 3699—3713.

Ogorodnikova, V.A., Volkhonskaya, N.I., 2006. Zooplankton of the Luga Bay of the Gulf of Finland (background status before the start of the port facilities operation). Ecological aspects of hydropower construction on the biota of the water area of the eastern part of the Gulf of Finland. St. Petersburg, vol. 331(1). 324—342, (in Russian).

Ojaveer, H., Kotta, J., 2015. Ecosystem impacts of the widespread non-indigenous species in the Baltic Sea: literature survey evidences major limitations in knowledge. Hydrobiologia 750, 171—185.

Ostov, I.S., 1971. Characteristic features of the hydrological and hydrochemical regime of the Gulf of Finland as the basis for its fishery development, Biol. Commerc. Resources of the Gulf of Finland. Leningrad 76, 18—45, (in Russian).

Panov, V.E., Bychenkov, D.E., Berezina, N.A., Maximov, A.M., 2003. Alien species introductions in the eastern Gulf of Finland: current state and possible management options. Proc. Estonian Acad. Sci. Biol. Ecol. 52 (3), 254—267.

Parent, G.J., Plourde, G.J., Turgeon, S.J., 2012. Natural hybridization between *Calanus finmarchicus* and *C. glacialis* (Copepoda) in the Arctic and Northwest Atlantic. Limnol. Oceanogr. 57, 1057—1066.

Petrusek, A., Seda, J., Machacek, J., Ruthova, S., Smilauer, P., 2008. *Daphnia* hybridization along ecological gradients in pelagic environments: the potential for the presence of hybrid zones in plankton. Proc. R. Soc. B. Biol. Sci. 363, 2931—2941.

Piasecki, W., Goodwin, A.E., Eiras, J.C., Nowak, B.F., 2004. Importance of copepod in freshwater aquaculture. Zool. Stud. 43 (2), 193—205.

Pierson, J.J., Kimmel, D.G., Roman, M.R., 2016. Temperature impacts on *Eurytemora carolleeae* size and vital rates in the upper Chesapeake Bay in winter. Estuar. Coasts 39 (4), 1122—1132.

Pollumae, A., Kotta, J., 2007. Factors describing the distribution of the zooplankton community in the Gulf of Finland in the context of interactions between native and introduced predatory cladocerans. Oceanologia 49 (2), 277—290.

Pollumaea, A., Valjataga, K., 2004. *Cercopagis pengoi* (Cladocera) in the Gulf of Finland: environmental variables affecting its distribution and interaction with *Bosmina coregoni* maritima. Proc. Estonian Acad. Sci. Biol. Ecol. 53 (4), 276—282.

Pritchard, V.L., Knutson, V.L., Lee, M., Zieba, J., Edmands, S., 2012. Fitness and morphological outcomes of many generations of hybridization in the copepod *Tigriopus californicus*. J. Evol. Biol. 26, 416—433.

Raupach, M.J., Mayer, C., Malyutina, M., Wägele, J.-W., 2009. Multiple origins of deep-sea Asellota (Crustacea: Isopoda) from shallow waters revealed by molecular data. Proc R Soc Lond Ser B 276, 799—808.

Ryabova, V.N., Pogrebov, V.B., 1991. Biological seasonality in the zooplankton of the Gulf of Finland. Hydrobiol. J. 27 (1), 19—24, (in Russian).

Sergeev, V.N., Ryabova, V.N., Belogolovaya, L.A., 1971. Features of the dynamics and distribution of zooplankton in the eastern part of the Gulf of Finland in 1969. Izvestiya GosNIORH 123, 52—64, (in Russian).

Spiridonov, M., Ryabchuk, D., Zhamoida, V., Sergeev, A., Sivkov, V., Boldyrev, V., 2011. Geological hazard potential at the baltic sea and its coastal zone: examples from the Eastern Gulf of Finland and the Kaliningrad Area. In: Harff, J., Björck, S., Hoth, P. (Eds.), The Baltic Sea Basin. Springer-Verlag, Berlin, Heidelberg, 337—364.

Sturmbauer, C., Opadiya, G.B., Niederstätter, H., Riedmann, A., Dallinger, R., 1999. Mitochondrial DNA reveals cryptic oligochaete species differing in cadmium resistance. Mol. Biol. Evol. 16, 967—974.

Sukhikh, N.M., Alekseev, V.R., 2013. *Eurytemora caspica* sp.nov. from the Caspian sea — one more new species within the *E. affinis* complex (Copepoda: Calanoida). Proc. Zool. Inst. RAS 317 (1), 85—100.

Sukhikh, N.M., Souissi, A., Souissi, S., Alekseev, V.R., 2013. Invasion of *Eurytemora* sibling species (Copepoda: Temoridae) from North America into the Baltic Sea and European Atlantic coast estuaries. J. Nat. Hist. 47 (5—12), 753—767.

Sukhikh, N.M., Castric, V., Polyakova, N.V., Souissi, S., Alekseev, V.R., 2016a. Isolated Populations of Eurytemora americana Williams (Crustacea, Copepoda) in the White Sea Rock Pools—Postglacial Relicts or Anthropogenic Invasion? Rus. J. Biol. Invas. 7 (4), 396—404.

Sukhikh, N.M., Souissi, A., Souissi, S., Winkler, G., Castric, V., Holl, A. C., Alekseev, V.R., 2016b. Genetic and morphological heterogeneity among populations of *Eurytemora affinis* (Crustacea: Copepoda: Temoridae) in European waters. C.R. Biol. 339, 197—206.

Sukhikh, N.M., Lazareva, V.I., Alekseev, V.R., 2018. Eurytemora caspica Sukhikh et alekseev in the Volga river basin. In: Abstract Book, All-Russian Scientific Conference: "Volga and its life". 22—26 October 2018, Borok, Russia p. 127, (in Russian).

Tamura, K., Stecher, G., Peterson, D., Filipski, A., Kumar, S., 2013. MEGA6: molecular evolutionary genetics analysis version 6.0. Mol. Biol. Evol. 30, 2725—2729.

Taylor, D.J., Hebert, P.D.N., 1993. Habitat-dependent hybrid parentage and differential introgression between neighboringly sympatric Daphnia species. Proc. Natl. Acad. Sci. USA 90, 7079—7083, http://dx.doi.org/10.1073/pnas.90.15.7079.

Thompson, J.D., Higgins, D.J., Gibson, T.J., 1994. CLUSTAL W: improving the sensitivity of progressive multiple sequence alignments through sequence weighting, position-specific gap penalties and weight matrix choice. Nucleic Acids Res 22, 4673—4680.

Uitto, A., Gorokhova, E., Valipakka, P., 1999. Distribution of the non-indigenous *Cercopagis pengoi* in the coastal waters of the eastern Gulf of Finland. ICES J. Mar. Sci. 56 (Suppl.), 49—57, http://dx.doi.org/10.1006/jmsc.1999.0613.

Wasmund, N., Augustin, C., Pollehne, F., Siegel, H., Zettler, M., 2013. Biologische ustandseinschätzung der Ostsee im Jahre 2012. Meereswiss Ber, Warnemünde, p. 92.

White, T.J., Burns, T., Lee, S., Taylor, J., 1990. Amplification and direct sequencing of fungal ribosomal RNA genes for phylogenetics. In: Innis, M.A., Gelfand, D.H., Shinsky, J.J., White, T.J. (Eds.), PCR Protocols: A Guide to Methods and Applications. Acad. Press, San Diego, California, 315—322.

Winkler, G., Souissi, S., Poux, C., Castric, V., 2011. Genetic heterogeneity among Eurytemora affinis populations in Western Europe. Mar. Biol. 158, 1841—1856.

Zakharov, V.M., 1989. Future prospects for population phenogenetics. Sov. Sci. Rev. Sect. F: Physiol. Gen. Biol. Rev. 4, 1—79, (in Russian).

Oceanologia (2019) 61, 239—251

Available online at www.sciencedirect.com

ScienceDirect

journal homepage: www.journals.elsevier.com/oceanologia/

ORIGINAL RESEARCH ARTICLE

Seasonal variations in the abundance and sinking flux of biogenic silica in Daya Bay, northern South China Sea

Xiufeng Zhao, Weifeng Yang *, Haoyang Ma, Junjie Li, Min Chen, Ziming Fang, Xiao Zhang, Jian Zeng, Yusheng Qiu, Minfang Zheng

State Key Laboratory of Marine Environmental Science and College of Ocean and Earth Sciences, Xiamen University, Xiamen, China

Received 25 August 2018; accepted 14 November 2018
Available online 23 November 2018

KEYWORDS
Biogenic silica;
Dissolved silicate;
Sinking flux;
Thorium;
Daya Bay

Summary Coastal seas account for >50% of the biogenic silica (BSi) production in marine environments. However, BSi sinking is poorly understood. Here, seasonal variations in the abundance and sinking flux of BSi were investigated in Daya Bay, in the northern South China Sea. The highest BSi concentrations occurred in summer, averaging 8.04 ± 5.48 μmol L^{-1} (±SD), followed by autumn (5.51 ± 3.11 μmol L^{-1}) and spring (3.76 ± 3.06 μmol L^{-1}). The lowest BSi concentration of 2.93 ± 1.34 μmol L^{-1} was observed in winter. Based on $^{234}Th/^{238}U$ disequilibria, the average BSi sinking fluxes were 7.08 ± 8.62, 10.01 ± 13.95, and 8.30 ± 13.06 mmol Si m^{-2} d^{-1} in spring, summer, and autumn, respectively. The lowest flux of 4.19 ± 3.98 mmol Si m^{-2} d^{-1} was measured in winter. Together with nitrogen fluxes, the Si:N sinking ratios were 0.8:1.0, 1.5:1.0, 1.6:1.0, and 1.4:1.0 in spring, summer, autumn, and winter, respectively, indicating that particle sinking induces the faster removal of Si compared to N in Daya Bay.

* Corresponding author at: State Key Laboratory of Marine Environmental Science and College of Ocean and Earth Sciences, Xiamen University, Xiamen 361102, China. Tel.: +86 5922189468.
E-mail address: wyang@xmu.edu.cn (W. Yang).
Peer review under the responsibility of Institute of Oceanology of the Polish Academy of Sciences.

Production and hosting by Elsevier

https://doi.org/10.1016/j.oceano.2018.11.003

1. Introduction

Silicon, a key nutrient element in oceans, is widely absorbed by plankton such as diatoms, siliceous sponges, radiolaria, and silicoflagellates (Bužančić et al., 2016; Stramska and Bialogrodzka, 2016). After assimilation by organisms, dissolved silicate (DSi) is transformed into particulate amorphous silicon, known as biogenic silica (BSi) (Sospedra et al., 2018). Knowledge of the production, sinking, and dissolution mechanisms of BSi is essential for understanding silicon cycling in the ocean (Krom et al., 2014; Pastuszak et al., 2008; Yang et al., 2015). Since the 1990s, a growing number of studies have attempted to quantify marine biogeochemical mechanisms of BSi cycling (Nelson et al., 1995; Ragueneau et al., 2000; Yang et al., 2015) and have elucidated the abundance of BSi in various oceanic environments (Laruelle et al., 2009; Tréguer and De La Rocha, 2013; Tréguer et al., 1995). In the open ocean, BSi dissolution and recycling mainly occur in the euphotic zone (56%) and at the water-sediment interface (30%); less than 3% of BSi produced in the upper ocean is permanently buried in sediments (Tréguer and De La Rocha, 2013). In estuarine and coastal zones, BSi normally accounts for a small fraction of particulate silica, while lithogenic silica (LSi) contributes over 90% (Ragueneau et al., 2005). However, BSi is essential to coastal ecosystems as it dissolves more easily than LSi and is assimilated by phytoplankton (Loucaide et al., 2008; Pastuszak et al., 2008; Roubeix et al., 2008). As diatoms frequently dominate phytoplankton communities in most coastal seas, these regions represent the most productive BSi areas. Earlier studies confirmed that coastal BSi accounted for over half of the total global BSi production (Nelson et al., 1995; Tréguer and De La Rocha, 2013). Additionally, diatom debris can increase the sinking efficiency of particulate organic carbon (POC) in seawater due to its ballast effect (Guinder et al., 2015; Nelson et al., 1995; Waite et al., 1997). POC sinking is a critical parameter in evaluating the efficiency of marine biological pumps. Therefore, BSi sinking would significantly influence the efficiency of biological pumps in coastal waters. A detailed investigation on BSi sinking in coastal seas could both increase the understanding of silicon cycling in coasts and benefit our evaluation of CO_2 sequestration capacity in such environments.

In oceans, BSi sinking is normally estimated using sediment trapping and/or radionuclide approaches. For example, by analysing particles collected in sediment traps, Nelson et al. (1996) and Li et al. (2017) reported sinking fluxes of BSi in the Ross Sea and the South China Sea (SCS), respectively. Several studies employed ^{234}Th, ^{210}Po, and ^{210}Pb to trace BSi sinking in the Southern Ocean (Buesseler et al., 2001a; Friedrich and Rutgers van der Loeff, 2002; Rutgers van der Loeff et al., 2002). The ^{234}Th/^{238}U disequilibrium was also employed to evaluate the effect of decaying cyclonic eddies on BSi export in the oligotrophic SCS (Yang et al., 2015). Boyd et al. (2000) combined sediment trapping with the ^{234}Th/^{238}U method to trace BSi and POC export during a phytoplankton bloom in the polar Southern Ocean, stimulated by iron fertilization. Overall, BSi sinking is less studied, especially in coastal waters, although the above reports revealed the essential role of BSi in removing silicon and POC from seawater.

As a radionuclide tracer to constrain particle sinking, ^{234}Th/^{238}U is widely employed to trace POC export from the upper ocean (Buesseler et al., 1992, 2006; Chen et al., 2003; Coale and Bruland, 1985). In seawater, ^{234}Th is formed from soluble ^{238}U. Due to its strong particle reactivity in seawater, ^{234}Th is efficiently removed from surface water by particle scavenging and sinking, resulting in a ^{234}Th deficit with respect to ^{238}U. The half-life of ^{234}Th is 24.1 d; therefore, the disequilibrium between ^{234}Th and ^{238}U reflects particle export over days to months (Yang et al., 2016). In the open ocean, physical processes are normally neglected when employing ^{234}Th/^{238}U (Le Moigne et al., 2013; Savoye et al., 2006). Several studies suggested that advection and diffusion terms contribute less than 10% to the ^{234}Th flux in the southern SCS (Cai et al., 2008; Yang et al., 2015). However, these physical processes significantly affect the ^{234}Th flux in coastal zones (Benitez-Nelson et al., 2000). Additionally, the ^{234}Th flux is probably subject to significant seasonal variations due to substantial changes in phytoplankton production in coastal waters. For instance, the export fluxes of ^{234}Th and POC exhibited more significant seasonal variations in the northern shelf than in the SCS basin (Cai et al., 2015). Although the ^{234}Th/^{238}U method can theoretically trace coastal BSi export, its application in coastal seas is rarely reported.

To investigate the abundance of BSi, as well as its sinking flux in Daya Bay (northern SCS), we performed a four-season investigation of both BSi and ^{234}Th/^{238}U. In this study, our objectives are: (1) to determine the abundance and seasonal variation in the BSi concentration, (2) to establish a ^{234}Th/^{238}U method for quantifying the BSi flux in Daya Bay that considers physical processes, and (3) to estimate the BSi fluxes in different seasons.

2. Material and methods

2.1. Study area

The semi-enclosed Daya Bay is located in the northern SCS (Fig. 1). Its area is 600 km^2 and approximately 60% of the bay is less than 10 m deep (Wang et al., 2008b). Since no major rivers discharge into Daya Bay, its seawater mostly originates from the SCS, which is characterized by its oligotrophic setting and minimal primary production (Yang et al., 2015). Consequently, the seawater in Daya Bay also exhibits low nutrient contents (Zheng et al., 2001), even though terrestrial nutrient input has increased since 1990 (Wang et al., 2008b). During the last three decades, especially since the Daya Bay Nuclear Power Station (DNPS) commenced operation, mariculture and human population expansion have significantly changed the environment in Daya Bay. For instance, the annual mean surface water temperature and Chl.*a* concentration increased by 1.1°C and 1.9 mg m^{-3}, respectively, from 1994 to 2004 compared with the period from 1983 to 1993 (Yu et al., 2007). Harmful algal blooms increased significantly (Yu et al., 2007), and both algal and major zooplankton species decreased (Wang et al., 2008b). Sediment mass accumulation rates also significantly increased in different sub-areas in Daya Bay (Wang, 2018; Yang et al., 2018).

The residence time of seawater in Daya Bay is approximately 90 d (Wang et al., 2008a). The nutrient and organic matter contents displayed significant spatio-temporal variation (Huang et al., 2008; Mou, 2018; Wang et al., 2004).

Therefore, it is probable that ^{234}Th in Daya Bay is subject to a large seasonal variation. Physical processes might significantly affect the quantification of ^{234}Th flux. The abundance and flux of BSi may also exhibit seasonal variations, since primary production displayed seasonal variations in Daya Bay (Song et al., 2004; Wu and Wang, 2007).

2.2. Sampling

Seawater samples were collected during four seasonal cruises on-board *YUEXIAYU* in Daya Bay from 2015 to 2016, i.e., spring (March), summer (July), autumn (October), and winter (December). The station distribution covered all of Daya Bay (Fig. 1). At most stations, both surface and bottom water were sampled. For several stations (i.e., S9, S10, S13, S14, and Z3), water was sampled at three depths. Only surface water was sampled at very shallow stations (i.e., S3 and S16). Once collected, 0.2 L of seawater was filtered through polycarbonate (PC) membrane with a 47 mm diameter and 0.4 μm pore size. The collected particles were washed with Milli-Q water and stored for BSi analysis. The seawater (0.5–2.0 L) was filtered through 25 mm diameter 1 μm quartz fibre (QMA, Whatman) to collect particles and filtrate for particulate and dissolved ^{234}Th analysis. Additionally, 1 L of seawater was filtered through a PC membrane of 0.4 μm pore size to determine the total suspended particulate matter (TSM). The seawater temperature and salinity were measured using a YSI 6600 multi-probe sensor.

2.3. BSi analysis

PC membranes for BSi analysis were dried at 50°C. The double wet-alkaline digestion method was then adopted to determine the BSi content (Ragueneau et al., 2005; Yang et al., 2015). Briefly, particles on PC membranes were digested in 4 mL of 0.2 mol L^{-1} NaOH solution in polyethylene centrifuge tubes at 100°C for 40 min to convert BSi to $Si(OH)_4$ (Brzezinski and Nelson, 1989). From each sample, 1 mL of solution was extracted to determine the silicate content via molybdosilicate blue spectrophotometry. The particles were then rinsed with Milli-Q water to remove leached silicate and dried. Subsequently, a second leaching, identical to the first, was performed to quantify the LSi content leached during the first leaching (Ragueneau et al., 2005). The BSi contents were calculated based on the two measurements (Yang et al., 2015).

2.4. ^{234}Th analysis

Particulate ^{234}Th samples were dried at 50°C for further analysis. The pre-concentration of dissolved ^{234}Th (i.e., ^{234}Th in filtrate) was based on the small-volume MnO_2 co-precipitation technique (Benitez-Nelson et al., 2001; Buesseler et al., 2001b; Fang et al., 2016). Briefly, the pH of 1.5 L of filtrate was adjusted to 8.0–8.2 using concentrated $NH_3{\cdot}H_2O$. Subsequently, 50 μL $KMnO_4$ solution (15 g L^{-1}) and 20 μL $MnCl_2{\cdot}4H_2O$ solution (100 g L^{-1}) were added by stirring to form MnO_2 particles. After standing for over 6 h, MnO_2-carrying ^{234}Th was filtered with a QMA membrane (25 mm diameter) and dried at 50°C. All dried samples were mounted under a Mylar film layer and two layers of aluminium foil for counting using a gas-flow proportional low-level RISØ beta counter (RISØ GM-25-5A). After 150 d, a second counting was performed for each sample to remove the contribution from other beta emitters (Benitez-Nelson et al., 2001). A counting efficiency of 48.5% was determined using a standard TC99 instrument (116–118 Bq, DTU Nutech, Denmark), similar to those (50 ± 1%) reported by Cai et al. (2006). Additionally, seawater from the intermediate zone of the SCS was employed to determine the chemical yield of ^{234}Th. The seawater was acidified to pH 1.0 with concentrated HCl and stored for over 150 d. The ^{234}Th was then analyzed using the same procedures as for the samples. The results indicated an average recovery of 94.7 ± 2.3% (±SD, n = 4). This is comparable to our recovery in a previous study (95.7 ± 1.0%, n = 5) (Ma et al., 2005), which verifies the reliability of the method. The ^{234}Th activities presented in this study were corrected to the sampling time. The ^{238}U activities were calculated using the relationship between ^{238}U and salinity (Owens et al., 2011).

2.5. ^{234}Th flux calculation

In Daya Bay, advection and diffusion probably affect the ^{234}Th flux calculation. Therefore, a method that considers these physical processes should be established. The tide in Daya Bay is irregular semidiurnal, and the meridional rectilinear current dominates the flow. Meanwhile, the southwest and northeast monsoons prevail in summer and winter, respectively (Lin et al., 2011; Wu et al., 2007). The residual current, which is affected by the monsoons, is expected to influence material distribution in Daya Bay. The seasonal variations in current velocity, based on the simulation of wind fields and the mean flow field of the northern SCS (Shi et al., 2009), displayed the trend winter > autumn > spring ≈ summer, which is similar to the wind speed trend. The coastal current flows nearly eastwards in summer and westwards in winter. These directions changed to northwest in spring and autumn (Shi et al., 2009). By combining the residual currents in summer and winter (Wu et al., 2007) with the seasonal variations in coastal currents, we estimated the flow fields over four seasons in Daya Bay. The horizontal velocity varied minimally with depth (Wu et al., 2007; Zheng et al., 1993) due to the shallowness (Fig. 1). Thus, velocity attenuation with depth was neglected in the horizontal advection term. For the diffusion term, ^{224}Ra was adopted for calculating the diffusion coefficient.

The sinking fluxes of ^{234}Th can be expressed according to the ^{234}Th/^{238}U disequilibria (Buesseler et al., 1992; Coale and Bruland, 1985; Cochran et al., 1995):

$$\frac{\partial A_{ThD}}{\partial t} = \lambda A_U - \lambda A_{ThD} - J, \quad (1)$$

$$\frac{\partial A_{ThP}}{\partial t} = J - \lambda A_{ThP} - P, \quad (2)$$

where $\partial A_{ThD}/\partial t$ and $\partial A_{ThP}/\partial t$ represent the changes in dissolved and particulate ^{234}Th with time; A_U, A_{ThD}, and A_{ThP} are the activities of ^{238}U, dissolved and particulate ^{234}Th, respectively; λ is the decay constant of ^{234}Th (0.0288 d^{-1}); J is the adsorption rate of dissolved ^{234}Th onto particles; and P

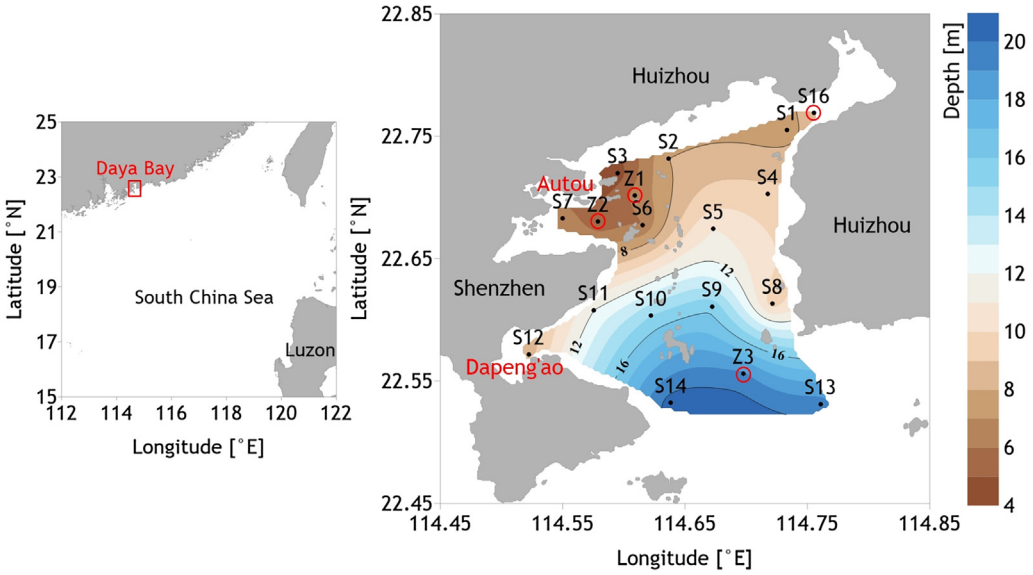

Figure 1 Sampling stations with bathymetry in Daya Bay, northern South China Sea. Stations Z1, Z2, Z3, and S16 were unoccupied in summer, while other stations were occupied during all cruises.

denotes the export rate of particulate ^{234}Th. By including advection and diffusion terms, the variation in dissolved ^{234}Th with time (Eq. (1)) becomes:

$$\frac{\partial A_{ThD}}{\partial t} = -V\cdot\nabla A_{ThD} + D\Delta A_{ThD} + \lambda A_U - \lambda A_{ThD} - J, \quad (3)$$

where ∇ is the Hamiltonian, Δ is the Laplacian ($\Delta = \nabla^2$), V (a vector quantity) denotes advection, and D is the eddy diffusivity. Combining Eqs. (2) and (3) yields,

$$\frac{\partial A_{Th}}{\partial t} = -V\cdot\nabla A_{ThD} + D\Delta A_{ThD} + \lambda A_U - \lambda A_{Th} - P, \quad (4)$$

where $\partial A_{Th}/\partial t$ is the change in the total ^{234}Th with time. For a steady state ($\partial A_{Th}/\partial t = 0$),

$$P = -V\cdot\nabla A_{ThD} + D\Delta A_{ThD} + \lambda A_U - \lambda A_{Th}. \quad (5)$$

In the horizontal direction, the advection term is more important than the diffusion term by a factor of 10. As upwelling and downwelling are rare in Daya Bay, the vertical diffusion is included. Then,

$$P = -V_H\left(\frac{\partial A_{ThD}}{\partial H}\right) + D_z\frac{\partial^2 A_{ThD}}{\partial Z^2} + \lambda A_U - \lambda A_{Th}, \quad (6)$$

where V_H is the horizontal residual current, D_Z is the vertical eddy diffusivity, $\partial A_{ThD}/\partial H$ is the horizontal gradient of dissolved ^{234}Th, and $\partial^2 A_{ThD}/\partial Z^2$ is the second derivative of dissolved ^{234}Th in the vertical direction. The flux of particulate ^{234}Th out of the water column is

$$F_{Th} = \int_0^h P dz = \int_0^h \left(-V_H\left(\frac{\partial A_{ThD}}{\partial H}\right) + \lambda A_U - \lambda A_{Th}\right) dz - D_z\left(\frac{\partial A_{ThD}}{\partial Z}\right)\Big|_{z=h}, \quad (7)$$

where h is the depth of the water column, $F_{Th} > 0$ denotes the net sinking flux, and $F_{Th} < 0$ represents the net flux from sediment resuspension into the seawater (Table 1).

3. Results

3.1. Hydrological environment

Daya Bay is influenced by the Asian Monsoon, with higher wind speeds in autumn and winter than in spring and summer (Shi et al., 2009). In summer, the average temperatures of the surface and bottom water in Daya Bay were 30.3 ± 0.7°C (±SD) and 27.5 ± 1.6°C, respectively, while the average salinities were 32.5 ± 4.6 and 35.7 ± 1.4 (Fig. 2), respectively. Temperature and salinity differed significantly between the surface and bottom waters (t-test, $p < 0.001$), suggesting stratification in summer (Fig. 2). In winter, strong northeast monsoons mixed the seawater. The average temperatures were 19.3 ± 1.3°C and 19.5 ± 0.8°C for surface and bottom waters, respectively, and the average salinities were 31.0 ± 1.5 and 31.7 ± 0.4, respectively. As in winter, the temperature and salinity in spring and autumn exhibited minimal differences between the surface and bottom waters (t-test, $p > 0.05$) (Fig. 2). The seasonal seawater stratification was consistent with the variation in the vertical stability in Daya Bay, which was highest in summer and lowest in winter (Han and Ma, 1991).

3.2. BSi abundance

BSi concentrations in Daya Bay were significantly higher than the 0.01–2.17 μmol L^{-1} measured in the northern SCS (Wang, 2012) (t-test, $p < 0.001$). In spring, BSi concentrations varied from 0.15 to 9.98 μmol L^{-1} with an average value of 3.76 ± 3.06 μmol L^{-1} (±SD, $n = 37$). High values were observed in the bay outlet (>7.19 μmol L^{-1}) and Dapengao in the southwest (>6.57 μmol L^{-1}). In summer, BSi concentrations fell to 1.47–23.93 μmol L^{-1} (avg. 8.04

Table 1 The particulate ^{234}Th sinking fluxes, BSi concentration to $^{234}Th_P$ ratios (BSi/$^{234}Th_P$), POC concentration to $^{234}Th_P$ ratios (POC/$^{234}Th_P$), PN concentration to $^{234}Th_P$ ratios (PN/$^{234}Th_P$), and sinking fluxes of BSi, POC, and PN in Daya Bay. The SS term is the particulate ^{234}Th flux that is calculated without considering physical processes; HT and VT are the particulate ^{234}Th fluxes resulting from horizontal advection and vertical diffusion, respectively. POC and PN data are from Mou (2018).

Station	Depth	V_H	D_Z	SS term	HA Term	VD Term	$^{234}Th_P$ flux	BSi/$^{234}Th_P$	POC/$^{234}Th_P$	PN/$^{234}Th_P$	BSi flux	POC flux	PN flux
	[m]	[cm s^{-1}]	[cm^2 s^{-1}]	[dpm m^{-2} d^{-1}]				[μmol dpm^{-1}]			[mmol m^{-2} d^{-1}]		
Spring													
S1	7.0	4.0	1.52	198 ± 15	160	−62	296 ± 15	0.91 ± 0.12	29.0 ± 3.7	8.29 ± 1.06	0.27 ± 0.04	8.6 ± 1.2	2.46 ± 0.34
S2	7.5	3.0	2.42	188 ± 13	−225	−230	−267 ± 13	3.82 ± 0.52	36.0 ± 4.9	9.87 ± 1.36	−1.02 ± 0.15	−9.6 ± 1.4	−2.64 ± 0.39
S4	9.0	3.0	2.63	293 ± 17	698	83	1075 ± 17	1.89 ± 0.15	25.1 ± 2.0	4.54 ± 0.37	2.04 ± 0.17	27.0 ± 2.2	4.88 ± 0.40
S5	10.5	3.0	2.50	155 ± 20	−489	475	142 ± 20	1.68 ± 0.11	15.0 ± 10.0	3.06 ± 0.20	0.24 ± 0.04	2.1 ± 0.3	0.43 ± 0.07
S6	5.5	2.5	2.32	−111 ± 19	−258	1203	834 ± 19	0.09 ± 0.01	10.6 ± 0.7	1.65 ± 0.11	0.08 ± 0.01	8.9 ± 0.6	1.37 ± 0.10
S7	6.0	2.0	1.71	218 ± 9	−22	−163	33 ± 9	2.39 ± 0.39	46.7 ± 7.6	14.6 ± 2.4	0.08 ± 0.03	1.6 ± 0.5	0.49 ± 0.16
S9	15.0	4.0	3.00	620 ± 15	1318	123	2062 ± 15	10.4 ± 1.4	49.0 ± 6.9	9.95 ± 1.39	21.5 ± 3.0	101 ± 14	20.5 ± 2.9
S10	14.5	6.0	0.91	475 ± 21	−1086	−53	−664 ± 21	13.2 ± 1.7	45.8 ± 5.9	6.96 ± 0.90	−8.74 ± 1.16	−30.4 ± 4.0	−4.63 ± 0.61
S11	11.5	4.0	3.30	414 ± 18	1312	49	1775 ± 18	6.77 ± 0.60	20.0 ± 1.8	4.45 ± 0.39	12.0 ± 1.1	35.6 ± 3.2	7.91 ± 0.70
S12	8.0	2.0	1.93	279 ± 13	74	−55	298 ± 13	12.0 ± 1.6	60.4 ± 8.3	9.28 ± 1.27	3.58 ± 0.52	18.0 ± 2.6	2.77 ± 0.40
S13	19.0	6.0	0.91	606 ± 21	−974	−65	−434 ± 21	12.9 ± 1.3	42.7 ± 4.3	9.58 ± 0.97	−5.59 ± 0.62	−18.5 ± 2.1	−4.16 ± 0.46
S14	20.0	7.0	1.52	838 ± 20	987	−43	1782 ± 20	13.4 ± 1.1	38.7 ± 3.2	6.33 ± 0.53	23.9 ± 2.0	69.0 ± 5.8	11.3 ± 1.0
Z3	18.5	5.0	0.37	566 ± 22	1190	−22	1734 ± 22	4.13 ± 0.28	17.3 ± 1.2	3.53 ± 0.24	7.16 ± 0.50	30.0 ± 2.1	6.12 ± 0.42
Summer													
S1	7.0	4.0	3.32	208 ± 14	52	135	395 ± 14	116 ± 44	335 ± 128	67.3 ± 25.8	45.8 ± 17.7	132 ± 51	26.6 ± 10.2
S2	6.0	3.0	0.21	249 ± 13	−659	288	−122 ± 13	34.1 ± 5.6	97.3 ± 16.0	17.7 ± 2.9	−4.15 ± 0.81	−11.9 ± 2.3	−2.15 ± 0.42
S4	8.0	3.0	5.03	291 ± 18	−435	−179	−323 ± 18	40.7 ± 9.5	98.9 ± 23.1	19.1 ± 4.4	−13.2 ± 3.1	−32.0 ± 7.7	−6.17 ± 1.48
S5	11.0	4.0	0.78	509 ± 31	279	41	829 ± 31	9.26 ± 1.53	93.1 ± 15.4	8.82 ± 1.46	7.68 ± 1.30	77.2 ± 13.1	7.31 ± 1.24
S6	8.0	4.0	6.00	344 ± 21	77	−108	314 ± 21	29.7 ± 6.5	132 ± 29	15.59 ± 3.42	9.33 ± 2.13	41.3 ± 9.4	4.89 ± 1.12
S7	6.5	3.0	7.73	238 ± 22	386	−339	285 ± 22	16.6 ± 2.4	99.0 ± 14.2	18.43 ± 2.64	4.73 ± 0.77	28.2 ± 4.6	5.25 ± 0.85
S8	7.5	6.0	4.55	244 ± 19	−582	461	122 ± 19	6.11 ± 0.69	21.2 ± 2.4	4.11 ± 0.46	0.75 ± 0.14	2.6 ± 0.5	0.50 ± 0.10
S10	14.0	7.0	0.15	574 ± 27	1361	−860	1075 ± 27	8.57 ± 0.98	23.0 ± 2.6	3.17 ± 0.36	9.21 ± 1.08	24.8 ± 2.9	3.41 ± 0.40
S12	7.0	3.0	1.30	262 ± 36	−609	−212	−559 ± 36	11.8 ± 2.4	63.9 ± 13.4	8.64 ± 1.81	−6.60 ± 1.44	−35.7 ± 7.8	−4.83 ± 1.06
S13	18.5	6.0	2.72	617 ± 27	133	−306	443 ± 27	1.93 ± 0.12	11.0 ± 0.7	2.06 ± 0.13	0.86 ± 0.07	4.9 ± 0.4	0.91 ± 0.08
S14	19.0	8.0	14.6	782 ± 32	−182	−167	433 ± 32	3.86 ± 0.42	19.8 ± 2.2	3.24 ± 0.35	1.67 ± 0.22	8.6 ± 1.1	1.40 ± 0.18
Autumn													
S1	8.5	4.0	2.05	62 ± 20	−385	−124	−446 ± 20	4.92 ± 0.48	39.6 ± 3.9	4.52 ± 0.44	−2.19 ± 0.24	−17.7 ± 1.9	−2.02 ± 0.22
S2	7.5	3.0	1.52	70 ± 17	22	17	109 ± 17	2.04 ± 0.16	13.8 ± 1.1	2.18 ± 0.18	0.22 ± 0.04	1.5 ± 0.3	0.24 ± 0.04
S4	9.5	3.0	0.48	−50 ± 26	−649	−145	−843 ± 26	3.61 ± 0.37	21.3 ± 2.2	3.47 ± 0.36	−3.04 ± 0.33	−17.9 ± 1.9	−2.93 ± 0.32
S5	11.5	4.0	3.48	152 ± 22	333	−301	185 ± 22	1.59 ± 0.14	17.1 ± 1.5	3.60 ± 0.31	0.29 ± 0.04	3.2 ± 0.5	0.66 ± 0.10
S6	8.0	4.0	3.00	44 ± 24	1256	108	1409 ± 24	2.63 ± 0.23	21.4 ± 1.9	2.96 ± 0.26	3.70 ± 0.33	30.1 ± 2.7	4.17 ± 0.37
S7	7.0	3.0	3.64	96 ± 18	570	−173	494 ± 18	2.89 ± 0.30	16.7 ± 1.7	3.07 ± 0.32	1.43 ± 0.16	8.3 ± 0.9	1.52 ± 0.17
S9	15.5	4.0	2.57	97 ± 28	−289	98	−94 ± 28	6.03 ± 0.52	20.4 ± 1.8	5.05 ± 0.43	−0.57 ± 0.18	−1.9 ± 0.6	−0.48 ± 0.15
S10	14.5	7.0	0.34	−22 ± 34	−1180	−3	−1204 ± 34	4.19 ± 0.33	10.5 ± 0.8	1.97 ± 0.16	−5.05 ± 0.43	−12.7 ± 1.1	−2.37 ± 0.20
S11	12.5	4.0	3.00	365 ± 27	1709	69	2143 ± 27	17.3 ± 2.3	59.0 ± 7.8	5.48 ± 0.73	37.0 ± 4.9	126 ± 17	11.74 ± 1.56
S12	8.0	3.0	23.1	188 ± 20	52	−740	−500 ± 20	20.0 ± 3.1	37.7 ± 5.9	6.28 ± 0.99	−10.0 ± 1.6	−18.9 ± 3.1	−3.14 ± 0.51

Table 1 (*Continued*)

Station	Depth	V_H	D_Z	SS term	HA Term	VD Term	$^{234}Th_P$ flux	$BSi/^{234}Th_P$	$POC/^{234}Th_P$	$PN/^{234}Th_P$	BSi flux	POC flux	PN flux
	[m]	[cm s^{-1}]	[cm^2 s^{-1}]	[dpm m^{-2} d^{-1}]				[μmol dpm^{-1}]			[mmol m^{-2} d^{-1}]		
S13	19.0	6.0	6.06	704 ± 30	−639	−154	−89 ± 30	7.09 ± 0.91	22.6 ± 2.9	3.31 ± 0.42	−0.63 ± 0.23	−2.0 ± 0.7	−0.29 ± 0.11
S14	19.5	7.0	9.34	487 ± 42	1340	−84	1743 ± 42	4.09 ± 0.43	9.0 ± 0.9	1.23 ± 0.13	7.13 ± 0.76	15.7 ± 1.6	2.14 ± 0.22
Z2	15.0	3.0	0.30	8 ± 55	−873	−9	−875 ± 55	2.69 ± 0.29	13.4 ± 1.4	2.10 ± 0.22	−2.35 ± 0.29	−11.7 ± 1.5	−1.83 ± 0.23
Z3	18.5	5.5	2.11	397 ± 29	−198	−240	−41 ± 29	6.08 ± 0.66	9.5 ± 1.0	1.46 ± 0.16	−0.25 ± 0.18	−0.4 ± 0.3	−0.06 ± 0.04
Winter													
S1	7.0	5.0	9.62	241 ± 10	−250	−36	−45 ± 10	8.79 ± 1.12	15.4 ± 2.0	3.64 ± 0.46	−0.40 ± 0.10	−0.7 ± 0.2	−0.16 ± 0.04
S2	6.5	4.0	7.00	214 ± 12	891	27	1131 ± 12	4.50 ± 0.44	11.5 ± 1.1	3.07 ± 0.30	5.09 ± 0.50	13.0 ± 1.3	3.47 ± 0.34
S4	9.8	4.0	11.0	147 ± 24	−177	589	558 ± 24	2.54 ± 0.24	13.7 ± 1.3	3.56 ± 0.33	1.42 ± 0.14	7.6 ± 0.8	1.99 ± 0.20
S5	11.5	4.0	0.81	365 ± 14	1177	−58	1484 ± 14	2.90 ± 0.26	12.1 ± 1.1	2.83 ± 0.26	4.30 ± 0.40	18.0 ± 1.7	4.20 ± 0.39
S6	8.0	3.0	6.67	96 ± 19	−466	−216	−586 ± 19	2.29 ± 0.19	17.7 ± 1.5	2.42 ± 0.20	−1.34 ± 0.12	−10.4 ± 0.9	−1.42 ± 0.12
S9	14.5	5.0	31.4	335 ± 17	123	1177	1635 ± 17	4.15 ± 0.34	10.9 ± 0.9	3.70 ± 0.30	6.78 ± 0.56	17.8 ± 1.5	6.05 ± 0.50
S10	14.0	7.0	7.89	528 ± 18	1814	318	2659 ± 18	4.77 ± 0.63	14.6 ± 1.9	2.85 ± 0.38	12.7 ± 1.7	38.7 ± 5.1	7.59 ± 1.01
S11	11.8	5.0	9.90	313 ± 23	140	−293	161 ± 23	1.82 ± 0.15	10.9 ± 0.9	2.15 ± 0.17	0.29 ± 0.05	1.8 ± 0.3	0.35 ± 0.06
S12	7.5	2.5	6.67	240 ± 13	14	−230	23 ± 13	4.26 ± 0.39	11.4 ± 1.0	2.93 ± 0.26	0.10 ± 0.06	0.3 ± 0.2	0.07 ± 0.04
S13	19.0	6.0	5.97	476 ± 22	−108	−329	38 ± 22	4.21 ± 0.38	11.8 ± 1.1	1.89 ± 0.17	0.16 ± 0.09	0.5 ± 0.3	0.07 ± 0.04
S14	19.5	8.0	7.00	711 ± 20	1358	−182	1887 ± 20	3.62 ± 0.33	9.7 ± 0.9	1.90 ± 0.17	6.84 ± 0.63	18.3 ± 1.7	3.58 ± 0.33
Z1	5.5	4.0	6.60	12 ± 18	−504	−314	−806 ± 18	4.22 ± 0.37	13.4 ± 1.2	2.81 ± 0.25	−3.40 ± 0.31	−10.8 ± 1.0	−2.26 ± 0.21
Z3	18.5	6.0	1.48	333 ± 24	−1300	257	−709 ± 24	3.73 ± 0.38	11.3 ± 1.1	2.31 ± 0.23	−2.64 ± 0.28	−8.0 ± 0.9	−1.64 ± 0.17

± 5.48 μmol L^{-1}, n = 26). These values were high in the northern region and decreased towards the outlet (Fig. 1). In autumn, BSi concentrations varied from 0.71 to 13.43 μmol L^{-1} (avg. 5.51 ± 3.11 μmol L^{-1}, n = 38) with high values in Dapengao (>12.74 μmol L^{-1}). In winter, BSi concentrations fell to 0.98–8.69 μmol L^{-1} (avg. 2.39 ± 1.34 μmol L^{-1}, n = 35). The annual mean BSi was 1.71 ± 1.79 μmol L^{-1} in the Changjiang Estuary and the adjacent area (Cao et al., 2013). In the upwelling system off Concepción, Chile, the annual average BSi reached 3.15 ± 3.59 μmol L^{-1} (Sánchez et al., 2008). In the Indian sector of the Subantarctic Ocean, BSi was less than 0.46 μmol L^{-1} (Leblanc et al., 2002). In comparison, the annual mean BSi concentration was 4.92 μmol L^{-1} in Daya Bay, representing an area of extremely high diatom production.

Overall, BSi concentrations in Daya Bay did not differ statistically between the surface and bottom water. The average BSi concentrations (±SD) in surface waters were 3.58 ± 3.28 μmol L^{-1} in spring, 7.83 ± 6.47 μmol L^{-1} in summer, 4.38 ± 2.85 μmol L^{-1} in autumn, and 2.80 ± 1.20 μmol L^{-1} in winter. In the bottom waters, BSi concentrations averaged 3.01 ± 2.41, 9.20 ± 4.50, 6.72 ± 3.39, and 3.27 ± 1.64 μmol L^{-1} in the four seasons. Temperature and salinity were also comparable (Fig. 2) in all the seasons except summer. The hydrological environments probably affect the vertical BSi distributions.

3.3. $^{234}Th/^{238}U$ disequilibrium

The activity concentrations of the total ^{234}Th in spring, summer, autumn, and winter in Daya Bay fell to 0.57–4.60 dpm L^{-1} (avg. 1.23 ± 0.77 dpm L^{-1}, n = 31), 0.46–2.10 dpm L^{-1} (avg. 1.17 ± 0.37 dpm L^{-1}, n = 26), 0.71–3.74 dpm L^{-1} (avg. 1.67 ± 0.65 dpm L^{-1}, n = 35), and 0.77–6.40 dpm L^{-1} (avg. 1.56 ± 0.98 dpm L^{-1}, n = 35), respectively (Table S1). Particulate ^{234}Th accounted for 49 ± 13%, 45 ± 20%, 55 ± 15%, and 59 ± 15% of the total ^{234}Th, respectively. In spring, the average $^{234}Th/^{238}U$ ratio was 0.56 ± 0.37. For most stations, ^{234}Th was in deficit with respect to ^{238}U ($^{234}Th/^{238}U < 1.0$), but excess ^{234}Th was observed in the northwest (Fig. 2). In summer, the $^{234}Th/^{238}U$ ratios were below 1.0 except at station S3, averaging 0.50 ± 0.18. In autumn and winter, the average $^{234}Th/^{238}U$ values were 0.80 ± 0.31 and 0.72 ± 0.46, respectively.

4. Discussion

4.1. Seasonal variations in BSi abundance

BSi concentration is highest in summer and lowest in winter (t-test, $p < 0.001$). The highest BSi abundance is consistent with the highest diatom abundance in summer in Daya Bay (Sun et al., 2006). BSi concentrations in autumn are slightly higher than in spring (t-test, $p < 0.05$) (Fig. 3). The seasonality of the BSi concentration in Daya Bay is similar to that observed in the upwelling system off Concepción, Chile (Sánchez et al., 2008). The concurrent ^{14}C-derived primary production in the surface water of Daya Bay followed the pattern sum-

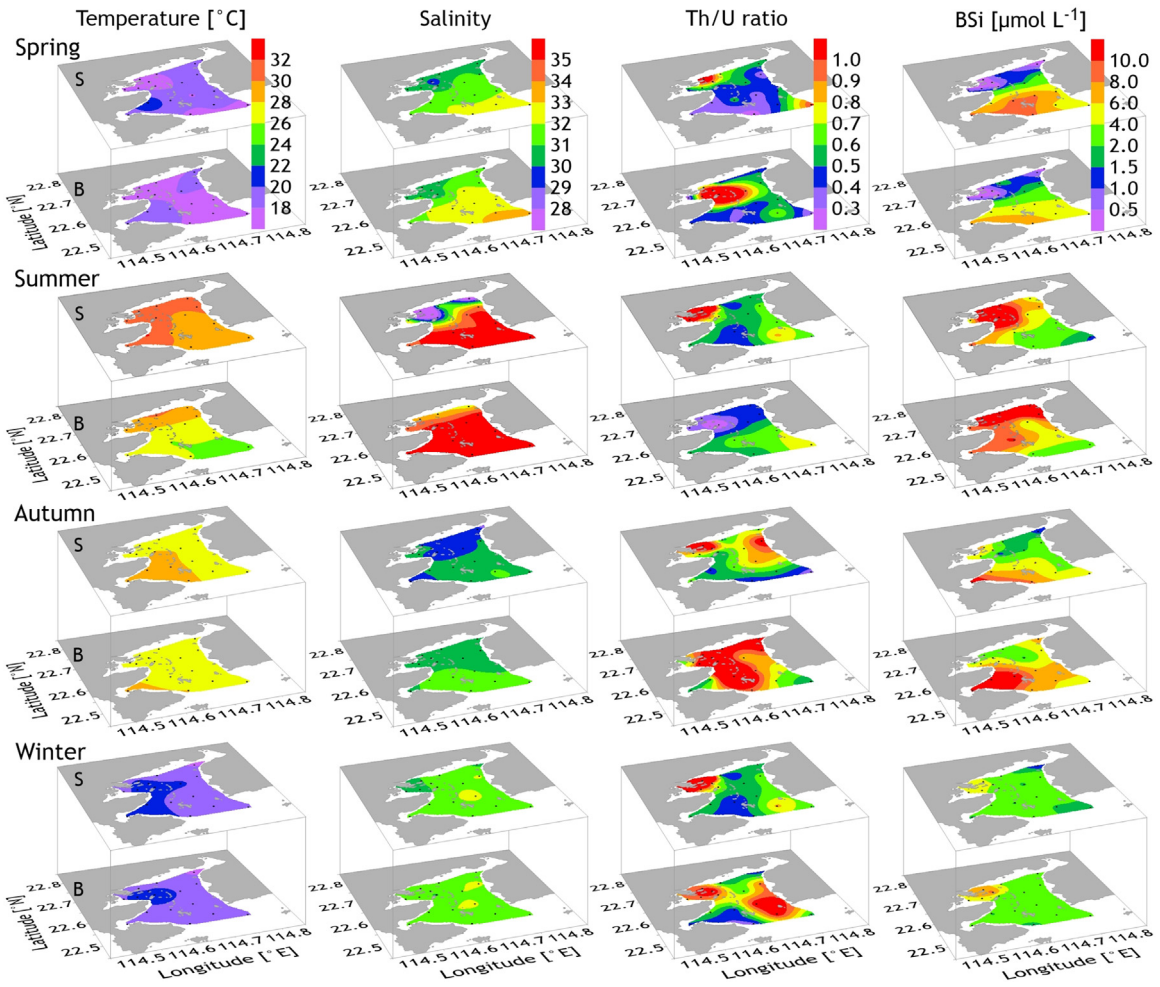

Figure 2 Seasonal distributions of temperature, salinity, $^{234}Th/^{238}U$ ratio, and BSi concentration in the surface (S) and bottom (B) waters in Daya Bay.

mer > spring > autumn > winter (Fig. 3; Mou, 2018). A dinoflagellate bloom, only appearing in spring in Daya Bay (Wang et al., 2005), was observed at S4 (Mou, 2018). Excluding the S4 data, the ^{14}C-derived primary production in spring is comparable to that in autumn. Therefore, the seasonal pattern of the BSi concentration appears to be controlled by the variation in primary production in Daya Bay. A previous study suggested that diatoms frequently dominate the phytoplankton community in Daya Bay (Wang et al., 2006). The diatom production probably regulates the seasonal abundance of BSi to a large extent in Daya Bay.

The BSi/POC (or Si/C) atomic ratios in particulate matter also reveal the dominance of diatoms in BSi abundance in situ. Combining the POC concentrations measured during the same cruises (Mou, 2018; Mou et al., 2017), the Si/C ratios in spring, summer, autumn, and winter were 0.01–0.58 (avg. 0.18 ± 0.16), 0.03–0.42 (avg. 0.27 ± 0.11), 0.02–0.72 (avg. 0.27 ± 0.16), and 0.07–0.57 (avg. 0.30 ± 0.09), respectively (Fig. 4). The surface sediments in Daya Bay had Si/C values of 0.4–2.5 (Wang, 2018). Clearly, most of the Si/C ratios in TSM are considerably lower than the values for sediments, suggesting that phytoplankton dominates the Si/C of TSM in Daya Bay. BSi concentrations display a significant positive correlation with Chl.*a* content in summer, autumn, and winter (Fig. 5), supporting this view. In spring, there is also a correlation between BSi and Chl.*a* after excluding several data affected by a dinoflagellate bloom (Fig. 5; Mou, 2018). Previous studies indicated that dinoflagellates only generate blooms in spring, although the mechanisms are unclear (Sun et al., 2006; Wang et al., 2005). A local nutrient input probably induced this bloom event.

Comparisons between our results and reported Si/C values in other oceanic settings further verify that BSi seasonality in Daya Bay is dominated by in situ diatom production. The mean Si/C ratio derived from 27 species under unlimited silicon was 0.13 (Brzezinski, 1985); notably, the mean Si/C ratios in Daya Bay are much higher than this value. However, our results are comparable to the values of 0.30–0.65 measured in the Antarctic Ocean (Leynaert et al., 1991; Nelson and Smith, 1986; Nelson et al., 1989; Tréguer et al., 1990). Therefore, particulate organic matter appears to be extremely siliceous in Daya Bay as in the open Antarctic Ocean (Shiomoto and Ishii, 1995). The extremely high Si/C ratios are ascribed to silica-rich diatoms. Although Si/C in diatoms has not been reported in Daya Bay, the Antarctic Ocean study may provide evidence. For instance, a high Si/C ratio of 0.61 was also measured in the Weddell-Scotia Sea during an abundance of *Nitzschia* spp. (Leynaert et al., 1991;

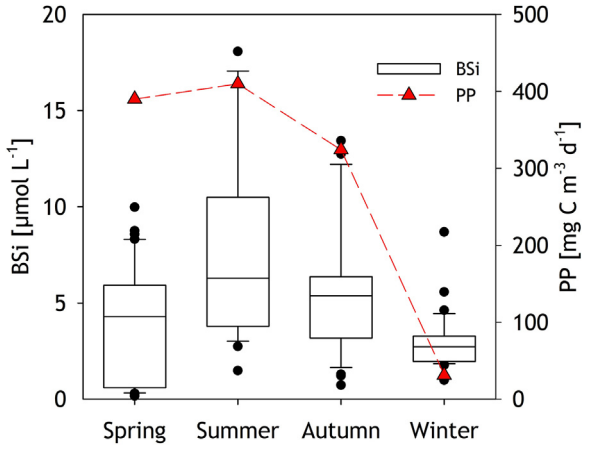

Figure 3 Seasonal variations in BSi concentration (box chart) and primary production (PP, triangle) in Daya Bay. In the diagram, the horizontal line within the box indicates the median of the sample. The lower (lower quartile) or upper (upper quartile) lines of each box denote 25% or 75% of data below the line. The black dots represent 25% of data above the upper line and below the lower line. PP data are from Mou (2018).

Tréguer and van Bennekom, 1991). Additionally, BSi contents per milligramme dry weight particles (i.e., in μmol mg^{-1}) display a maximum average of 2.23 ± 1.27 μmol mg^{-1} in summer, followed by autumn (1.48 ± 1.41 μmol mg^{-1}), spring (1.26 ± 1.37 μmol mg^{-1}), and winter (0.52 ± 0.19 μmol mg^{-1}). This seasonality directly confirms that diatoms provide the highest contribution to suspended particles in summer. Since BSi has a ballast effect, leading to the rapid sinking of particulate matter (Guinder et al., 2015; Nelson et al., 1995; Waite et al., 1997), POC and other biogenic particulate components could be efficiently removed from seawater and enter sediment after production. Thus, organic matter degradation mostly occurs in surface sediments in Daya Bay rather than in a water column as observed in mesopelagic waters (Yang et al., 2009).

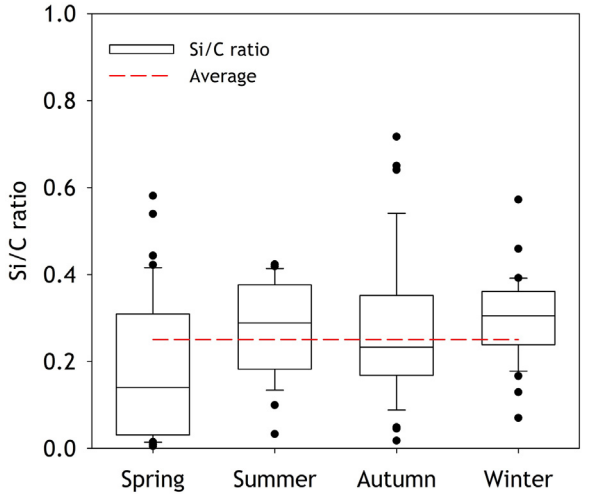

Figure 4 Seasonal variations in Si/C atomic ratios in TSM in Daya Bay.

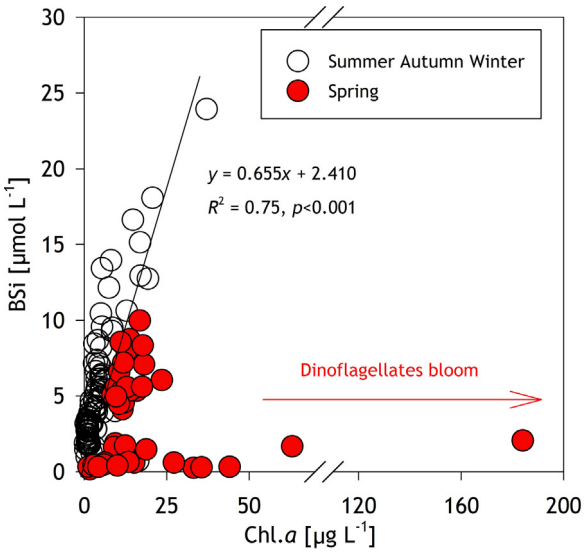

Figure 5 Relationships between BSi concentrations and Chl.*a* content in different seasons in Daya Bay. Chl.*a* data are taken from Mou (2018).

4.2. High BSi concentrations and low nutrients in Daya Bay

It is noteworthy that BSi concentrations in Daya Bay are five-fold higher than in the adjacent northern SCS (<0.50 μmol L^{-1}; Cao et al., 2012) and the southern SCS (<0.36 μmol L^{-1}; Yang et al., 2015). The concentrations are even higher than in the upwelling area in western Luzon (<1.83 μmol L^{-1}; Liu et al., 2012) and the upwelling system off Concepción, Chile (3.15 ± 3.59 μmol L^{-1}) (Sánchez et al., 2008). The seawater in Daya Bay mostly originates from the SCS. However, several small rivers and maricultures occasionally add nutrients into Daya Bay, which can result in phytoplankton blooms (Yu et al., 2007), Daya Bay, overall, does not display higher nutrient concentrations than in SCS seawater (Zheng et al., 2001). In comparison, both BSi concentrations and primary production in Daya Bay are significantly higher than in the SCS. This suggests that some mechanisms might sustain high diatom production in Daya Bay.

A recent report suggested that the dissolved inorganic nitrogen (DIN) concentration in Daya Bay is lower than that of silicate despite an increase in DIN over the past three decades (Wu et al., 2017). Specifically, DSi is not the limiting nutrient in Daya Bay. Efficient nitrogen cycling in Daya Bay might be key to the high diatom production. A laboratory simulation indicated that rapid organic nitrogen degradation causes rapid cycling of nitrogen nutrients in Daya Bay (Zheng et al., 2001). Meanwhile, the mechanisms explaining the high BSi and low nutrients in Daya Bay remain poorly understood, this phenomenon reveals that Daya Bay is an area of efficient BSi production.

4.3. ^{234}Th fluxes

Compared with ^{234}Th/^{238}U values in the northern shelf of the SCS (Cai et al., 2015), there are more significant deficits in

^{234}Th in Daya Bay in summer (*t*-test, $p < 0.001$); however, no significant differences were found between the bay and the shelf in the other three seasons (*t*-test, $p > 0.05$). Based on the disequilibria between ^{234}Th and ^{238}U, it was estimated that the horizontal advection terms constitute 47 ± 22%, 35 ± 17%, 60 ± 28%, and 44 ± 27% of particulate ^{234}Th fluxes in spring, summer, autumn, and winter, respectively; the vertical diffusion terms constituted 19 ± 22%, 24 ± 9%, 19 ± 19%, and 29 ± 22% of particulate ^{234}Th fluxes, respectively. These values are much higher than those in the SCS basin (<10%) (Cai et al., 2008). Therefore, ^{234}Th fluxes and ^{234}Th-derived BSi fluxes, including the physical terms, are more representative than the general ^{234}Th method.

At most stations, the ^{234}Th sinking fluxes of particles are above zero, suggesting an overall net sinking of particles in Daya Bay. The lowest flux of 487 ± 292 dpm m^{-2} d^{-1} (n = 8) occurred in summer (*t*-test, $p < 0.05$), corresponding to the prevention of particle sinking due to temperature-induced stratification. During the other three seasons, ^{234}Th exhibited comparable fluxes, i.e., 1003 ± 746 dpm m^{-2} d^{-1} (n = 10) in spring, 1014 ± 789 dpm m^{-2} d^{-1} (n = 6) in autumn, and 1064 ± 878 dpm m^{-2} d^{-1} (n = 9) in winter (Fig. 6). At several stations, negative ^{234}Th fluxes were measured, indicating sediment resuspension. The negative fluxes mostly appeared at stations close to land, suggesting that sediment resuspension may be due to strong hydrodynamic forcing in shallow waters. The average resuspension fluxes of ^{234}Th appear similar in different seasons, averaging 455 ± 163 (n = 3), 335 ± 179 (n = 3), 512 ± 403 (n = 8), and 537 ± 294 (n = 4) dpm m^{-2} d^{-1} for spring, summer, autumn, and winter, respectively (Fig. 6).

4.4. BSi fluxes

The sinking fluxes of biogenic components (BSi, POC, and PN) were calculated based on the ^{234}Th flux and the ratio of component X to the ^{234}Th activity on TSM (i.e., X/Th_P) in bottom waters:

$$F_X = F_{Th} \times \left(\frac{X}{Th_P}\right), \tag{8}$$

where F_X is the flux of biogenic particulate components.

For all seasons, the sinking fluxes of BSi varied from 0.08 ± 0.01 to 45.84 ± 17.66 mmol Si m^{-2} d^{-1} (Fig. 6), covering a large range. The lowest BSi flux of 4.19 ± 3.98 mmol Si m^{-2} d^{-1} occurred in winter, corresponding to its lowest primary production and abundance. In other seasons, the BSi fluxes appeared comparable, with values of 7.08 ± 8.62 mmol Si m^{-2} d^{-1} in spring, 10.01 ± 13.95 mmol Si m^{-2} d^{-1} in summer, and 8.30 ± 13.06 mmol Si m^{-2} d^{-1} in autumn (Fig. 6). Our results are comparable to the burial flux of BSi, which varied from 0.27 mmol Si m^{-2} d^{-1} to 19.2 mmol Si m^{-2} d^{-1} in the surface sediments in Daya Bay (Wang, 2018). Although summer exhibited the highest BSi concentrations (Fig. 3), the BSi flux did not differ statistically from that from spring to autumn (Fig. 6), which is probably due to the rapid BSi dissolution in summer that is induced by high temperature and stratification. The resuspension fluxes of BSi in spring, summer, autumn, and winter were 5.12 ± 3.17, 7.97 ± 3.80, 3.01 ± 3.03, and 1.95 ± 1.16 mmol Si m^{-2} d^{-1}, respectively (Fig. 6).

To date, few studies have reported BSi export in marine environments. In the northern SCS, the sinking flux of BSi that was estimated with a sediment trap at 500 m averaged 0.20 ± 0.09 mmol Si m^{-2} d^{-1} (Dong et al., 2016). In the southern SCS, BSi fluxes out of the euphotic zone were 0.18 ± 0.15 and 0.40 ± 0.20 mmol Si m^{-2} d^{-1} inside and outside a decaying cyclonic eddy, respectively (Yang et al., 2015). Clearly, BSi fluxes in Daya Bay were much higher than in the open SCS, indicating that Daya Bay is an efficient BSi burial site. In the

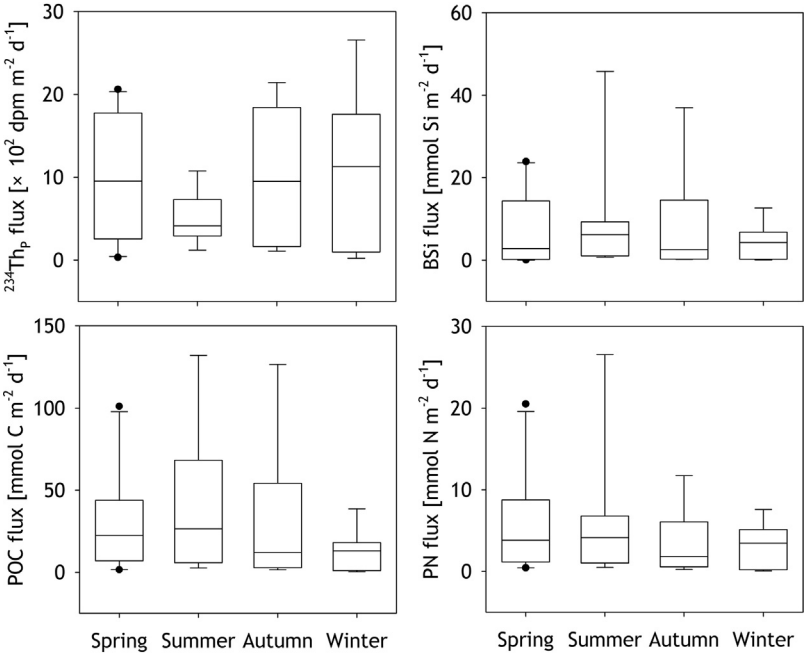

Figure 6 Seasonal variations in sinking fluxes of ^{234}Th$_p$, BSi, POC, and PN in Daya Bay. The sinking fluxes of POC and PN were estimated based on the POC and PN data measured during the same cruises (Mou et al., 2017; Mou, 2018).

Southern Ocean, one of the highest BSi production regions, BSi export fluxes out of the upper ocean varied from 2.4 to 32.4 mmol Si m^{-2} d^{-1} with an average of 20.4 mmol m^{-2} d^{-1} (Friedrich and Rutgers van der Loeff, 2002), exceeding the values in Daya Bay. These results reveal an extremely large variation in BSi export in worldwide marine environments. Therefore, the global quantification of BSi export requires extensive studies in different marine environments.

Our established ^{234}Th method allows us to estimate the sinking fluxes of POC and PN in TSM similarly to the estimation of BSi flux. Using the data from our cruises (Mou, 2018; Mou et al., 2017), the sinking fluxes of POC averaged 30.2 ± 30.4 mmol C m^{-2} d^{-1} in spring, 40.0 ± 41.6 mmol C m^{-2} d^{-1} in summer, and 30.9 ± 43.8 mmol C m^{-2} d^{-1} in autumn (Fig. 6). While winter exhibited the lowest value of 12.9 ± 11.6 mmol C m^{-2} d^{-1}. The fluxes of PN in spring, summer, autumn, and winter, averaged 5.82 ± 5.91, 6.28 ± 7.98, 3.41 ± 3.93, and 3.04 ± 2.53 mmol N m^{-2} d^{-1}, respectively (Fig. 6). Therefore, the average C:Si:N ratio during sinking was estimated as 5.1:0.8:1.0 in spring, indicating the preferential removal of nitrogen. However, the ratios in the other three seasons, i.e., 6.7:1.5:1.0 in summer, 7.0:1.6:1.0 in autumn, and 4.5:1.4:1.0 in winter, suggested that Si was more efficiently removed than nitrogen from seawater into sediment. Furthermore, BSi is more refractory than particulate organic nitrogen (Pastuszak et al., 2003; Zheng et al., 2001). Thus, particle sinking in Daya Bay appears to decrease the Si:N ratio in seawater. Since the 1980s, the Si:N ratio in seawater has decreased in Daya Bay, which is attributed to the local use of fertilizer (Qiu, 2001; Wei, 2005). A series of studies also confirmed that land-derived nutrients, including DSi and inorganic nitrogen, and BSi regeneration in the estuarine regions, significantly influence the Si:N ratio in seawater in the Baltic Sea (Conley et al., 2008; Danielsson et al., 2008; Humborg et al., 2006; Pastuszak et al., 2003, 2008). Our results provide another mechanism by which the nutrient structure is influenced in some coastal seas (Agirbas et al., 2017; Yucel, 2018), although the role of particle sinking in regulating the Si:N ratio requires further investigation. Studies in the Baltic Sea suggested that the long-term decreases in DSi and DSi:DIN (Danielsson et al., 2008) are linked to eutrophication (Conley et al., 2008) as well as the hydrologically generated input decrease (Humborg et al., 2006). Eutrophication may enhance the transformation of DSi to BSi, causing more BSi to sink into sediments, which would require a much longer time than nitrogen and phosphorus to return into seawater (Pastuszak et al., 2003).

5. Conclusions

Seasonal variations in the abundance and sinking flux of BSi were investigated in Daya Bay. BSi concentrations were much higher in summer than in other seasons. The lowest BSi concentration was in winter. The seasonal variation in BSi abundance was similar to the temporal trend of primary production, and correlated with the dominance of diatoms in the phytoplankton community. Advection and diffusion significantly affect the ^{234}Th/^{238}U method of tracing particulate sinking in Daya Bay. Based on our ^{234}Th/^{238}U method considering physical terms, the BSi sinking fluxes displayed seasonal variations, with the lowest values in winter and similar fluxes in other seasons. Simultaneously, sediment resuspension in very shallow waters was found in Daya Bay. Overall, these results suggested that Daya Bay is effective in burying BSi compared to particulate nitrogen, indicating the preferential removal of silicon over nitrogen. This result provides a feasible mechanism for interpreting the long-term decrease in the Si:N ratio in seawater in Daya Bay.

Acknowledgements

The authors appreciate the constructive suggestions from two anonymous reviewers and editors, and thank Q. Li for providing eddy diffusivity, and K. Zhang and B. Wang for PP data analysis. This work was supported by the National Key Basic Research Special Foundation Programme of China (2015CB452902 & 2015CB452903) and NSFC (41476061).

Appendix A. Supplementary data

Supplementary data associated with this article can be found, in the online version, at doi:10.1016/j.oceano.2018.11.003.

References

Agirbas, E., Koca, L., Aytan, U., 2017. Spatio-temporal pattern of phytoplankton and pigment composition in surface waters of southeastern Black Sea. Oceanologia 59 (3), 283–299, http://dx.doi.org/10.1016/j.oceano.2017.03.004.

Benitez-Nelson, C.R., Buesseler, K.O., Crossin, G., 2000. Upper ocean carbon export, horizontal transport, and vertical eddy diffusivity in the southwestern Gulf of Maine. Cont. Shelf Res. 20 (6), 707–736, http://dx.doi.org/10.1016/S0278-4343(99)00093-X.

Benitez-Nelson, C.R., Buesseler, K.O., Rutgers van der Loeff, M.M., Andrews, J., Ball, L., Crossin, G., Charette, M., 2001. Testing a new small-volume technique for determining ^{234}Th in seawater. J. Radioanal. Nucl. Chem. 248 (3), 795–799, http://dx.doi.org/10.1023/A:1010621618652.

Boyd, P.W., Watson, A.J., Law, C.S., Abraham, E.R., Trull, T., Murdoch, R., Bakker, D.C., Bowie, A.R., Buesseler, K.O., Chang, H., Charette, M., Croot, P., Downing, K., Frew, R., Gall, M., Hadfield, M., Hall, J., Harvey, M., Jameson, G., La Roche, J., Liddicoat, M., Ling, R., Maldonado, M.T., McKay, R.M., Nodder, S., Pickmere, S., Pridmore, R., Rintoul, S., Safi, K., Sutton, P., Strzepek, R., Tanneberger, K., Turner, S., Waite, A., Zeldis, J., 2000. A mesoscale phytoplankton bloom in the polar Southern Ocean stimulated by iron fertilization. Nature 407 (6805), 695–702, http://dx.doi.org/10.1038/35037500.

Brzezinski, M.A., 1985. The Si:C:N ratio of marine diatoms: Interspecific variability and the effect of some environmental variables. J. Phycol. 21, 347–357.

Brzezinski, M.A., Nelson, D.M., 1989. Seasonal changes in the silicon cycle within a Gulf Stream warm-core ring. Deep-Sea Res. Pt. A 36 (7), 1009–1030, http://dx.doi.org/10.1016/0198-0149(89)90075-7.

Buesseler, K.O., Bacon, M.P., Cochran, J.K., Livingston, H.D., 1992. Carbon and nitrogen export during the JGOFS North Atlantic bloom experiment estimated from ^{234}Th:^{238}U disequilibria. Deep-Sea Res. Pt. A 39 (7–8), 1115–1137, http://dx.doi.org/10.1016/0198-0149(92)90060-7.

Buesseler, K.O., Ball, L., Andrews, J., Cochran, J.K., Hirschberg, D.J., Bacon, M.P., Fleer, A., Brzezinski, M., 2001a. Upper ocean export of particulate organic carbon and biogenic silica in the Southern Ocean along 170 W. Deep-Sea Res. Pt. II 48 (19–20), 4275–4297, http://dx.doi.org/10.1016/S0967-0645(01)00089-3.

Buesseler, K.O., Benitez-Nelson, C.R., Rutgers van der Loeff, M.M., Andrews, J., Ball, L., Crossin, G., Charette, M., 2001b. An intercomparison of small- and large-volume techniques for ^{234}Th in seawater. Mar. Chem. 74 (1), 15—28, http://dx.doi.org/10.1016/S0304-4203(00)00092-X.

Buesseler, K.O., Benitez-Nelson, C.R., Moran, S.B., Burd, A., Charette, M., Cochran, J.K., Coppola, L., Fisher, N.S., Fowler, S.W., Gardner, W.D., Guo, L., Gustafsson, Ö., Lamborg, C., Masque, P., Miquel, J.C., Passow, U., Santschi, P.H., Savoye, N., Stewart, G., Trull, T., 2006. An assessment of particulate organic carbon to thorium-234 ratios in the ocean and their impact on the application of ^{234}Th as a POC flux proxy. Mar. Chem. 100 (3—4), 213—233, http://dx.doi.org/10.1016/j.marchem.2005.10.013.

Bužančić, M., Gladan, Ž., Marasović, N., Kušpilić, I., Grbec, G.B., 2016. Eutrophication influence on phytoplankton community composition in three bays on the eastern Adriatic coast. Oceanologia 58 (4), 302—316, http://dx.doi.org/10.1016/j.oceano.2016.05.003.

Cai, P., Dai, M., Lv, D., Chen, W., 2006. An improvement in the small-volume technique for determining ^{234}Th in seawater. Mar. Chem. 100 (3—4), 282—288, http://dx.doi.org/10.1016/j.marchem.2005.10.016.

Cai, P., Chen, W., Dai, M., Wan, Z., Wang, D., Li, Q., Tang, T., Lv, D., 2008. A high-resolution study of particle export in the southern South China Sea based on ^{234}Th:^{238}U disequilibrium. J. Geophys. Res. 113, C04019, http://dx.doi.org/10.1029/2007JC004268.

Cai, P., Zhao, D., Wang, L., Huang, B., Dai, M., 2015. Role of particle stock and phytoplankton community structure in regulating particulate organic carbon export in a large marginal sea. J. Geophys. Res. 120 (3), 2063—2095, http://dx.doi.org/10.1002/2014JC010432.

Cao, Z., Frank, M., Dai, M., Grasse, P., Ehlert, C., 2012. Silicon isotope constraints on sources and utilization of silicic acid in the northern South China Sea. Geochim. Cosmochim. Acta 97, 88—104, http://dx.doi.org/10.1016/j.gca.2012.08.039.

Cao, L., Liu, S., Ren, J., 2013. Seasonal variations of particulate silicon in the Changjiang (Yangtze River) Estuary and its adjacent area. Acta Oceanol. Sin. 32 (4), 1—10.

Chen, M., Huang, Y., Cai, P., Guo, L., 2003. Particulate organic carbon export fluxes in the Canada Basin and Bering Sea as derived from ^{234}Th/^{238}U disequilibria. Arctic 56 (1), 32—44, http://dx.doi.org/10.14430/arctic600.

Coale, K.H., Bruland, K.W., 1985. ^{234}Th:^{238}U disequilibria within the California Current. Limnol. Oceanogr. 30 (1), 22—33, http://dx.doi.org/10.4319/lo.1985.30.1.0022.

Cochran, J.K., Barnes, C., Achman, D., Hirschberg, D.J., 1995. Thorium-234/Uranium-238 disequilibrium as an indicator of scavenging rates and particulate organic carbon fluxes in the Northeast Water Polynya, Greenland. J. Geophys. Res. 100 (C3), 4399—4410, http://dx.doi.org/10.1029/94JC01954.

Conley, D.J., Humborg, C., Smedberg, E., Rahm, L., Papush, L., Danielsson, Å., Clarke, A., Pastuszak, M., Aigars, J., Ciuffa, D., Mörth, C.-M., 2008. Past, present and future state of the biogeochemical Si cycle in the Baltic Sea. J. Mar. Syst. 73 (3—4), 338—346, http://dx.doi.org/10.1016/j.jmarsys.2007.10.016.

Danielsson, Å., Papush, L., Rahm, L., 2008. Alterations in nutrient limitations—Scenarios of a changing Baltic Sea. J. Mar. Syst. 73 (3—4), 263—283, http://dx.doi.org/10.1016/j.jmarsys.2007.10.015.

Dong, Y., Li, Q.P., Wu, Z., Zhang, J., 2016. Variability in sinking fluxes and composition of particle-bound phosphorus in the Xisha area of the northern South China Sea. Deep-Sea Res. Pt. I 118, 1—9, http://dx.doi.org/10.1016/j.dsr.2016.10.007.

Fang, Z., Yang, W., Chen, M., Zheng, M., Hu, W., 2016. Abundance and sinking of particulate black carbon in the western Arctic and Subarctic Oceans. Sci. Rep. 6, 29959, http://dx.doi.org/10.1038/srep29959.

Friedrich, J., Rutgers van der Loeff, M.M., 2002. A two-tracer (^{210}Po-^{234}Th) approach to distinguish organic carbon and biogenic silica export flux in the Antarctic Circumpolar Current. Deep-Sea Res. Pt. I 49 (1), 101—120, http://dx.doi.org/10.1016/S0967-0637(01)00045-0.

Guinder, V.A., López-Abbate, M.C., Berasategui, A.A., Negrin, V.L., Zapperi, G., Pratolongo, P.D., Severini, M.D.F., Popovich, C.A., 2015. Influence of the winter phytoplankton bloom on the settled material in a temperate shallow estuary. Oceanologia 57 (1), 50—60, http://dx.doi.org/10.1016/j.oceano.2014.10.002.

Han, W., Ma, K., 1991. Study on the process of sea water exchange in Daya Bay. Mar. Sci. 15 (2), 64—67, (in Chinese).

Huang, X., Guo, F., Huang, L., 2008. Researches on surface sediment environment in marine culture area of Daya Bay. J. Trop. Oceanogr. 27 (5), 37—42, (in Chinese).

Humborg, C., Pastuszak, M., Aigars, J., Sigmund, H., Mörth, C.-M., Ittekkot, V., 2006. Decreased silica land—sea fluxes through damming in the Baltic Sea catchment - significance of particle trapping and hydrological alterations. Biogeochemistry 77 (2), 265—281, http://dx.doi.org/10.1007/s10533-005-1533-3.

Krom, M.D., Kress, N., Fanning, K., 2014. Silica cycling in the ultra-oligotrophic eastern Mediterranean Sea. Biogeosciences 11 (3), 4211—4223, http://dx.doi.org/10.5194/bg-11-4211-2014.

Laruelle, G.G., Roubeix, V., Sferratore, A., Brodherr, B., Ciuffa, D., Conley, D.J., Dürr, H.H., Garnier, J., Lancelot, C., Le Thi Phuong, Q., Meunier, J.D., Meybeck, M., Michalopoulos, P., Moriceau, B., Ní Longphuirt, S., Loucaides, S., Papush, L., Presti, M., Ragueneau, O., Regnier, P., Saccone, L., Slomp, C.P., Spiteri, C., van Cappellen, P., 2009. Anthropogenic perturbations of the silicon cycle at the global scale: Key role of the land-ocean transition. Global Biogeochem. Cycl. 23 (4), GB4031, http://dx.doi.org/10.1029/2008GB003267.

Le Moigne, F.A.C., Henson, S.A., Sanders, R.J., Madsen, E., 2013. Global database of surface ocean particulate organic carbon export fluxes diagnosed from the ^{234}Th technique. Earth Syst. Sci. Data 5 (2), 295—304, http://dx.doi.org/10.5194/essd-5-295-2013.

Leblanc, K., Quéguiner, B., Fiala, M., Blain, S., Morvan, J., Coraisier, R., 2002. Particulate biogenic silica and carbon production rates and particulate matter distributioninthe Indiansector of the Subantarctic Ocean. Deep-Sea Res. II 49 (16), 3189—3206, http://dx.doi.org/10.1016/S0967-0645(02)00078-4.

Leynaert, A., Tréguer, P., Quéguiner, B., Morvan, J., 1991. The distribution of biogenic silica and the composition of particulate organic malter in the Wedell-Scotia Sea during spring 1988. Mar. Chem. 35 (1—4), 35—447, http://dx.doi.org/10.1016/S0304-4203(09)90035-4.

Li, H., Wiesner, M.G., Chen, J., Ling, Z., Zhang, J., Ran, L., 2017. Long-term variation of mesopelagic biogenic flux in the central South China Sea: Impact of monsoonal seasonality and mesoscale eddy. Deep-Sea Res. Pt. I 126, 62—72, http://dx.doi.org/10.1016/j.dsr.2017.05.012.

Lin, L., Wang, Y., Sun, C., Li, N., Wang, H., Mitchell, B.G., Wu, M., Song, H., Wu, J., 2011. Demonstration of a new indicator for studying upwelling in the northern South China Sea. Oceanologia 53, 605—622, http://dx.doi.org/10.5697/oc.53-2.605.

Liu, Y., Dai, M., Chen, W., Cao, Z., 2012. Distribution of biogenic silica in the upwelling zones in the south china sea. Adv. Geosci. 28, 55—65, http://dx.doi.org/10.1142/9789814405683_0005.

Loucaide, S., Cappelle, P.V., Behrends, T., 2008. Dissolution of biogenic silica from land to ocean: Role of salinity and pH. Limnol. Oceanogr. 53 (4), 1614—1621, http://dx.doi.org/10.4319/lo.2008.53.4.1614.

Ma, Q., Chen, M., Qiu, Y., Huang, Y., 2005. MnO_2 precipitation and direct beta counting technique for determining ^{234}Th in small-volume seawater. Acta Oceanol. Sin. 27 (4), 68—75, (in Chinese with English Abstract).

Mou, X., 2018. The isotopic composition of carbon and nitrogen in suspended particulate organic matter in the Daya Bay and the Jiaozhou Bay. (Master thesis). Xiamen University, 1—157, (in Chinese with English Abstract).

Mou, X., Chen, M., Zhang, K., Zeng, J., Yang, W., Zhang, R., Zheng, M., Qiu, Y., 2017. Stable carbon and nitrogen isotopes as tracers of sources of suspended particulate organic matter in the Daya Bay in summer. Acta Oceanol. Sin. 39 (2), 39–52, http://dx.doi.org/10.3969/j.issn.0253-4193.2017.02.004 (in Chinese).

Nelson, D.M., Smith, W.O., 1986. Phytoplankton bloom dynamics of the western Ross Sea ice edge II. Mesoscale cycling of nitrogen and silicon. Deep-Sea Res. 33, 1389–1412, http://dx.doi.org/10.1016/0198-0149(86)90042-7.

Nelson, D.M., Smith Jr., W.O., Muench, R.D., Gordon, L.I., Sullivan, C.W., Husby, D.M., 1989. Particulate matter and nutrient distributions in the ice-edge zone of the Weddell Sea: relationship to hydrography during late summer. Deep-Sea Res. 36 (2), 191–209, http://dx.doi.org/10.1016/0198-0149(89)90133-7.

Nelson, D.M., Tréguer, P., Brzezinski, M.A., Leynaert, A., Quéguiner, B., 1995. Production and dissolution of biogenic silica in the ocean: Revised global estimates, comparison with regional data and relationship to biogenic sedimentation. Global Biogeochem. Cycl. 9 (3), 359–372, http://dx.doi.org/10.1029/95GB01070.

Nelson, D.M., DeMaster, D.J., Dunbar, R.B., Smith Jr., W.O., 1996. Cycling of organic carbon and biogenic silica in the Southern Ocean: Estimates of water-column and sedimentary fluxes on the Ross Sea continental shelf. J. Geophys. Res. 101 (C8), 18519–18532, http://dx.doi.org/10.1029/96JC01573.

Owens, S.A., Buesseler, K.O., Sims, K.W.W., 2011. Re-evaluating the ^{238}U-salinity relationship in seawater: Implications for the ^{238}U–^{234}Th disequilibrium method. Mar. Chem. 127 (1–4), 31–39, http://dx.doi.org/10.1016/j.marchem.2011.07.005.

Pastuszak, M., Nagel, K., Grelowski, A., Mohrholz, V., Zalewski, M., 2003. Nutrient dynamics in the Pomeranian Bay (Southern Baltic): impact of the Oder River outflow. Estuaries 26 (5), 1238–1254.

Pastuszak, M., Conley, D.J., Humborg, C., Witek, Z., Sitek, S., 2008. Silicon dynamics in the Oder estuary, Baltic Sea. J. Mar. Syst. 73 (3–4), 250–262, http://dx.doi.org/10.1016/j.jmarsys.2007.10.013.

Qiu, Y., 2001. The characteristics of nutrients variation in the Daya Bay. Acta Oceanol. Sin. 23 (1), 85–93, (in Chinese with Eglish Abstract).

Ragueneau, O., Tréguer, P., Leynaert, A., Anderson, R.F., DeMaster, D.J., Dugdale, R.C., Dymond, J., Fischer, G., François, R., Heinze, C., Maier-Reimer, E., Martin-Jézéquel, V., Nelson, D.M., Quéguiner, B., 2000. A review of the Si cycle in the modern ocean: recent progress and missing gaps in the application of biogenic opal as a paleoproductivity proxy. Glob. Planet Change 26 (4), 317–365, http://dx.doi.org/10.1016/S0921-8181(00)00052-7.

Ragueneau, O., Savoye, N., Del Amo, Y., Cotton, J., Tardiveau, B., Leynaert, A., 2005. A new method for the measurement of biogenic silica in suspended matter of coastal waters: using Si:Al ratios to correct for the mineral interference. Cont. Shelf Res. 25 (5–6), 697–710, http://dx.doi.org/10.1016/j.csr.2004.09.017.

Roubeix, V., Becquevort, S., Lancelot, C., 2008. Influence of bacteria and salinity on diatom biogenic silica dissolution in estuarine systems. Biogeochemistry 88 (1), 47–62, http://dx.doi.org/10.1007/s10533-008-9193-8.

Rutgers van der Loeff, M.M., Buesseler, K.O., Bathmann, U., Hense, I., Andrews, J., 2002. Comparison of carbon and opal export rates between summer and spring bloom periods in the region of the Antarctic Polar Front, SE Atlantic. Deep Sea Res. II 49 (18), 3849–3869, http://dx.doi.org/10.1016/S0967-0645(02)00114-5.

Sánchez, G.E., Pantoja, S., Lange, C.B., González, H.E., Daneri, G., 2008. Seasonal changes in particulate biogenic and lithogenic silica in the upwelling system off Concepción (~36°S), Chile, and their relationship to fluctuations in marine productivity and continental input. Cont. Shelf Res. 28 (18), 2560–2594, http://dx.doi.org/10.1016/j.csr.2008.07.010.

Savoye, N., Benitez-Nelson, C.R., Burd, A., Cochran, J.K., Charette, M., Buesseler, K.O., Jackson, G.A., Roy-Barman, M., Schmidt, S., Elskens, M., 2006. ^{234}Th sorption and export models in the water column: a review. Mar. Chem. 100 (3–4), 234–249, http://dx.doi.org/10.1016/j.marchem.2005.10.014.

Shi, H., Cai, X., Song, Y., 2009. Simulation of wind fields and mean flow field of the North Part of South China Sea. In: Qiao, B. (Ed.), Conference Proceedings of Marine Pollution Prevention and Emergency Technology, vol. 2China Environmental Science Press, Beijing, pp. 242–250, (in Chinese).

Shiomoto, A., Ishii, H., 1995. Distribution of biogenic silica and particulate organic matter in coastal and oceanic surface waters off the South Shetland Islands in summer. Polar Biol. 15 (2), 105–113.

Song, X., Huang, L., Zhang, J., Huang, X., Zhang, J., Yin, J., Tan, Y., Liu, S., 2004. Variation of phytoplankton biomass and primary production in Daya Bay during spring and summer. Mar. Pollut. Bull. 49 (11–12), 1036–1044, http://dx.doi.org/10.1016/j.marpolbul.2004.07.008.

Sospedra, J., Niencheski, F.H., Falco, S., Andrade, C.F.F., Attisano, K. K., Rodilla, M., 2018. Identifying the main sources of silicate in coastal waters of the Southern Gulf of Valencia (Western Mediterranean Sea). Oceanologia 60 (1), 52–64, http://dx.doi.org/10.1016/j.oceano.2017.07.004.

Stramska, M., Bialogrodzka, J., 2016. Satellite observations of seasonal and regional variability of particulate organic carbon concentration in the Barents Sea. Oceanologia 58 (4), 249–263, http://dx.doi.org/10.1016/j.oceano.2016.04.004.

Sun, C., Wang, Y., Sun, S., Zhang, F., 2006. Analysis dynamics of phytoplankton community characteristics in Daya Bay. Acta Ecol. Sin. 26 (12), 3948–3958.

Tréguer, P., De La Rocha, C., 2013. The world ocean silica cycle. Annu. Rev. Mar. Sci. 5, 477–501, http://dx.doi.org/10.1146/annurev-marine-121211-172346.

Tréguer, P., van Bennekom, A.J., 1991. The annual production of biogenic silica in the Antarctic Ocean. Mar. Chem. 35 (1–4), 477–487, http://dx.doi.org/10.1016/S0304-4203(09)90038-X.

Tréguer, P., Nelson, D.M., Gueneley, S., Zeyons, C., Morvan, J., Buma, A., 1990. The distribution of biogenic and lithogenic silica and the composition of particulate organic matter in the Scotia Sea and the Drake Passage during autumn 1987. Deep-Sea Res. 37 (5), 833–851, http://dx.doi.org/10.1016/0198-0149(90)90009-K.

Tréguer, P., Nelson, D.M., van Bennekom, A.J., DeMaster, D.J., Leynaert, A., Quéguiner, B., 1995. The silica balance in the world ocean: a re-estimate. Science 268 (5209), 375–379, http://dx.doi.org/10.1126/science.268.5209.375.

Waite, A., Fisher, A., Thompson, P.A., Harrison, P.J., 1997. Sinking rate versus cell volume relationships illuminate sinking rate control mechanisms in marine diatoms. Mar. Ecol. Prog. Ser. 157, 97–108, http://dx.doi.org/10.3354/meps157097.

Wang, D., 2012. Distribution, export, and seasonal variation of biogenic silica in the northern South China Sea. Xiamen University, 1–80, (in Chinese with English Abstract).

Wang, B., 2018. Based on isotopes and geochemical indicators, rebuilding the source composition and productivity changes of sediments from the Daya Bay. (Master thesis). Xiamen University, 1–113, (in Chinese with English Abstract).

Wang, Z., Qi, Y., Li, J., Xu, N., Chen, J., 2004. Analysis and evaluation trophic status in aquaculture areas of Daya Bay. Mar. Environ. Sci. 23 (2), 25–28, (in Chinese with English Abstract).

Wang, Z., Chen, J., Xu, N., Qi, Y., 2005. Dynamics on cell densities of diatom, dinoflagellate and relationship with environmental factors in Aotou area, Daya Bay, South China Sea. Oceanol. Limnol. Sin. 36 (2), 186–192.

Wang, Z., Qi, Y., Chen, J., Xu, N., Yang, Y., 2006. Phytoplankton abundance, community structure and nutrients in cultural areas of Daya Bay, South China Sea. J. Mar. Syst. 62 (1–2), 85–94, http://dx.doi.org/10.1016/j.jmarsys.2006.04.008.

Wang, C., Lin, J., Chen, P., Zhang, S., 2008a. Numerical simulation on water exchange in Daya Bay, South China. Fisher. Sci. 4 (4), 8–15, (in Chinese).

Wang, Z., Lou, Z., Sun, C., Sun, S., 2008b. Ecological environment changes in Daya Bay, China, from 1982 to 2004. Mar. Poll. Bull. 56 (11), 1871—1879, http://dx.doi.org/10.1016/j.marpolbul.2008.07.017.

Wei, G., 2005. The long term variation of the nutrient structure in southwest Daya Bay. Ecol. Sci. 24 (1), 1—5, (in Chinese).

Wu, M., Wang, Y., 2007. Using chemometrics to evaluate anthropogenic effects in Daya Bay, China. Estuar. Coast. Shelf Sci. 72 (4), 732—742, http://dx.doi.org/10.1016/j.ecss.2006.11.032.

Wu, R., Cai, S., Wang, S., Zhang, W., 2007. Three-dimensional numerical simulation of tidal current and residual current at Daya Bay. J. Trop. Oceanogr. 26 (3), 18—23, (in Chinese).

Wu, M., Wang, Y.S., Wang, Y.T., Yin, J., Dong, J., Jiang, Z., Sun, F., 2017. Scenarios of nutrient alterations and responses of phytoplankton in a changing Daya Bay, South China Sea. J. Mar. Syst. 165, 1—12, http://dx.doi.org/10.1016/j.jmarsys.2016.09.004.

Yang, W., Huang, Y.P., Chen, M., Qiu, Y., Peng, A., Zhang, L., 2009. Export and remineralization of POM in the Southern Ocean and the South China Sea estimated from ^{210}Po/^{210}Pb disequilibria. Chinese Sci. Bull. 54, 2118—2123, http://dx.doi.org/10.1007/s11434-009-0043-4.

Yang, W., Chen, M., Zheng, M., He, Z., Zhang, X., Qiu, Y., Xu, W., Ma, L., Lin, Z., Hu, W., Zeng, J., 2015. Influence of a decaying cyclonic eddy on biogenic silica and particulate organic carbon in the tropical South China Sea based on ^{234}Th-^{238}U disequilibrium. PLoS ONE 10 (8), e0136948, http://dx.doi.org/10.1371/journal.pone.0136948.

Yang, W., Zhang, X., Chen, M., Qiu, Y., 2016. Unusually low ^{234}Th in a hydrothermal effluent plume over the Southwest Indian Ridge. Geochem. Geophys. Geosyst. 17 (9), 3815—3824, http://dx.doi.org/10.1002/2016GC006580.

Yang, W., Zhao, X., Zhang, F., Fang, Z., Ma, H., Chen, M., Qiu, Y., Zheng, M., 2018. Identification of the earlier human-induced sedimentation change in Daya Bay, northern South China Sea using ^{210}Pb and ^{137}Cs. Mar. Poll. Bull. 126, 334—337, http://dx.doi.org/10.1016/j.marpolbul.2017.11.025.

Yu, J., Tang, D., Wang, S., Lian, J., Wang, Y., 2007. Changes of water temperature and harmful algal bloom in the Daya Bay in the Northern South China Sea. Mar. Sci. Bull. 9 (2), 26—33.

Yucel, N., 2018. Spatio-temporal variability of the size-fractionated primary production and chlorophyll in the Levantine Basin (northeastern Mediterranean). Oceanologia 60 (3), 288—304, http://dx.doi.org/10.1016/j.oceano.2017.12.003.

Zheng, S., Li, L., Zeng, G., 1993. Probability distribution of current speed in Dapeng'ao. Daya Bay. J. Oceanogr. Taiwan Strait 12 (3), 242—247, (in Chinese with English Abstract).

Zheng, A., Shen, H., Liu, J., Li, W., Chen, Q., 2001. The mechanism of low nutrients high productivity in Daya Bay. Mar. Sci. 25 (11), 48—52, (in Chinese with English Abstract).

Oceanologia (2019) 61, 252–264

Available online at www.sciencedirect.com

ScienceDirect

journal homepage: www.journals.elsevier.com/oceanologia/

ORIGINAL RESEARCH ARTICLE

Erosion and deposition processes from field experiments of hydrodynamics in the coastal mangrove area of Can Gio, Vietnam

Hoa Tien Le Nguyen *, **Hong Phuoc Vo Luong**

Department of Oceanology, Meteorology and Hydrology, University of Science, Vietnam National University, Ho Chi Minh City, Vietnam

Received 16 August 2018; accepted 23 November 2018
Available online 1 December 2018

KEYWORDS
Hydrodynamics;
Suspended sediment concentrations (SSCs);
Erosion;
Mangrove forests;
Can Gio Mangrove Biosphere Reserve

Summary Studying hydrodynamic processes is necessary for understanding the sediment erosion–deposition mechanism in mangrove areas. The hydrodynamic effects within the mangrove area of the Dong Tranh Estuary in the Can Gio Mangrove Biosphere Reserve in Ho Chi Minh City (HCMC), Vietnam are very complicated and are caused by the mixed impacts of waves, tides, currents and suspended sediment concentrations (SSCs). In this study, the measurements of hydrodynamics such as waves, currents and SSCs were conducted in the dry (Feb. 2012) and wet (Jun. 2014) seasons. Three stations were set up within the estuary, mud-flat and mangrove forest. The analysed results showed that the hydrodynamics in all three stations were strongly influenced during the first dry monsoon season and the next wet one. The waves were the main factor during the dry season and contributed more SSC turbulence in the mud-flat, potentially causing erosion at the study site. Meanwhile, the current velocities in both the estuary and mud-flat sites were major factors during the wet season. In the mangrove forest, the SSC during the dry season changed due to the tidal cycle. Additionally, two measurements for the change in the topographies and shorelines were conducted from 2014 to 2017. The results show that the study site has been eroding rapidly (0.61 m month^{-1}). Although this study shows a soil retention role for the mangrove forests, the wave energy dissipation occurs mainly within the mud-flat due to the bottom topography. The study site is proven to be eroding.

* Corresponding author at: Vietnam National University, 227 Nguyen Van Cu Street, Ward 4, District 5, Ho Chi Minh City, Vietnam. Tel.: +84 916716013. Fax: +84 28 3835 8463.
E-mail addresses: lnhtien@hcmus.edu.vn (H.T. Le Nguyen), vlhphuoc@hcmus.edu.vn (H.P. Vo Luong).
Peer review under the responsibility of Institute of Oceanology of the Polish Academy of Sciences.

ELSEVIER Production and hosting by Elsevier

https://doi.org/10.1016/j.oceano.2018.11.004

1. Introduction

Mangrove forests occupy the entire intertidal zone along the tropical and subtropical coastlines, which play an important role in reducing coastal erosion. Mangroves often protect coastlines due to their ability to dissipate wave energy (Cao et al., 2016; Horstman et al., 2014; Massel et al., 1999; Parvathy and Bhaskaran, 2017; Vo-Luong and Massel, 2006). Many species of mangroves also have extensive cable root systems that assist in binding the sediment particles. In this way, mangrove-covered shorelines are less likely to erode or will erode more slowly than unvegetated shorelines during periods of high wave energy (Saenger, 2002). In addition, salt marshes or mangrove forest have value for coastal hazard mitigation and climate change adaptation with three specific ecosystem services: wave attenuation, shoreline stabilisation, and floodwater attenuation (Shepard et al., 2011).

There are various studies about the hydrodynamic processes in mangrove forests. Wolanski (1995) presented the principles of the processes that directly impact the sediment transport in mangrove forests, and, later, Furukawa and Wolanski (1996) described the structure, distribution and settling velocity of the agglutinate sediment. Bryce et al. (2003) studied the hydrodynamic and geomorphological controls on suspended sediment transport in mangrove creek systems with a case study in Cocoa Creek, Townsville, Australia. Capo et al. (2006) measured and analysed the surface sediment as well as the suspended sediment concentrations (SSCs) in the mangrove forest in Konkoure Estuary, Guine. Recently, from practical surveys and the application of two numerical models, FVCOM and ESSed, Li et al. (2014) showed the effects of the mangrove forests and intertidal areas on the dynamics of suspended sediment in the Darwin seaport, Australia.

In Vietnam, which has 270,000 hectares of mangrove forests (FAO, 2015), many hydrodynamic studies have been done. Mazda et al. (1997, 2006) showed that the mangrove forests can attenuate the wave energy in the Tong King Delta. Van Santen et al. (2007) studied a mangrove system in the Ba Lat Estuary of the Red River in the dry season (Feb./Mar. 2000) and in the wet season (Jul./Aug. 2000). The study demonstrated that the bare mud bank of an estuary is highly dynamic until the mangroves cover it. Although the sediment delivery to the vegetated zones is low, the protective effect of the vegetation against erosion by the waves and currents is high. Bao (2011) studied at two coastal mangrove forest areas in Vietnam, including the Red River Delta and Can Gio mangrove forests, and showed that the wave height decays exponentially with the distance from the mangrove front. Norris et al. (2017) examined the role of pneumatophores as a spatial control on the dissipation of the turbulent kinetic energy in the southern edge of Cu Lao Dung in the Mekong Delta. The turbulent dissipation reaches its maximum at the forest fringe, where pneumatophore densities are the highest. The dissipation depends on the tides, wave heights and water depths. High turbulent energy at the forest fringe may suspend fine sediments that can be redistributed elsewhere in the forest.

Can Gio was designated as the first Mangrove Biosphere Reserve in Vietnam under the Man and the Biosphere Programme of UNESCO in 2000 (Vo Quoc and Kuenzer, 2012). Can Gio is an ideal scientific research area. Mazda et al. (2002) determined the erosion mechanism of the coast of Long Hoa village. The first necessary condition is that the strong tidal flows move the bottom sediments along the coast of Long Hoa alongside the river mouths. The second condition is that the changes in the mangrove vegetation density due to human intervention have prevented the amplitude of the tidal flows from becoming steady. Therefore, the erosion is due to the tidal forces and not due to the wave action. Vo-Luong and Massel (2006, 2008) measured and studied the Nang Hai Creek at Dong Tranh Estuary for two years (2004 and 2005), mainly during the dry season. The results prove that the effect of the wave breaking plays an important role on the wave attenuation in a sparse forest. Waves are one of the primary factors that influence the sediment transport and cause coastal erosion, even though the wave fields are rather weak. However, the results are estimated and analysed only during the North East monsoon. Vo Luong (2012) used a “tracer stick” method and “coloured sample” method to measure the erosion and deposition of the surface sediment in Nang Hai Creek. The results showed that there is a clear occurrence of erosion–deposition processes, and the erosion process is dominant. In addition, the author applied a one-dimensional model to calculate the vertical SSCs. The results showed that SSCs at the bottom are much higher than those at the surface. The results also prove that SSCs depend on the wave intensity and tidal current velocity, thus concluding that the mangrove vegetation can encourage the deposition of sediment and protect the coastland from high waves and storms. Bay et al. (2012) suggested a mathematical model to simulate the sediment transport affected by the tides and winds in which the numerical results showed a trend of sediment accretion-erosion and concurred with the satellite observations. However, it is important to note that the model does not mention the mangrove forests and only simulates the sediment transport on the coastal zone of Can Gio. Vinh and Truong (2012) carried out a field investigation, GIS and numerical modelling (MIKE 21) to determine and analyse the erosion mechanism in the Nga Bay River and found that the actual erosion rate is approximately 10 m year^{-1}. The main factors found were currents, waves and ship-generated waves. However, the authors only studied the erosion mechanism in the riverbanks and river mouth. Recently, Schwarzer et al. (2016) studied the sediment dynamics in a mangrove forest on timescales from the spring-neap tidal cycles to the seasonal cycles (dry season versus wet season) to investigate the inter-tidal sediments forming the forest soil and the suspended matter dynamics in a creek that floods and discharges in the mangrove forest. The study was conducted in the Khe Nhan Creek, Rach Oc Creek and Nang Hai Creek in the Dong Tranh River.

Those studies showed that the mangrove forests in Can Gio are faced with high risks of erosion, especially in the Dong Tranh River and Nga Bay River Mouth. Hence, it is necessary to increase the research relevant to the dynamic factors for the coastal stabilisation and erosion mechanisms in mangrove forests.

Therefore, the aims of this study are to evaluate and explain the main hydrodynamics impact on erosion and deposition processes in mangrove areas. The measured and observed data of the hydrodynamics in mangrove areas, such as waves, currents, tides and SSCs, have been worked out in the Nang Hai site at Can Gio (HCMC) in the dry season (Feb. 2012) and the wet season (Jun. 2014). Furthermore, the study

measures and analyses the changes in the measured shorelines and topographies at the study site from 2014 to 2017.

2. Data collection

2.1. Study site

The field experiments for this study were done in the mangrove region in the Dong Tranh River (Fig. 1a). This region is a branch of the Saigon-Dong Nai River located in the HCMC, Vietnam (Hong and San, 1993). The study site was located between the Capes Ly Nhon and Long Hoa side of the estuary; therefore, it was less affected by the strong wind-induced waves (Vo-Luong and Massel, 2006). The tidal regime in Can Gio is an irregular semi-diurnal regime with an average tidal amplitude from 2 m (mean tide) to 4 m (spring tides) (Vo Quoc and Kuenzer, 2012).

The Nang Hai mangrove area was chosen as the study site and equipped with three stations: ST0 in the estuary (Fig. 1c), ST1 in the mud-flat and ST2 in the mangrove forest (Fig. 1b). Station ST1 and ST2 are approximately 2000 m apart from ST0. Station ST1 is approximately 30 m from ST2. The positions of the three stations were:

- Station in the estuary (ST0): 10°22′46.38″N; 106°51′57.12″E,
- Station in the mud-flat (ST1): 10°23′27.18″N; 106°52′48.12″E,
- Station in the mangrove forest (ST2): 10°23′27.43″N; 106°52′49.31″E.

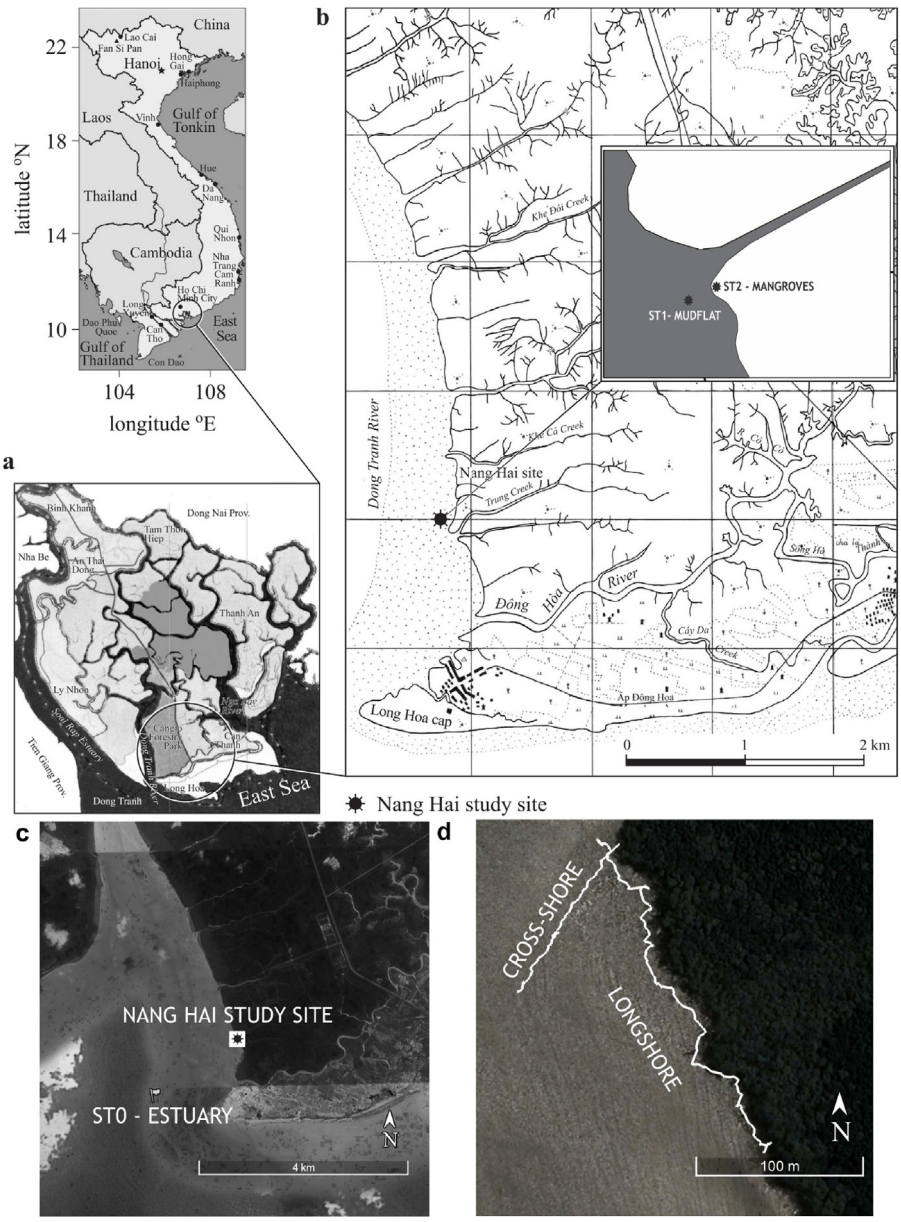

Figure 1 Location of the experimental area: (a) Vietnam and Can Gio Mangrove Biosphere Reserve, HCMC, Vietnam; (b) Nang Hai study site; (c) station ST0 in the estuary and (d) the measured cross-shore profile and measured longshore transect.

Table 1 The physical settings of the instruments at the study site.

Instruments	Measured factors	Physical settings
Valeport MIDAS DWR 27110	Water level	Sampling rate [Hz]: 4
	Current	Interval [mins]: 30
Valeport MIDAS DWR 27111	Turbidity [mV]	No. of samples: 2048
	Wave	
AEM-213D	Current	Interval [mins]: 60 No. of samples: 4800
INFINITY-Turbi ATU75W2	Turbidity [FTU]	Interval [mins]: 60 No. of samples: 4800
INFINITY-WH	Wave	Interval [mins]: 30 No. of samples: 4800

The field experiments were conducted during the dry season (Feb. 2012) and wet season (Jun. 2014), and every field campaign completed lasted for seven days. The primary measured factors were the water level depths, current velocities, wave heights and SSCs (from turbidity measurements). Additionally, the changes in the shorelines and topographies were measured from 2014 to 2017 (Fig. 1d).

2.2. Methods

2.2.1. Hydrodynamics

The measurements of the hydrodynamic factors were obtained by using various types of instruments: Valeport MIDAS DWR, AEM-213D, AEM-USB, INFINITY-Turbi ATU75W2 and INFINITY-WH (Table 1). The Valeport MIDAS DWR was fitted with sensors to measure the water level depths, current velocities, wave heights and SSCs (from turbidity measurements) (Fig. 2a). The instruments AEM-213D, INFINITY-Turbi ATU75W2 and INFINITY-WH had sensors levelled at 5 cm above the bottom bed (Fig. 2b). Table 2 shows the positions of the instruments at the study site in the dry and wet seasons.

2.2.2. Suspended sediment concentrations

To measure SSCs, the instruments required calibration. In the field experiments, the units of concentration in the instruments are mV (for Valeport MIDAS DWR) or FTU (for INFINITY-Turbi ATU75W2) (Fig. 2a and b). To convert the FTU/mV values into real concentrations, the water samples were required for calibration. The water samples were taken every 30—60 min within 24 h at all three stations. Then, the water samples were analysed in the laboratory (Fig. 2c).

2.2.3. Topography and shoreline changes

To analyse the changes of the topography and shoreline, data was collected in two ways (Fig. 1d):

- *Longshore changes*: the shoreline is considered to be the boundary between the mangroves and the mud-flat. The length of the measured boundary was 200 m (Fig. 1d). By using the GPS map 76CSx, data was collected along the mangrove boundary from 2014 to 2017. In total, four analyses were recorded on 20th Jan. 2014, 4th Feb. 2015, 17th Dec. 2016 and 25th May 2017. The data was processed by the DSAS tool (Digital Shoreline Analysis System) in ArcGIS 10.3.
- *Cross-shore changes*: the measured profile extended from the mangrove forests to the mud-flat and passed through the boundary. The measured length of the profile was approximately 120—140 m from the mangrove to the mud-flat in intervals of 1—2 m. Three referenced points were set up at the boundary, the mud-flat and the mangrove. The referenced point at the boundary was called the "zero point". The distance from the zero point to the mangrove is approximately 20—40 m. The distance from the zero point to the mud-flat is approximately 100 m. The SOKKIA level instrument was used eight times to measure on the dates: 20th Jan. 2014, 25th Jun. 2014, 26th Nov. 2014, 4th Feb. 2015, 19th Oct.

(a) Valeport at station ST1


(b) AEM, INFINITI Turbi and INFINITI WH at station ST2


(c) Water sample filtration in the laboratory

Figure 2 Measuring at the study site (a, b) and the water sample filtration in the laboratory (c).

Table 2 Observed time and positions of the instruments.

Stations	The dry season (Feb. 6th–13th, 2012)	The wet season (Jun. 20th–26th, 2014)
ST0	Valeport MIDAS DWR 27110 (Feb. 6th–9th, 2012)	Valeport MIDAS DWR 27111
ST1	Valeport MIDAS DWR 27111	- Valeport MIDAS DWR 27110 - AEM-213D
ST2	Valeport MIDAS DWR 27110 (Feb. 9th–13th, 2012)	- AEM-USB - INFINITY-Turbi ATU75W2 - INFINITY-WH

2015, 12th Jan. 2016, 18th Dec. 2016 and 25th May 2017. There were seven phases as follows:

- The first phase (20th Jan. 2014–25th Jun. 2014): dominant dry season,
- The second phase (25th Jun. 2014–26th Nov. 2014): dominant wet season,
- The third phase (26th Nov. 2014–4th Feb. 2015): dry season,
- The fourth phase (4th Feb. 2015–19th Oct. 2015): dominant wet season,
- The fifth phase (19th Oct. 2015–12th Jan. 2016): dominant dry season,
- The sixth phase (12th Jan. 2016–18th Dec. 2016): both seasons,
- The seventh phase (Dec. 2016–25th May 2017): dominant dry season.

2.3. Calibration results

From the data analysed in the laboratory and the field experiments, there were a total of five results for the correlation between the analysed SSCs and the recorded output from the instrument sensors (D&A Ins Co., 2004). Fig. 3 is an example for the calibration result at station ST0 in the estuary. All results show that the value of *R*-squared is between 63% and 91%. The calibration results are highly reliable. The regression equations of every station are as follows:

In the dry season (Feb. 2012):

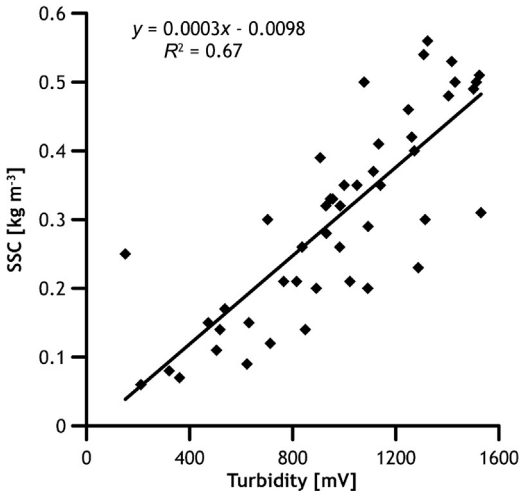

Figure 3 An example of the calibration results of Valeport MIDAS DWR at station ST0 in the estuary.

- ST0 and ST2: $y = 0.0074x + 0.0069$; $R^2 = 0.90$
- ST1: $y = 0.0003x + 0.0174$; $R^2 = 0.91$

In the wet season (Jun. 2014):

- ST0: $y = 0.0003x - 0.0098$; $R^2 = 0.67$
- ST1: $y = 0.0025x + 0.0509$; $R^2 = 0.73$
- ST2: $y = 0.0001x$; $R^2 = 0.63$

where y: SSC – [kg m^{-3}], x: record output – [mV] or [FTU].

3. Results

3.1. In the estuary

In the estuary (ST0), the tidal ranges during both seasons were found to be approximately the same (3.30 m in the dry season (Fig. 4a) and 3.20 m in the wet season (Fig. 4d)), while the current velocity data showed minor changes and a small variance between the seasons (0.19 m s^{-1} in the dry season (Fig. 4b) and 0.15 m s^{-1} in the wet season (Fig. 4e)). However, the significant wave heights in the dry season (Fig. 4c) were much higher than the ones in the wet season (Fig. 4f), as they were recorded to reach up to 0.55 m in the dry season but only approximately 0.24 m in the wet season. Consequently, the average SSCs in the dry season (0.15 kg m^{-3} – Fig. 4a) were higher than in the wet season (0.10 kg m^{-3} – Fig. 4d).

The results show that during the dry season, the SSCs were affected by the water level fluctuations, current velocities and significant wave heights (Fig. 4a–c). On the two first tidal days, the waves were weak (Fig. 4c) but the current velocities (Fig. 4b) and the SSCs (Fig. 4a) were high. Especially during the third tidal day, the SSC reached its highest values because the significant wave heights and the current velocities values reached their recorded peaks. Therefore, the waves had a strong impact on the variability of SSCs at station ST0 during the dry season. In contrast, during the wet season, the relationship between SSCs and waves was weaker than the relationship between SSCs and current velocities. With the increase of the current velocities, the SSCs also increased; hence, in the wet season, SSCs are mainly controlled by the currents. In general, any changes in the hydrodynamics will have a direct influence on SSCs in both the dry and wet seasons.

3.2. In the mud-flat

In the mud-flat (ST1), the results show that the water levels in the dry season (Fig. 5a) are higher than the ones in the wet season (Fig. 5d). The maximum water level was 2.26 m in the

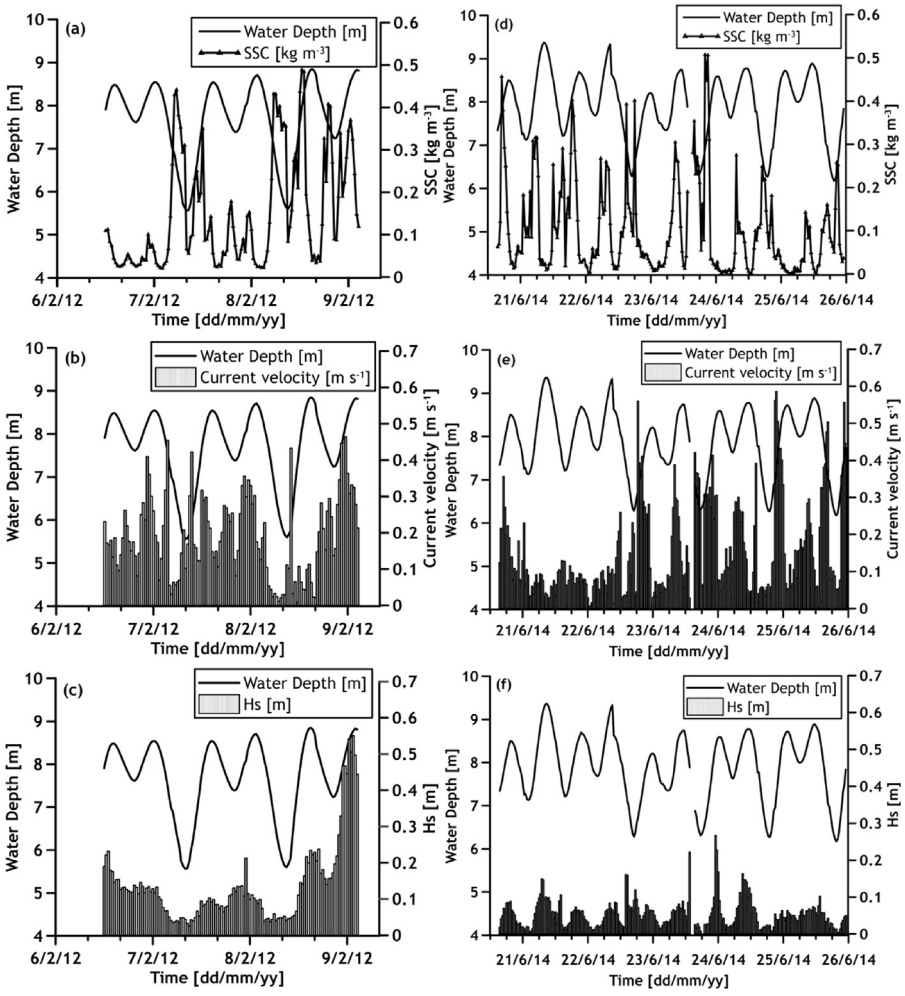

Figure 4 Water depths, SSCs, current velocities, and significant wave heights (Hs) in the estuary (ST0) in the dry season (a—c) and in the wet season (d—f).

dry season and 1.68 m in the wet season. However, the current velocities in both seasons were low, recording only 0.12 m s^{-1} as its maximum. The results show that the flood current velocities were higher than the ebb current velocities. Tidal asymmetry occurred mainly during the dry season and was not obvious in the wet season (Fig. 5b and e). The significant wave heights in the dry season were approximately 0.11 m on average (Fig. 5c), which were much higher than the ones in the wet season (only 0.04 m on average (Fig. 5f)). The low water depth during the wet season can be considered as one of the main reasons for the small wave heights due to the wave energy dissipation. In addition, the significant wave heights in the wet season were not high in the estuary; hence, the significant wave heights in the mud-flat were not high.

The relationship between the current velocities and significant wave heights was complicated. In the dry season, on the two first tidal days (10:30 AM 6th Feb. 2012—10:00 AM 8th Feb. 2012), the significant wave heights were not high (approximately 0.07 m on average — Fig. 5c) whereas on the other tidal days (10:30 AM 8th Feb. 2012—7:00 AM 12th Feb. 2012), the significant wave heights were higher (approximately 0.15 m on average — Fig. 5c). Meanwhile, the current velocities were similar during the time measured (Fig. 5b). However, the peak of the wave and the peak of the current velocity occurred at the same time (Fig. 5b and c). Within the wet season, on the fifth tidal day (09:00 PM 24th Jun. 2014—12:00 PM 25th Jun. 2014), the significant wave heights were weak (Fig. 5f) but the current velocities were strong (Fig. 5e). The current velocities were similar during the time measured and higher at the flood tide. This proves that the current velocities were affected strongly by the tides.

Fig. 5a and d shows that the SSCs in the dry and wet seasons were similar (approximately 0.11 kg m^{-3} on average), but the fluctuation of SSCs in the dry season was stronger than the one in the wet season. In particular, at 01:00 AM 10th Feb. 2012, the peak SSC in the dry season reached 0.59 kg m^{-3}, and the peak SSC coincided with the maximum current velocity and high significant wave height (Fig. 5a). However, the anomalous value was quite different from the surrounding values.

In the dry season, the significant wave heights can reach up to 0.36 m (Fig. 5c). Under strong waves, from 8th Feb. 2012 to 12th Feb. 2012, the average SSC was 0.13 kg m^{-3}, while under weak waves, from 6th Feb. 2012 to 7th Feb. 2012, the average SSC was 0.06 kg m^{-3} (Fig. 5a and c). It can be shown that the SSCs during the high waves are more than twice as high as the SSCs during the small waves, which is similar to the results in the wet season. It can be explained

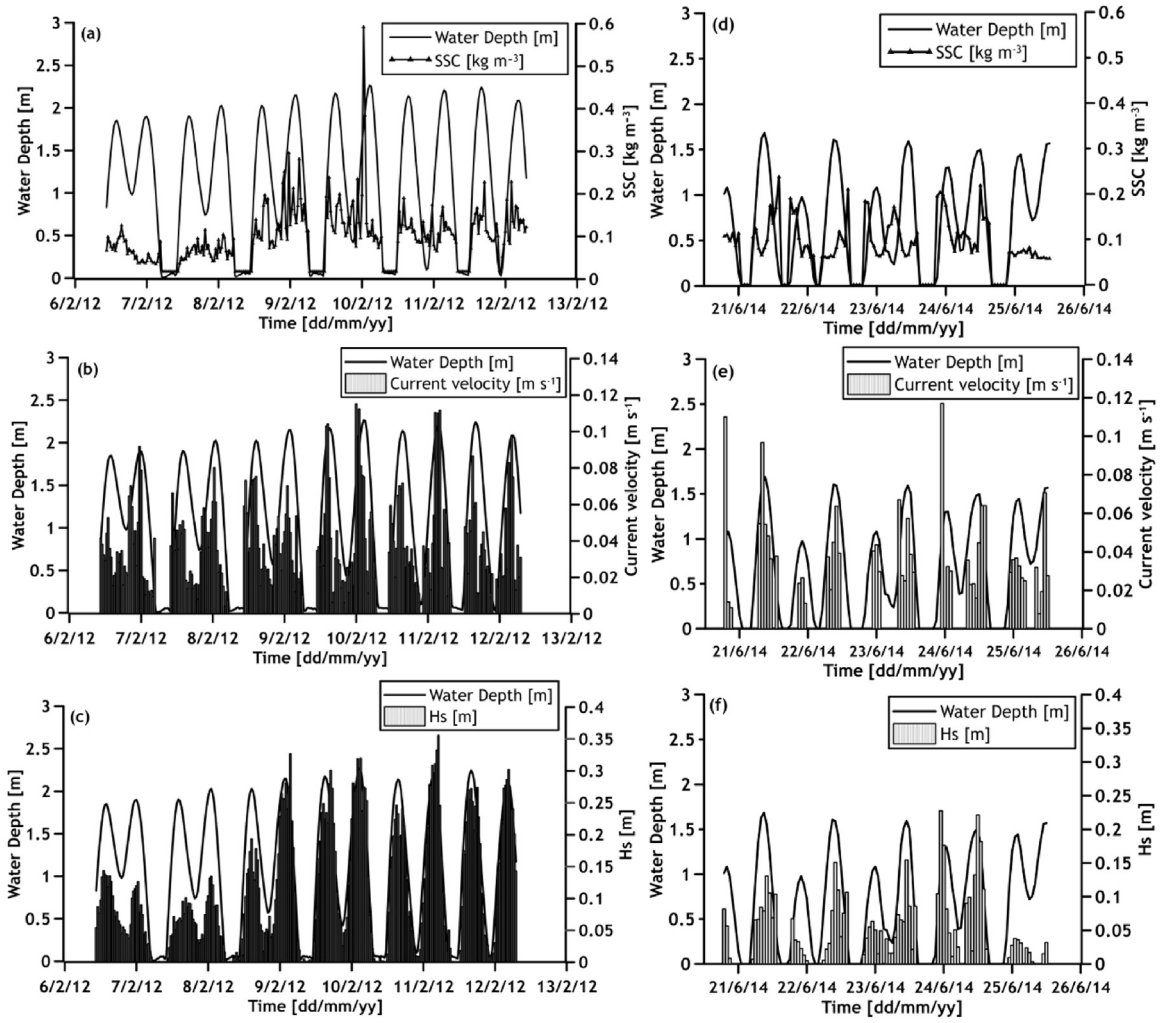

Figure 5 Water depths, SSCs, current velocities, and significant wave heights (Hs) in the mud flat (ST1) in the dry season (a–c) and the wet season (d–f).

that the high waves can pump up the suspended matters from the bottom and cause a higher turbulence.

The amount of SSC input or output to the mud-flat during the tidal cycles are different in both the dry and wet seasons. The deposition trend will occur when the SSCs during the flood tide are higher than during the ebb tide. In the opposite case, an erosion trend will occur. Fig. 5a shows that, in the dry season, the deposition trend was higher than the erosion trend. However, the deposition and erosion trends in the wet season were not clear (Fig. 5d). This may be due to the hydrodynamics of the waves and currents in the dry season being stronger than the ones in the wet season. In general, the deposition trend could be considered to be the main trend in the mud-flat for both seasons. The current velocity could be the main factor controlling the SSC distribution.

3.3. In the mangrove forest

Fig. 6 shows the bathymetry from the mud-flat to the mangrove forest on 25th Jun. 2014. There was a large difference (approximately 1.2 m) between the mud-flat station ST1 and the mangrove forest station ST2, hence the water levels in the mangrove forest (ST2) were found to be low. The highest water level reached approximately 0.93 m in the dry season (Fig. 7a) and only 0.27 m in the wet season (Fig. 7d). Because the water level depths in the wet season were too low, the significant wave heights and the current velocities were small; hence, the impact of the hydrodynamics on SSCs could not be shown effectively (Fig. 7d–f). Therefore, only the hydrodynamics in the dry season can be considered in this section.

In the dry season, the significant wave heights and current velocities were also low. The maximum current velocity was found to be approximately 0.07 m s^{-1} (Fig. 7b) and the maximum significant wave height was approximately 0.36 m (Fig. 7c). The peak current velocities almost occurred at high slack water.

In the mangrove forest, the current velocities during the flood tide were higher than the ones during the ebb tide (Fig. 7b). Consequently, the average SSCs during the flood tide were higher than during the ebb tide (Fig. 7a). The SSCs changed in accordance with the current velocities. It proves that the current velocity played a more dominant role on the SSCs within the mangroves (ST2), especially when the water levels were low enough.

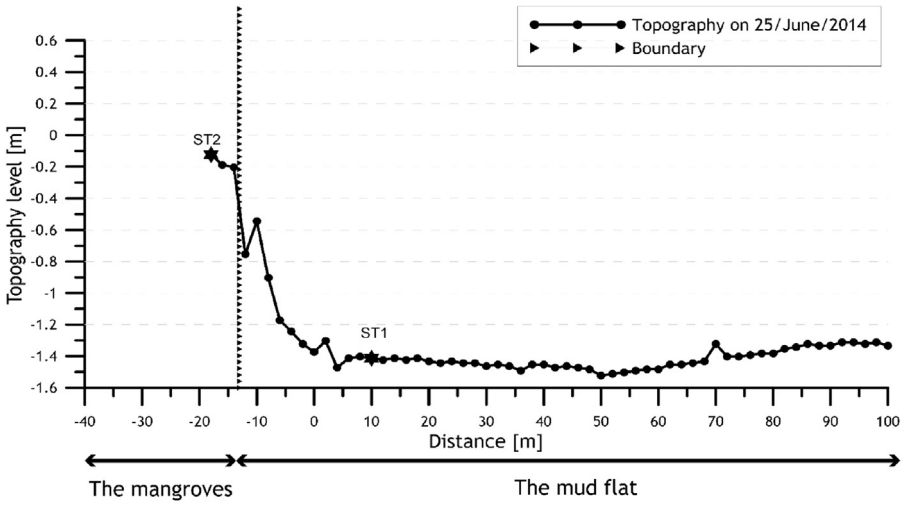

Figure 6 Topography at study site on 25th Jun. 2014.

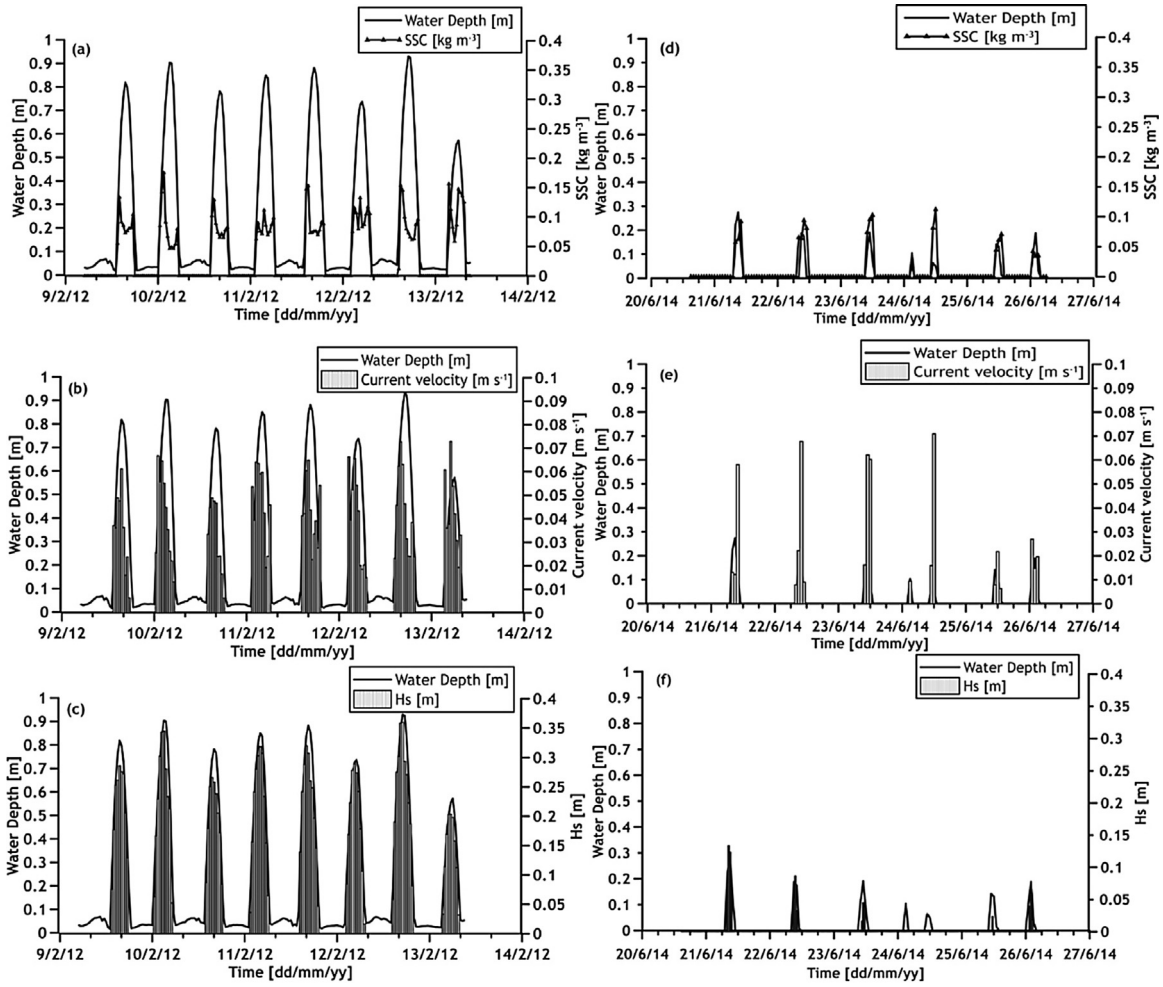

Figure 7 Water depths, SSCs, current velocities, and significant wave heights (Hs) in the mangroves (ST2) in the dry season (a—c) and the wet season (d—f).

Table 3 Calculated suspended sediment rate Q during the flood tides, ebb tides and total Q on one tidal day.

Cases	Station ST2 – in the mangrove forest		
Q [kg m^{-1} s^{-1}]	Q_{flood}	Q_{ebb}	Q_{tol}
Case I: strong waves (H_s average = 0.24 m)	$+22 \times 10^{-3}$	-6×10^{-3}	$+16 \times 10^{-3}$
Case II: weak waves (H_s average = 0.14 m)	$+12 \times 10^{-3}$	-4×10^{-3}	$+8 \times 10^{-3}$

Note: "+": the seaward of Q, "–": the landward of Q.

To illustrate the role of the mangrove forest in the accumulation during the dry season, the sediment transport rate Q (the suspended sediment transport per unit width) during the incoming tides and outgoing tides in one tidal period was calculated in Eq. (1) (Mehta and Li, 2003).

$$Q = \int_0^h U_{tol}(z)C(z)dz, \quad (1)$$

in which $C(z)$ is the vertical variation of the SSCs. $U_{tol}(z)$ is the total velocities in the water column due to the tidal currents and wave-induced velocity in Eq. (2).

$$U_{tol} = U_{tide} + U_{wave}. \quad (2)$$

It is found that the tidal currents are positive on the flood tide and negative on the ebb tide. Therefore, the value of the vertical sediment transport rate Q at the observed point will be positive for the tidal flow to the forest and negative for the tidal ebb to the ocean.

For practical applications, $U_{tol}(z)$ could be used as the mean total velocity due to the tides and waves. Because the water level depths in the mangrove were so low, the tidal currents and wave-induced velocities could be considered vertically uniform. $U_{tol}(z)$ and $C(z)$ were based on the field experimental data at ST2.

The suspended sediment rate on one tidal day was calculated in two cases: strong waves (from 2:30 PM to 7:30 PM 12th Feb. 2012) and weak waves (from 3:30 AM to 7:30 AM 13th Feb. 2012). The calculated results at the study site are shown in Table 3.

For both cases of strong and weak waves, the suspended sediment rates at the flood tide were three times higher as the ones at the ebb tide. Therefore, the total suspended sediment rate Q_{tol} resulted in positive values. The total Q_{tol} under the strong waves was more than twice as high as the total Q_{tol} under the weak waves. This result indicates that the strong hydrodynamics caused high turbulence; therefore, the vertical suspended sediment rate Q_{tol} achieved high values as well. In addition, for the tidal flow to the mangrove forests, the vertical suspended sediment rate Q_{tol} had positive values.

In general, the mangrove SSCs were mainly affected by the currents. In addition, the SSCs during the flood tides were higher during the ebb tides. This proves the role of the mangrove forests in accumulation in the coastal area.

3.4. Topography and shoreline change

Fig. 8 shows how the topography at Nang Hai changed over three years (from 20th Jan. 2014 to 25th May 2017). The boundary between the mud-flat and the mangrove forest was being eroded rapidly. In one year (from Jan. 2014 to Feb. 2015), the mangrove boundary was shifted approximately 5 m inwards. In three years (from Jan. 2014 to May 2017), the boundary was shifted inwards approximately 25 m. Hence, the displacement rate was calculated at approximately 0.61 m month^{-1} in 41 months (Jan. 2014–May 2017). Although the boundary between the mangrove and mud-flat had been eroded, the bathymetry in the mud-flat had accumulated during the measured time. In general, the range of the average depth deposition reached up to 0.40 m, but the

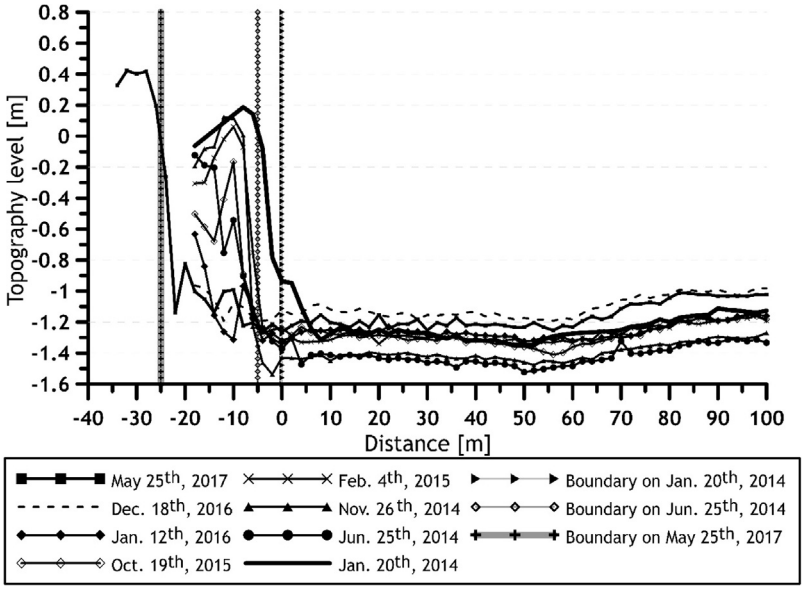

Figure 8 Changes in the topography at the study site from 2014 to 2017.

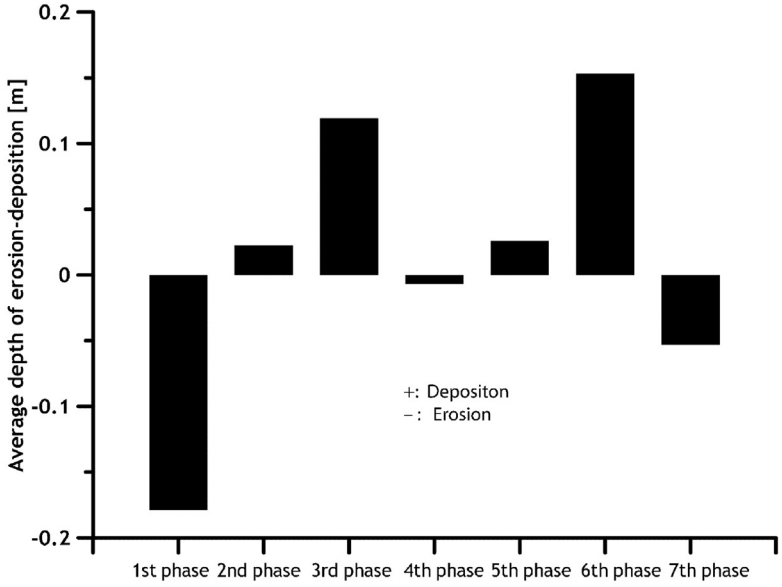

■The mud flat	-0.18	0.02	0.12	-0.01	0.03	0.15	-0.05
Dominance	Dry season	Wet season	Dry season	Wet season	Dry season	Both season	Dry season

Figure 9 The erosion—deposition process from 2014 to 2017 in the mud flats (ST1).

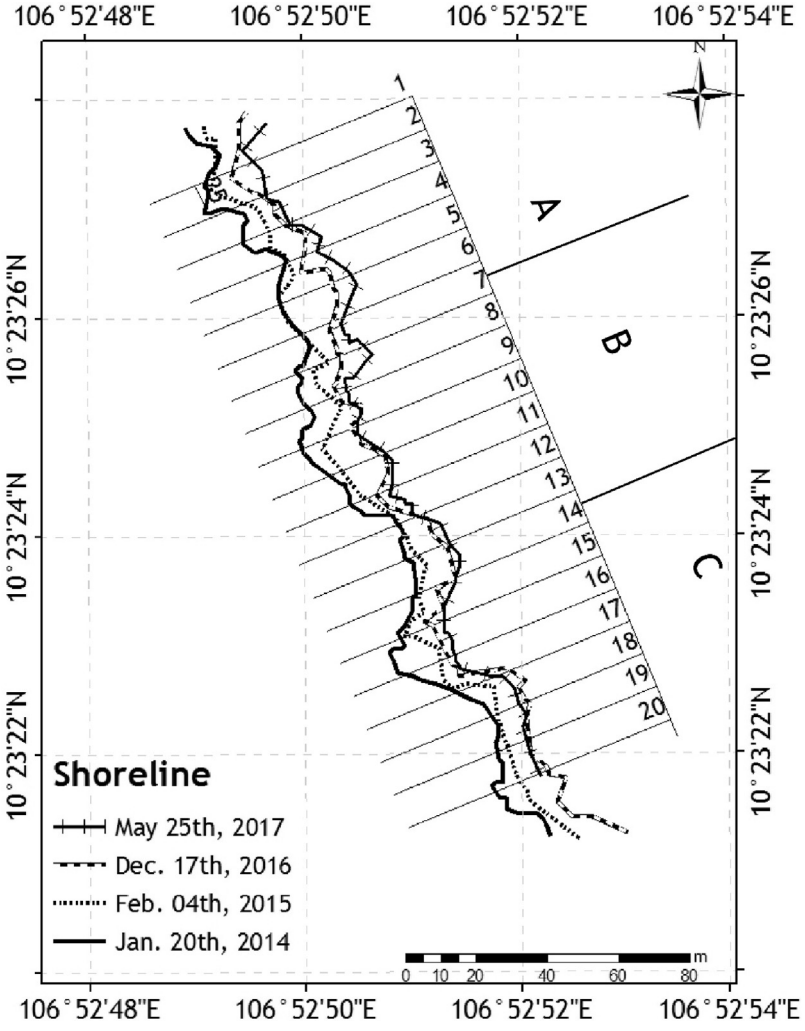

Figure 10 Measured shoreline changes from 2014 to 2017.

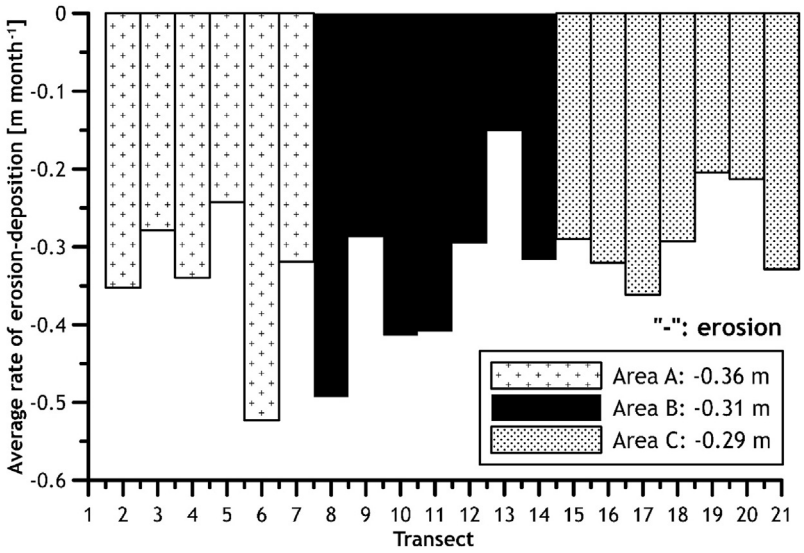

Figure 11 The average rate of erosion at the study site from 2014 to 2017.

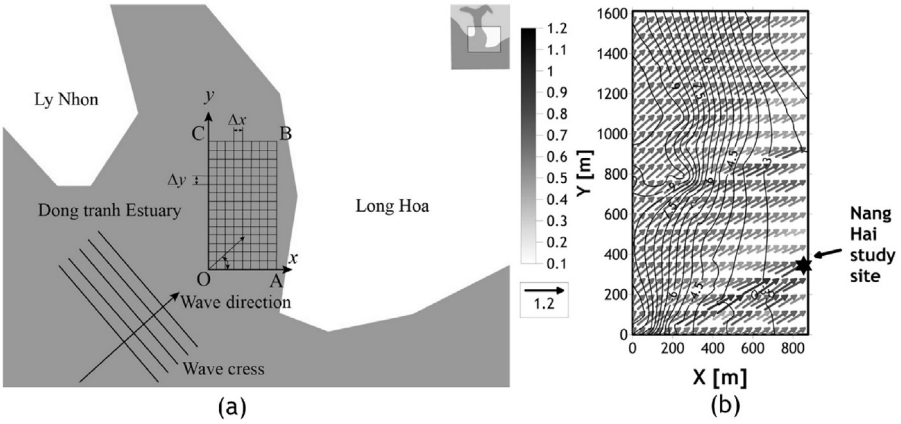

Figure 12 Calculated results at the Dong Tranh Estuary (Vo Luong et al., 2008): (a) the calculated area and (b) the result of the wave fields.

deposition and erosion processes occurred alternately. The measured SSC results at ST1 (Section 3.2) also proved that deposition occurred within the mud-flat. In the 1st, 3rd and 7th phases, the erosion process occurred, while the deposition process occurred in the 2nd, 4th, 5th and 6th phases. The deposition in the mud-flat could be explained by two reasons. First, the flood tides were strong enough to bring sediment into the mud-flat (Section 3.2). Second, the erosion at the boundary may contribute to the settlement of the sediment in the mud-flat. Fig. 9 shows that the difference in the sediment in the dry season was higher than that in the wet season. In the dry season, the average depth erosion reached up to 0.18 m in the first phase and to an average depth deposition of 0.12 m in the third phase. Meanwhile, in the wet season, the average depth erosion was 0.01 m in the 4th phase, while the average depth deposition was only 0.02 m in the 2nd phase.

Fig. 10 shows the observation of the mangrove shoreline changes by using GPS from 20th Jan. 2014 to 25th May 2017. In general, the entire shoreline used as the study site has been eroded. The shoreline was divided into three areas (A, B and C), and the Nang Hai site was situated in area A where the strongest erosion process occurred. The degradation rate was calculated as approximately 0.36 m month^{-1} in area A (Fig. 11). The results could be shown to be aligned with the results from the topography methods by using levelling instruments. However, the calculated rate of the cross-shore changes by topography was higher (0.61 m month^{-1}). There were many possible causes, such as error from GPS instrument; error within the measurement recorded, or error from the calculation in ArcGIS (DSAS tool), etc. Moreover, by using the wave refraction model, Vo Luong et al. (2008) proved that the Nang Hai study site was affected strongly by the wave fields (Fig. 12). In summary, the higher the wave heights were, the stronger the erosion–deposition processes.

However, the causes of erosion at the study site were not only due to the hydrodynamics but also due to human activities. Previous studies, such as Mazda et al. (2002) and Vinh and Truong (2012), showed that human intervention also affected the erosion mechanism in the Nga Bay River, which is not far from the study site. In recent years, Tin and Vinh (2013) showed that sand extraction between the Dong Tranh

Gulf and Ganh Ray Gulf affected the erosion—deposition processes significantly. These activities may impact the sediment mechanism, causing the erosion—deposition processes at the study site.

4. Conclusions

The observations and measurements from the mangrove areas of the Dong Tranh Estuary, Vietnam, showed strong relationships between the hydrodynamic processes and suspended sediment dynamics. In the estuary, the SSCs were very complicated due to the mixed impacts of the waves and currents in both seasons. The waves had a strong impact on the variability of the SSCs in the dry season. In the mud-flat, the current velocities were the main factor that dictated SSC distribution. In the mangrove forest, the SSCs were influenced strongly by the currents in the dry season and had a strong tidal asymmetry. Addtionally, most of the measured results showed that the hydrodynamics in the dry season were stronger than the ones in the wet season. Hence, the hydrodynamics in the mangrove areas were influenced strongly by monsoons.

The results of the shoreline and topography changes show that in the mud-flat, the erosion and deposition processes occurred alternately, and that the deposition was more dominant than the erosion. The erosion—deposition intensity in the dry monsoon was stronger than the one in the wet monsoon. In the mangrove forest, the erosion process always occurred, especially at the sloping mangrove edge, where the erosion was at its strongest. The measured results showed that the hydrodynamics in the mangroves were weak; meanwhile, the hydrodynamics in front of the mangrove edge were strong. Thus, the hydrodynamics can be considered one of the causes of erosion in the mangrove edge.

In conclusion, similar to previous studies, this study is concurrent with a soil retention role for mangrove forests. However, the study site is being eroded. It is noticeable that the wave energy dissipation in the mangrove was not large, and that the wave energy dissipation occurred in the mud-flat due to the bottom topography. Human activity was not considered in the study. Addtionally, the measured time in the study was not long enough and only occurred in the El Nino period (Nov. 2014—Apr. 2016). Hence, it is necessary to conduct future work for a longer term to determine the factors affecting the erosion—deposition processes at the study site.

Acknowledgements

This work was supported by the NAFOSTED (grant numbers: ĐT. NCCB-ĐHU'D.2012-G/10). We would like to express our great gratitude to late Professor Stanisław Massel for the invaluable advice.

References

Bao, T.Q., 2011. Effect of mangrove forest structures on wave attenuation in coastal Vietnam. Oceanologia 53 (3), 807—818, http://dx.doi.org/10.5697/oc.53-3.807.

Bay, N.T., Toan, T.T., Phung, N.K., Tri, N.Q., 2012. Numerical investigation on the sediment transport trend of can Gio Coastal Area (Southern Vietnam). J. Mar. Environ. Eng. 9 (3), 191—210.

Bryce, S., Larcombe, P., Ridd, P.V., 2003. Hydrodynamic and geomorphological controls on suspended sediment transport in mangrove creek systems, a case of study: Cocoa Creek, Townsville, Australia. Estuar. Coast. Shelf Sci. 56 (3—4), 415—531, http://dx.doi.org/10.1016/S0272-7714(02)00192-0.

Cao, H., Chen, Y., Tian, Y., Feng, W., 2016. Field investigation into wave attenuation in the mangrove environment of the South China Sea Coast. J. Coastal Res. 32 (6), 1417—1427, http://dx.doi.org/10.2112/JCOASTRES-D-15-00124.1.

Capo, S., Sottolichio, A., Brenon, I., Castaing, P., Ferry, L., 2006. Morphology, hydrography and sediment dynamics in a mangrove estuary: the Konkoure Estuary, Guinea. Mar. Geol. 230 (3—4), 199—215, http://dx.doi.org/10.1016/j.margeo.2006.05.003.

FAO, 2015. Global Forest Resources Assessment 2015. Food and Agriculture Organization of the United Nations, 244 pp.

Furukawa, K., Wolanski, E., 1996. Sedimentation in mangrove forest. Mang. Salt Marsh. 1 (1), 3—10.

Hong, P.N., San, H.T., 1993. Mangroves of Vietnam. IUCN—The World Conservation Union, Bangkok, Thailand, 173 pp.

Horstman, E.M., Dohmen-Janssen, C.M., Narra, P.M.F., van den Berg, N.J.F., Siemerink, M., Hulscher, S.J.M.H., 2014. Wave attenuation in mangroves: a quantitative approach to field observations. Coast. Eng. 94, 47—62, http://dx.doi.org/10.1016/j.coastaleng.2014.08.005.

Li, L., Wang, X.H., Andutta, F., Williams, D., 2014. Effects of mangroves and tidal flats on suspended-sediment dynamics: Observation and numerical study of Darwin Harbour, Australia. J. Geophys. Res.-Oceans 119 (9), 5854—5873, http://dx.doi.org/10.1002/2014JC009987.

Massel, S.R., Furukawa, K., Brinkman, R.M., 1999. Surface wave propagation in mangrove forests. Fluid Dyn. Res. 24 (4), 219—249, http://dx.doi.org/10.1016/S0169-5983(98)00024-0.

Mazda, Y., Magi, M., Kogo, M., Hong, P.N., 1997. Mangroves as a coastal protection from waves in the Tong King Delta, Vietnam. Mang. Salt Marsh. 1 (2), 127—135.

Mazda, Y., Magi, M., Nanao, H., Kogo, M., Miyagi, T., Kanazawa, N., Kobashi, D., 2002. Coastal erosion due to long-term human impact on mangrove forests. Wetl. Ecol. Manag. 10 (1), 1—9, http://dx.doi.org/10.1023/A:1014343017416.

Mazda, Y., Magi, M., Ikeda, Y., Kurokawa, T., Asano, T., 2006. Wave reduction in a mangrove forest dominated by *Sonneratia* sp. Wetl. Ecol. Manag. 14 (4), 365—378, http://dx.doi.org/10.1007/s11273-005-5388-0.

Mehta, A., Li, Y., 2003. Principles and Process — Modelling of Cohesive Sediment Transport. University of Florida, 86 pp.

Norris, B.K., Mullarney, J.C., Bryan, K.R., Henderson, S.M., 2017. The effect of pneumatophore density on turbulence: a field study in a Sonneratia-dominated mangrove forest, Vietnam. Cont. Shelf Res. 147, 114—127, http://dx.doi.org/10.1016/j.csr.2017.06.002.

Parvathy, K.G., Bhaskaran, P.K., 2017. Attenuation in presence of mangrove: a sensitivity study for varying bottom slopes. Int. J. Ocean Climate Syst. 8 (3), 126—134, http://dx.doi.org/10.1177/1759313117702919.

Phuoc, V.L.H., 2012. Concentration of suspended sediments in mangrove forests (Nang Hai study site, Ho Chi Minh city). Scientific research project of Viet Nam National University — Ho Chi Minh city (in Vietnamese).

Saenger, P., 2002. Mangrove Ecology, Silviculture and Conservation. Kluwer Academic Publishers, Netherlands, 360 pp.

Schwarzer, K., Thanh, N.C., Ricklefs, K., 2016. Sediment re-deposition in the mangrove environment of Can Gio, Sai Gon River estuary (Vietnam). J. Coastal Res. 75 (Sp. Iss.), 138—142, http://dx.doi.org/10.2112/SI75-028.1.

Shepard, C.C., Crain, C.M., Beck, M.W., 2011. The protective role of coastal marshes: a systematic review and Meta-analysis. PLoS ONE 6 (11), e27374, http://dx.doi.org/10.1371/journal.pone.0027374.

Tin, H.T., Vinh, B.T., 2013. Exploitation, evaluation of reserve and environmental impact assessment of the sand extraction in Can Gio coastal zone. Kick-off Seminar on ASEAN-Japan Build-up Cooperative Education Program for Global Human Resource Development in Earth Resources Engineering. Bangkok, Thailand.

Van Santen, P., Augustinus, P.G.E.F., Janssen-Stelder, B.M., Quartel, S., Tri, N.H., 2007. Sedimentation in an estuarine mangrove system. J. Asian Earth Sci. 29 (4), 566—575, http://dx.doi.org/10.1016/j.jseaes.2006.05.011.

Vinh, B.T., Truong, N.H., 2012. Erosion mechanism of Nga Bay Riverbanks (Ho Chi Minh City, Vietnam). ASEAN Eng. J. C 3 (2), 132—141.

Vo Luong, H.P., Toan, N.D., An, D.T., Hanh, T.C., 2008. Computation of wave field in the Dong Tranh estuary, can Gio by using wave refraction model. J. Geol. Ser. B 31—32, 164—170.

Vo Quoc, T., Kuenzer, C., 2012. Can Gio Mangrove Biosphere Reserve Evaluation 2012: Current Status, Dynamics and Ecosystem Services. IUCN, Ha Noi, Vietnam, 100 pp.

Vo-Luong, H.P., Massel, S.R., 2006. Experiment on wave motion and suspended sediment concentration at Nang Hai, Can Gio mangrove forest, Southern Viet Nam. Oceanologia 48 (1), 23—40.

Vo-Luong, H.P., Massel, S.R., 2008. Energy dissipation in non-uniform mangrove forests of arbitrary depth. J. Mar. Syst. 74 (1—2), 603—622, http://dx.doi.org/10.1016/j.jmarsys.2008.05.004.

Wolanski, E., 1995. Transport of Sediment in mangrove swamps. Hydrobiologia 295 (1—3), 31—42.

Oceanologia (2019) 61, 265—275

Available online at www.sciencedirect.com

ScienceDirect

journal homepage: www.journals.elsevier.com/oceanologia/

ORIGINAL RESEARCH ARTICLE

The response of cyclonic eddies to typhoons based on satellite remote sensing data for 2001—2014 from the South China Sea

Fangjie Yu [a,b], **Qiongqiong Yang** [a], **Ge Chen** [a,b,*], **Qiuxiang Li** [a]

[a] *College of Information Science and Engineering, Ocean University of China, Qingdao, China*
[b] *Laboratory for Regional Oceanography and Numerical Modeling, Qingdao National Laboratory for Marine Science and Technology, Qingdao, China*

Received 19 August 2018; accepted 26 November 2018
Available online 11 December 2018

KEYWORDS
Tropical cyclones;
Mesoscale eddy;
Eddy kinetic energy

Summary Eddies are known to be affected by typhoons, and in recent years, the general three-dimensional structure, as well as features of the spatial and temporal distributions of eddies have been determined. However, the type of eddy that is most likely to be affected by a typhoon remains unclear. In this paper, quantitative and qualitative methods were used to study the eddies that are most sensitive to upper-ocean tropical cyclones (TCs) from the perspective of eddy characteristics, and the quantitative results showed that not all eddies were enhanced under the influence of typhoons. Enhancement of the eddy amplitude (Amp), radius (Rad), area (A), or eddy kinetic energy (EKE) accounted for 92.3% of the total eddy within the radius of the typhoon. Qualitative analyses showed the following: First, eddies located on different sides of the typhoon tracks were differently affected, as eddies on the left side were more intensely affected by the typhoon than eddies on the right side, and second, eddies with short lifespans or small radii were more susceptible to the TCs.

* Corresponding author at: College of Information Science and Engineering, Ocean University of China, Qingdao, China. Tel.: +86 053266781265.
E-mail address: gechen@ouc.edu.cn (G. Chen).
Peer review under the responsibility of Institute of Oceanology of the Polish Academy of Sciences.

Production and hosting by Elsevier

https://doi.org/10.1016/j.oceano.2018.11.005

1. Introduction

The South China Sea (SCS) is the largest semi-enclosed marginal water body in the Northwest Pacific. Its average depth is 1800 m, and its maximum depth is up to 5400 m. Each year, many TCs pass through the SCS (Liu and Xie, 1999) (Fig. 1), and many studies have shown that their strong winds stir and vertically mix the upper ocean (Guan et al., 2014; Knaff et al., 2013; Price, 1981; Wang et al., 2012), and Mixing of the upper and subsurface water causes the sea surface temperature (SST) to cool (Chiang et al., 2011; Guan et al., 2014; Lin et al., 2017; Liu and Xie, 1999; Potter et al., 2017; Sun et al., 2015).

Due to the influence of seabed topography and kuroshio invasion, many mesoscale eddies occur in the SCS (Chelton et al., 2011b; Du et al., 2016; Wang, 2003; Xiu et al., 2010) that have far-reaching impacts on the mixing of sea water, the transport of deep-sea sediment, and the distributions of marine organisms, energy, heat, and nutrients. As one of the characteristics of oceans, mesoscale eddies can also regulate air–sea interactions (Chelton et al., 2011a; Lin et al., 2005; Patnaik et al., 2014; Shay et al., 2000; Zheng et al., 2010).

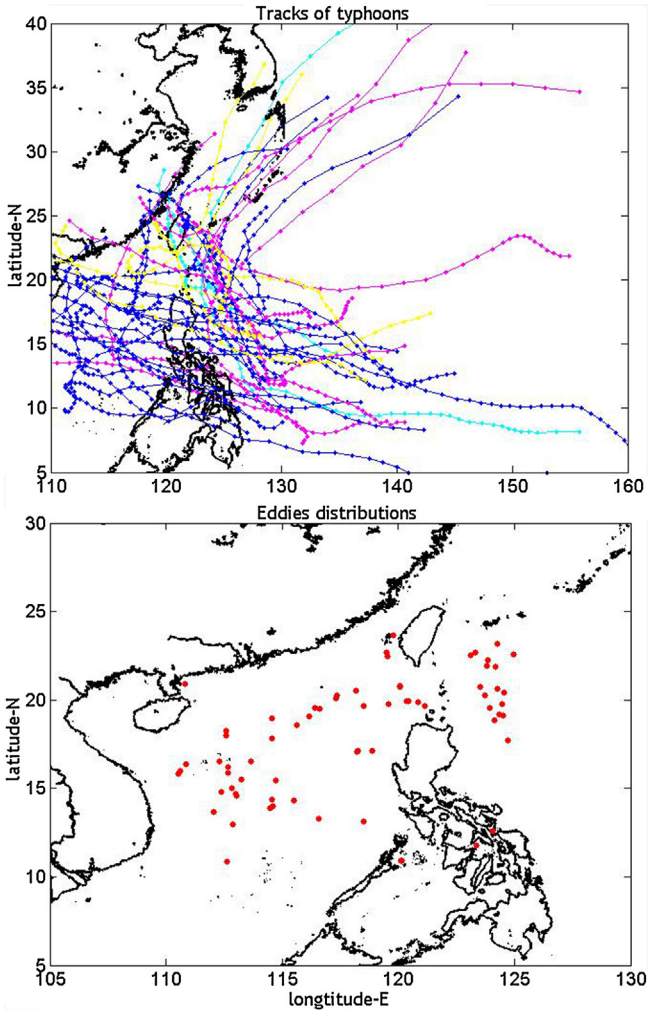

Figure 1 Tracks of typhoons and spatial distributions of eddies.

The interaction between eddies and TCs is an important branch of air–sea interactions, and the study of this interaction improves our understanding of ocean circulation dynamics (Hisaki, 2003; Wang et al., 2009; Zheng et al., 2010). In the past few decades, scholars have suggested that typhoons promote eddy generation. Hu and Kawamura (2004) found that for each case of a looping tropical cyclone, a cyclonic eddy with an obvious sea-level depression appears in the sea area where the cyclone takes a loop form, and a cold core forms with a difference in SST greater than 2°C compared to the surrounding areas (Chen et al., 2012; Chow et al., 2008; Gordon et al., 2017; Hu and Kawamura, 2004; Mahadevan et al., 2008; Zhang et al., 2016). Furthermore, the responses of the cyclonic eddies (CEs) to typhoon forcing in the Western North Pacific Ocean (WNPO) were analyzed using Argo profiles, and the results indicated that the inflow of warm and fresh water, heats and freshens the subsurface in the CEs to compensate for the cooling. Eddies primarily cool at the surface (0–10 m depth) but deep upwelling occurs from the top of the thermocline (200 m in depth) to greater ocean depths shortly after typhoon forcing (Liu et al., 2017). By using satellite and altimeter data to research the response of eddies to typhoons, the eddy core has found to have an obvious sea-level depression after a typhoon, resulting in both mixed layers and SST cooling (Jaimes et al., 2011; Shang et al., 2008); Cyclonic eddies have been found to be enhanced by typhoons, and one noticeable feature was a change in the three-dimensional structure accompanied by reaxisymmetrization and elliptical deformation processes in the horizontal plane (Lu et al., 2016; Wang et al., 2009). Additionally, by comparing the EKE and available gravitational potential energy of COEs before and after typhoons, Sun et al. (2014) found that the energy of a COE can be increased by a slow-moving typhoon, and the EKE can change on order of O (10^{14}–10^{15} J) (Shang et al., 2015; Sun et al., 2014). Finally, among maximum wind speed, typhoon translation speed and the typhoon forcing time (T_f), changes in the geometric and physical parameters of eddies have been found to mostly be related to the T_f, which is determined by typhoon translation speed and size and typhoon intensity (Sun et al., 2014).

In summary, many breakthroughs have occurred in the response of eddies to TCs over the last ten years, but important questions remain unanswered. For example, will the properties of the eddy constrain how it is affected by a typhoon and if so, which kind of eddy responds more strongly? In this paper, the data used for eddy identification and tracking are introduced in Section 2, which is followed by results of the qualitative analysis based on specific eddy and typhoon cases (Section 3). Finally, conclusions are offered that include suggestions for future research (Section 4).

2. Material and methods

2.1. Typhoon data

In this paper, typhoon “best-track data sets” (BTDS) were obtained from the U.S Joint Typhoon Warning Center (JTWC), and each contained typhoon maximum sustained wind (MSW) speeds in knots (i.e., the 1-min mean maximum sustained wind speed at a height of 10 m), the latitude and longitude of

the typhoon center, and the typhoon radius in sea miles. According to the TC classification standard of the JTWC, a TC is defined as a typhoon when its MSW exceeds 63 knots, and as the MSW surpasses 113 knots, a TC is defined as super typhoons. Only TCs in the Northwest Pacific with MSW $\geq$64 knots from 2001 to 2014 were used in this study. The duration of the TCs in the SCS was counted with an accuracy of 0.5 days because the time interval of the BTDS was 6 h (Table 1).

2.2. Satellite data and eddy parameters

Altimeter data from Archiving, Validation, and Interpretation of Satellite Oceanographic Data (AVISO 2014) were used in this study, and they were generated from a combination of data from TOPEX/Poseidon, Jason-1 and Jason-2, and Environmental Satellite. AVISO delayed-time altimeter data from January 1993 to December 2015 are daily, two-satellite merged global seal-level anomalies (SLA) with a spatial resolution 0.25 $\times$ 0.25°. Sea surface temperature (SST) data were acquired from remote sensing systems with a resolution of 25 km. The altimeter data were used to identify, detect and track mesoscale eddies, while SST data were adopted to validate the tracking results. The algorithm used to identify, detect and track mesoscale eddies used in this study was provided by Liu et al. (2016) and Sun et al. (2017). The meridional component, u_g, and the zonal component, v_g, of the geostrophic velocity of the ocean current as well as A and EKE (e.g., Xu et al., 2011) were calculated as follows:

$$A = N\times 0.25\times 0.25\times 111\times 111\times|\cos(lat)|, \quad (1)$$

$$u_g = -\frac{g}{f}\frac{\partial SLA}{\partial y}, \quad v_g = \frac{g}{f}\frac{\partial SLA}{\partial x}, \quad (2)$$

$$EKE = \sum_{i=1}^{n}\frac{1}{2}(u_g^2 + v_g^2)\rho A_i H_i. \quad (3)$$

In those formulas, N is the number of pixel occupied by the eddy, and 0.25 $\times$ 111 transforms the angle into a distance (in kilometer). The variables u_g and v_g are the vertical and horizontal velocity of geostrophic flow, respectively; ρ is a constant value of the density of the seawater equal to 1020 kg m^{-3}; and H_i is the ocean depth. To better illustrate that the eddy is affected by the typhoon this article takes the state of eddy before the typhoon transit as a reference point, the average values of the eddy properties (Amp, Rad, A, EKE) one week after typhoon transit were calculated, and we further calculated the ratio of the eddy attribute values before and after being affected by the typhoon. The reason that ratios were used rather than differences is that an eddy can form at different sizes and because the growth of its properties is also limited. After being affected by a typhoon, the ratio of two eddies with the same property difference may vary greatly; part of the eddy changes significantly during the week after a typhoon and then changes only slightly. Therefore, this article takes the week after the typhoon as the study period and to highlight the impact of typhoons on the upper ocean, the maximum SST and SLA variation are taken at $\pm$2.25° from the eddy center.

Table 1 Information of typhoons.

Typhoon name	Time/day (stay in the SCS)	V_max/knots (Typhoon encountered eddy)	Number of the eddies
PABUK(2001)	2.00	90	2
WUTIP(2001)	5.75	115	3
IMBUDO(2003)	2.25	90	1
MORAKOT(2003)	3.75	120	1
MAEMI(2003)	2.00	65	1
NEPARTAK(2003)	5.75	115	1
CONSON(2004)	2.00	125	1
HAITANG(2005)	4.00	95	1
TALIM(2005)	1.25	115	1
CHANCHU(2006)	6.25	65	4
PRAPIROON(2006)	5.25	115	1
XANGSANE(2006)	4.75	115	3
CIMARON(2006)	10.50	115	3
UTOR(2007)	5.50	75	2
PABUK(2007)	3.00	65	1
SEPAT(2007)	2.00	140	1
PEIPAH(2007)	6.50	75	1
MITAG(2007)	2.50	75	1
NEOGURI(2008)	6.00	100	2
NURI(2008)	3.50	80	2
HAGUPIT(2008)	3.50	100	1
LINFA(2009)	6.75	70	1
MORAKOT(2009)	1.75	80	1
PARMA(2009)	12.00	65	1
FANAPI(2010)	2.25	105	1
MEGI(2010)	5.25	110	4
SONGDA(2011)	1.75	140	2
MUIFA(2011)	5.25	70	1
NESAT(2011)	4.50	75	2
NALGAE(2011)	4.50	65	1
JELAWAT(2012)	2.25	130	1
TINH(2012)	4.25	75	2
BOPHA(2013)	5.00	115	1
SOULIK(2013)	1.25	80	1
NARI(2013)	4.75	80	2
KROSA(2013)	4.75	100	3
HAIYAN(2013)	3.25	95	1
RAMMASUN(2014)	5.00	125	3
MATMO(2014)	1.50	80	1
KALMAEGI(2014)	3.50	70	2

3. Results and discussion

3.1. New eddy generated by Typhoon MEGI (2010)

Typhoon MEGI formed on October 11 and passed through the SCS at 90 knots on October 18, and its direction was from east to west. During its 126-h residency, the intensity of the typhoon increased from 90 knots to 115 knots; MEGI finally left the SCS on October 24 at 30 knots.

The four subgraphs in Fig. 2 illustrate daily SST and SLA on four different days influenced by Typhoon MEGI in the region,

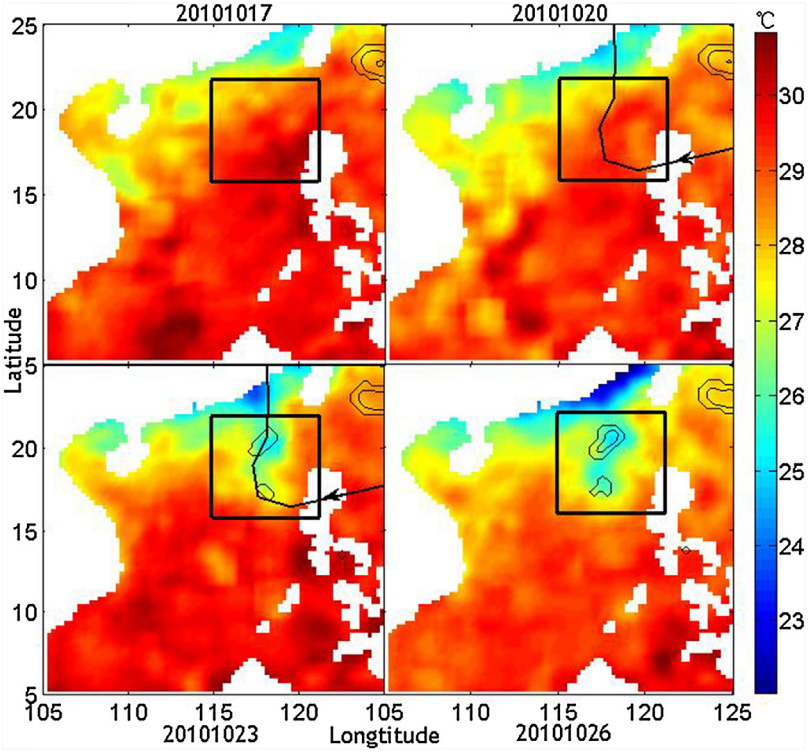

Figure 2 The SST colored, from October 17, 2010 to October 26, 2010. October 17, 2010 was the SST status before the typhoon. October 20, 2010, October 23, 2010, October 26, 2010 were SST status on day 2, day 5 and day 8 after the typhoon, respectively. The curve plots the path of the typhoon, and the arrow marks the direction of the typhoon, the closed loop was the area of SLA < -12 cm (cold eddy zone).

it is obvious that the SST and SLA significantly reduced in the black box area during MEGI period. Before the typhoon's arrival (2010.10.17), the lowest SST of the area of new eddy generation was 27.8°C, and the temperature fell to 27.2°C on the third day (20101020). Then, on the sixth day (2010.10.23) after MEGI, the lowest SST was 25.3°C, which was accompanied by a >12-cm sea-level depression and the appearance of a closed loop. During the 126-h typhoon period, the maximum reduction in SST in the region was 2.53°C, and the maximum reduction of the SLA reached 11.3 cm. In summary, under the influence of the typhoon, a new eddy was generated below the sea on October 23, 2010 (Fig. 2), and this new eddy was well developed and lasted for more than several weeks.

3.2. Typhoon enhanced preexisting eddy

UTOR was a tropical cyclone during the Pacific typhoon season in 2006. The storm formed on December 7, was maintained for 8 days and then dissipated on December 15. The maximum intensity of UTOR during its lifecycle was 100 knots, and UTOR passed the SCS on December 11 with an intensity of 75 knots. Within the range of the radius of UTOR, a mesoscale eddy occurred (recorded as No. 25 eddy in Table 2a, Fig. 4).

Fig. 3 shows the eddy properties of the No. 25 and No. 55 eddy in their whole lifetime. It can be seen from the figure that during the entire life cycle of the eddy, the properties of the eddy are always fluctuating. From the left side of Fig. 3, the SLA, Amp, Rad, Area and EKE of the No. 25 eddy were all significantly changed after affected by UTOR, and the maximum (minimum of the SLA) of each parameter occurred either during or after UTOR. Moreover, compared with other periods, the vital signs of the eddy were relatively stable during the typhoon. The No. 25 eddy was located to the right of the center of UTOR (position of the eddy core relative to the UTOR path) with a radius of 156.92 km and a lifespan of 46 days. After the typhoon passed, the SST in the eddy area decreased by 3.31°C (Fig. 4), and the parameters of No.25 eddy changed. Among them, the SLA decreased by 7.04 cm, and the amplitude, radius, area and EKE increased by1.29 times, 0.92 times, 0.92 times, and 1.15 times respectively, compared to before the typhoon.

Typhoon NARI originated on October 7, 2013 in the Philippines east of the SCS and dissipated on October 16. Its life cycle was 10 days, and its maximum intensity reached 100 knots. When the typhoon passed the SCS, there was an eddy under the typhoon (recorded as the No. 55 eddy in Table 2b, Fig. 5).

The right side of Fig. 3 shows that the SLA, Amp, Rad, Area and EKE of the No. 55 eddy significantly changed after being affected by NARI, and the maximum (minimum of the SLA) of each parameter occurred during or after the typhoon. Moreover, compared with other periods, the vital signs of the eddy were relatively stable during the typhoon. The No. 55 eddy had a lifespan of 42 days and a radius of 52.43 km, and after the typhoon passed, the SST in the eddy area dropped by 2.32°C. The SLA of the eddy core as well as the eddy amplitude, radius, area, and EKE exhibited very significant changes: the SLA decreased by 4.41 cm while the eddy

Table 2a Parameters of 65 eddies.

Eddy	Cold/warm eddy	Location	Lifetime/days	Amp/times	Rad/times	A/times	EKE/times
1	Cold	R	13	1.38	1.15	1.90	5.81
2	Cold	R	13	2.03	1.03	1.19	1.61
3	Cold	R	24	0.79	0.81	0.50	0.33
4	Cold	R	32	1.52	1.15	1.48	1.90
5	Cold	R	24	1.37	1.00	1.59	3.26
6	Cold	L	13	1.51	1.41	2.23	1.51
7	Cold	R	13	0.57	0.92	0.58	3.30
8	Cold	L	13	0.78	0.95	0.75	6.61
9	Cold	R	109	1.12	1.09	0.75	1.59
10	Cold	L	36	1.13	1.10	1.23	2.02
11	Cold	L	14	0.76	0.99	0.68	4.92
12	Cold	L	17	1.07	1.05	1.22	1.19
13	Cold	R	10	2.62	1.57	1.50	4.63
14	Cold	R	32	1.34	1.05	1.11	2.02
15	Cold	R	29	0.36	0.61	0.35	0.14
16	Cold	R	10	0.21	0.43	0.19	0.01
17	Cold	L	15	0.94	0.92	0.93	1.22
18	Cold	L	37	1.35	1.10	2.03	3.77
19	Cold	L	13	2.04	1.60	2.66	8.13
20	Cold	L	13	1.39	1.35	1.81	3.02
21	Cold	R	15	2.13	1.39	0.60	1.63
22	Cold	R	15	2.00	1.48	2.33	13.08
23	Cold	R	15	1.55	1.26	1.66	2.86
24	Cold	R	23	2.35	1.24	1.50	5.09
25	Cold	R	46	1.29	0.92	0.92	1.15
26	Cold	L	12	0.73	1.16	1.20	1.18
27	Cold	L	21	1.54	1.77	2.17	2.91
28	Cold	L	14	2.22	1.27	1.60	1.25
29	Cold	R	18	3.83	1.52	4.87	1.16
30	Cold	R	67	1.16	1.02	0.90	2.14
31	Cold	L	20	0.64	0.78	0.88	0.26
32	Cold	R	27	1.09	0.95	1.09	1.13
33	Cold	L	58	1.18	1.07	0.56	1.19
34	Cold	R	51	1.13	0.97	0.88	1.19
35	Cold	R	27	0.95	0.80	0.65	1.23
36	Cold	L	13	2.62	1.35	1.30	2.39
37	Cold	L	14	1.17	1.00	1.13	1.52
38	Cold	L	45	8.32	3.05	10.25	45.66
39	Cold	R	42	0.75	0.74	0.57	2.24
40	Cold	R	20	0.91	0.70	0.14	0.04
41	Cold	R	42	0.66	0.83	1.01	32.33
42	Cold	R	42	0.64	0.84	1.04	4.86
43	Cold	R	49	0.89	0.87	1.36	2.58
44	Cold	L	27	1.07	0.81	0.26	3.01
45	Cold	R	43	0.78	0.92	0.85	7.73
46	Cold	R	17	0.81	0.91	1.10	0.53
47	Cold	L	24	1.03	1.12	1.26	1.51

amplitude, radius, area, and EKE increased by 1.61 times, 1.06 times, 1.11 times, and 1.99 times, respectively, compared to before the NARI crossed.

With its enhanced amplitude, radius, area, or EKE, the eddy accounted for 92.3% of the total eddies within the radius of the typhoon. The rate of increase in the properties is highly variable among different eddies. In the study, the longest eddy lifespan was 109 days, and the amplitude, radius, area, and EKE of this eddy changed by 1.12, 1.09, 0.75, and 1.59 times, respectively (recorded as the No. 9 eddy in Table 2a). Compared to other eddies that were enhanced by typhoons, this eddy was relatively minimally enhanced. As shown in the next section, this paper takes the perspective of the eddy as a starting point and considers the position of the eddy relative to the typhoon path as well as the lifetime and radius of the eddy to study the reasons for restricted influence of a typhoon.

Table 2b Parameters of 65 eddies.

Eddy	Cold/warm eddy	Location	Lifetime/days	Amp/times	Rad/times	A/times	EKE/times
48	Cold	L	17	0.91	0.99	1.70	137.04
49	Cold	L	21	1.01	0.97	1.11	1.14
50	Cold	R	60	0.92	0.93	1.36	1.44
51	Cold	R	68	1.45	1.08	16.39	26.07
52	Cold	R	21	2.87	1.63	2.39	12.76
53	Cold	L	12	2.37	1.11	2.74	1.79
54	Cold	R	42	1.85	1.13	1.27	3.26
55	Cold	R	42	1.61	1.06	1.11	1.99
56	Cold	L	30	2.40	1.30	2.79	21.27
57	Cold	L	15	1.10	1.20	1.63	6.17
58	Cold	R	51	1.82	1.23	1.12	1.04
59	Cold	R	69	2.14	1.50	2.20	4.37
60	Cold	R	17	1.21	1.11	1.25	1.65
61	Cold	R	17	1.41	1.27	1.80	4.27
62	Cold	R	10	1.78	2.45	7.56	1.20
63	Cold	R	13	3.18	2.28	32.33	4.48
64	Cold	R	13	1.22	1.24	1.33	1.89
65	Cold	R	17	3.06	1.31	1.89	1.55

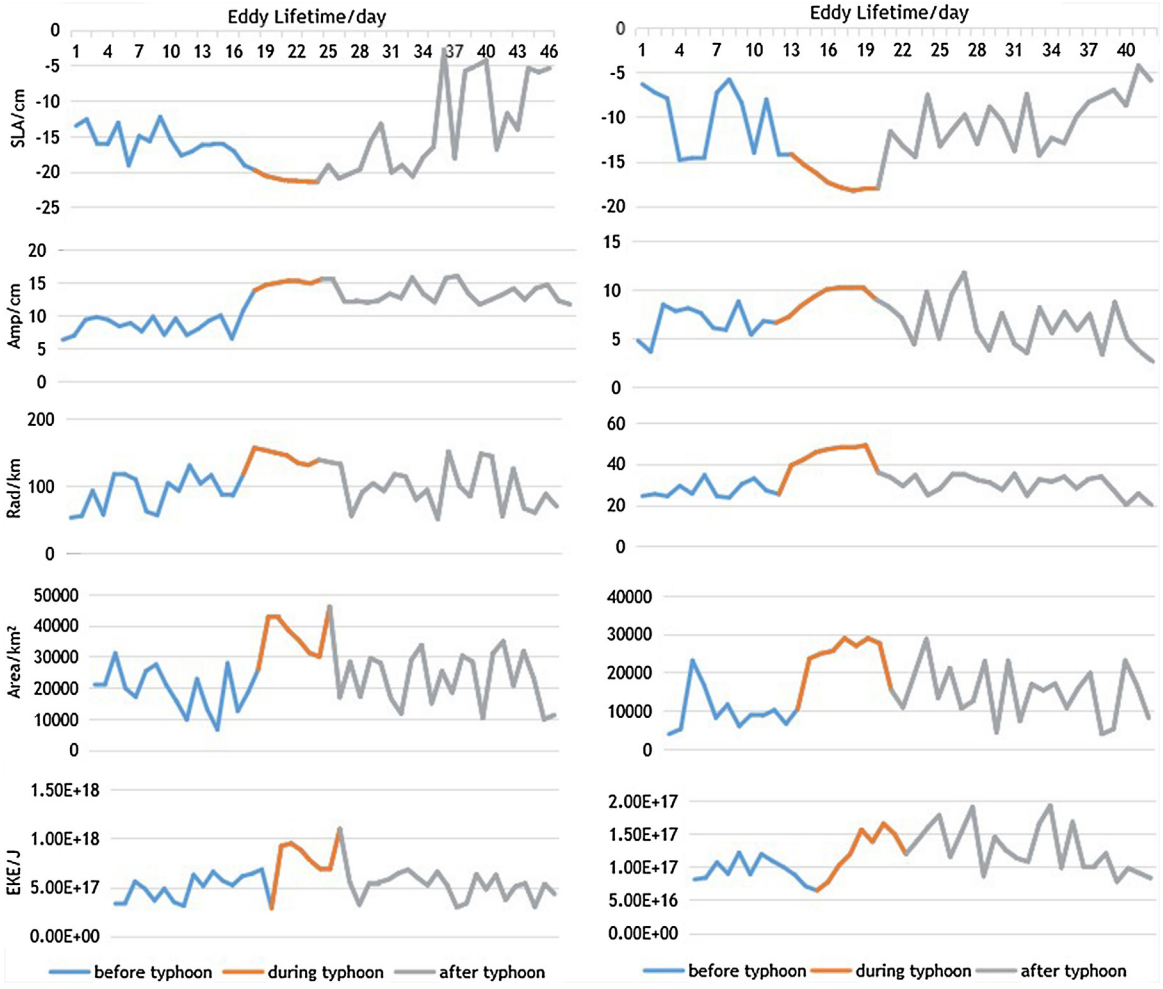

Figure 3 The No. 25 eddy (left) and No. 55 eddy (right) parameters in their whole lifecycle.

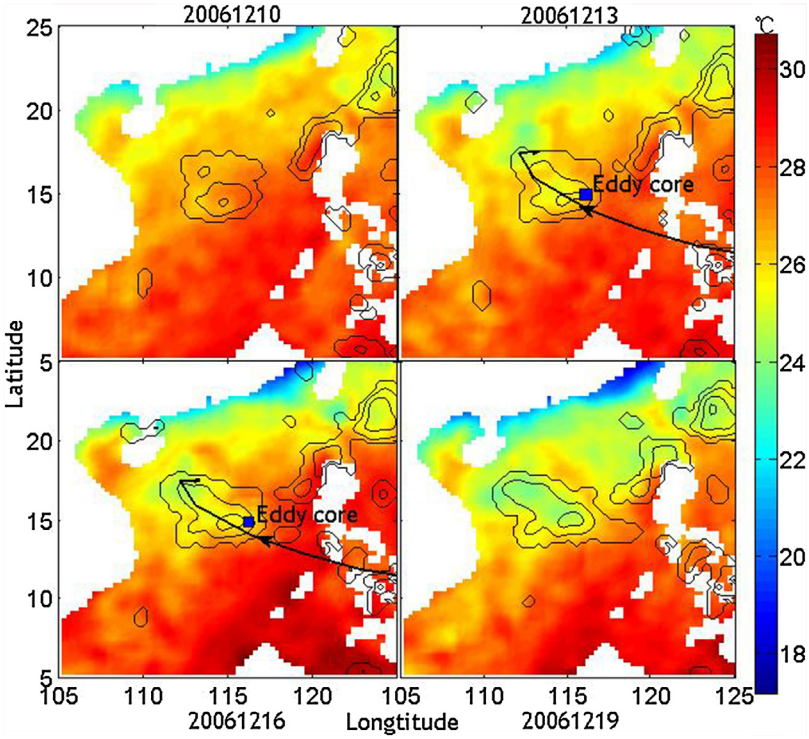

Figure 4 Same as Fig. 2, except for typhoon UTOR, UTOR passed the SCS on December 11, 2006.

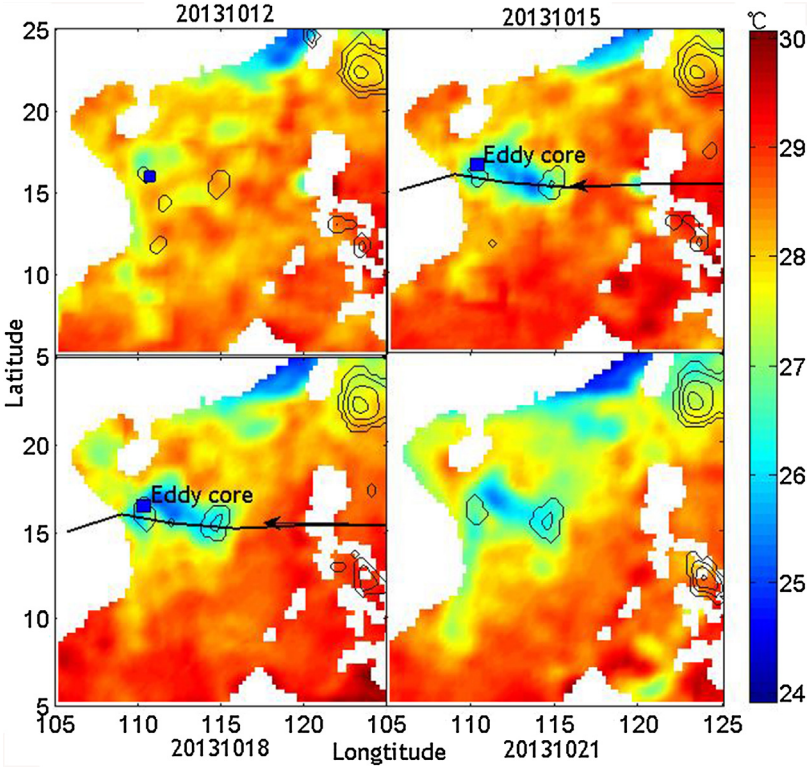

Figure 5 Same as Fig. 2, except for the typhoon NARI, NARI passed the SCS on October 13, 2013.

3.3. Qualitative analysis

The eddy to the left of the typhoon and that to the right were numbered 24 and 41, respectively, accounting for 37% and 63% of the total. Fig. 6 shows that the eddies changed on both sides of the path of the typhoon after the typhoon passed, and seven days after passage, the eddies to the left of the path exhibited greater changes in the SLA, Amp, area and EKE than those to the right. The overall growth trend of the ones on the left of the path was also greater than that for the eddies to the right.

The eddies studied were divided into two groups: those whose radius was larger than the average radius of 75.6 km, referred to as the large eddy group, and those with a smaller-than-average radius km, referred to as the small eddy group. There were 23 eddies in the large eddy group, accounting for 35% of the total, and the small eddy group consisted of 42 eddies, accounting for 65% of the total. Fig. 7 shows the two eddy groups and the changes in their property after the typhoon passed. The result indicates that after being influenced by the typhoon, the eddies with a small radius underwent a more significant increase in their Amp, Rad, area and EKE than those with a large radius. However, after the typhoon passed, the large-eddy Amp and EKE grew only slightly, and their radii and areas decreased. All of these results indicated that a small eddy is more susceptible to a typhoon.

We further divided the eddies into two groups: eddies with lifetimes of 10—20 days were marked as the short-lived group, and eddies with lifetimes longer than 21d were considered as long-lived. There were 32 and 33 short- and long-lived eddies, respectively, each accounting for 50% of the study data. Fig. 8 shows that the values of the two eddy groups increased after being affected by the typhoon, but eddies with a lifespan of 10—20 days exhibited a more intense increase in their Amp, rad, area and EKE than those with lifespan longer than 21 days. The results indicate that short-lived eddies are more susceptible to typhoons than long-lived eddies.

In summary, eddies located on the left of the typhoon path are more intensely affected than eddies on the right. Eddies with the short lifespans and small radii are more susceptible to typhoons.

3.4. Causal relationship

The results of statistical analysis show that the eddy on the left of the typhoon was more intense affected by typhoon than the eddy located on the right side of the typhoon. The difference between the conclusion of this paper and those of others lies in that this paper aims at studying eddies growth rate after being affected by typhoon rather than increment, the latter is concerned with the change in quantity, while this article focuses on indicating the ease or complexity of eddies

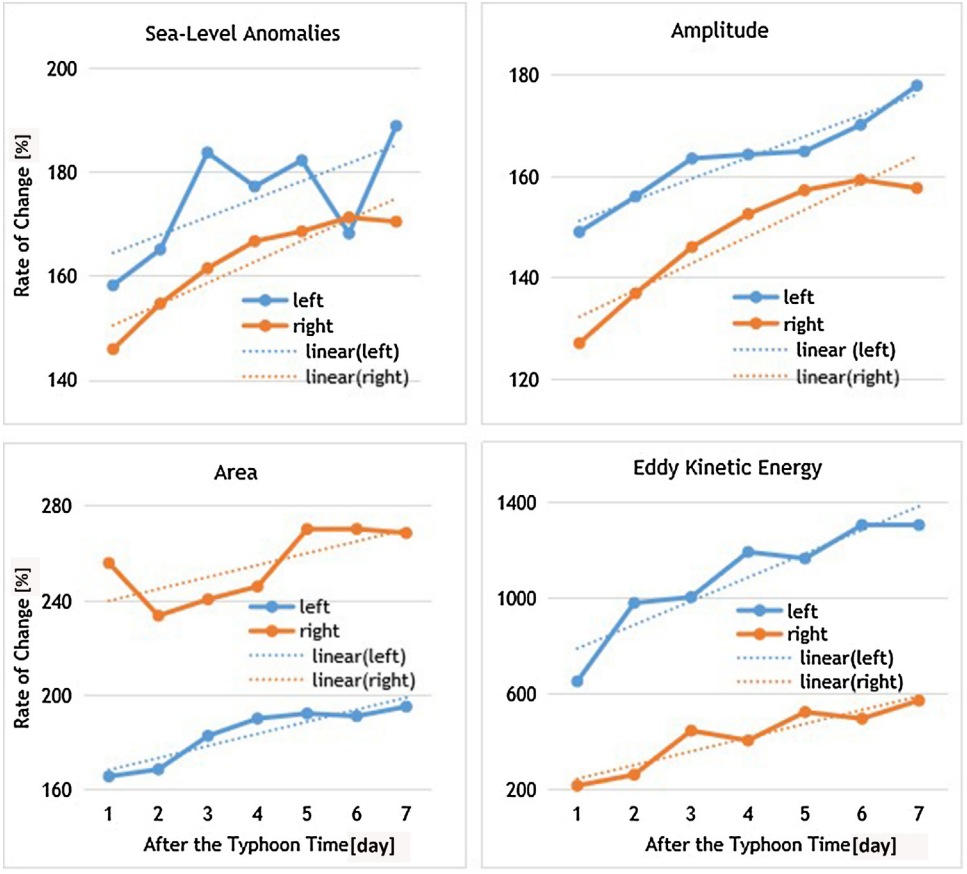

Figure 6 After the typhoon, eddy properties change, on both sides of the typhoon path.

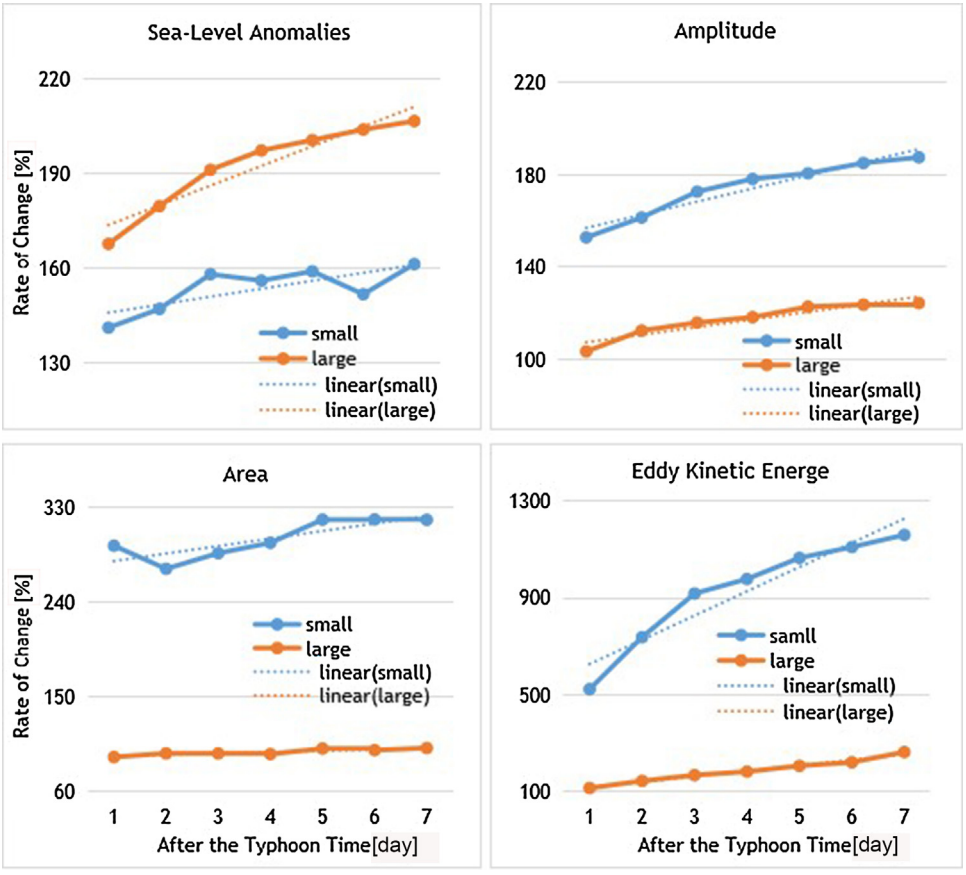

Figure 7 After the typhoon, properties change of large and small eddies.

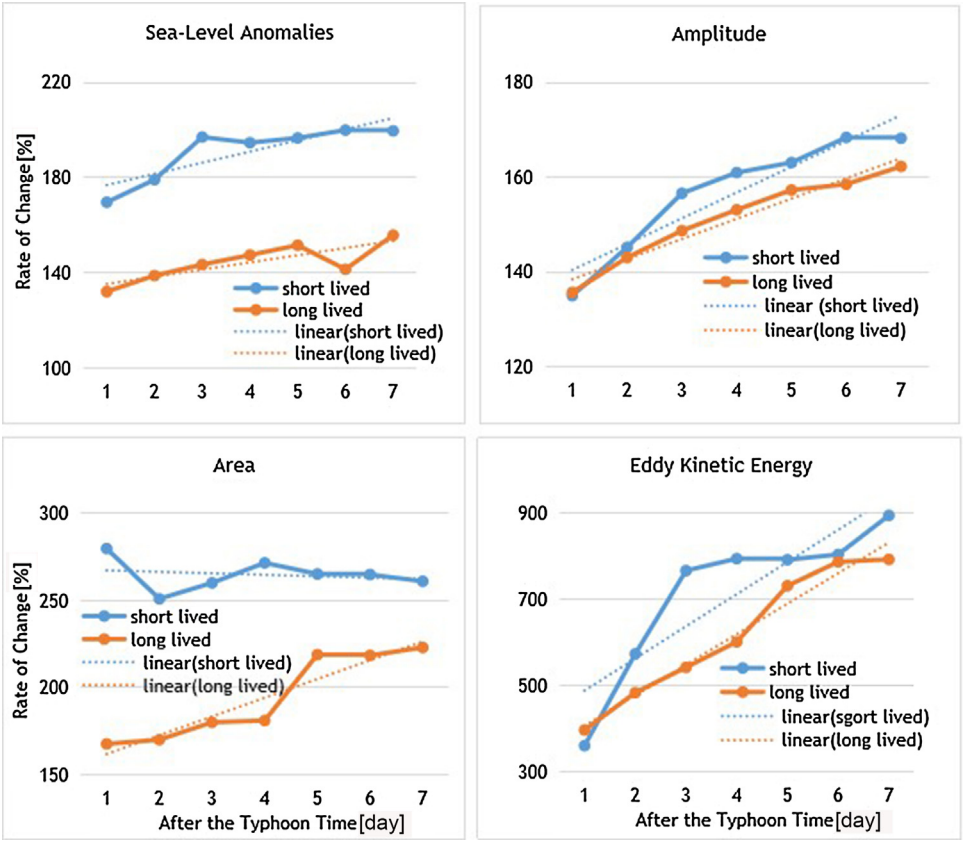

Figure 8 After the typhoon, properties change of short lived eddies and longevity eddies.

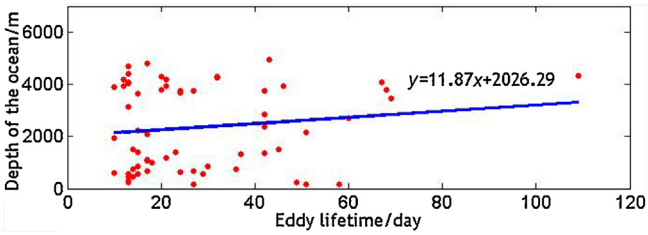

Figure 9 Relationships between eddy lifetime and depth of ocean at the eddy center.

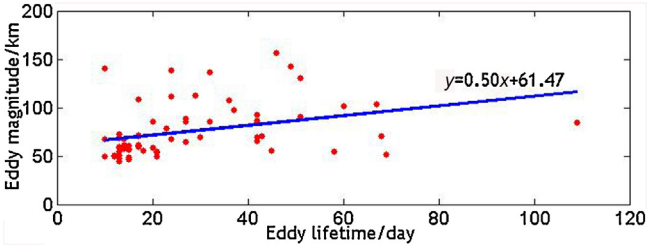

Figure 10 Relationships between eddy lifetime and eddy magnitude.

affected by typhoon. To further study why a short-lived, small-sized eddy was more intensely enhanced by typhoons, the depth of the eddy center and the eddy radius were plotted across the entire eddy life cycle. Fig. 9 shows that long-lived eddies appear more often in deeper sea areas and there appears to be a positive correlation between the lifespan of the eddy and its size. Fig. 10 shows the relationships between the lifespan of the eddy and the depth of the ocean at its center, and it illustrates that short-lived eddies occur more often in shallow seas. This conclusion is consistent with data indicating that strong eddies usually penetrate much deeper into the ocean than weak ones (Xiu et al., 2010).

4. Conclusions

In this study, typhoon and eddy intersection data for 2001 to 2014 for the South China Sea were first generated using typhoon data from JTWC; eddies were then identified and tracked using data from Liu et al. (2016). The data set contained a total of 65 eddies with an average eddy life of 28.03 days and an average radius of 75.6 km. After being affected by a typhoon, not all eddies were enhanced. Typhoon can enhance the eddy, but can't stop the eddy dissipate. When encountered the typhoon in the late stage of its lifecycle, the eddy is hard to be enhanced, it may be explained that the energy dissipated of the eddy itself is greater than that delivered by the typhoon. There are three typical cases demonstrated that typhoons would generate new eddies and enhance preexisting eddies in Section 3. Then, several conclusions were reached through qualitative analysis. First, the Amp, rad and EKE are sharply intensified in eddies located on the left side of the track of the typhoon, and the growth trend is more severe than that of eddies to the right of the track. Second, after being influenced by a typhoon, the Amp, rad, area and EKE of small-sized eddies increase more intensely, and this trend is more prominent compared to eddies with a large magnitude. Third, short-lived eddies are more susceptible to typhoons than long-lived eddies, especially regarding the difference in the eddy radius and area. Finally, the dynamics for the response of mesoscale eddy to the tropical cyclones involves wind stress, and sea surface wind stress was the only way in which the atmosphere can transmit momentum directly to the ocean. This paper was based on the perspective of eddy characteristics, so the wind stress is not introduced in detail, but the specific introduction will be further introduced in the later research on typhoon. Then, it will be possible to expand the study area in the sea, increase the amount of data, and control a single variable to conduct more detailed research about the eddy properties and identify the influence of tropical cyclones alone.

Acknowledgments

The research was supported by following programs: (1) National key research and development program of China (Grant No. 2016YFC1402608, Grant No. 2016YFC1401008); (2) Qingdao National Laboratory for Marine Science and Technology (Grant No. QNLM2016ORP0105); (3) The Fundamental Research Funds for the Central Universities (Grant Nos. 201413064, 201613010).

References

Chelton, D.B., Gaube, P., Schlax, M.G., Early, J.J., Samelson, R.M., 2011a. The influence of nonlinear mesoscale eddies on near-surface oceanic chlorophyll. Science 334 (6054), 328—332, http://dx.doi.org/10.1126/science.1208897.

Chelton, D.B., Schlax, M.G., Samelson, R.M., 2011b. Global observations of nonlinear mesoscale eddies. Prog. Oceanogr. 91 (2), 167—216, http://dx.doi.org/10.1016/j.pocean.2011.01.002.

Chen, G., Gan, J., Xie, Q., Chu, X., Wang, D., Hou, Y., 2012. Eddy heat and salt transports in the South China Sea and their seasonal modulations. J. Geophys. Res.-Oceans. 117 (C5), http://dx.doi.org/10.1029/2011JC007724.

Chiang, T., Wu, C., Oey, L., 2011. Typhoon Kai-Tak: an ocean's perfect storm. J. Phys. Oceanogr. 41 (1), 221—233, http://dx.doi.org/10.1175/2010JPO4518.1.

Chow, C., Hu, J., Centurioni, L.R., Niiler, P.P., 2008. Mesoscale Dongsha Cyclonic Eddy in the northern South China Sea by drifter and satellite observations. J. Geophys. Res. 113 (C4), http://dx.doi.org/10.1029/2007JC004542.

Du, Y., Wu, D., Liang, F., Yi, J., Mo, Y., He, Z., Pei, T., 2016. Major migration corridors of mesoscale ocean eddies in the South China Sea from 1992 to 2012. J. Mar. Syst. 158, 173–181, http://dx.doi.org/10.1016/j.jmarsys.2016.01.013.

Gordon, A.L., Shroyer, E., Murty, V.S.N., 2017. An intrathermocline Eddy and a tropical cyclone in the Bay of Bengal. Sci Rep.-UK 7, 46218, http://dx.doi.org/10.1038/srep46218.

Guan, S., Zhao, W., Huthnance, J., Tian, J., Wang, J., 2014. Observed upper ocean response to typhoon Megi (2010) in the Northern South China Sea. J. Geophys. Res.-Oceans. 119 (5), 3134–3157, http://dx.doi.org/10.1002/2013JC009661.

Hisaki, Y., 2003. Horizontal variability of near-inertial oscillations associated with the passage of a typhoon. J. Geophys. Res. 108 (C12), 12 pp., http://dx.doi.org/10.1029/2002JC001683.

Hu, J.Y., Kawamura, H., 2004. Detection of cyclonic eddy generated by looping tropical cyclone in the northern South China Sea: a case study. Acta Oceanol. Sin. 23 (2), 213–224.

Jaimes, B., Shay, L.K., Halliwell, G.R., 2011. The response of quasigeostrophic oceanic vortices to tropical cyclone forcing. J. Phys. Oceanogr. 41 (10), 1965–1985, http://dx.doi.org/10.1175/JPO-D-11-06.1.

Knaff, J.A., DeMaria, M., Sampson, C.R., Peak, J.E., Cummings, J., Schubert, W.H., 2013. Upper oceanic energy response to tropical cyclone passage. J. Clim. 26 (8), 2631–2650, http://dx.doi.org/10.1175/JCLI-D-12-00038.1.

Lin, I.I., Wu, C.C., Emanuel, K.A., Lee, I.H., Wu, C.R., Pun, I.F., 2005. The interaction of Supertyphoon Maemi (2003) with a warm ocean eddy. Mon. Weather Rev. 133 (9), 2635–2649, http://dx.doi.org/10.1175/MWR3005.1.

Lin, S., Zhang, W., Shang, S., Hong, H., 2017. Ocean response to typhoons in the western North Pacific: composite results from Argo data. Deep-Sea Res. Pt. I 123, 62–74, http://dx.doi.org/10.1016/j.dsr.2017.03.007.

Liu, W.T., Xie, X.S., 1999. Spacebased observations of the seasonal changes of South Asian monsoons and oceanic responses. Geophys. Res. Lett. 26 (10), 1473–1476, http://dx.doi.org/10.1029/1999GL900289.

Liu, Y., Chen, G., Sun, M., Liu, S., Tian, F., 2016. A parallel SLA-based algorithm for global mesoscale Eddy identification. J. Atmos. Ocean. Tech. 33 (12), 2743–2754, http://dx.doi.org/10.1175/JTECH-D-16-0033.1.

Liu, S., Sun, L., Wu, Q., Yang, Y., 2017. The responses of cyclonic and anticyclonic eddies to typhoon forcing: the vertical temperature-salinity structure changes associated with the horizontal convergence/divergence. J. Geophys. Res.-Oceans. 122 (6), 4974–4989, http://dx.doi.org/10.1002/2017JC012814.

Lu, Z., Wang, G., Shang, X., 2016. Response of a preexisting cyclonic ocean Eddy to a Typhoon. J. Phys. Oceanogr. 46 (8), 2403–2410, http://dx.doi.org/10.1175/JPO-D-16-0040.1.

Mahadevan, A., Thomas, L.N., Tandon, A., 2008. Comment on "eddy/wind interactions stimulate extraordinary mid-ocean plankton blooms". Science 320 (5875), 448, http://dx.doi.org/10.1126/science.1152111.

Patnaik, K.V.K.R., Maneesha, K., Sadhuram, Y., Prasad, K.V.S.R., Murty, T.V.R., Brahmananda Rao, V., 2014. East India Coastal Current induced eddies and their interaction with tropical storms over Bay of Bengal. J. Oper. Oceanogr. 7 (1), 58–68, http://dx.doi.org/10.1080/1755876X.2014.11020153.

Potter, H., Drennan, W.M., Graber, H.C., 2017. Upper ocean cooling and air–sea fluxes under typhoons: a case study. J. Geophys. Res.-Oceans. 122 (9), 7237–7252, http://dx.doi.org/10.1002/2017JC012954.

Price, J.F., 1981. Upper ocean response to a hurricane. J. Phys. Oceanogr. 11 (2), 153–175, http://dx.doi.org/10.1175/1520-0485(1981)011<0153:UORTAH>2.0.CO;2.

Shang, S., Li, L., Sun, F., Wu, J., Hu, C., Chen, D., Ning, X., Qiu, Y., Zhang, C., Shang, S., 2008. Changes of temperature and bio-optical properties in the South China Sea in response to Typhoon Lingling, 2001. Geophys. Res. Lett. 35 (10), 6 pp., http://dx.doi.org/10.1029/2008GL033502.

Shang, X., Zhu, H., Chen, G., Xu, C., Yang, Q., 2015. Research on cold core eddy change and phytoplankton bloom induced by typhoons: case studies in the South China Sea. Adv. Meteorol. 2015, 1–19, http://dx.doi.org/10.1155/2015/340432.

Shay, L.K., Goni, G.J., Black, P.G., 2000. Effects of a warm oceanic feature on hurricane opal. Mon. Weather. Rev. 128 (5), 1366–1383, http://dx.doi.org/10.1175/1520-0493(2000)128<1366:EOAWOF>2.0.CO;2.

Sun, L., Li, Y., Yang, Y., Wu, Q., Chen, X., Li, Q., Li, Y., Xian, T., 2014. Effects of super typhoons on cyclonic ocean eddies in the western North Pacific: a satellite data-based evaluation between 2000 and 2008. J. Geophys. Res.-Oceans. 119 (9), 5585–5598, http://dx.doi.org/10.1002/2013JC009575.

Sun, J., Oey, L., Chang, R., Xu, F., Huang, S., 2015. Ocean response to typhoon Nuri (2008) in western Pacific and South China Sea. Ocean Dynam. 65 (5), 735–749, http://dx.doi.org/10.1007/s10236-015-0823-0.

Sun, M., Tian, F., Liu, Y., Chen, G., 2017. An improved automatic algorithm for global eddy tracking using satellite altimeter data. Remote Sens.-Basel. 9 (3), 206, http://dx.doi.org/10.3390/rs9030206.

Wang, G., 2003. Mesoscale eddies in the South China Sea observed with altimeter data. Geophys. Res. Lett. 30 (21), 6 pp., http://dx.doi.org/10.1029/2003GL018532.

Wang, G., Ling, Z., Wang, C., 2009. Influence of tropical cyclones on seasonal ocean circulation in the South China Sea. J. Geophys. Res. 114 (C10), http://dx.doi.org/10.1029/2009JC005302 11 pp.

Wang, H., Wang, D., Liu, G., Wu, H., Li, M., 2012. Seasonal variation of eddy kinetic energy in the South China Sea. Acta Oceanol. Sin. 31 (1), 1–15, http://dx.doi.org/10.1007/s13131-012-0170-7.

Xiu, P., Chai, F., Shi, L., Xue, H., Chao, Y., 2010. A census of eddy activities in the South China Sea during 1993–2007. J. Geophys. Res. 115 (C3), http://dx.doi.org/10.1029/2009JC005657 15 pp.

Xu, C., Shang, X., Huang, R.X., 2011. Estimate of eddy energy generation/dissipation rate in the world ocean from altimetry data. Ocean Dynam. 61 (4), 525–541, http://dx.doi.org/10.1007/s10236-011-0377-8.

Zhang, Z., Tian, J., Qiu, B., Zhao, W., Chang, P., Wu, D., Wan, X., 2016. Observed 3D structure, generation, and dissipation of oceanic mesoscale eddies in the South China Sea. Sci. Rep.-UK 6 (1), 11 pp., http://dx.doi.org/10.1038/srep24349.

Zheng, Z., Ho, C., Zheng, Q., Lo, Y., Kuo, N., Gopalakrishnan, G., 2010. Effects of preexisting cyclonic eddies on upper ocean responses to Category 5 typhoons in the western North Pacific. J. Geophys. Res. 115 (C9), 11 pp., http://dx.doi.org/10.1029/2009JC005562.

Oceanologia (2019) 61, 276–290

Available online at www.sciencedirect.com

ScienceDirect

journal homepage: www.journals.elsevier.com/oceanologia/

ORIGINAL RESEARCH ARTICLE

A cost-effective method for estimating long-term effects of waves on beach erosion with application to Sitia Bay, Crete

Flora E. Karathanasi [a,b,*], **Kostas A. Belibassakis** [a]

[a] *School of Naval Architecture & Marine Engineering, National Technical University of Athens, Athens, Greece*
[b] *Institute of Oceanography, Hellenic Centre for Marine Research, Anavyssos, Greece*

Received 24 July 2018; accepted 5 December 2018
Available online 19 December 2018

KEYWORDS
Beach erosion;
Bed level evolution;
Wave/current modelling;
Shields criterion;
Sitia-Crete coast

Summary Considering the significant role of beaches for the sea environment and welfare of coastal communities, a variety of process-based models are applied in order to examine and understand the interaction of hydrodynamic processes with seabed material at different time scales. However, a long-term view of this interaction requires a great amount of computational time. In this work a cost-effective methodology is proposed to surpass this shortcoming and estimate bed level evolution. The technique is relied on an objective criterion to assess spectral wave time series of wave height, period and direction and identify the wave conditions that contribute to the initiation of sediment movement. After implementing the so-called Shields criterion, the full wave climate is reduced to two classes of representative wave conditions: the over-critical ones, mainly responsible for long-term erosion, and the sub-critical wave conditions. By applying a well-known process-based model, the representative wave conditions are used as input for the wave-current-sediment transport simulation and rates of bed level changes are obtained, on the basis of which the long-term effects of waves on beach erosion are estimated. Taking into account that erosion is a threatening phenomenon along the sandy beaches of Mediterranean Sea, the present method is demonstrated at a sandy coast of Sitia Bay, Crete. The bed levels derived from the proposed methodology and the full time series are compared. The results indicate reasonable agreement at the selected locations with deviations under 7%, and conformity of the tendency of seabed evolution, rendering the new methodology a useful tool.

* Corresponding author at: School of Naval Architecture and Marine Engineering, National Technical University of Athens, Zografos 15773, Athens, Greece. Tel.: +30 210 7721103
E-mail address: flora@mail.ntua.gr (F.E. Karathanasi).
Peer review under the responsibility of Institute of Oceanology of the Polish Academy of Sciences.

ELSEVIER | Production and hosting by Elsevier

https://doi.org/10.1016/j.oceano.2018.12.001

1. Introduction

Understanding erosion and accretion processes in a coastal area and accurately forecasting coastal evolution is essential in order to prioritize mitigation measures and manage planning decisions and prospective interventions as regards the protection of the coastal environment and its sustainable development. Numerous scientific studies have been conducted over the past decades dealing with coastal erosion and morphological changes; see, for instance, the recent review papers on coastal erosion under climate change scenarios by Ranasinghe (2016) and Toimil et al. (2017). Nevertheless, it is yet a challenging field of research since the sufficient and proper understanding of the underlying processes and dynamics is still lacking due to the complex and non-linear interactions of the involved processes; see, e.g. Davidson-Arnott (2009).

Process-based models have been widely used to simulate morphological processes and estimate sediment transport rates and bathymetry evolution for different time scales during recent years. Such models are based on mathematical formulation and assumptions in order to assess sediment transport processes, and are ideal for short-term simulations (hours to weeks); however, for medium- and long-term processes, they suffer from inherent constraints such as the high computational time, sensitivity to initial conditions and numerical instabilities. Some relevant and recent studies based on process-based models are the works of Ramakrishnan et al. (2018), who simulated morphological changes under normal wave conditions and storm events during a four-month period along a pocket beach at the east coast of India, of Dubarbier et al. (2015), who simulated beach profile evolution on the timescales from hours to months encompassing both slow onshore and rapid offshore sandbar migration events at two sites, and of Corbella and Stretch (2012), who examined the impacts of decadal trends on storm induced beach erosion based on a non-stationary multivariate statistical model combined with three process-based models.

In order to reduce computational time that is required for simulations of morphological models with time period of one year or greater, retaining an acceptable accuracy of the predictions, wave input reduction methods have been suggested. The core idea of these techniques is to reduce the size of the wave input data at a coastal area of interest with some sets of representative wave conditions based on specific criteria. A detailed analysis of five techniques dealing with input reduction has been performed by Benedet et al. (2016). In that study, one-year reference wave data representing the full wave climate at a south-east coast of Florida, USA, were transformed to four different numbers of representative wave conditions. Specifically, the full wave climate was reduced to 30, 20, 12 and 6 representative wave cases in order to run the corresponding models in sequence for a smaller time period; these numbers were selected based on sensitivity tests carried out by the authors. According to the frequency of occurrence of each wave condition in a full year, the sediment transport patterns were estimated for each proposed technique along with the simulation of the detailed wave climate, used as benchmark. The results obtained by each technique were compared with the corresponding results of the benchmark in terms of root mean square error. The analysis showed that for a small number of wave conditions (i.e. 12 and 6) the method with the best performance is the "Energy Flux Method", where directional bins of equal wave energy flux were formed; on the other hand, as the size of representative wave cases was increasing, all methods had a similar performance. Furthermore, Walstra et al. (2013) introduced an input reduction method at two wave-dominated coasts with dissimilar long-term offshore wave direction characteristics. Their analysis also demonstrated that apart from storm events, which contribute to the largest morphological changes, it is essential to preserve in the reduced wave climate the wave energy conditions with low or intermediate intensity for a more realistic long-term sandbar behaviour.

The same rationale is also adopted when examining coastal erosion in terms of wave action, where there are two main viewpoints. The first one refers to the episodic events (e.g. storms, tsunamis) that act for a short time window (hours to some days) but can cause significant and sudden damages, from loss of land and destruction of coastal infrastructure to direct impacts on coastal communities and the adjacent coastal ecosystems, among others. The second one deals with the accumulative wave action, where erosion behaviour is governed by the interaction of storm events and calm periods. In a previous work by the authors (Belibassakis and Karathanasi, 2017), the first viewpoint was examined with application to the Varkiza coast in the Saronic Gulf (western Aegean Sea); the present study focuses on the second viewpoint. To this end, in this work a cost-effective method is introduced based on the use of process-based models combined with the philosophy of wave input reduction techniques. The proposed technique relies wave input reduction on a grain motion initiation criterion in terms of orbital velocity, from which two basic categories are separated: (i) the one dealing with wave conditions that contribute to the wave-induced initiation of sediment movement at depths around the closure depth, and (ii) the other one including the low energetic wave conditions. Other reference works as regards the onset of sediment motion under waves are those of Hallermeier (1980), Soulsby (1997), and Van Rijn (1993). Consequently, the computational efficiency of estimating bed level can be drastically increased with the proposed methodology instead of using the full wave time series, while the accuracy level can be retained into acceptable limits.

As an application the coast of Sitia, in the eastern part of Crete Isl., is examined as a specific case study. The main reasons for selecting this particular coast lie in its vulnerability to erosion phenomena and its touristic character; see Fig. 1(a). Specifically, a recent study (Alexandrakis et al., 2015) based on aerial photographs between 1945 and 2014, indicated that the coastline has been retreated for a distance of the order of 45 m (representing the maximum value) while in Foteinis and Synolakis (2015), the mean coastal retreat rate at Sitia was estimated at 0.32 m/yr, among the highest erosion rates in Crete, utilizing aerial photographs (1960–2004), satellite images (2003–2012) and field survey measurements (2009–2012). Indicatively, aerial and satellite images from Google Earth show that 7 m is the maximum loss during the period 2002–2015; see also Fig. 1(b). In 2016, the collapse of the retaining wall of the coastal road brought the erosion matter to a climax leaving some villages in the

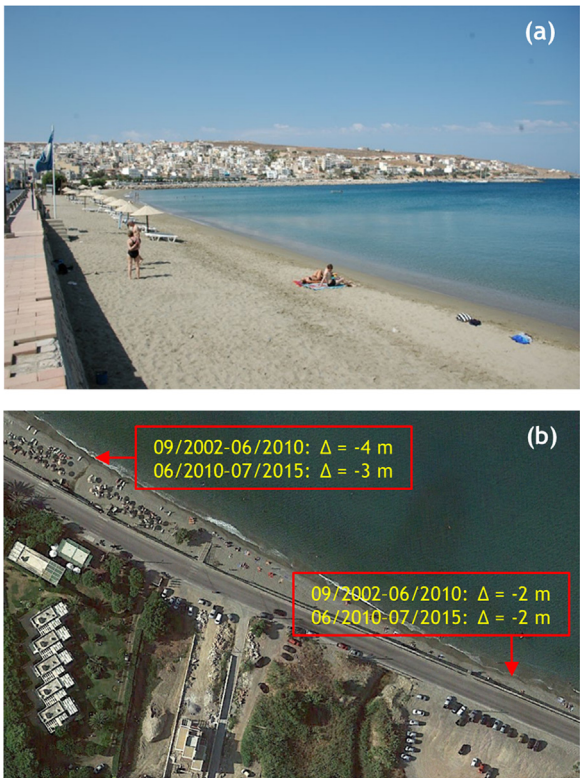

Figure 1 (a) Western part of the beach at Sitia Bay. (b) Coastline retreat at the central part.

north-eastern part inaccessible until the end of repair works. However, from Google Earth images, it seems that in 2017 there was a widening along the beach, which can be attributed to natural processes since no beach nourishment took place. Additionally, the touristic activities in the wider area have become more intensive the last years rendering confronting, prediction and management of erosion even more imperative. A preliminary study as regards the sediment transport patterns under two alternative wave scenarios (i.e. mean sea state, harsh wave conditions that contribute to initiation of sediment motion) and three different topographies of the seabed (i.e. current state, two submerged breakwaters at the isobaths of 5 m, port extension in the sea) has been conducted by the same authors at the same study area (Karathanasi et al., 2017). One of the main conclusions of this study as regards the harsh wave conditions for all the examined seabed topographies was the clockwise current circulation that contributed to the sediment movement westward.

Since the availability of in situ wave measurements from oceanographic buoys is rather limited in space and time, the analysis is based on statistical parameters, like significant wave height and peak period, derived from wave models that are quickly accessed nowadays. Thereupon, in this study time series of wave statistical parameters are derived from the Mediterranean Sea Waves forecast system, which is based on the third-generation wave model WAM Cycle 4.5.4 (Günther and Behrens, 2012). Moreover, current velocity time series are obtained from the Med-currents system, whose equations are solved by an Ocean General Circulation Model based on the NEMO model (version 3.6); for more details, see Clementi et al. (2017). Both datasets can be accessed at http://marine.copernicus.eu/services-portfolio/access-to-products/. The process-based numerical model used for the detailed description of currents, waves, sediment transport and bed level update and their interdependence is the MIKE 21 Coupled Model FM (DHI, 2016). The same numerical wave model has been applied in relevant recent studies; see, e.g. Aouiche et al. (2016), Belibassakis and Karathanasi (2017), Daghigh et al. (2017), Gad et al. (2018), and Gharibreza et al. (2018).

The structure of the present paper is as follows: in Section 2, the proposed methodology is presented, which provides the bed level for a specified time period, after appropriately reducing the available wave time series. A detailed description of the study area is given in Section 3 and an overview of the model setup, including the bathymetry of the model domain, the analyzed wave climate and the input data for the various modules can be found in Section 4. Subsequently, in Section 5, the results of this procedure are presented and compared with the results from the simulation of the full time series. Discussion and further comments are given in Section 6, and in the final section, the main findings of this work are summarized along with some suggestions for further research.

2. Methodology

When a long-term time series of wave data is available nearshore, the core of the proposed methodology is based on the rationale of wave input reduction. The wave conditions that contribute to the onset of sediment motion below the closure depth of a sandy bed level, called hereafter “over-critical wave conditions”, form the determinative factor of this analysis. With the term “closure depth”, we define the transition zone in which the influence of waves on bed stresses, and hence sediment transport, is significantly lower than within the region of wave breaking (i.e. surf zone) or the region where the effects of wave energy dissipation are dominant (i.e. upper shoreface zone) (Ortiz and Ashton, 2016). Hence the underlying assumption as regards closure depth is its dependence on the harsh wave conditions. In this context, it is possible to significantly reduce computation times and speed up the whole analysis. The proposed approach uses the wave statistical parameters such as significant wave height H_S and peak period T_P, along with some basic hydrodynamic parameters (e.g. wave height, sea water density) and sediment characteristics (e.g. d_{50}, density of sediment), to estimate bottom orbital velocity u_b and wave shear velocity u_{*w}, rendering the methodology fully applicable and handy, since in the majority of the cases such summary data are available (e.g. wave model outputs, archived wave data).

Before proceeding with the description of the methodology, for the sake of simplicity, let us first provide the appropriate definitions regarding the points used in the analysis that are mentioned in the subsequent sections:

- the offshore points that correspond to the available wave time series, forming the input for the boundary of the outer model domain with the coarse spatial resolution, are denoted by P_{out};

- the points that are used as input for the boundaries of the inner model domain with the fine spatial resolution, obtained after applying a wave transformation scheme, are denoted by P_{inn}, and the middle point of the northern boundary is denoted by $P_{inn,m}$;
- the point that represents the closure depth is denoted by P_{cd}, and the corresponding depth h_{cd} is defined by the Hallermeier (1981) equation given by:

$$h_{cd} = 2.28H_{eff} - 68.5\left(\frac{H_{eff}^2}{gT_{eff}^2}\right), \tag{1}$$

where H_{eff} is the effective wave height, exceeded 12 h in a single year (i.e. the greatest 0.137% waves during a year) and T_{eff} is the associated wave period.

2.1. Description of the cost-effective method

According to linear wave theory, the bottom (or near-bed) orbital velocity of a monochromatic wave is related to water depth and surface wave conditions as follows:

$$u_b = \frac{\pi H}{T\sinh(kh)}, \tag{2}$$

where H is the wave height, T is the wave period and $k = 2\pi/\lambda$ is the wavenumber (λ is the wavelength) and h is the water depth. Eq. (2) is extended for multichromatic waves in the coastal environment by applying it for all frequencies of the wave spectrum corresponding to each sea state and summing the components. Thus, a representative bottom orbital velocity u_{br} is calculated; see, e.g. Madsen (1994). Following the method suggested by Wiberg and Sherwood (2008), a generic form of the wave spectrum is used to estimate bottom orbital velocity from the values of H_S and T_P of the reference wave data (i.e. the entire time series of the available wave data) at a point that represents the closure depth, denoted by P_{cd}. Among the commonly used wind-generated wave spectra, JONSWAP spectrum (Hasselmann et al., 1973) is adopted,

$$S_\eta(\omega) = B\left(\frac{H_S}{4}\right)^2 \frac{\omega_p^4}{\omega^5}\exp\left[-\frac{5}{4}\left(\frac{\omega}{\omega_P}\right)^{-4}\right]\gamma^{(\omega/\omega_P)}, \tag{3}$$

where $\omega_P = 2\pi/T_P$ is the peak angular frequency, $B = 3.29$, $\gamma = 3.3$ and $\phi(\omega/\omega_P) = \exp[-0.5\beta^{-2}(\omega/\omega_P - 1)^2]$ with $\beta = 0.07$ for $\omega \leq \omega_P$ and $\beta = 0.09$ for $\omega > \omega_P$.

The representative orbital velocity u_{br} is then calculated from the following relation

$$u_{br} = \sqrt{2\left(\sum_i S_{u,i}\Delta\omega_i\right)}, \tag{4}$$

with $S_{u,i} = \frac{4\pi^2}{T_i^2\sinh^2(k_i h)} S_{\eta,i}$.

For the sediment transport purposes, another important property of waves is the bed shear stress τ_{bw} that can be associated with u_b and a wave friction factor f_w by:

$$\tau_{bw} = \frac{1}{2}\rho_w f_w u_b^2, \tag{5}$$

where ρ_w is the sea water density. f_w is calculated by the following empirical relationship (Fredsøe and Deigaard, 1992):

$$f_w = \begin{cases} 0.04\frac{\alpha^{-0.25}}{k}, & \frac{\alpha}{k} > 50 \\ 0.4\frac{\alpha^{-0.75}}{k}, & \frac{\alpha}{k} < 50, \end{cases} \tag{6}$$

where $\alpha = 0.5H/\sinh(kh)$ is the wave orbital amplitude and k_N is the Nikuradse's bed roughness parameter equal to $2.5d_{50}$, where d_{50} is the median sediment grain diameter.

Wave shear velocity u_{*w} is defined as follows:

$$u_{*w} = \sqrt{\frac{\tau_{bw}}{\rho_w}}. \tag{7}$$

The dimensionless bed shear stress, i.e. the Shields parameter θ^*, defined as

$$\theta^* = \frac{u_{*w}^2}{(s-1)gd_{50}}, \tag{8}$$

with $s = \rho_s/\rho_w$ denoting the ratio between the density of bed material and sea water (ρ_s is the density of the sediment) and g denoting the acceleration caused by gravity (9.81 m/s^2), is used to indicate the lower threshold value for initiation of sediment motion for the cases that $\theta^* > \theta_{cr}$, where $\theta_{cr} = 0.045$ is the critical bed shear stress.

Based on the above threshold value of initiation of sediment movement, the proposed methodology can be applied on the available wave time series at P_{cd} in order to indicate the specific timesteps that represent these wave conditions yielding a value of θ^* higher than 0.045 (i.e. over-critical wave conditions). Let us note that in case the available wave time series is available at an offshore location, like P_{out} points, a wave transformation process should be necessarily implemented in order to obtain the corresponding time series at the closure depth. Having these over-critical wave conditions at P_{cd} to hand, the corresponding conditions at the boundary of the inner model need to be extracted, represented by $P_{inn,m}$. Since the temporal resolution of the wave time series is 1 hour and given the distance between the offshore boundary (of the inner model) and P_{cd} ($\sim$1.6 km), the over-critical wave conditions at the boundary of the inner model that contribute to the initiation of sediment motion are identified based on the same timestep that gives each over-critical wave condition at P_{cd}. Then, these over-critical conditions are classified at $P_{inn,m}$ into specific intervals of H_S and T_P (0.5 m and 1 s, respectively) with equidistant binning (i.e. constant bin-size) and the corresponding mean wave direction θ_m is calculated for each class. This schematization (into (H_S, T_P, θ_m) triplets) is essential in order to proceed with the proposed methodology described in detail in the remaining part of this section.

Apart from the over-critical wave conditions, in which the morphological changes are large, the conditions where wave-induced currents are dominant should be additionally considered for a more realistic long-term behaviour of bed level. Assuming that waves below 0.5 m at the boundary of the inner model do not produce significant erosion/accretion patterns in the shore, the calm wave climate, called hereafter "sub-critical wave conditions", is grossly classified for values of H_S smaller than the threshold values and higher than 0.5 m. In this case, the intervals for H_S remain 0.5 m and for T_P the interval is varying (from 1 s to 4 s). The corresponding mean wave directions θ_m for the selected pairs (H_S, T_P) is also calculated.

The final triplets of both the over- and sub-critical wave conditions comprise the input for MIKE 21 Coupled Model Flexible Mesh (called hereafter MIKE21 CFM) simulations, which is the process-based model used in this work; see also Sections 4 and 5. From these simulations the rate of bed level change q is extracted for a 2-week simulation period with 1-hour timestep. This time period allows a detailed sediment response for the specific triplets and a more accurate estimation of a mean rate q. Let us note that the rates estimated for the over- and sub-critical wave conditions are appropriately weighted based on the frequency of occurrence of each selected class.

After the schematization of the over- and sub-critical wave conditions, from the simulation results, the rate of bed level change is estimated based on the sediment continuity equation. The mean rate of bed level change q [m/day] for each triplet is calculated by

$$a = \frac{\sum_{i=2}^{n} q_i}{n-1}, \tag{9}$$

where n is the total number of timesteps during the 2-week simulation period. The rate of the first timestep q_1 is considered as an initialization rate of the simulations and for this reason, it is excluded from Eq. (9).

For the proposed methodology, the bed level is estimated by

$$h(jt) = h(jt-1) + q, \quad j = 1, \ldots, n, \tag{10}$$

at the tth 1-hour interval for each (H_S, T_P, θ_m) triplet.

Based on the above mentioned description and definitions, the frame of the cost-effective methodology is presented in Fig. 2. Recapitulating the steps that should be followed for implementing the proposed methodology, the following key-aspects should be addressed:

1. Obtain wave time series at P_{inn} points and P_{cd}, if wave data are only available offshore;
2. Calculate bottom orbital velocity, wave shear velocity and bed shear stress at P_{cd};
3. If $\theta^* > \theta_{cr}$ at P_{cd}, then identify the corresponding values of H_S and T_P at P_{cd}. Based on the timestep of each pair, extract the corresponding over-critical values of (H_S, T_P) at $P_{inn,m}$. Then, group these pairs and calculate mean value of θ_m for each class;
4. If $\theta^* < \theta_{cr}$ at P_{cd}, then identify these values of H_S that are both higher than 0.5 m and different from the over-critical values (from step 3) along with the corresponding values of T_P. Then, group these pairs and calculate mean value of θ_m for each class;
5. Calculate the rates of bed level change with MIKE21 CFM for both over- and sub-critical values for each (H_S, T_P, θ_m) triplet;
6. Finally, calculate bed level at any location of the inner model domain via Eq. (10).

3. Study area

The area of interest is Sitia beach that is located in the north-eastern part of the Prefecture of Lassithi, Crete, on the west side of the homonymous bay; see Fig. 3. It is a 2-km long beach with variable width of maximum value around 35 m, and exhibits a typical U-shape in the NW-SE orientation. Due to the shape and orientation of the examined beach, the wave action is confined to the north and north-eastern directions, which is the primary factor for the settlement of sediments. At the western part of the beach there is a river system (Pantelis- or Stomios-river), following dry and wet periods, that discharges into the bay, and there is also the homonymous port that can accommodate both small fishing vessels and larger merchant and passenger vessels.

Fig. 3 also presents an overview of the points mentioned in Section 2 for the case study of this work. Let us note that in this case study h_{cd} = 6.5 m, thus P_{cd} was selected on the isobath of 6.5 m and in the middle of the longshore direction of the beach.

The homonym town, Sitia, has become a tourist attraction the last decades, mainly during the summer period, while tourist infrastructures (e.g. hotels, restaurants), and in general human activities, place pressure on the coastal environment. Moreover, the main road that connects Sitia with other tourist destinations at the eastern part of the island, such as the palm forest Vai, was developed to a great extent beside the coastal front.

To this end, erosion phenomena are evident due to both the intensive residential and infrastructure-based development of the wider area along with the physical conditions that seem to be more frequent and of longer duration.

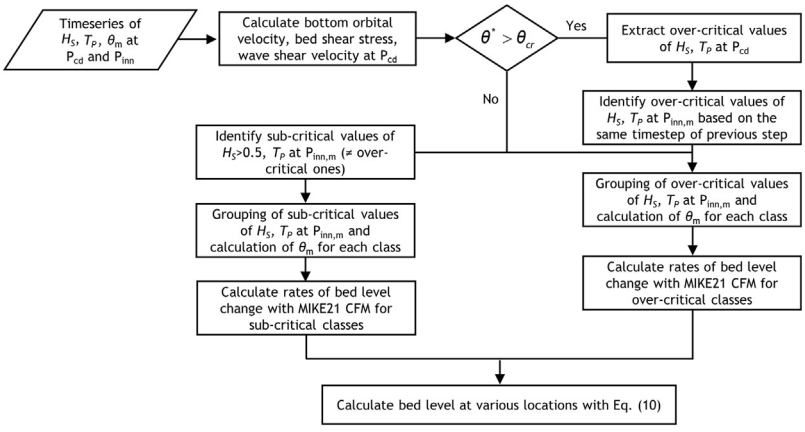

Figure 2 Flow chart of the proposed methodology.

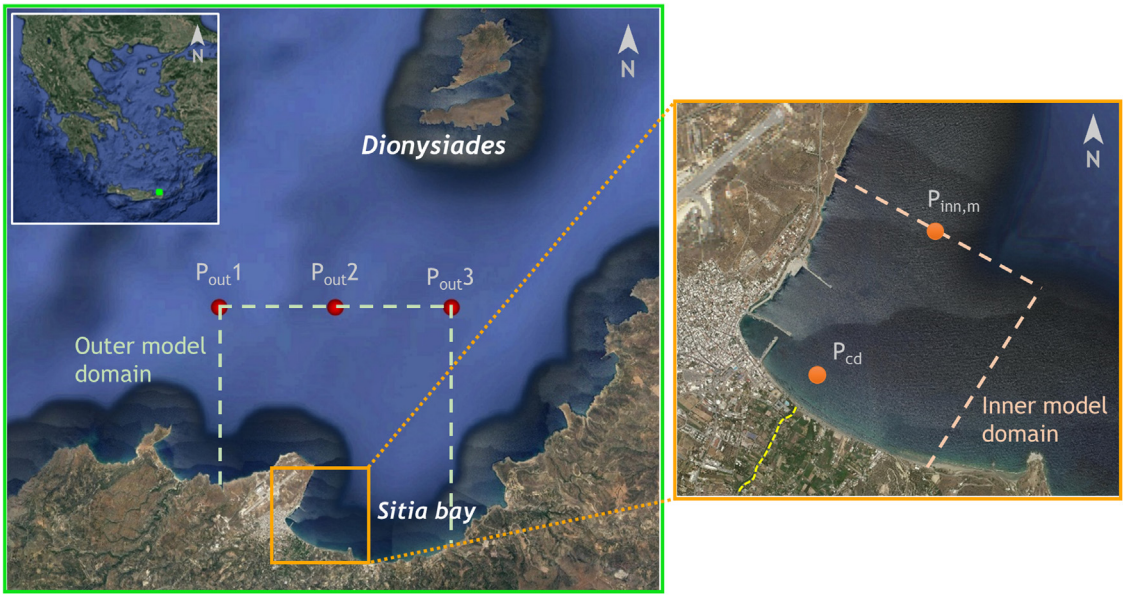

Figure 3 Aerial map of Sitia Bay along with the offshore locations of the input data for the outer model domain (left map), and the study area of Sitia beach (inner model domain) along with the locations of $P_{inn,m}$ and P_{cd} (right map) used in the analysis. *Source*: Google Earth.

Specifically, at the end of 2016 the front of the coastal road that is contiguous to the eastern part of the beach collapsed after the accumulative action of intense weather conditions that took place the last few years, causing several problems and safety issues to the local residents and tourists. Moreover, the sediment supply of the beach is relatively limited while the construction of the adjacent harbour at the western part of the coast, in order to serve the needs for tourism and fishing, puts additional pressures and intensifies erosion rates.

4. Model setup

As mentioned above, the process-based numerical model that is used in this study is MIKE21 CFM developed by the Danish Hydraulic Institute (DHI). MIKE21 CFM is a depth-averaged two-dimensional numerical model used to study and simulate a wide range of coastal hydrodynamic problems including the description and interaction of the relevant processes, such as currents, waves and sediment transport in coastal areas, among others. This numerical modelling software package includes several interrelated modules, of which the following are used for the purpose of this study: (i) the hydrodynamic (HD) module; (ii) the spectral wave (SW) module, and; (iii) the sand transport (ST) module. Through a dynamic coupling, hydrodynamic and spectral wave computations are performed simultaneously to calculate sediment transport rates and update bathymetry at each timestep. Specifically, sediment modelling is established on: (i) a depth-averaged hydrodynamic model, based on the depth-integrated incompressible Reynolds averaged Navier-Stokes equations; (ii) a phase-averaged wave model, based on the wave action conservation equation, and; (iii) sediment transport tables calculated in advance for every combination of current, wave, bathymetry and sediment conditions appearing in the simulation; for a more detailed description of the three modules, see Belibassakis and Karathanasi (2017).

In the following subsections, the boundary conditions and the model parameters used for the model simulations are described for each module, along with some necessary information as regards the model grid and wave climate.

4.1. Bathymetry and unstructured grid

As already mentioned, in this analysis, the outer model domain is used for the transformation of the wave conditions from the available wave time series towards the shore. This model domain covers a distance of 7.5 km in the longshore direction and 7.8 km for the cross-shore one. The total number of triangular elements in the outer domain is 1,284 with 759 nodes while the maximum size of the elements is approximately 0.12 km^2; see also Fig. 4(a). The bathymetry of the outer model domain presented in Fig. 4 (b), shows that the seabed topography is quite mild. From the shoreline up to the isobath of −75 m, the contours are parallel and the maximum depth (−226 m) is observed at the north-western part of the domain.

As regards the inner model domain, it is divided into two nested grid domains, going gradually from the outer area with the lower resolution (i.e. level 1) up to the computational grid with the highest resolution (i.e. level 2), where the smaller triangular elements represent areas where the accuracy in the wave, current and sediment transport calculations are important; see also Fig. 5(a) for the representation of the different levels and the final mesh generation of the examined area. Specifically, level 1 extends both in the longshore and cross-shore directions approximately 1.7 km with the area of each triangular element not exceeding 6,580 m^2. Let us note in advance that the appropriate forces are imposed at the boundaries of the outmost level (i.e. level 1) for the generation of

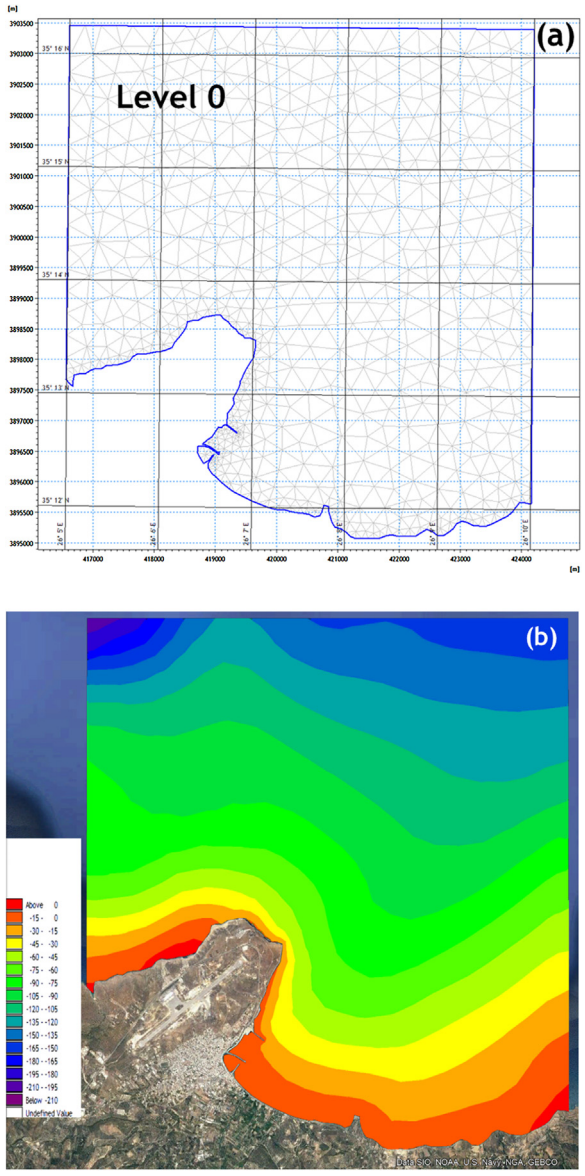

Figure 4 (a) Mesh with triangles for the outer model. (b) The bathymetry of the outer model domain.

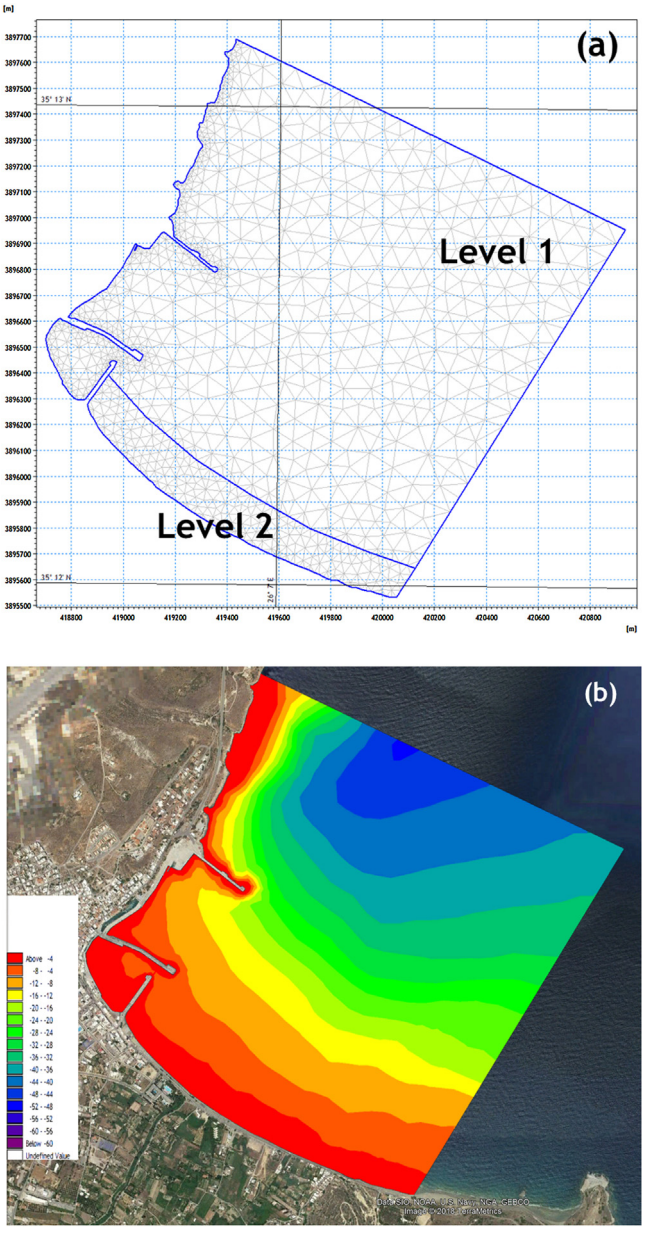

Figure 5 (a) Mesh with triangles using two levels for the inner model domain. (b) The inner model domain showing the bathymetry of the examined area.

flow and wave conditions, which in turn define the corresponding boundary conditions of the inmost level (i.e. level 2). The second, and more detailed, computational grid (level 2) extends in the longshore and cross-shore directions 1,400 m and 140 m, respectively, with maximum area of each triangular cell up to 1,050 m^2. The total number of grid cells in the inner domain is 2,135 with 1,282 nodes.

The bathymetry data of the inner model domain were digitized from maps of different spatial scales obtained from the Hellenic Navy Hydrographic Service (HNHS). The above data were enriched for the outer model domain with bathymetric grid points from the European Marine Observation and Data Network (EMODnet) Digital Bathymetry database with 1/8 of an arc minute (~230 m) resolution (Marine Information Service, 2016).

In Fig. 5(b), the 2D bathymetric representation of the study area is displayed in Google Earth for levels 1 and 2. The isobaths from −20 m to lower depths are generally parallel to the shoreline and are evenly flattened going from the offshore part towards the shore. The highest depth (close to −50 m) is encountered in the north-western part of level 1 while the 10-m isobath is about 410 m from the coastline. In the eastern part of Sitia beach, there are beachrocks aligned parallel to the shoreline starting approximately from −1.5 m depth and ending to the coast. The formations act as natural submerged breakwaters mitigating erosion phenomena at this part of the coast.

4.2. Wave conditions

As regards the wave characteristics of the wider study area, the analysis is relied on 1-year time series, between 01/01/

2016 and 31/12/2016, at the middle point of the boundary of the outer model, i.e. at $P_{out}2$ (see also Fig. 3, left map), with geographical coordinates 35.271°N–26.125°E, obtained from the Mediterranean Sea Waves database. The relevant information include significant wave height H_S, peak wave period T_P and mean wave direction θ_m (measured clockwise from north), with an 1-hour resolution. These time series were used as input for the wave propagation from the offshore to the near-shore using MIKE21 CFM (SW and HD modules). After this simulation, the spectral time series were extracted for the northern and eastern boundaries of the inner model domain (with the finest triangular elements), presented in the right map of Fig. 3, in order to be used as input for the rest simulations.

The basic statistical measures at $P_{out}2$ include mean value (*m*), standard deviation (*sd*), minimum (*min*) and maximum (*max*) values, 50th percentile (*p50*), skewness (*sk*) and kurtosis (*ku*), and the results are presented in Table 1. On average, the wave intensity is characterized low with mean values $m_{H_S} = 0.9$ m, $m_{T_P} = 5.08$ s and $m_{\theta_m} = 394.1°$. The most intense wave incident occurred on 6th February 2016 with $H_S = 4.8$ m and corresponding $T_P = 9.23$ s and $\theta_m = 344.4°$ during a two-day storm. The value of sk_{T_P} (0.23), close to zero, indicates that the distribution of the corresponding data is close to be symmetrical while the highest value of *ku* (7.1) is given by H_S indicating a sharp peak of the distribution.

As regards θ_m, the low value of *sd* (0.6) corresponds to a circular dataset that is highly concentrated, which can be also verified in Fig. 6, while *sk* value close to zero (−0.01) denotes a unimodal distribution. The wave rose of H_S at $P_{out}2$ is depicted in Fig. 6, along with the corresponding frequencies of occurrence. The scattering of wave directions is limited to the sector [285°, 15°] due to the topography and coast orientation of the study area with the prevailing wave directions coming from the north direction (sector [300°, 315°]), which are attributed to the very large fetch (390 km). The highest frequency of occurrence (13%) as regards wave propagation in the dominant direction is observed for values of H_S between 0.5 m and 1 m while the corresponding values of T_P exhibiting the highest frequency of occurrence are between 4 s and 6 s. Intense sea states ($H_S > 2.5$ m) with the highest frequency of occurrence (2%) correspond to the sector [345°, 0°].

4.3. Input data

For practical reasons, the period of the simulation is confined to one year, i.e. from January 1 to December 31, 2016. As already mentioned the bathymetry resolution for the inner model domain gets progressively finer as we move from level 1 to level 2, which is the area of interest as concerns the simulation results and the evaluation of the methodology. The timestep is set to $\Delta t = 3600$ s, equal with the time interval of the available time series. Prior to the description of the input data for the one-year wave time series, let it be mentioned that the authors kept some parameters at their default values since no in situ measurements were available for calibration of the model.

As regards HD module, the most essential input data include: wave radiation stress gradients that force the flows, bed resistance, eddy viscosity and boundary conditions. Eddy viscosity is based on the Smagorinsky coefficient with a constant value at 0.28, bed resistance expressed through the Manning number was fixed (32 m$^{1/3}$/s) in the entire inner model domain apart from its south-eastern part due to the presence of bedrock formations while density is not updated during the simulation (barotropic mode). Let us note that tidal potential is very low in Sitia Bay thus it is not considered in the model setup. At the open boundaries, current velocities (varying in time and along boundary) are used as input obtained from the simulation results of the outer model while at the closed boundary, the normal velocity component is set to zero, assuming full slip boundary conditions.

As in the HD module, the instationary mode as regards time formulation was adopted in the SW module as well, with a directionally decoupled parametric formulation. The conditions at the open boundaries (at the north and east side of the model domain) were kept constant in space (along the boundary line) and varying in time while the boundary data consisted of significant wave height H_S, peak wave period T_P, mean wave direction θ_m and directional spreading index *n*. Additional model parameters were wave breaking specified by the gamma parameter $\gamma_{wb} = 0.8$ constant in space, bottom friction specified by the Nikurdase roughness k_N, which was varying in space ranging from 6.25 mm to 0.25 for level 1, and 1.9 mm for level 2 while for the bedrock formations the value of 62.5 mm was selected.

Regarding the setting up of the ST module, sediment transport rates and bed level changes under the combined action of waves and currents are calculated through interpolation of sediment transport tables. These tables are generated in advance and include the following parameters: root-mean square wave height, peak period, current speed, wave height-to-water depth ratio, angle between current and waves, median grain diameter d_{50} and sediment grading. The ST calculations are activated at the initial th timestep while the timestep factor is set to 1, meaning that sediment transport rates and bed level are calculated every timestep. Apart from the flow (HD) and wave (SW) forcings, the specification of sediment properties and the considerations of morphological impact on hydrodynamics are two important features that need to be provided for the area of interest. To this end, as regards the granulometric composition of the bottom sediments in the study area, the sea bottom consists

Table 1 Basic statistics of the wave parameters obtained from the spectral time series at $P_{out}2$ between 01/2016 and 12/2016. Square brackets denote units of the corresponding wave parameter where necessary.

	N	*m*	*sd*	*min*	*p50*	*max*	*sk*	*ku*
H_S [m]	8784	0.9	0.7	0.1	0.7	4.8	1.8 [–]	7.1 [–]
T_P [s]		5.08	1.53	1.37	5.21	10.15	0.23 [–]	2.9 [–]
θ_m [°]		394.1	0.6 [–]	–	396.7	–	−0.01 [–]	0.7 [–]

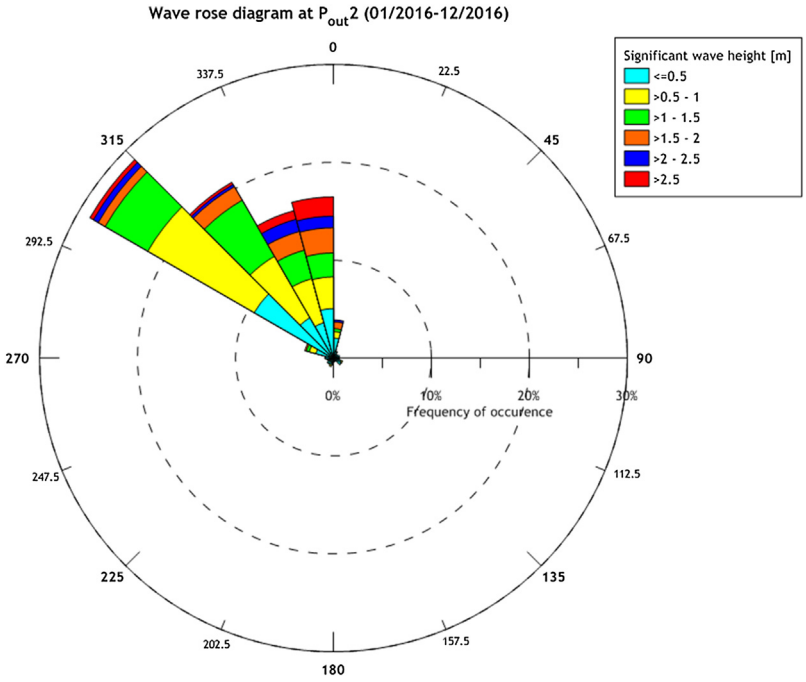

Figure 6 Rose diagram of significant wave height and wave direction at $P_{out}2$ for the period 01/2016—12/2016. Intervals for H_S and θ_m are ΔH_S = 0.5 m and $\Delta\theta_m = 15^\circ$, respectively.

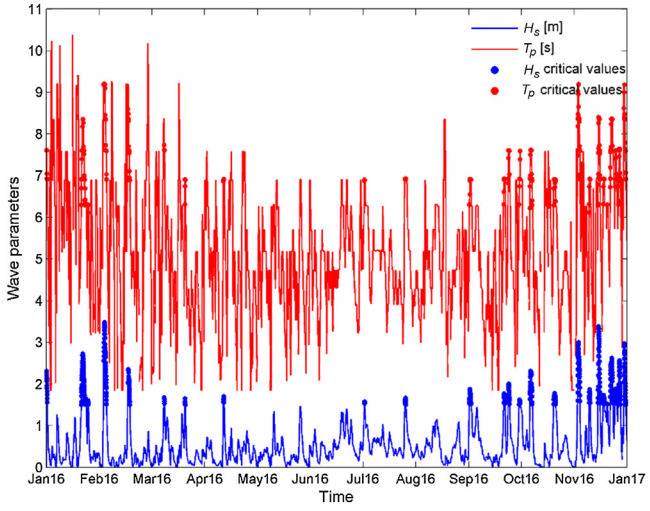

Figure 7 Time series of H_S and T_P at $P_{inn,m}$ for the year 2016. Blue and red dots indicate over-critical values of H_S and T_P, respectively.

of sand with an average diameter of d_{50} around 0.65—0.85 mm up to the isodepths of 1.5—2 m and with d_{50} between 0.08 mm and 0.25 mm for depths above 15 m (Anagnostou et al., 2017). Sediment grading was kept fixed, equal to 1.45, at the entire model domain. The initial bed layer thickness for all levels was set to 0.5 m apart from the bedrock part (0.0001 m).

In terms of the representative wave conditions (both over- and sub-critical ones), the parameters of the model setup remained the same except for the time formulation (quasi stationary mode) and the start time of the ST calculations since all modules were synchronized to start at the same timestep.

5. Results

5.1. Representative wave conditions

In this work, the time period of the analyzed wave data is confined between 01/2016 and 12/2016; henceforth, when

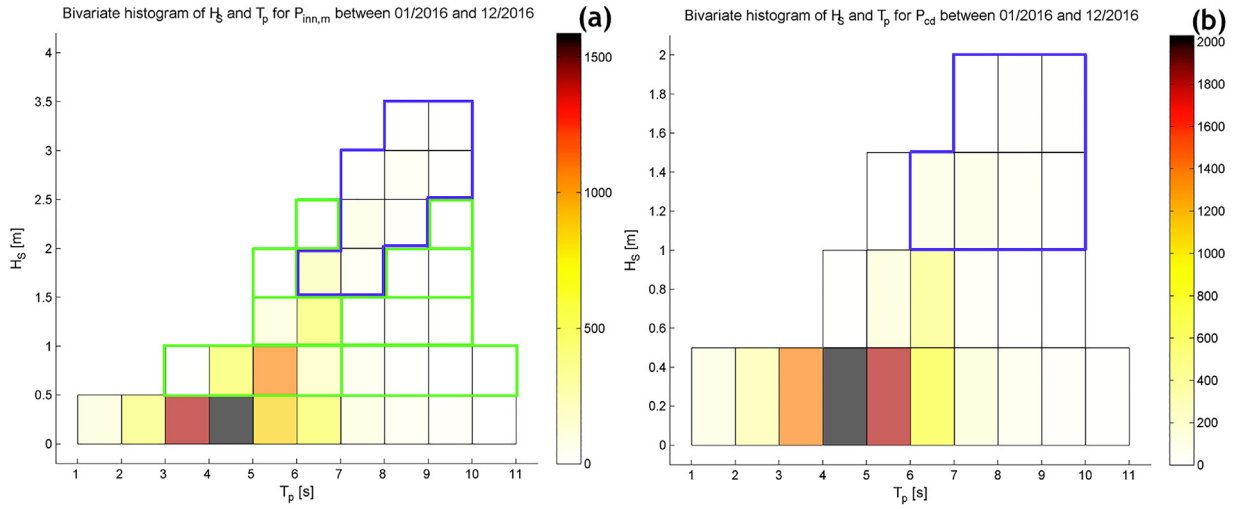

Figure 8 Bivariate histogram of (H_S, T_P) for (a) $P_{inn,m}$, and (b) P_{cd} for the year 2016. The blue closed polygon indicates the over-critical values and the green rectangles indicate the sub-critical pairs.

Table 2 Name of location, geographical coordinates, depth and distance from shore for the examined locations.

Location	Geographical coordinates (long., lat.) [°]	Depth [m]	Distance from shore [m]
A	(26.1090°, 35.2060°)	−1.23	26
B	(26.1101°, 35.2050°)	−1.42	38
C	(26.1113°, 35.2041°)	−1.38	37
D	(26.1129°, 35.2030°)	−1.08	37
E	(26.1143°, 35.2024°)	−1.57	41
F	(26.1158°, 35.2017°)	−1.02	39
G	(26.1172°, 35.2013°)	−0.87	40
H	(26.1188°, 35.2007°)	−0.58	45

we refer to the full time series of 2016 we use the term "reference wave data". The time series of the reference wave data for H_S and T_P at $P_{inn,m}$ is presented in Fig. 7. Consecutive intense wave conditions, with H_S above 1.5 m, occurred mainly during the last two months of the examined year. In the majority of the timesteps, high values of H_S correspond to high values of T_P as regards the examined location, rendering these pairs candidates for the initiation motion of sediments. According to the methodology, the first step is to calculate representative orbital velocity, bed shear stress and wave shear velocity by using the H_S and T_P time series of P_{cd} by applying Eqs. (4), (5) and (8), respectively. Based on the calculation of the Shields parameter and its threshold value, the over-critical wave conditions at P_{cd} are determined. Classifying the reference wave data at P_{cd} into classes of H_S and T_P with intervals 0.5 m and 1 s, respectively, we obtain Fig. 8(b). From this figure it can be noticed that the lower threshold values for the onset of sediment transport, based on the Shields criterion, correspond to waves higher than 1 m with peak period between 6 s and 10 s and mean wave direction around 25°–29° as regards P_{cd}.

Identifying the corresponding wave conditions at the boundary of the inner model, i.e. at $P_{inn,m}$, the corresponding threshold values are presented in Fig. 8(a) with the blue outline having minimum values 1.5 m and 6 s for H_S and T_P, respectively, and in the range $[355°,\ 5°]$ for θ_m. As a whole,

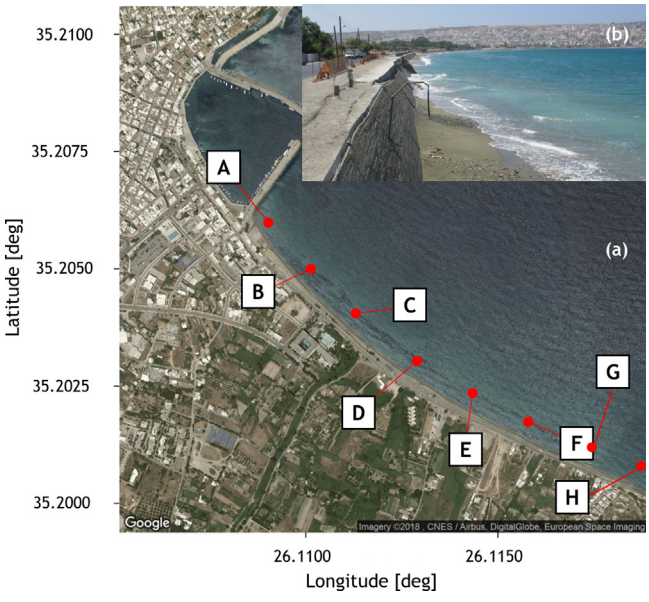

Figure 9 (a) Map of the examined area (from Google Earth) indicating the locations for the estimation of bed level based on the proposed methodology at Sitia beach. (b) Photo near location G indicating erosion problem.

nine representative intense wave conditions (i.e. over-critical pairs) were taken into account for the estimation of rates of bed level change over the examined period. From the same figure, the calm (sub-critical) wave conditions were derived by further grouping these classes into eight representative calm wave conditions with the same interval for H_S and a varying one for T_P, depending on the bivariate histogram. Let us remind that small values of H_S (i.e. $<$0.5 m) are not considered in the next steps of the technique since the model runs of the sensitivity analysis, performed by the same authors, demonstrated that such waves present almost negligible quantities of sediment transport rates. Altogether, 17 (H_S, T_P) pairs, along with the corresponding values of θ_m, are considered in the analysis, which were simulated separately.

5.2. Application of the methodology at the examined coast

Eight shallow locations are selected for examining the methodology described in Section 2; their geographical location, depth and distance from shore are given in Table 2. These points cover a distance of approximately 1,100 m along the coast with their in-between distance being around 150 m; their location on the map is shown in Fig. 9(a).

As regards the over-critical (H_S, T_P) pairs, the values of rates of bed level change for locations C, D, E, F, G and H are negative, with values between −0.003 m/day and −0.036 m/day. In general, the eastern locations (i.e. E, F, G and H) present the highest negative rates of bed level change while the western locations A and B are characterized by negative and positive rates of varying magnitude. With respect to the sub-critical (H_S, T_P) pairs, smaller, negative and positive, rates of bed level change are provided by all locations compared to the above pairs with the highest positive value (0.034 m/day) encountered at location E and the highest negative value (−0.033 m/day) at location F.

A more analytic representation for estimating bed level with the proposed methodology is given in Fig. 10 for location A, and in Fig. 11 for location F regarding specific representative (H_S, T_P) pairs. At the left panels of the above figures, the vertical lines denote the time windows of the over-critical (H_S, T_P) pairs in terms of sediment initiation; in the examined annual time scale, 30 time frames were identified by the methodology. At the right panels of the same figures, the rates of bed level change are plotted for the two different types of representative wave conditions (i.e. over- and sub-critical). As it was expected, the rates of bed level change for the over-critical (H_S, T_P) pair present higher values compared with the sub-critical pairs at both locations.

Specifically, as regards location A, the pattern of the over-critical wave case shows some resemblance with the sub-critical one; in both cases, the rate of bed level change strongly fluctuates during the 2-week simulation, taking mainly positive values, while at the 8th day of simulation a relative stabilization is evident. On the other hand, for location F, the rates present a dissimilar behaviour from location A; the rate of bed level change seems to be stabilized around zero after eight days of simulation for the over-critical representative wave conditions while it takes constantly negative values, after the second day of simulation, with bigger fluctuations for the sub-critical ones.

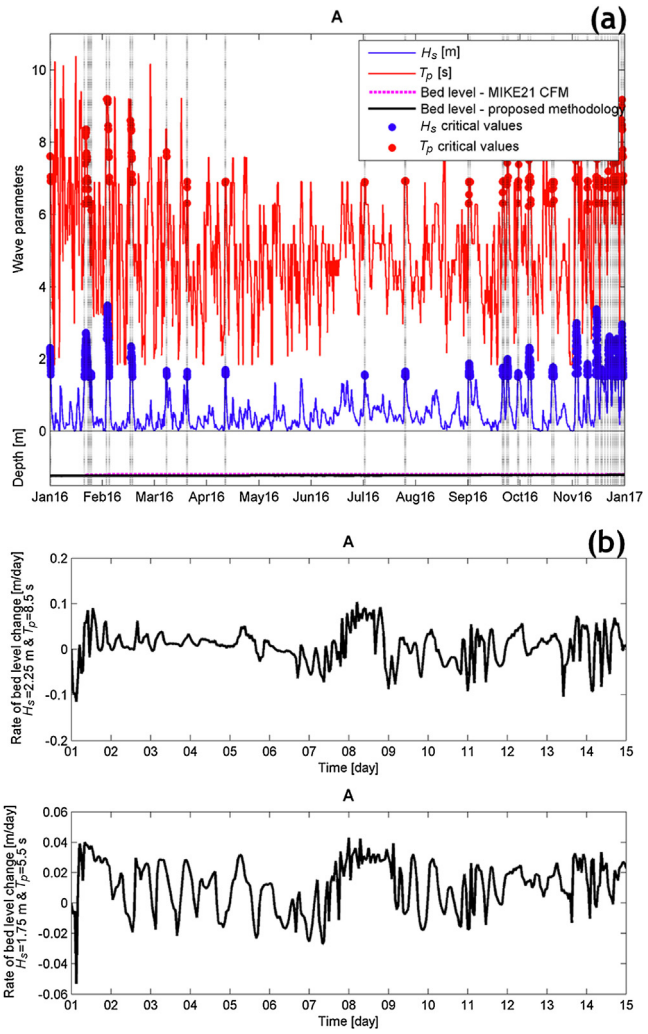

Figure 10 (a) Wave parameters along with bed levels obtained from the two approaches. (b) Rates of bed level change obtained from the proposed methodology for one over-critical and one sub-critical representative wave condition at point A.

In Fig. 12, the values of bed level obtained from the simulations results of MIKE21 CFM with the reference wave data as input, represented by the dashed line, and the proposed methodology, represented by the solid line, are plotted at the examined locations. From this figure, the following comments can be summarized:

- Locations B and D exhibit a very good agreement between the two approaches; throughout the year, the corresponding bed levels follow the same tendency and are very close with each other while as regards the last month, the deviation between the two bed level values is 0.7 cm and 0.4 cm, respectively, which are the smallest differences among the examined cases.
- Locations A and C, which follow a bathymetric profile with smooth to intermediate slopes (not shown here), and location H as well, exhibit medium-size deviations at the end of 2016, with values between 2.2 cm and 2.8 cm, respectively; however, the resemblance of the pattern that the two lines follow throughout the year is rather poor.

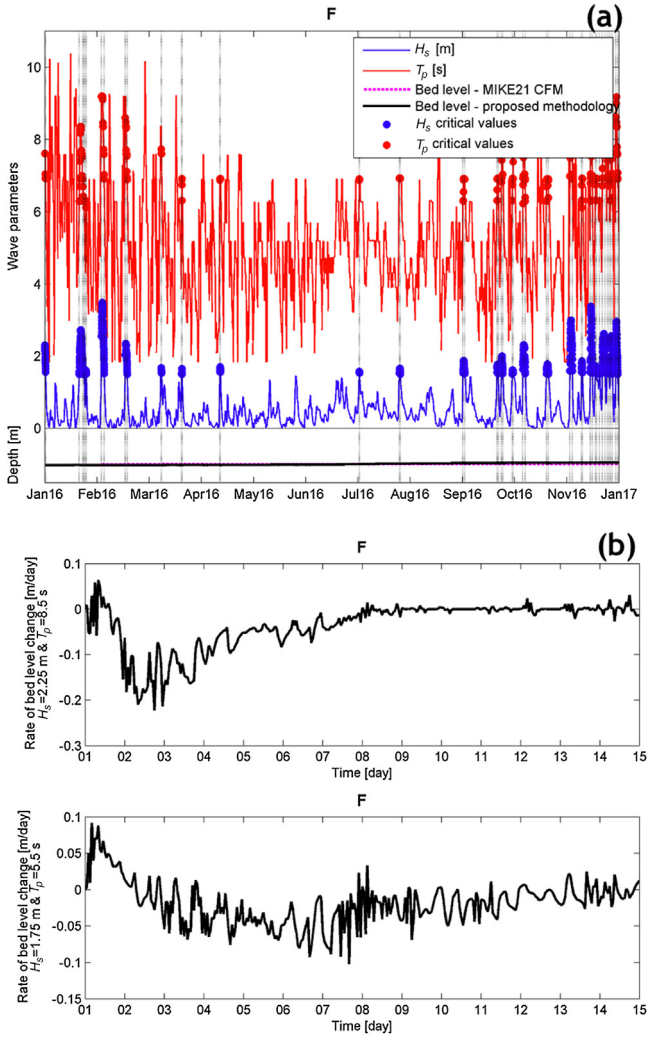

Figure 11 (a) Wave parameters along with bed levels obtained from the two approaches. (b) Rates of bed level change obtained from the proposed methodology for one over-critical and one sub-critical representative wave condition at point F.

- The locations E and F, with the latter having a steep bathymetric profile, exhibit the second largest deviation at the end of 2016 (4.5 cm) but the lines indicating the bed levels are in accordance in terms of the trend.
- Location G (see also Fig. 9(b)) presents the highest deviation (6.6 cm) compared with the reference time series.
- The bed level slope at locations A, B and C is positive indicating accretion in the western side of the Sitia coast while location D is characterized by a small negative slope (i.e. erosion pattern). Locations E and F present a steeper positive slope than the western locations, and locations G and H exhibit a higher negative slope than location D, implying more distinct erosion patterns. Overall, this behaviour coincides quite satisfactorily with the real situation encountered in the Sitia coast during the examined period, where the eastern part has been eroded to a great extent leading to the collapse of the retaining wall of the coastal road.

6. Discussion

The scope of this work was to reduce the reference wave data (of one-year duration) into two groups, i.e. (i) the over-critical (H_S, T_P) pairs that fulfil the Shields criterion leading to sediment initiation, and (ii) the sub-critical (H_S, T_P) pairs that do not fulfil this criterion, in order to significantly reduce computational times and compare the estimated bed level values with the full case. The results of the proposed methodology compared to the ones obtained from utilizing the entire time series of the available wave data present similar trends, and the differences remain under 7%.

In this connection, some notable aspects should be remarked. Various sources of uncertainties as regards the discrepancies can be attributed to the assumptions that are imposed throughout the adopted technique. For instance, turbulence caused by wave breaking is not considered although it can be a source of sediment mobilization. Other uncertainties deal with the calculation of bottom orbital velocity, related indirectly with the Shields criterion, that does not take into account the presence of currents while the assumed spectral form might also influence bottom orbital velocity. For more details in terms of the potential sources of error in the calculation of bottom orbital velocity from wave spectral parameters such as H_S and T_P, see further assumptions provided by Wiberg and Sherwood (2008). Furthermore, in the context of the sensitivity analysis, the authors followed an alternative way to estimate bottom orbital velocity and friction factor. The corresponding values derived from the simulation results of the reference wave data reached common over-critical combinations of H_S and T_P.

Another potential source of uncertainty could be the estimation method of the mean rates of bed level change. Many dissimilar ways were tested by the authors including mean rates from one week, different mean rates based on the (H_S, T_P) pairs and the examined location, mean rates calculated with a smaller time interval during the simulation runs etc. However, the adopted approach showed consistently better performance in terms of bed level prediction.

Let us also highlight that a more proper and fair comparison would be to assess both results from model simulations with in situ measurements of bed level at the site of interest. The absence of real measurements has a twofold effect: (i) it places the comparison into relative terms, and (ii) it renders model calibration infeasible, thus the model results per se should be used with caution. Nevertheless, such comparison is beyond the scopes of this study. Moreover, due to the lack of real measurements, it is also recommended not to apply speed-up techniques since they require careful calibration and validation.

Another worth-mentioning fact refers to the distribution of wave direction. Specifically, the range of wave directions that affect significantly the morphological (bed level) conditions of the examined beach is very narrow since in the majority northern wave directions are dominant. This feature along with the gentle bottom slope and the uniformity of the coast as regards its shape render the study area a simple and easy example to implement this methodology compared to more complex cases.

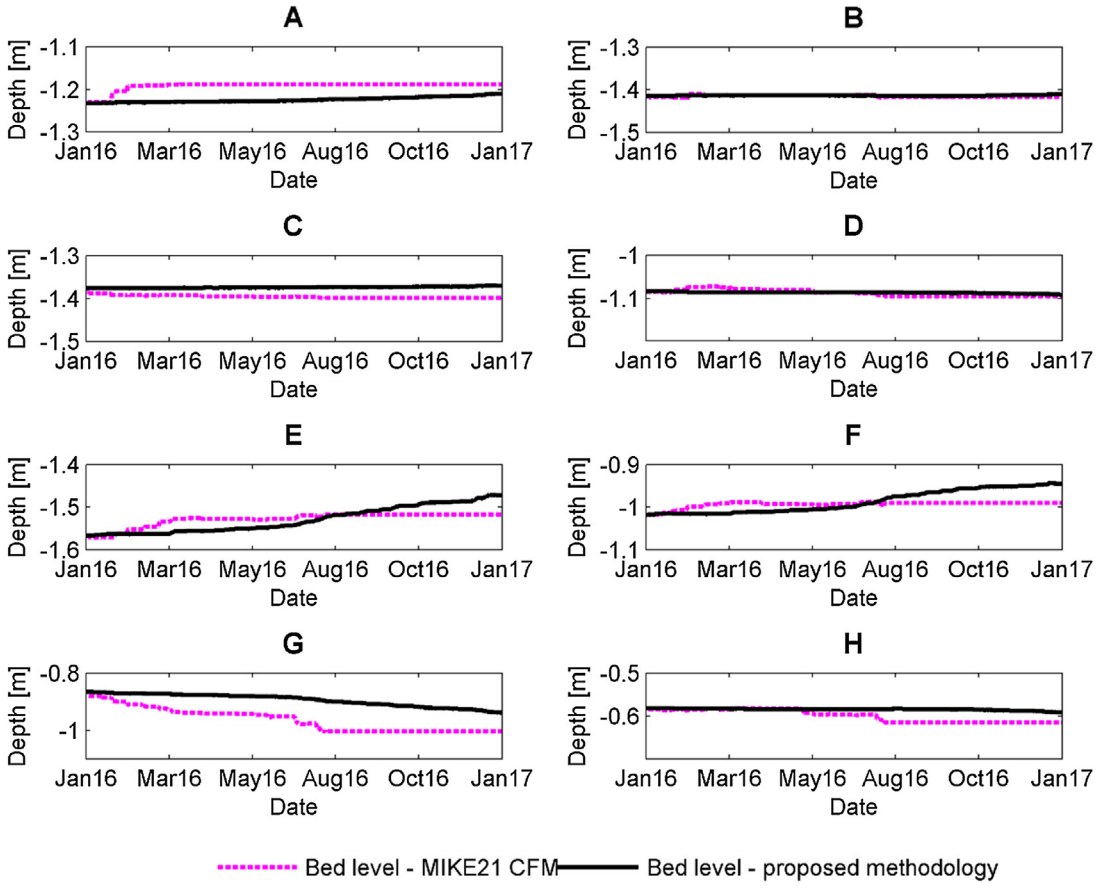

Figure 12 Bed levels derived from MIKE21 CFM (dashed red line) and the proposed methodology (solid black line).

In reference with the overall computation time of the model simulations, there is a striking discrepancy between the two approaches. For MIKE21 CFM with the full reference wave data as input, the total runtime was 542 h while for the 17 representative wave cases of the proposed methodology, the corresponding runtime was 2 h. Let us note that all simulations were conducted on an i7-2600 CPU server with 16 GB RAM and 3.40 GHz processor. Although current version of DHI is designed for parallel computing using graphics processors and could significantly accelerate the calculation process, still the present approach contributes to a significant runtime reduction, which for the particular non-parallel computing setup used is of the order of 99.6%. The latter result is quite impressive compared to the outcome presented in Fig. 12, at least for the case-study examined, characterised by mild bottom topography and coastal characteristics, and regularly in the distribution of offshore wave directions.

7. Conclusions

A cost-effective methodology is introduced to estimate long-term effects of waves represented by specific pairs of wave characteristics instead of the full wave time series, which is very demanding as regards computational cost. The proposed method is relatively easy to be applied and input reduction consists in defining the representative wave classes through (H_S, T_P) pairs with reference to the Shields parameter criterion. A number of 17 representative wave conditions were derived from the reference wave data of the available time series with one-year duration. From the moment the over-critical wave conditions are found, the sub-critical wave classes can also be identified along with the corresponding frequency of occurrence; in this way, the full time series of wave height, period and direction can be appropriately classified into representative wave conditions. Having these triplets to hand, the dynamic coupled current-wave modelling, including the interaction with sediment transport, for each representative condition provides the desirable rates of bed level change, from which the final bed level can be estimated.

Comparing the values of bed level from the representative wave conditions with those from the reference time series, there was a good agreement for the examined locations, with the differences remaining under 7% at eight selected locations along the examined coast. Moreover, the bed evolution tendencies of the proposed methodology at the examined locations conform with the outcome from the full wave time series and the situation encountered in reality. For this reason, the suggested technique can be considered as a useful tool for reducing considerably computational cost in particular.

The results from the present analysis verify the fact that both intense wave conditions and calm periods should be taken into account when bed level (or shoreline) evolution is

examined. However, the proposed method was applied to a wave-dominated coast in the Sitia Bay with a limited range of incoming wave directions. Consequently, further improvements and validations should be made in order to take into consideration additional factors that influence sediment transport and bed level, such as currents, and examine the methodology at more complex areas, where preferably in situ measurements are available. Moreover, the impacts of a finer resolution of the involved wave parameters during the discretization process and a longer reference time series can be also analyzed.

Acknowledgments

F. Karathanasi would like to thank the GIS section of HCMR for providing the digitized bathymetric data, and F. Gad for the fruitful conversations on the 2DH model. The authors are also thankful to Ch. Anagnostou for useful data and discussion concerning the examined site, E. Moussoulis from DHI-Greece for providing the software licence and for his prompt feedback to the raised questions as regards model configuration, and the two anonymous reviewers for their helpful comments that greatly improved this manuscript.

References

Alexandrakis, G., Gkionis, G., Petrakis, S., Kozyrakis, G., Kampanis, N.A., 2015. Study for the Effective Management of the Erosion Problem, the Protection and Recasting of the Coastline and the Reduction of Incoming Wave Energy, in the Sitia City Beachfront, and Makri Gialos. Technical Report. Coastal & Marine Research Laboratory (CRL), Institute of Applied & Computational Mathematics – Foundation for Research and Technology, Heracleion, 115 pp. (in Greek).

Anagnostou, C., Belibassakis, K., Karathanasi, F., 2017. Coastal erosion in the Sitia Crete Bay – rehabilitation of the coast based on nourishment techniques as an alternative to hard work interventions. In: 7th National Conference on Management and Improvement of Coastal Zones, 20–22 November, Athens, 421–430.

Aouiche, I., Daoudi, L., Anthony, E.J., Sedrati, M., Harti, A., Ziane, E., 2016. The impact of storms in the morphodynamic evolution of a human-impacted semi-sheltered beach (Agadir Bay, Morocco). J. Afr. Earth Sci. 115, 32–47, http://dx.doi.org/10.1016/j.jafrearsci.2015.12.011.

Belibassakis, K.A., Karathanasi, F.E., 2017. Modelling nearshore hydrodynamics and circulation under the impact of high waves at the coast of Varkiza in Saronic-Athens Gulf. Oceanologia 59 (3), 350–364, http://dx.doi.org/10.1016/j.oceano.2017.04.001.

Benedet, L., Dobrochinski, J.P.F., Walstra, D.J.R., Klein, A.H.F., Ranasinghe, R., 2016. A morphological modeling study to compare different methods of wave climate schematization and evaluate strategies to reduce erosion losses from a beach nourishment project. Coast. Eng. 112, 69–86, http://dx.doi.org/10.1016/j.coastaleng.2016.02.005.

Clementi, E., Pistoia, J., Delrosso, D., Mattia, G., Fratianni, C., Storto, A., Ciliberti, S., Lemieux, B., Fenu, E., Simoncelli, S., Drudi, M., Grandi, A., Padeletti, D., Di Pietro, P., Pinardi, N., 2017. A 1/24 degree resolution Mediterranean analysis and forecast modeling system for the Copernicus Marine Environment Monitoring Service. Extended abstract. In: 8th EuroGOOS Conference, Bergen, 27–28.

Corbella, S., Stretch, D.D., 2012. Predicting coastal erosion trends using non-stationary statistics and process-based models. Coast. Eng. 70, 40–49, http://dx.doi.org/10.1016/j.coastaleng.2012.06.004.

Daghigh, H., Khaniki, A.K., Bidokhti, A.A., Habibi, M., 2017. Prediction of bed ripple geometry under controlled wave conditions: wave-flume experiments and MIKE21 numerical simulations. Indian J. Geo Mar. Sci. 46 (3), 529–537, http://nopr.niscair.res.in/handle/123456789/40808.

Davidson-Arnott, R., 2009. Introduction to Coastal Processes and Geomorphology. Cambridge Univ. Press, Cambridge, 442 pp.

DHI, 2016. MIKE 21 & MIKE 3 Flow Model FM, Hydrodynamic and Transport. Scientific Documentation.

Dubarbier, B., Castelle, B., Marieu, V., Ruessink, G., 2015. Process-based modeling of cross-shore sandbar behavior. Coast. Eng. 95, 35–50, http://dx.doi.org/10.1016/j.coastaleng.2014.09.004.

Foteinis, S., Synolakis, C.E., 2015. Beach erosion threatens Minoan beaches: a case study of coastal retreat in Crete. Shore Beach 83 (1), 53–62.

Fredsøe, J., Deigaard, R., 1992. Mechanics of Coastal Sediment Transport. World Scientific, Singapore, 369 pp.

Günther, H., Behrens, A., 2012. The WAM model. Validation document Version 4.5.4. Institute of Coastal Research Helmholtz-Zentrum Geesthach (HZG), 92 pp.

Gad, F.K., Hatiris, G.A., Loukaidi, V., Dimitriadou, S., Drakopoulou, P., Sioulas, A., Kapsimalis, V., 2018. Long-term shoreline displacements and coastal morphodynamic pattern of North Rhodes Island, Greece. Water 10 (7), 849, http://dx.doi.org/10.3390/w10070849.

Gharibreza, M., Nasrollahi, A., Afshar, A., Amini, A., Eisaei, H., 2018. Evolutionary trend of the Gorgan Bay (southeastern Caspian Sea) during and post the last Caspian Sea level rise. Catena 166, 339–348, http://dx.doi.org/10.1016/j.catena.2018.04.016.

Hallermeier, R.J., 1980. Sand motion initiation by water-waves – 2 asymptotes. J. Waterw. Port C. Div. 106 (3), 299–318.

Hallermeier, R.J., 1981. A profile zonation for seasonal sand beaches from wave climate. Coast. Eng. 4 (3), 253–277, http://dx.doi.org/10.1016/0378-3839(80)90022-8.

Hasselmann, K., Barnett, T.P., Bouws, E., Carlson, H., Cartwright, D. E., Enke, K., Ewing, J.A., Gienapp, H., Hasselmann, D.E., Kruseman, P., Meerburg, A., Müller, P., Olbers, D.J., Richter, K., Sell, W., Walden, H., 1973. Measurements of wind-wave growth and swell decay during the Joint North Sea Wave Project (JONSWAP). In: group, J. (Ed.), Hydraulic Engineering Reports. Deutches Hydrographisches Institut, Hamburg, p. 95.

Karathanasi, F., Belibassakis, K., Anagnostou, C., 2017. Simulation of wave field and sediment transport at the Sitia bay. In: 7th National Conference on Management and Improvement of Coastal Zones, 20–22 November, Athens, 33–42.

Madsen, O.S., 1994. Spectral wave-current bottom boundary layer flows. In: Coast. Eng.; Proceedings 24th International Conference Coastal Engineering Research Council, American Society of Civil Engineers, Kobe, Japan (1994), 384–398, http://dx.doi.org/10.9753/icce.v24.%p.

Marine Information Service, 2016. EMODnet Digital Bathymetry (DTM). Marine Information Service, http://dx.doi.org/10.12770/c7b53704-999d-4721-b1a3-04ec60c87238.

Ortiz, A.C., Ashton, A.D., 2016. Exploring shoreface dynamics and a mechanistic explanation for a morphodynamic depth of closure. J. Geophys. Res. Earth 121 (2), 442–464, http://dx.doi.org/10.1002/2015jf003699.

Ramakrishnan, R., Agrawal, R., Remya, P.G., NagaKumar, K.C.V., Demudu, G., Rajawat, A.S., Nair, B., Nageswara Rao, K., 2018. Modelling coastal erosion: a case study of Yarada beach near Visakhapatnam, east coast of India. Ocean Coast. Manage. 156, 239–248, http://dx.doi.org/10.1016/j.ocecoaman.2017.08.013.

Ranasinghe, R., 2016. Assessing climate change impacts on open sandy coasts: a review. Earth-Sci. Rev. 160, 320–332, http://dx.doi.org/10.1016/j.earscirev.2016.07.011.

Soulsby, R., 1997. Dynamics of Marine Sands: A Manual for Practical Applications. Thomas Telford Publications, London, 249 pp.

Toimil, A., Losada, I.J., Camus, P., Díaz-Simal, P., 2017. Managing coastal erosion under climate change at the regional scale. Coast. Eng. 128, 106–122, http://dx.doi.org/10.1016/j.coastaleng.2017.08.004.

Van Rijn, L.C., 1993. Principles of Sediment Transport in Rivers, Estuaries and Coastal Seas. Aqua Publications, Amsterdam, The Netherlands, 690 pp.

Walstra, D.J.R., Hoekstra, R., Tonnon, P.K., Ruessink, B.G., 2013. Input reduction for long-term morphodynamic simulations in wave-dominated coastal settings. Coast. Eng. 77, 57–70, http://dx.doi.org/10.1016/j.coastaleng.2013.02.001.

Wiberg, P.L., Sherwood, C.R., 2008. Calculating wave-generated bottom orbital velocities from surface-wave parameters. Comput. Geosci.-UK 34 (10), 1243–1262, http://dx.doi.org/10.1016/j.cageo.2008.02.010.